THE DESIGN OF AN INTELLIGENT MACHINE FOR UPPER-LIMB PHYSICAL THERAPY

by

JAIN CHARNNARONG

B.Eng. Mechanical Engineering

Chulalongkorn University

(1988)

SUBMITTED TO THE DEPARTMENT OF

MECHANICAL ENGINEERING

IN PARTIAL FULFILLMENT OF THE REQUIREMENTS

FOR THE DEGREE OF

MASTER OF SCIENCE IN MECHANICAL ENGINEERING

at the

MASSACHUSETTS INSTITUTE OF TECHNOLOGY

August 1991

Signature of Author Signature redacted
Department of Mechanical Engineering
August 27, 1991

Certified by Signature redacted
Dr. Andre Sharon
Thesis Supervisor

Accepted by Signature redacted
Professor Ain A. Sonin
Chairman, Departmental Committee on Graduate Studies

THE DESIGN OF AN INTELLIGENT MACHINE FOR UPPER-LIMB PHYSICAL THERAPY

by

Jain Charnnarong

Submitted to the Department of Mechanical Engineering
on August 27, 1991 in Partial Fulfillment of the
Requirements for the Degree of Master of Science in
Mechanical Engineering

Abstract

Growth in robotic technology for the past two decades has focused primarily on manufacturing applications. Recently, the focus has shifted to service industries, including medical rehabilitation. The objective of this research is to apply robotic technology to physical rehabilitation of the human upper limb by: 1) providing a tool to increase the effectiveness of physical therapists; 2) providing a test-bed to study the potential of robotics in physical therapy; and 3) providing a tool to study the interaction between man and machine.

A prototype robotic aid for upper limb physical therapy has been designed and fabricated. The mechanical design of this prototype minimizes friction and end-point inertia such that end-point impedance can be easily modulated over a wide range through control action. This enables the robot to vary its firmness and "feel", thus varying its contribution in interacting with patients.

Thesis Supervisor: Andre Sharon, Ph.D.
Title: Associate Director, Laboratory of Manufacturing and Productivity

Acknowledgments

This thesis describes a research project being conducted at the Newman Laboratory for Biomechanics and Rehabilitation at Massachusetts Institute of Technology. Financial support for the research was provided by the National Science Foundation.

My supervisor, Andre Sharon, provided invaluable guidance and suggestions from the first day we started the project. After two years of hard work and of what seemed to be insurmountable obstacles, Andre turned out to be not only my thesis supervisor but also a close friend whose encouragement and support kept me going and enabled me to persevere.

Neville Hogan, my advisor, had a major role in directing this research. Neville's knowledge, imagination, and dedication have made him a leader in his field. It was an honor and pleasure to work with him. This research is truly the outcome of Neville's keen imagination in pushing robotic technology to its fullest limits and applications.

Hermano Igo Krebs' useful advice helped shape the design of this robot especially in the controller architecture. John Mical Mansfield and Ernie Fasse provided practical information about actuators and sensors. Ernie has tremendous experiences with a similar robot in the Bizzi lab. He has contributed invaluable guidance and suggestions for the design of this teaching aid. Padmanaban Srikrishna (Krishna) had joined the research project just a few months before I started writing this thesis. Krishna's work on control and dynamics taught me a lot about the end-effector that I haven't focused on much in the design stage. He pointed out some design defects just in time before we sent the drawings to our machine shop. Crispin Miller and his marvelous intelligence on hardware and software helped shape this manipulator design from the initial stage. Patrick Royer, Denis Rancourt, and Justin Won also contributed practical techniques and knowledge in electronics, control, and modelling.

Beside students in Neville's group, I would like to give special thank to Kenneth Salisbury, Kamal Youcef-Toumi, and Harry Asada who provided very useful information on direct-drive and cable drive technologies. Special thanks to Hagen Schemfp at the Woodhole Oceanographic Institute for providing useful information on speed reducers. Without helpful group of the machinists in the Laboratory for Manufacturing and Productivity (LMP), I might have not been able to complete the hardware design and fabrication.

Chen-An Chen, Scot Banks, Yvonne Grierson, and Dan DiLorenzo are marvelous office mates who helped encourage me through all the hard work during the design process. Lucille Blake, Sarakorn Gerjarusak, and Krishna were so helpful in proof reading this thesis.

Finally, I would like to give special thank to my parents and both sisters who try to listen, understand, and guide me through all difficulties. You may never know how much your love, guidance, and support really mean to me.

To

His Majesty King Bhumibol Adulyadej of Thailand
who gave me an honorable opportunity

My Beloved Mother and Father
Your love and kindness are always deeply appreciated

Table of Contents

Abstract....2

Acknowledgment....3

Table of Contents....5

List of Figures....10

List of Tables....12

Chapter 1: Introduction....14
- 1.1 Motivation....15
- 1.2 Specific Aims....15
- 1.3 Prototype Design....16
- 1.4 Impact on the Disabled Population....17

Chapter 2: Anthropometry
- 2.1 Physically Disabled People....19
  - 2.1.1 Workspace....24
  - 2.1.2 Hand Dimensions....27
- 2.2 Joint Motions....31
  - 2.2.1 Wrist Movement....32
  - 2.2.2 Finger Movement....34
  - 2.2.3 Shoulder Movement....35
  - 2.2.4 Elbow and Forearm Movement....37
- 2.3 Human Strength and Designed Interaction Force....38

Chapter 3: Design Specifications
- 3.1 End–point Properties....42
  - 3.1.1 Interaction Force at the End-Point....42
  - 3.1.2 End–point Friction....43
  - 3.1.3 End–point Inertia....43

3.1.4 End-point Stiffness..... 43
3.1.5 End–point Impedance Properties.....43
3.1.6 Backdrivability..... 43
3.2 Workspace
3.2.1 Size of Workspace..... 44
3.2.2 Visibility and Accessibility.....44
3.2.3 Mobility of the Teaching Aid Workstation..... 44
3.3 Power Source.....44
3.4 Control Architecture..... 45
3.5 Transducers
3.5.1 Position Transducer.....45
3.5.2 Force/Torque Transducer..... 45
3.5.3 Velocity Transducers..... 45
3.6 End-Effector
3.6.1 Modular Package.....46
3.6.2 Degrees of Freedom.....46
3.7 Safety Considerations
3.7.1 System Failure Detection.....47
3.7.2 Safety Release Mechanism.....47

Chapter 4: Kinematic Selection
4.1 Common Kinematic Configurations..... 49
4.1.1 Cartesian Frame..... 50
4.1.2 Cylindrical Frame..... 51
4.1.3 Spherical Coordinate Frame..... 52
4.1.4 SCARA Frame..... 54
4.2 Comparison of Prismatic and Revolute Joints
4.2.1 Energy Consumption..... 55
4.2.2 End-point Static Friction..... 57
4.2.3 End–point Inertia.....61
4.3 Selection of Arm configuration
4.3.1 End–point Friction of Arms.....62
4.3.2 End–point Inertia of Arms..... 74
4.3.3 Chapter Conclusion.....84

Chapter 5: Transmission and Actuator Selection

5.1 Linear and Rotary Drives....87
5.1.1 Linear Actuators....88
5.1.2 Rotary Actuators....91
5.2 Impact of Speed Reducers on Transmission Systems....92
5.3 Direct–drive Versus Cable Drive....99
5.4 Bearing Selection....103
5.4.1 Bearing Friction....104
5.4.2 Lubricant Selection....110
5.5 Chapter Conclusion....112

Chapter 6: Sensor Selection

6.1 Position Sensors....114
6.1.1 Position Resolutions....114
6.1.2 High-Accuracy Optical Shaft Encoders....115
6.1.3 High-Accuracy Resolvers and Synchros....117
6.2 Angle Measurement Using Resolvers....120
6.2.1 Direct Angle Technique....120
6.2.2 Phase Analog Technique....120
6.2.3 Sampling Technique....121
6.2.4 Tracking Resolver to Digital Converter....121
6.2.5 Dual Converters....125
6.3 Position Sensor Selection....126
6.3.1 Resolver-to-Digital Converter Selection....126
6.3.2 Resolver Selection....127
6.3.3 Position Sensor Architecture....130
6.4 Velocity Sensor Selection....131
6.4.1 DC Tachometers....131
6.4.2 Tachometer Selection....133
6.5 Torque Sensor Selection....136

Chapter 7: Actuator and Arm Design

7.1 Installation Requirements for Actuator Package Design....140
7.1.1 RBE-3003-AOX Brushless Motor....140
7.1.2 SSJH-44-B-2 Resolver....142
7.1.3 TG-2936-B Tachometer....143

7.1.4 TRT-200 Reaction Torque Sensor..... 144
7.2 Actuator Design
7.2.1 Actuator Package..... 144
7.2.2 Transmission Design..... 147
7.3 Actuator Package Wiring and Connections
7.3.1 Wiring in Actuator Package..... 148
7.3.2 Connector Arrangement..... 150
7.4 Future Improvements of the Actuator Package
7.4.1 Demand on Tachometer..... 152
7.4.2 Possibility of Weight Reduction..... 152
7.4.3 Heat Dissipation..... 153
7.4.4 Magnetic Shields..... 153
7.5 Determination of Profile and Wall thickness of the Arm Member..... 153
7.5.1 Cross Section Profiles of Arm Members..... 154
7.5.2 Load Calculation and Selection of Arm Members..... 156
7.6 Arm Design..... 161
7.6.1 Shoulder Joint and Joint 2-3..... 163
7.6.2 Arm Construction..... 164
7.6.3 Construction of Link 4 Joints..... 165
7.6.4 End-point Joint..... 166
7.6.5 Wiring and Electrical Connectors..... 167

Chapter 8: End-Effector Design
8.1 Requirements on End-Effector..... 170
8.2 Choices of Supporting Point..... 170
8.3 Pronation/Supination
8.3.1 Mechanism..... 172
8.3.2 Actuators and Sensors..... 175
8.4 Hand Holding Arrangement..... 175
8.5 Flexion/Extension and Abduction/Adduction
8.5.1 Mechanism..... 177
8.5.2 Actuators and Sensors..... 184
8.6 Safety Lock..... 184

Chapter 9: Conclusion
9.1 Design of Manual Teaching Aid..... 190

9.2 Future Work....192
9.2.1 Biorobot Design....192
9.2.2 Man-machine Interaction....193

Bibliography....194

Appendices
Appendix A: Detail Mechanical Design Drawings....199
A.1 Arm Subassembly....200
A.2 Foundation Subassembly....225
A.3 End-Effector Subassembly....234
A.4 Actuator Package Subassembly....250
Appendix B: Actuator and Sensors Details
B.1 RBE-3003-AOX Brushless Motor....272
B.2 SSJH-44-B2 Multi-Speed Resolver....277
B.3 TRT-200 Reaction Torque Sensor....280
B.4 TG-2936-B Tachometer....283
B.5 168-K400 Series Resolver-to-Digital Converter....285
B.6 Bearings....289
B.7 DGPH-1610-B-1T high torque miniature motor....298

List of Figures

2.1 Anthropometrics of Average Chairbounded Man and Woman.....21
2.2 Clearances and Reach of Wheelchaired Person at Seated Position..... 23
2.3 Work Area on Table Top for Wheelchair Seated Small Female..... 25
2.4 Selected Workspace..... 26
2.5 Selected Hand Dimensions for the Manual Teaching Aid.....30
2.6 Wrist Flexion and Extension..... 33
2.7 Wrist Abduction and Adduction..... 33
2.8 Radial and Ulnar Finger Movement..... 34
2.9 Flexion and Extension Finger Movement.....34
2.10 Internal and External Shoulder Movement.....35
2.11 Hyperextension and Flexion Shoulder Movement.....36
2.12 Abduction Shoulder Movement.....36
2.13 Flexion Elbow Movement..... 37
2.14 Pronation and Supination of Forearm.....38
2.15 Arm Strength in Seated Position of Weak Man and Woman..... 39

4.1 Cartesian Configuration.....51
4.2 Cylindrical Configuration.....52
4.3 Spherical Coordinate Configuration.....53
4.4 SCARA Configuration.....54
4.5 Prismatic and Revolute Joints.....56
4.6 Ratio of Kinetic Energy of Revolute to Prismatic Joints.....57
4.7 Model of Prismatic and Revolute Joints for Friction Determination.....58
4.8 Reflected End-Point Friction for Prismatic and Revolute Joints..... 60
4.9 Ratio of End-Point inertia of Revolute to Prismatic Joints.....62
4.10 Revolute Joint with Pivot Friction.....63
4.11 (a) and (b) Friction on Two Individual links..... 65,66
4.12 Friction Parallelogram.....67
4.13 Friction Compensation Algorithm..... 68
4.14 End-Point Friction Parallelogram of designed SCARA Arm.....69
4.15 Overhung Cartesian Frame..... 70
4.16 Estimated Friction of Telescopic Arm of Cartesian Frame.....71
4.17 Estimated Friction on Lower Carriage of Cartesian Frame..... 72
4.18 Friction Distribution of Cartesian Frame in the Workspace and Graphical Comparison to SCARA Frame..... 72
4.19 Friction Distribution of Cylindrical Frame on the workspace and Graphical Comparison to SCARA Frame..... 72
4.20 Inertia Distribution of Cartesian Frame on the Workspace and Graphical Comparison to SCARA Frame..... 75
4.21 Five Bar Parallel Mechanism.....76
4.22 (a) End-Point Inertia Ellipsoids of Designed Parallel Mechanism.....81
(b) Friction Parallelograms and Inertia Ellipsoids of Designed Parallel Mechanism.....82
4.23 Inertia Distribution of Cylindrical Frame in the Workspace and Graphical Comparison to SCARA Frame..... 83

5.1 Contact Condition of Friction/Traction Drive..... 89
5.2 Actuator and Ideal Speed Reducer.....93
5.3 (a) Reflected Output Friction for Different Speed Reduction Ratio..... 95
(b) Actuator Weight for Different Speed Reduction Ratio.....95
(c) Reflected Output Inertia for Different Speed Reduction Ratio.....96

5.4 Linkages and Cable Drive for Forearm....100
5.5 Preliminary Design of Cable Drive for Forearm....101
5.6 Pre-Tension Force on Cable....102
5.7 Deformation of a Rolling Element and the Raceway in the Direction of Rolling Motion....105
5.8 Motion in Cageless Bearings....106

6.1 Optical Encoder Construction....116
6.2 Resolver Construction....118
6.3 Equivalent Resolver Schematics....122
6.4 Basic Resolver Tracking System....122
6.5 Solid State Tracking System....124
6.6 True Size Cross Section of SSJH-44-B-2 Multi Speed Resolver....129
6.7 Architecture of Position Measurement Interfacing....130
6.8 Tachometer Output Waveform....132
6.9 True Size Cross Section of TG-2936-B Tachometer....135
6.10 True Size Cross Section of TRT-200 Reaction Torque Sensor....137

7.1 Example of Stator Mounting....141
7.2 Example of Rotor Mounting....141
7.3 Cross Section of Designed Actuator Package....145
7.4 Cross Section of Designed Actuator Package with Shoulder Joint....147
7.5 Wiring Routes of Actuator Package....149
7.6 Connector Arrangements on Rear Housing Unit....151
7.7 Square and Circular Tube Structure....154
7.8 Ratio of Moment of Area of Square to Circular Tubes....155
7.9 Lift and Press Strength of Weak Man and Woman....157
7.10 SCARA Arm with Vertical End-Point Load....158
7.11 Top View of Arm Assembly....162
7.12 Cross Section of Shoulder Joint....163
7.13 Front View of Link 2....164
7.14 Joint Constructions of Link 4....165
7.15 End-Point Joint at Normal Position....166
7.16 End-Point Joint at Overloaded Condition....166
7.17 Internal Electrical Wiring and Outside Loops....168

8.1 Choices of Supporting Point....171
8.2 Posture of Mechanism in Forearm Pronation....173
8.3 Posture of Mechanism in Forearm Supination....174
8.4 True Size View of Pronation/Supination DC Motor....175
8.5 Forearm Holding Arrangement with Plastic Splint....176
8.6 Output Torque Characteristic of Independent and Dependent Drive Concepts....178
8.7 Differential Mechanism for Flexion/Extension and Abduction/Adduction....179
8.8 Differential Mechanism in Wrist Abduction/Adduction Posture....181
8.9 Differential Mechanism in Wrist Flexion Posture....182
8.10 Differential Mechanism in Wrist Extension Posture....183
8.11 Separation of Splint Holder with Magnet Lock....185

9.1 The Designed SCARA Arm....188
9.2 Cross Section View of the Manual Teaching Aid....189
9.3 Front View of the End-Effector....190
9.4 Side View of the End-Effector....191

List of Tables

2.1 Distribution of U.S. Disabilities by Diagnosis....19
2.2 Accompanied Anthropometrics Data for Fig. 2.1....21
2.3 Work Area on Table Top for Seated Wheelchaired Small Female....25
2.4 Hand Thickness of Male and Female USAF and NAVY Personnel....27
2.5 Hand Length of Male and Female in Military and Civilian Samples....28
2.6 Hand Breadth Measured at Metacarpal....28
2.7 Hand Breadth Measured at Thumb....29

3.1 Design Specification of Wrist Movement....46

4.1 Estimated Reflected Inertia to End-Point of Cartesian Frame....75

5.1 Reflected Static Friction, Rotor Inertia, and Actuator Weight for Different Speed Reducer Ratios....94
5.2 Friction coefficient for Various Rolling Bearings....107
5.3 Comparison of Deep Groove and Angular Contact Ball Bearings....108
5.4 Load Torque Values, z and *y* , for Ball Bearings....109
5.5 Viscous Torque Factors....109
5.6 Criterion for Grease Selection....110
5.7 Properties of Recommended Grease for Low Friction Running Applications....110

6.1 Resolution of Position Sensors....115
6.2 Comparison of Position Sensors....115
6.3 Resolver-to–Digital Converter Performances....127
6.4 Profiles of Potentially Applicable Resolvers....128
6.5 Tachometer Specification....133
6.6 Tachometer Performances....134
6.7 Performance of TRT-200 Reaction Torque Sensor....137

7.1 Minimum Expected Mechanical Properties of 6061-T6 Aluminium Alloy....160
7.2 Comparison of Safety Factor of 1.5 inches Square Tube With Various Thickness....161

Chapter 1

Introduction

1. Introduction

The ability to manipulate and control objects in our environment is an important human characteristic. A severely disabled individual, however, is usually limited in the direct control of the environment or, in other words, unable to use a vast array of tools and gadgets that most humans take for granted. Robots are able to help disabled people[33] in the daily living activities, as well as serving as educational tools and therapeutic devices. Robots were first introduced to rehabilitation applications as mechanical personal attendants[13] (PCAs) for daily living activities; however, therapeutic applications for robots are novel. A current literature search has shown that the recent introduction of robotics to the disabled, published in an occupational therapy journal, fails to mention the concept of therapeutic applications[5]. Only a few groups are currently working in this area.

Khali and Zomlefer[19] constructed a continuous passive motion robot. Harwin, Ginige, and Jackson of the Cambridge group[16] developed a manipulator to assist in the developmental education of young children with severe physical impairments.

Dijkers and his colleagues[13] developed a robotic aid for upper-extremity reeducation movement after a stroke; This group also looked into safety, system utility, and patient and therapist acceptance. It appears, however, that none of these robotic therapeutic applications have gone far enough to allow robots to "fully interact" with patients. In other words, they do not dynamically "sense" and "control" impedance in man-machine interaction.

Dijkers only quantified patient performance by keeping records of time and number of movements of the patient's hand between his/her lap and a switch on the end-effector of the robot arm which stops at predetermined points in space. Ideally,

patient performance should be quantified in terms of position, speed, acceleration, force, time, and number of movements along the patient's hand trajectory.

Dynamic interaction between a robot and its environment has proved to be a difficult task. It involves integration of sensors in the robotic system and development of special control schemes to enhance the robot response. Most commercially available industrial robots employ purely position control schemes, while only a few use force control strategies. Mortensen[24] looked into switching between force and position control on a single axis. Craig and Raibert[7] proposed an appropriate control strategy with a combination of motion control along the tangent of a kinematic constraint and force control along the normal. Whitney[37] summarized various issues concerning force control strategies such as dynamic stability. Some research efforts have addressed dynamic interaction between robot and its environment. Hogan[17],[18] developed impedance control to precisely manage interaction between the robot arm and its environment.

1.1 Motivation

Performance advances and cost reductions have brought computer technology to the field of education. The existing packages for computer aided education (CAE) are limited only to audiovisual display (text, graphics, and audio).

Physical contact and manual manipulation are essential in education and cognitive development. In the world of therapy, direct "hand-over-hand" instruction is an effective technique for teaching, especially patients at an early stage of cognitive development who may not understand graphic, verbal, and gestural instructions.

1.2 Specific Aims

The main goal of this research is to apply recent technological advances and to add the critical tactile, proprioceptive and kinaesthetic sensori-motor dimensions to

educational applications. The proposed device is a "workstation" that will record motor actions that the therapist wants to shape and play them back repeatedly to the patient who may practice the motor skill without continuous physical involvement of the therapist. The machine will allow the therapist to take care of several patients at the same time and will quantify the progress of the patients over time.

The key element of the proposed workstation is a computer-controlled manipulator which safely holds and guides a person's hand. Instructions may be prepared in two ways: (1) the therapist "wears" the device and performs required motion while the computer records the information. (2) The therapist lets the patient "wear" the device and provides traditional "hand-over-hand" instruction to the patient and the machine at the same time.

One positive feature of the proposed machine is that the recorded actions may be replayed repeatedly with different degrees of "firmness" (The "firmness" refers to the degree of motion assistance and guidance). A "firm" robot would permit little motion deviation from nominal action. It would firmly but gently "drag" the patient's hand and arm along the proper path. At the other extreme of "firmness," the device would offer little or no resistance and guidance, but would record the patient's motion performance. These degrees of "firmness" may be specified by the therapist or may be varied by the computer based on the patient's actions.

1.3 Prototype Design

The machine can be categorized into three parts:

(1) Robot arm A parallel mechanism was selected to provide two degrees of freedom in a horizontal plane. End-point inertia of 4/3 kilograms with less than 5 ounces friction was achieved. In addition, the mechanism is compact when fully folded.

(2) Transmission design After a long study of various transmissions, direct-drive has been employed because of its low friction, high stiffness, and light weight. The design allows two actuators to be installed face-to-face in order to drive the arm mechanism. Each of the actuator units comprise a brushless DC motor along with position, torque, and velocity sensors.

(3) A hand-holding unit with three actively controlled rotational degrees of freedom has been employed at the end-point of the arm. Unlike most robot wrists and end-effectors, the required rotational travel is limited at 45 degrees of flexion/extension, 90 degrees of pronation/supination, and 30 degrees of abduction/adduction.

Two electromagnetic actuators work together to provide abduction/adduction and flexion/extension of wrist movements through a differential gear. In case of emergency, the patient may pull free from the hand holder unit without assistance.

1.4 Impact on the Disabled Population

The device will bring computer and robotic technology to cognitive development and education. While it cannot replace a skilled therapist, it can greatly increase the therapist's effectiveness. In addition, the device will quantitatively monitor forces, position, speed of motion, etc. This recorded information will be used to quantify progress of learning in subjective areas such as "feel" or rigidity. It may also enhance the patient's motivation and ability to learn and practice motion, especially in the case of young disabled patients.

Chapter 2

Anthropometry

2. Anthropometry

2.1 Physically Disabled People

The U.S. Department of Health, Education, and Welfare estimated in 1970 that 69 million people in the United States alone had physical limitations or disabilities. Table 2.1[1] shows a distribution of disabilities by diagnosis.

Disability	Number of Individuals
Visual:	
25% Vision loss	4,105,000
50% Vision loss	184,000
75% Vision loss	618,000
100% Vision loss	483,000
Orthopedic aids:	
Wheelchairs	409,000
Crutches	443,000
Canes	2,156,000
Walkers	404,000
Braces	1,102,000
Artificial Limbs	172,000
Special Shoes	2,337,000
Auditory:	
Deaf	1,800,000
Hard of Hearing	18,300,000
cardiovascular:	7,600,000
Respiratory:	14,500,000
Mental Retardation:	5,120,000
Arthritis:	18,300,000
Aging: Over age 65	7,000,000
Childhood: Age 5-12	32,550,000
Pregnancy:	3,730,000
	Total = 121,313,000

Total U.S. population = 215,000,000

Table 2.1 Distribution of U.S. Disabilities by Diagnosis

[1] Michigan Center for a Barrier-Free Environment by Salem, *Barrier Free Design*, 1977.

Data obtained statistically in 1972[2] showed that 15.0 percent and 13.6 percent of women and men of the total U.S. population considered themselves disabled. Age is clearly an important parameter in disability and the degree of severity. About 8 percent of those under forty-five years old claimed that they were disabled, compared to 19 percent and 29 percent of those aged forty-five to fifty-four and fifty-five to sixty-four, respectively. Similarly, in terms of severity of disability the group aged thirty-five to forty-four, the groups aged forty-five to fifty-four and the group aged fifty-five to sixty-four had two, four, and eight times the group aged twenty to thirty four, respectively. The same source of information also reflected that among those who were disabled, or 15 million people in 1972, 36 percent or more than 5 million people, had musculoskeletal disorders. As far as activity limitations involved with the upper limb, 28.6 percent had limitation in reaching, 21.0 percent had problems with handling and fingering, 33 percent had difficulties in lifting or carrying weights up to 10 pounds, and 58.8 percent had difficulties in lifting or carrying weights over 10 pounds. Unfortunately, over 75 percent of upper-limb disabled people are left to cope with their limitation.

From our observation at the Spaulding Rehabilitation Hospital[3], most of the upper-limb disabilities are accompanied by some degree of paralysis and muscle dysfunction. Statistics of 1972 showed that among the disabled people, 21.7 percent had no activity limitations while 12.6, 11.7, 10.6, 7.9, and 35.4 percent had one, two, three, four, and five or more limitations, respectively. Most of the upper-limb disabled people at Spaulding Rehabilitation Hospital are chairbound. Causes of disability range from accidents to aging. Patients may be as young as five to over sixty-five years old with different body sizes, reach, and wheelchairs. Regardless of the different body size or wheelchairs, the manual teaching aid must be designed to accommodate and

---

2 Dept. of Health and Human Service, *Disability Survey 72*, Research report no. 56, April 1981

3 Spaulding Rehabilitation Hospital, 125 Nashua St., Boston

guarantee accessibility to these people. With regard to the anthrometrics involved, Fig 2.1 illustrates body segments and reaches of the average man and woman in standard wheelchairs.

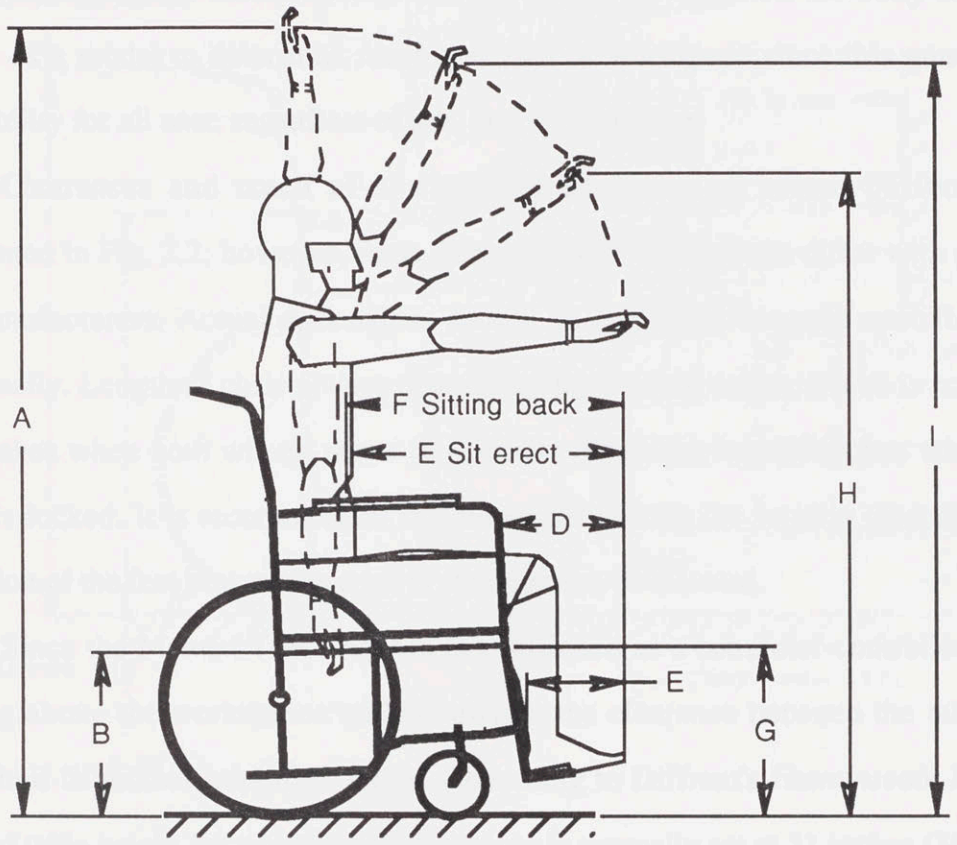

Fig. 2.1 Anthropometrics of Average Chairbounded Man and Woman
(Use with Table 2.2)
Sources: Humanscale 7/8/9

	MALE		FEMALE	
	in	cm	in	cm
A	62.25	158.1	56.75	144.1
B	16.25	41.3	17.5	44.5
C	8.75	22.2	7.0	17.8
D	18.5	47.0	16.5	41.9
E	25.75	65.4	23.0	58.4
F	28.75	73.0	26.0	66.0
G	19.0	48.3	19.0	48.3
H	51.5	130.8	47.0	119.4
I	58.25	148.0	53.24	135.2

Table 2.2 Accompanying Anthropometrics Data for Fig. 2.1

Since reach is an essential parameter in the design of this robotic aid design, all dimensions in Table 2.2 are based on 2.5th percentile of statistical human dimensions to allow those users with small body sizes, such as small woman and youth patients, to use the machine. It is recommended that the design be based on the body of small women as a model to determine reach and size of workspace since this guarantees accessibility for all user, regardless of sex, age, or body size.

Clearances and reach of a wheelchaired person at seated position[4] are represented in Fig. 2.2; however, exact dimensions of wheelchairs differ with models and manufacturers. Actual dimensions should be measured for each specific chair individually. Length of chair always determines the turning radius, which is normally 31.5 inches when both wheels move in opposite directions and 36 inches when one wheel is locked. It is recommended that when calculating the turning clearance, the protrusion of the feet beyond the edge of the footrests be allowed.

Since the Manual Teaching Aid is envisioned as a computer-controlled robot working above the workstation table's surface; the clearance between the table and wheelchair is another important factor. According to Diffrent's *Humanscale 7/8/9* [5], standard table height for wheelbounded persons is normally set at 31 inches (78.7 cm) with a minimum height of 21 inches (53.3 cm) to allow underneath clearance. Forward-reach ability still depends, nevertheless, on the user body size. Again, the farthest point in the designed workspace from the user's body must still be within the reaching limit of a small female or a youth user. Figure 2.2 illustrates easy and maximum forward reach for youth age six to nine to average adult[6]. Note that easy and maximum forward reach for a small female is 18.5 inches (47 cm) and 31.3 inches (79.5 cm), respectively.

---

[4] The American National Standards Institute ANSI Pub. A117-1961, Revalidated 1971

[5] Diffrient, Tilley, Harman, *Humanscale 7/8/9*, MIT press, Cambridge, 1981

[6] Diffrient, Tilley, Harman, *Humanscale 1/2/3* , MIT press, Cambridge, 1981

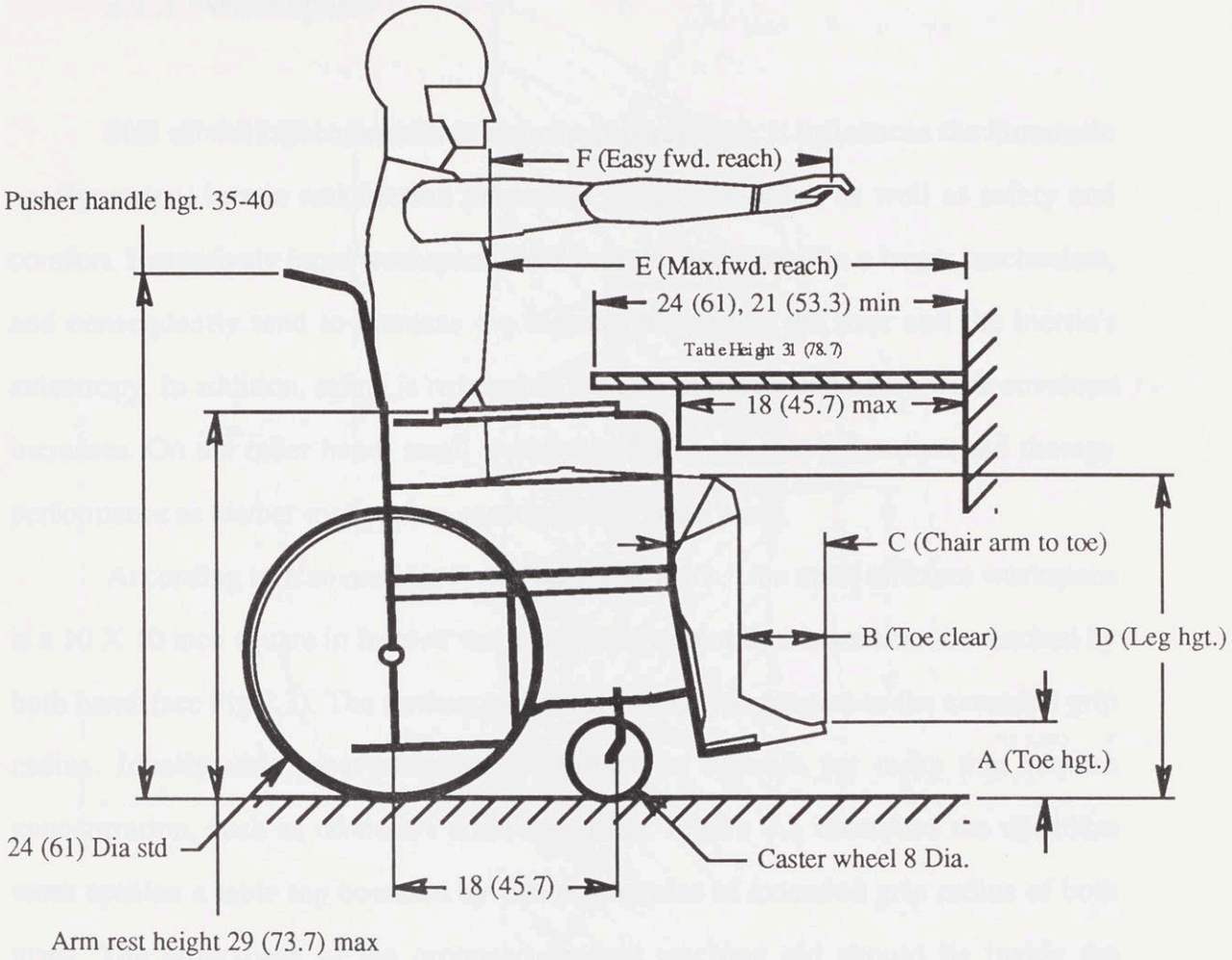

Body size	A	B	C	D	E	F
Youth Age 6-9	11.9(25.2)	4.5(11.4)	11.5(29.2)	23.3(59.2)	26.3(66.8)	15.3(38.9)
Youth Age 9-12	8.4(21.3)	5(12.7)	13.3(33.8)	22.3(5606)	30.6(77.7)	18.1(46)
Small female	8.8(22.4)	4.5(11.4)	12.5(31.80	23.5(59.7)	31.3(79.5)	18.5(47)
Avg.female/small male	6.5(16.5)	5.8(14.7)	14.5(36.8)	24.5(62.2)	34.2(86.9)	20.2(51.3)
Avg.male/Large female	5.8(14.7)	7.3(18.5)	16.5(41.9)	25.5(64.8)	36.3(92.2)	21.3(54.1)
Avg. Adult	6.2(15.7)	6.6(16.8)	15.5(39.4)	25(63.5)	35.3(89.7)	20.8(52.8)

Fig. 2.2 Clearances and Reach of Wheelchaired Person at Seated Position
Source: Humanscale 7/8/9,

2.1.1 Workspace

Size of workspace is another important parameter. It influences the kinematic configuration, inertia and friction properties at the end-point, as well as safety and comfort. Excessively large workspace, for example, may result in a larger mechanism, and consequently tend to increase the inertia reflected to the user and the inertia's anisotropy. In addition, safety is reduced as the size of the mechanism's work envelope increases. On the other hand, small workspace limits the user's freedom and therapy performance as his/her motions are constrained in small areas.

According to *Humanscale 7* on "seated at work," the most efficient workspace is a 10 X 10 inch square in front of the body. Every point in this area can be reached by both hands(see Fig 2.3). The farthest part from the body is tangent to the extended grip radius. Ideally, this most efficient workspace is suitable for tasks that require concentration, such as miniature scale operation. Figure 2.3 illustrates the optimum work area on a table top bounded by two semicircles of extended grip radius of both arms. The workspace of the proposed manual teaching aid should lie inside the optimum work area, and at the same time, be large enough to cover the most efficient work area in front of the user's body.

Based on the criteria that reach is a critical design factor, 15 inches was selected as the length of therapy workspace. This 15 inch dimension represents the difference between the extended grip radius and the average sitting distance between the body's shoulder line and the table's edge. In addition, the width of the workspace was selected to be 18 inches which is equal to the standard width of a wheelchair for a small female. This 15X18 area is directly in front of the user's body, covering the most efficient work area.

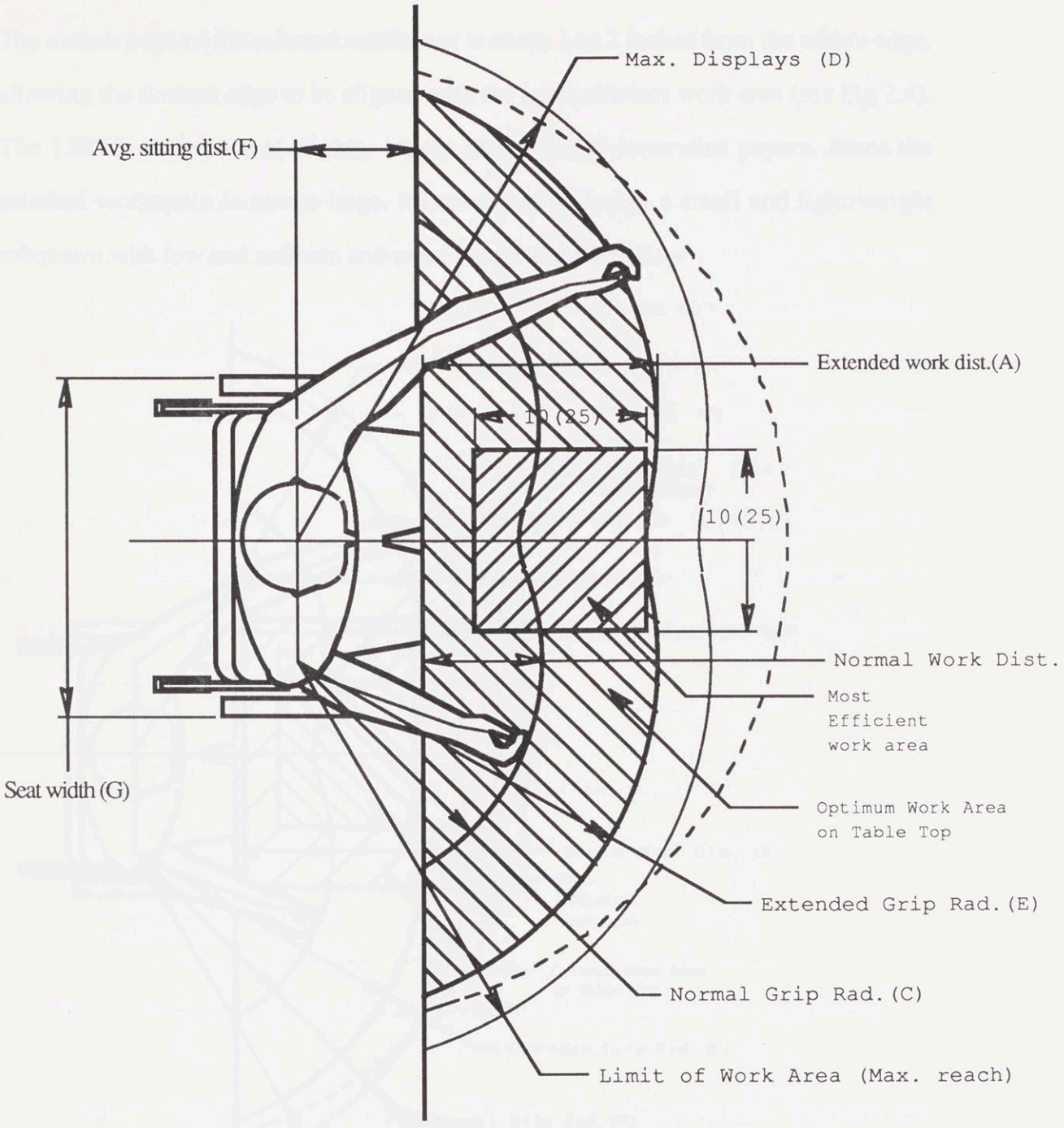

Select	A	B	C	D	E	F	G
Youth age 10	13.8(35.1)	7.4(18.8)	13.8(35.1)	30.9(78.5)	20.2(51.3)	6.4(16.3)	16(40.6)
Small female	15.5(39.4)	7.9(20.1)	14.9(37.8)	31(78.7)	22.5(57.2)	7(17.80	16(40.6)
Sm.male/avg female	16.3(41.4)	8.2(20.8)	16(40.6)	31.1(79)	24.1(61.2)	7.8(19.8)	18(45.7)
Avg. adult	16.7(42.4)	8.6(21.8)	16.6(42.2)	31.2(79.2)	24.9(74.4)	8(20.3)	18(45.7)\
Avg.male/Lg.female	17.2(43.7)	9(22.9)	17.4(44.2)	31.3(79.5)	25.6(65)	8.4(21.3)	18(45.7)

Fig.2.3 and Table 2.3 Work Area on Table Top for Wheelchair Seated Small Female
Source: Humanscale 1/2/3

The closest edge of the selected workspace is about 1 or 2 inches from the table's edge, allowing the farthest edge to be aligned with the most efficient work area (see Fig 2.4). The 15X18 workspace is slightly bigger than two US letter-size papers. Since the selected workspace is not so large, it is possible to design a small and light-weight robot arm with low and uniform end-point inertia and friction.

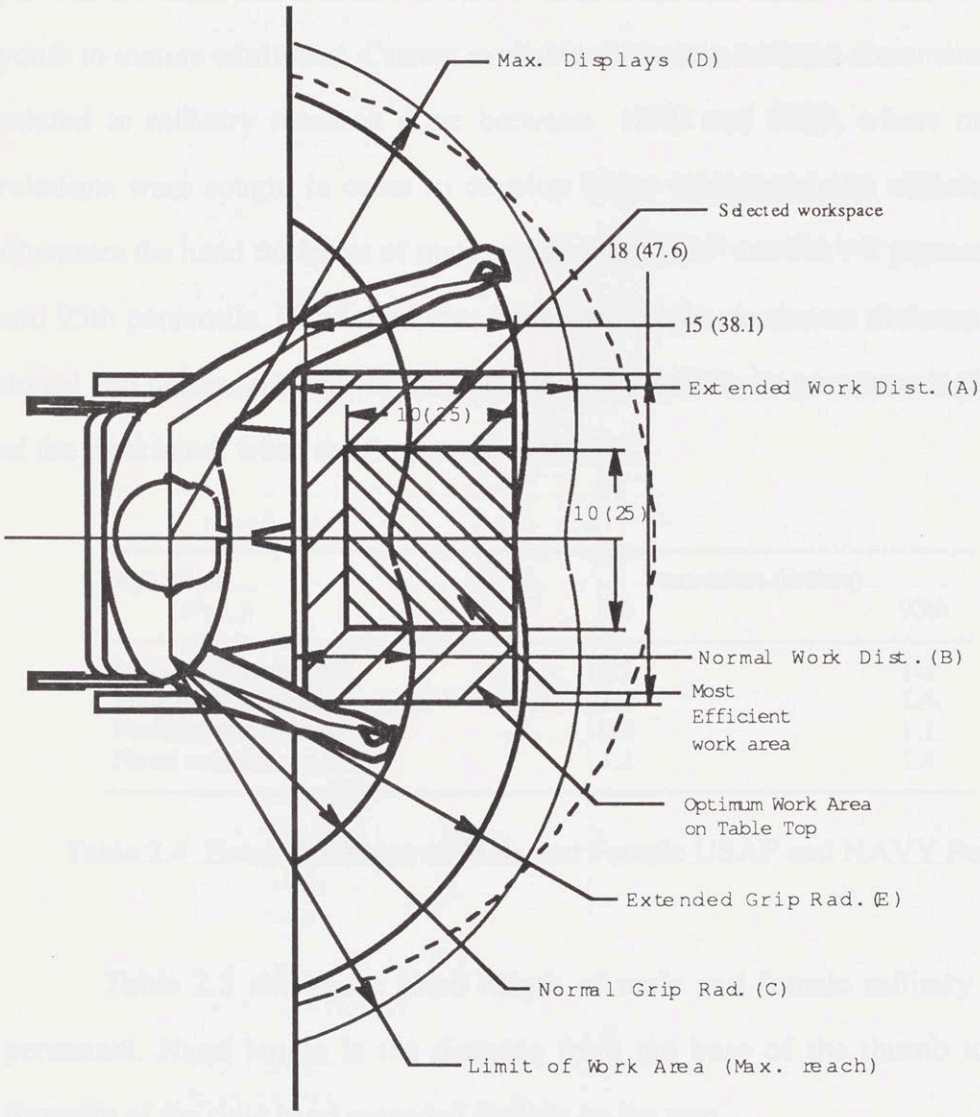

Fig 2.4 Selected Workspace[7]

[7] Derive from Diffrient, Tilley, Harman, *Humanscale 7*, MIT Press, 1981

2.1.2 Hand Dimensions

Hand dimensions are extremely important parameters to the manual teaching aid. The machine is going to hold the human hand and palm and control their posture and movement. In other words, interaction between the machine and the user will take place at the hand. The machine should be able to accommodate various hand sizes from youth to mature adulthood. Current available references on hand dimensions are mainly related to military research done between 1940 and 1950, where man–machine relations were sought in order to develop better equipment and vehicles. Table 2.4 illustrates the hand thickness of male and female USAF and NAVY personnel in the 5th and 95th percentile. Hand thickness is defined as the maximum distance between the dorsal and palmar surfaces of the knuckle of the middle finger where it joins the palm of the right hand, when the fingers are extended.

Population	Percentiles (inches)	
	5th	95th
Male flight personnel	1.1	1.3
Male basic trainees	1.1	1.4
Female basic trainees	0.8	1.1
Naval aviators	1.1	1.4

Table 2.4 Hand Thickness of Male and Female USAF and NAVY Personnel[8]

Table 2.5 shows the hand length of male and female military and civilian personnel. Hand length is the distance from the base of the thumb to the middle fingertip of the right hand extended straight on the arm.

---

[8] Van Cott, Kinkade, *Human Engineering Guide to Equipment Design*, McGraw-Hill, 1963

Population	Percentiles (inches) 5th	95th
MALE:		
Air Force personnel	6.9	8.0
Cadets	7.1	8.2
Gunners	3.9	8.1
Basic trainees	6.9	8.2
Army personnel:		
Aviators	6.9	8.1
Separatees, white	7.0	8.2
Separatees, black	7.3	8.7
Truck and bus drivers	7.1	8.1
Naval aviators	7.0	8.1
FEMALE:		
Air Force personnel		
Pilots	6.4	7.4
Flight nurses	6.5	7.4
Basic trainees	6.2	7.3
Army personnel	6.4	7.4
College students	6.2	7.2

Table 2.5 Hand Length of Male and Female in Military and Civilian Samples[9]

Population	Percentiles (inches) 5th	95th
MALE:		
Air Force personnel	3.2	3.7
Cadets	3.1	3.7
Gunners	3.1	3.6
Basic trainees	3.2	3.7
Army personnel:		
Separatees, white	3.1	3.8
Separatees, Negro	3.2	3.8
Truck and bus drivers	3.2	3.8
Army aviators	3.2	3.8
Naval aviators	3.3	3.8
FEMALE:		
Air Force personnel:		
Pilots	2.8	3.3
Flight nurses	2.8	3.2
Basic trainees	2.7	3.4
Army personnel	2.7	3.4

Table 2.6 Hand Breadth Measured at Metacarpal[10]

9 Van Cott, Kinkade, *Human Engineering Guide to Equipment Design*, McGraw-Hill, 1963

10 Van Cott, Kinkade, *Human Engineering Guide to Equipment Design*, McGraw-Hill, 1963

Table 2.6 presents the hand breadth at the metacarpal of U.S. male military and civilians. The breadth is defined as the maximum distance across the ends of the metacarpal bones, where the fingers join the palm of the index and little fingers of the right hand extended straight and stiff with the fingers together. (Metacarpal is the name of an anatomical point located at the distal end of the middle metacarpal bone.)

Table 2.7 shows the hand breadth at the thumb (D in Figure 2.5) for various segments of the population.

Population	Percentiles (inches)	
	5th	95th
Male flight personnel	3.7	4.4
Male basic trainees	3.7	4.5
Female basic trainees	3.2	4.0
Naval aviators	3.9	4.5

Table 2.7 Hand Breadth Measured at Thumb[11]

Concluding from hand dimensions of Tables 2.4 to 2.7, the design should be able to accommodate the sizes of human hands shown in Fig 2.5. Maximum values shown in Fig. 2.5 are selected from the 95th percentile of male subjects, and the minimum is from 5th percentile of female subjects. We assume that hand dimensions of youth who are capable of using the robotic aid are close to that of the 5th percentile.

---

11 Van Cott, Kinkade, *Human Engineering Guide to Equipment Design*, McGraw-Hill, 1963

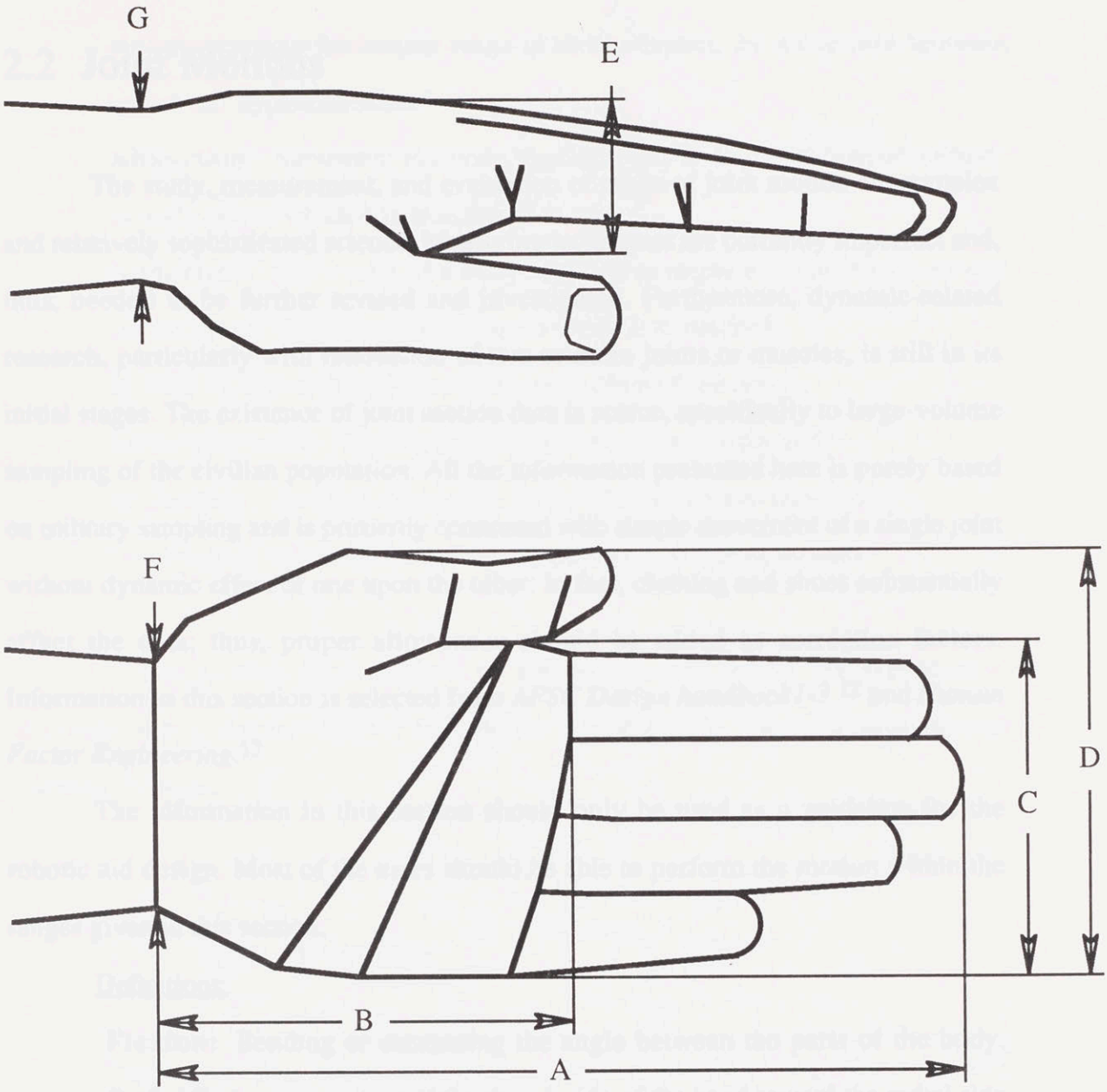

Dimensions	(inches) Max	Min
A	8.3	6.6
B	4.6	3.8
C	3.8	2.8
D	4.5	3.0
E	2.8	1.8
F	2.9	2.1
G	2.0	1.5

Fig. 2.5 Selected Hand Dimensions for the Manual Teaching Aid

2.2 Joint Motions

The study, measurement, and evaluation of range of joint motion are complex and relatively sophisticated science. Measuring techniques are currently imperfect and, thus, needed to be further revised and investigated. Furthermore, dynamic-related research, particularly with interaction of two or more joints or muscles, is still in its initial stages. The existence of joint motion data is scarce, specifically to large-volume sampling of the civilian population. All the information presented here is purely based on military sampling and is primarily concerned with simple movement of a single joint without dynamic effect of one upon the other. In fact, clothing and shoes substantially affect the data; thus, proper allowances should be added as correction factors. Information in this section is selected from *AFSC Design handbook1-3* [12] and *Human Factor Engineering*.[13]

The information in this section should only be used as a guideline for the robotic aid design. Most of the users should be able to perform the motion within the ranges given in this section.

Definitions:

Flexion: Bending or decreasing the angle between the parts of the body. *Radial flexion*: movement of the thumb side of the hand toward the radial side of the forearm segments; *ulnar flexion*: the opposite side of the hand's movement toward the ulnar side of the forearm segment.

Extension: Straightening or increasing the angle between the parts of the body. It is generally defined as the return from flexion. When a joint is

---

12 *Human Factors Engineering*, 3rd ed.

13 *AFSC Design Handbook 1-3*, Jan 1977, Department of the Air Force, Headquarters Air Force Systems Command, Andrews AFB, DC 20334, pp. 16-17

extended beyond the normal range of its movement, the movement becomes known as "hyperextension."

Abduction: Movement of a body segment away from the midline of the body or body part to which it is attached.

Adduction: Movement of a body segment or segment combination toward the midline of the body or body part to which it is attached.

Medial rotation: Turning toward the midline of the body.

Lateral rotation: Turning away from the midline of the body.

Pronation: Rotating the forearm so that the palm faces downward.

Supination: Rotating the forearm so that the palm faces upward.

In this section, joint motions of the wrist and shoulder are presented in schematic forms. Again, note that each motion is independent from interaction of other joints or muscles.

2.2.1 Wrist Movement

There are two rotational degrees of freedom in the human wrist, flexion/extension and abduction/adduction. Figure 2.6 illustrates wrist flexion and extension. Flexion is normally limited to 70 degrees while extension is slightly less than 65 degrees. Figure 2.7 shows abduction and adduction movements. Adduction travel is 30 degrees while abduction is only 15 degrees. When both rotational movements interact, abduction is unachievable as the wrist is fully flexed. On the other hand, if the wrist is fully adducted, small degrees of flexion/extension are allowed.

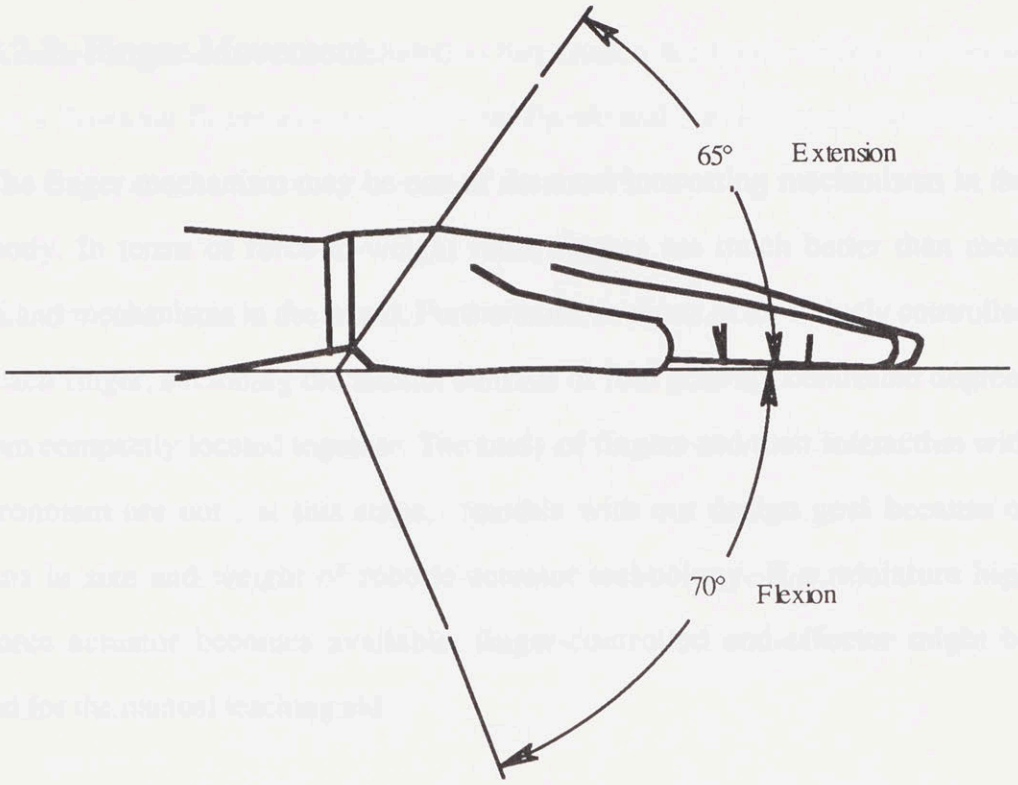

Fig. 2.6 Wrist Flexion and Extension

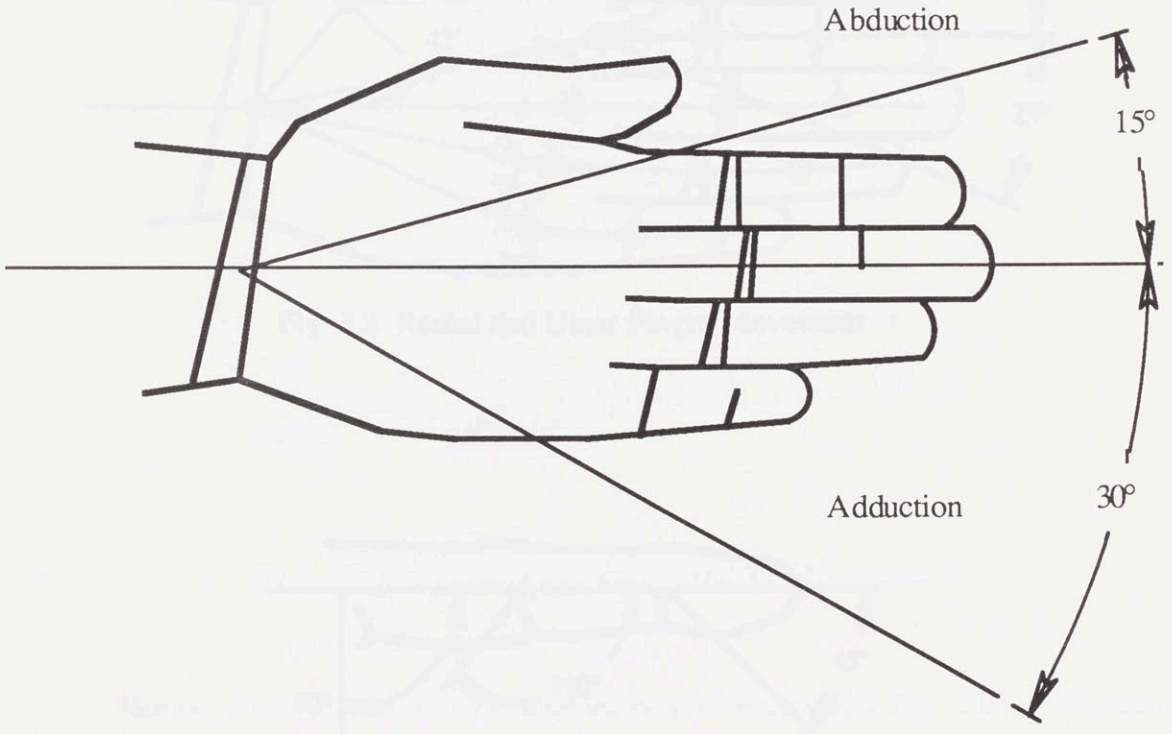

Fig. 2.7 Wrist Abduction and Adduction

2.2.2 Finger Movement

The finger mechanism may be one of the most interesting mechanisms in the human body. In terms of force-to-weight ratio, fingers are much better than most machines and mechanisms in the world. Furthermore, in terms of an actively controlled system, each finger, excluding the thumb, consists of four actively controlled degrees of freedom compactly located together. The study of fingers and their interaction with the environment are not , at this stage, feasible with our design goal because of limitations in size and weight of robotic actuator technology. If a miniature high torque/force actuator becomes available, finger-controlled end-effector might be developed for the manual teaching aid.

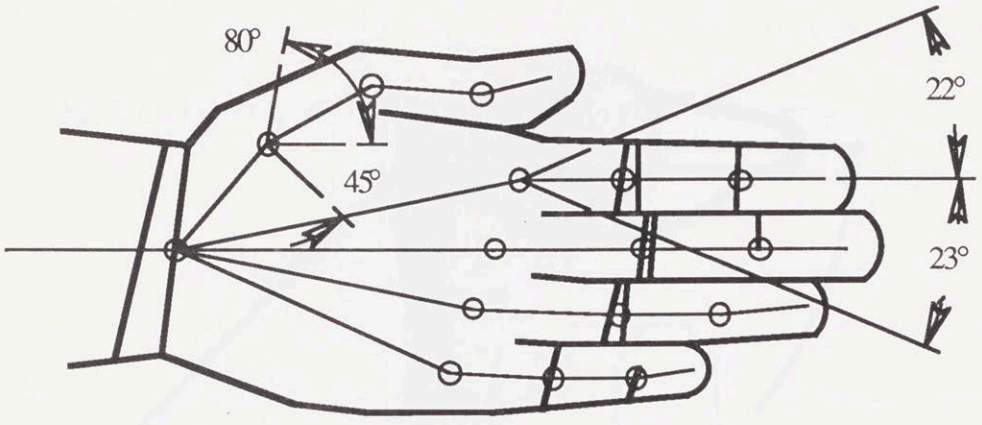

Fig. 2.8 Radial and Ulnar Finger Movement

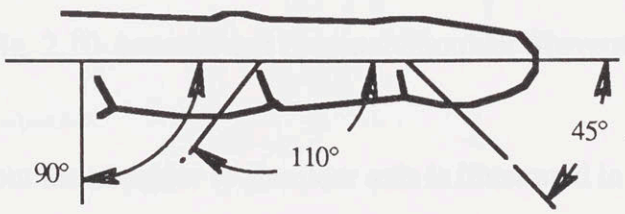

Fig. 2.9 Flexion and Extension Finger Movement

Finger-movement data is included in this section for future reference. Figures 2.8 and 2.9 illustrate finger movement of the thumb and index finger which are the most dominant ones for most hand-operation tasks.

2.2.3 Shoulder Movement

Shoulder joints have the most powerful muscles on the upper limb. There are 3 degrees of freedom in the joint. Data presented below only illustrate shoulder movement in one single degree of freedom, one vertical and two horizontal. The motion about the vertical axis is called internal and external shoulder rotation which is illustrated in Fig. 2.10.

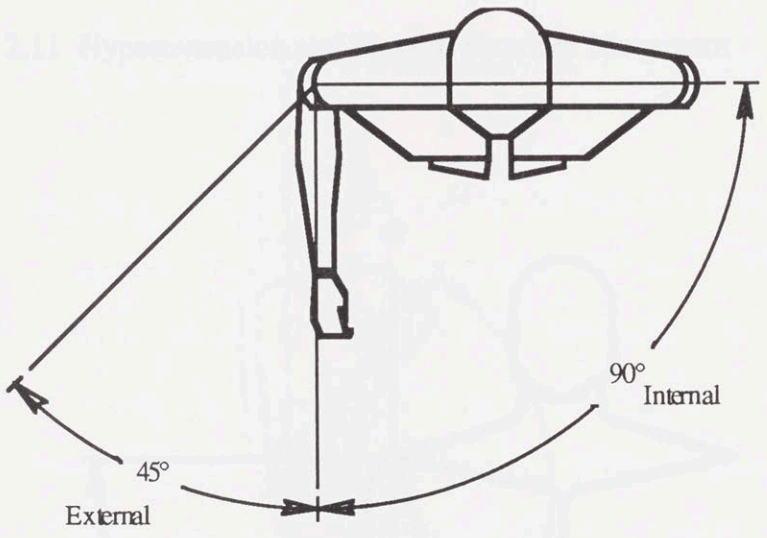

Fig. 2.10 Internal and External Shoulder Movement

Motion about the shoulder to shoulder axis is illustrated in Fig. 2.11 as forward elevation, flexion, and hyperextension. In Fig. 2.12, shoulder abduction is shown.

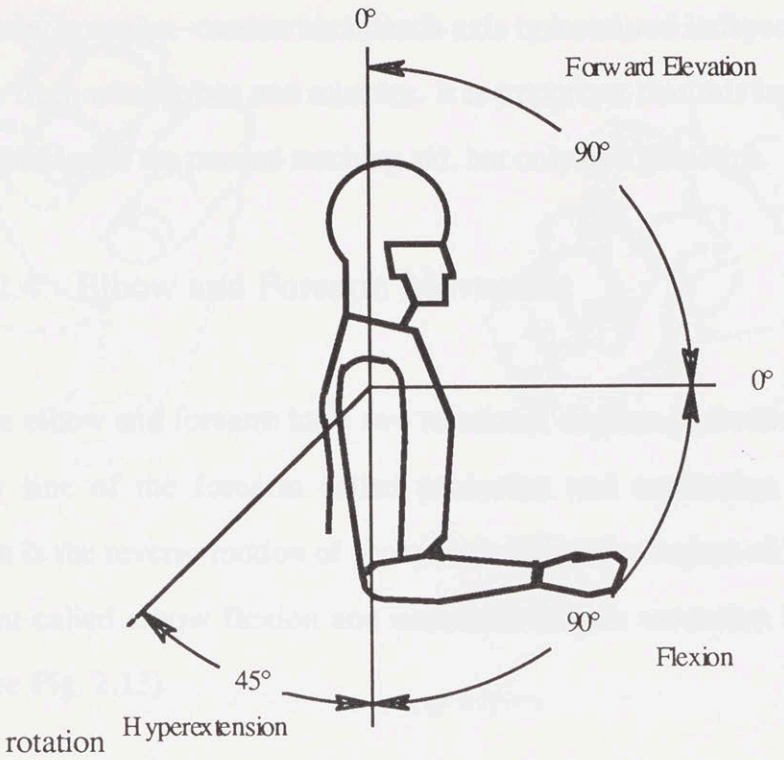

Fig. 2.11 Hyperextension and Flexion Shoulder Movement

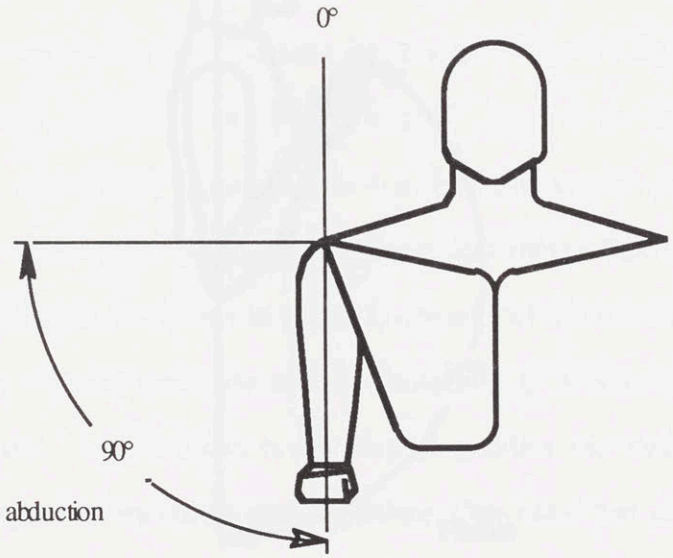

Fig. 2.12 Abduction Shoulder Movement

Again, note that motion about each axis is measured independently from any interaction from other joints and muscles. It is important that this information not be used in the design of the manual teaching aid, but only as a guideline.

2.2.4 Elbow and Forearm Movement

The elbow and forearm have two rotational degrees of freedom. One is about the center line of the forearm called pronation and supination (see Fig 2.14), (supination is the reverse motion of pronation). The other degree of freedom is about elbow joint called elbow flexion and extension. Again extension is the reverse of flexion (see Fig. 2.13).

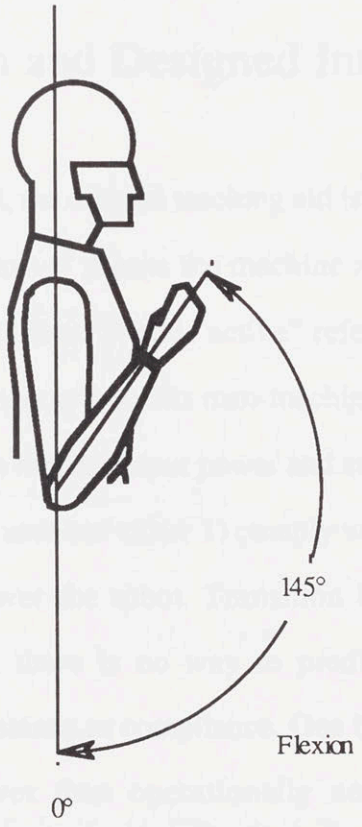

Fig. 2.13 Flexion Elbow Movement

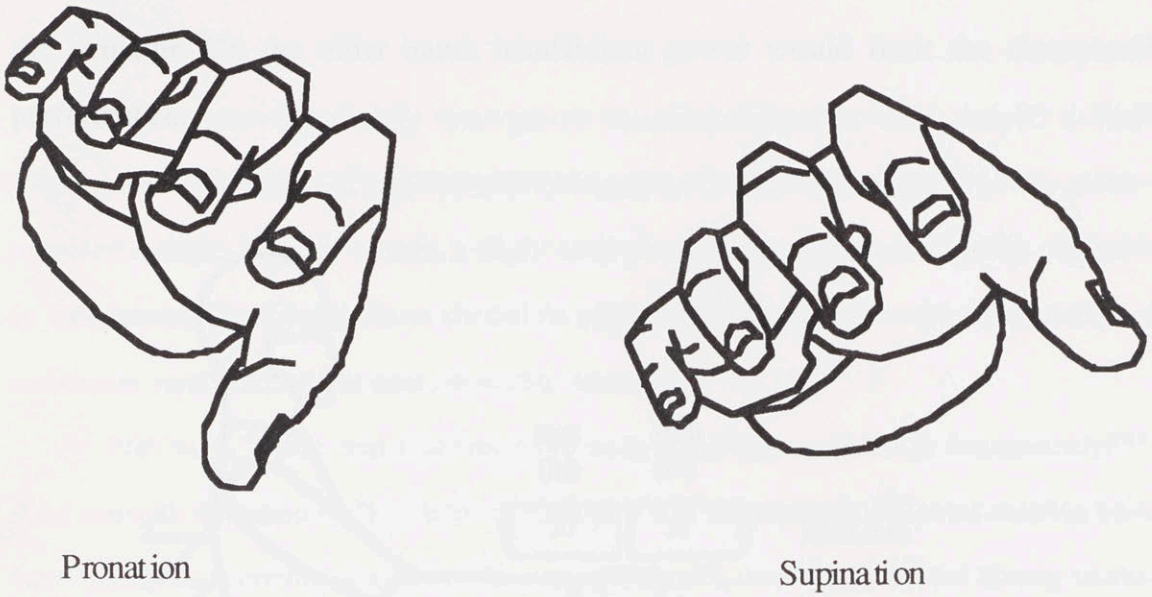

Fig. 2.14 Pronation and Supination of Forearm

2.3 Human Strength and Designed Interaction Force

As presently envisioned, the manual teaching aid is a robot that operates in both passive and active modes. "Passive" means the machine absorbs the energy produced by the user, dissipates it out as heat. While "active" refers to the operating mode in which the machine introduces energy into this man-machine system. In the active mode the manipulator clearly requires higher output power and energy than the passive mode.

In active operation, the user can either 1) comply with the robot's assistance and guidance or 2) try to overpower the robot. Transition between these two states is unmodelled. In other words, there is no way to predict the switching time, the sequence, or the degree of resistance or compliance. One basic rule of design is to give the robot slightly more power than operationally necessary. Excessive power, however, would threaten the user's safety and would increase the size and weight of

the actuator. On the other hand, insufficient power would limit the therapeutic performance.

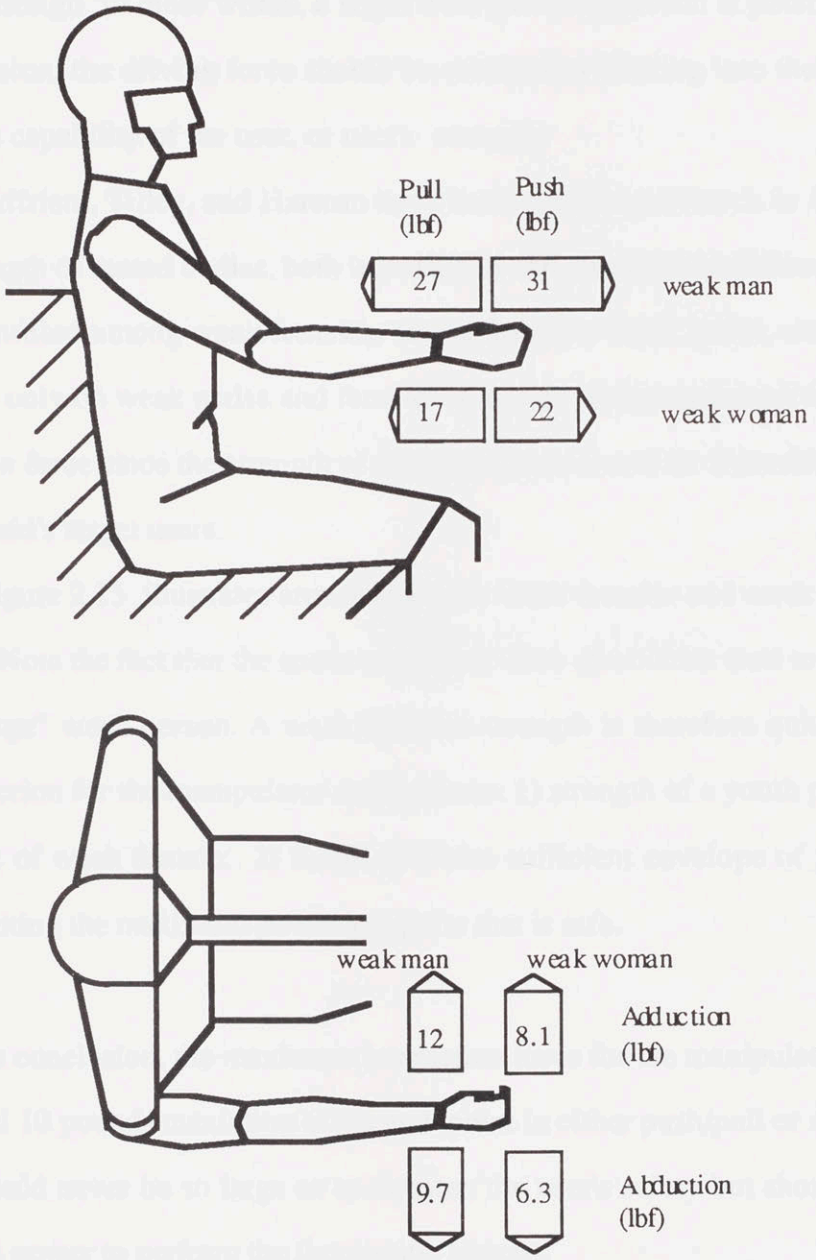

Fig. 2.15 Arm Strength in Seated Position of Weak Man and Woman

If the robot has slightly more power than necessary, it is much simpler to limit output power for each particular manipulating task than to boost power from an under–powered design. In other words, a slight over-power approach is potentially superior. In conclusion, the driving force should be selected by looking into the information of resistance capability of the user, or user's strength.

Diffrient, Tilley, and Harman have done excellent research in *humanscale7*[14]. Arm strength of seated bodies, both in push/pull and sideways in different reaches have been quantified among weak females, strong females, weak males, and strong males. Focusing only on weak males and females is a good design approach for selecting the interaction force since the strength of this population is not far from that of the manual teaching aid's target users.

Figure 2.15 illustrates arm strength for weak females and weak males in seated position. Note the fact that the users with upper-limb disabilities tend to be weaker than an "average" weak person. A weak female's strength is therefore quite likely to be a good criterion for the manipulator design since: 1) strength of a youth patient is not far from that of weak female; 2) it still provides sufficient envelope of power to teach, while limiting the maximum power to a point that is safe.

In conclusion, the maximum interaction force for the manipulator is selected to be around 10 pounds maximum at the end–point in either push/pull or side to side. The force should never be so large as to threaten the user's safety but should still provide sufficient power to perform the therapeutic lessons.

---

[14] Diffrient, Tilley, Harman, *Humanscale7*, MIT Press, 1981

Chapter 3

Design Specifications

3 Design Specifications

3.1 End-Point Properties

The proposed manipulator will behave either as a passive or active platform from which the user will work. The interaction between human and machine is a very interesting phenomenon. During the passive mode, the robotic aid absorbs energy produced by the user and dissipate it as heat. In the meantime, the effectiveness of the man-machine interaction can be evaluated by how the user perceives the kinematic and kinetic properties of the robot's mechanism, such as friction and inertia reflected to the end-point. In other words, end-point properties would determine the degree of the user's comfort, as well as the suitability and effectiveness of the machine. If the machine has excessive end-point friction, for example, it would certainly be difficult for an upper-limb impaired person to move its end-point. On the other hand, if the robot has excessive end-point inertia, the user would perceive resistance to acceleration and deceleration of the end-point. Some of these properties affect the performance of the robot itself, especially in the active mode. Unless a more powerful actuator is used, excessive inertia will certainly degrade the performance bandwidth. Some of the important specifications of the manual teaching aid are described in the following sections.

3.1.1 Interaction Force at the End-Point

End-point interaction force is specified at 10 pounds *maximum*. The number was selected considering the strength of weak females (Section 2.3). However, the machine is designed to produce more than 10 pounds at the end–point, but is limited to 10 pounds through the control algorithm.

3.1.2 End-point Friction

End-point static friction of about 3 +/-1 ounces or less (without control of impedance) at every point inside the workspace is desired. The correction term (+/-1 ounce) is the anisotropic factor. The difference between stiction and dynamic friction should not be greater than a ratio of 2:1.

3.1.3 End-point Inertia

Inside the workspace, effective inertia of the mechanism and actuators reflected to the end-point is desired to be in the range of 2/3 to 4/3 kilograms (without control of impedance and end-effector) in any direction.

3.1.4 End-point Stiffness

End-point stiffness of 0 to 2 Newton/millimeter is desired.

3.1.5 End-point Impedance Properties

Between 0 to 7 Hertz, end–point impedance should behave like viscous friction. Frequencies above 7 Hertz are not a concern in this application. Directional variation of any impedance parameters should be less than 2:1.

3.1.6 Backdrivability

In the case of passive operation, the machine must comply to the user in different degrees. The lowest degree implies that the user needs minimal effort to back drive the robot; in the other words, the machine will definitely comply to the user with minimal end-point friction and inertia resistance.

3.2 Workspace

3.2.1 Size of Workspace

The workspace size for the machine is 15X18 inches as described in Section 2.1.1. The workspace is placed in front of the user body as shown in Fig.2.4. Protrusion of the linkage and mechanism behind the device should be minimized.

3.2.2 Visibility and Accessibility

The workspace should be kept uncluttered to allow standard therapeutic procedures. Maximum visibility must be guaranteed to permit the therapist and the patients to see and locate every point inside the selected workspace. The hand holding unit should allow "hand-over-hand" operation between the therapist and his/her patient.

3.2.3 Mobility of the Teaching Aid System

Two people should be able to easily transport the robotic aid workstation. The maximum weight of the robot should not exceed 70 pounds (controller not included). A compact and foldable mechanism is preferable to give a nice, clean package.

3.3 Power Sources

Since the most convenient power source available in any rehabilitation hospital is electrical, electromagnetic devices should be the primary actuators. Standard single-phase 110 Volts AC is preferable for the energy source.

3.4 Control Architecture

A digitally supervised analog loop is selected as the controller platform. The architecture has long been proven to be effective in similar applications such as Abul-Haj's cybernetic elbow prostheses[15] and Faye's manipulandum[16].

3.5 Transducers

3.5.1 Position Transducer

Absolute position transducers should be the prime selection for position feedback sensors. Absolute type sensors eliminate calibration procedures during start up. Resolution of 16 bits per single mechanical revolution or more is required with accuracy up to the least significant bit. The transducers should be installed with actuators which provide a nice, clean driving package. Again, position sensors must be interfaced to the selected controller platform without difficulties.

3.5.2 Force/Torque Transducer

Force/Torque transducers must be installed in the system to give contact force information to the controller. Maximum end-point force is specified at 10 pounds (Section 2.3 and 3.1.1).

3.5.3 Velocity Transducer

High-accuracy velocity transducers are to be installed in the actuator package. They should be able to track rotational velocity between 8 to 0.008 radian/second with less than 8 percent signal-to-noise ratio. Friction contribution from these velocity

---

15 Abul-Haj C.J., Hogan N., *Functional Assessment of Control Systems for Cybernetic Elbow Prostheses*, IEEE Transactions on Biomedical Engineering, 1990

16 Faye I. C., *An Impedance Controlled Manipulandum For Human Movement Studies*, MIT SM Thesis, 1986

transducers must be minimized. If possible, the transducers are to be installed inside the actuator package.

3.6 End-effector

3.6.1 Modular Package

The end-effector should be designed as an independent package from the robot to allow several different end-effectors for different operations to be installed on the robot.

3.6.2 Degrees of Freedom

In the current stage of this research, the end-effector has a three-rotational-degree-of-freedom-hand-holding unit that allows pronation / supination, flexion / extension, and abduction / adduction on the users' wrist. The allowable degrees of freedom are:

Wrist motion	Degrees (°)	Remark
Pronation	40	from flip-down palm position
Supination	40	from flip-down palm position
Flexion	30	
Extension	15	
Abduction	15	
Adduction	20	

Table 3.1 Design Specification of Wrist Movement

Each rotational degree of freedom should be actively controlled by active actuators installed within the end-effector unit.

3.7 Safety Consideration

3.7.1 System Failure Detection

The device will incorporate failure detection devices which will shut down the system on sensing excessive forces, acceleration, etc. The responses of these events will disable the actuators and brake them by short-circuiting their electrical terminals. The stored dynamic energy in the mechanism will be converted into back emf and be dissipated as heat in the electrical winding.

3.7.2 Safety Release Mechanism

In addition to system failure detection, the user may pull his/her hand free of the machine without assistance through a specially designed locking mechanism which breaks and separates from the hand-holding unit when subjected to a certain force level.

Chapter 4

Kinematic Selection

4 Kinematic Selection

The specifications in Chapter 3, especially end–point inertia and friction properties, provide good guidelines for selecting and designing the robot configuration. The selected configuration will contribute strong kinematic and dynamic coupling to the user, determining quality and effectiveness of this man-machine "interaction." In terms of kinematics, positions and orientations are fundamental motion planning parameters. Different configurations may result in different degrees of complexity of forward and inverse kinematics to determine position and orientation. On the other hand, in terms of kinetics, the focus should be on dynamic performance of the configuration due to physical construction, mass distribution, actuator placement, and speed reduction. Two similar configurations with the same dimensions, for example, might contain substantially different dynamic properties due to mass-distribution inequality. A wise configuration selection may alleviate complexity and computation time in the control algorithm

4.1 Common Kinematic Configurations

Since the selected workspace for upper limb therapy is quite small, most of the conventional arm configurations such as Cartesian, cylindrical, and spherical are applicable. As presently envisioned, the manual teaching aid arm will only operate on a horizontal plane. The major reason for this decision is that the active control of motions out of horizontal plane require actuators that can overpower the rest-weight of the user should he/she lean towards the manipulator. This would require large motors and power supplies. If motion is constrained to a horizontal plane, the payload can be

supported by a structural frame which substantially reduces size, weight, and power consumption of the system.

The most widely used configurations are Cartesian (Rectangular), Cylindrical, Spherical, and SCARA (Selective Compliance Assembly Robot Arm).[17] The objective in this Chapter is to qualitatively characterize each configuration in terms of their end-point properties and select the best configuration for the manual teaching aid.

4.1.1 Cartesian Frame

Cartesian or rectangular frames are used mostly for simple-and high-precision applications, such as positioning or loading/unloading parts (see Fig. 4.1). This configuration is less complex to control since each degree of freedom is kinematically and dynamically decoupled resulting in less computation. In the other words, joint coordinates are independent from one another with no dynamic coupling effect among motions in all axes. A Cartesian frame is applicable to various types of transmissions, for example, linear screw actuator or hydraulic cylinder. Cartesian configuration, however, has some negative aspects such as difficulties in protecting linear sliding surfaces from dirt and contamination and the need for bellows to protect linear guide ways. These increase weight, resistance, and limit the work envelope. Cartesian frames are rather bulky and heavy compared to other configurations for the same operation and the same work space[18]. As a consequence, the effective inertia reflected to the end-point is larger.

---

[17] Makino, H. and Furuya, N., *Selective compliance assembly robot arm*, Proc. 1st Int. Conf. on Assembly Automation, Brighton, IFS, Kempston, UK, 1980

[18] Rivin, E.I. *Mechanical Desing of Robots*, New York, McGraw-Hill, 1988.

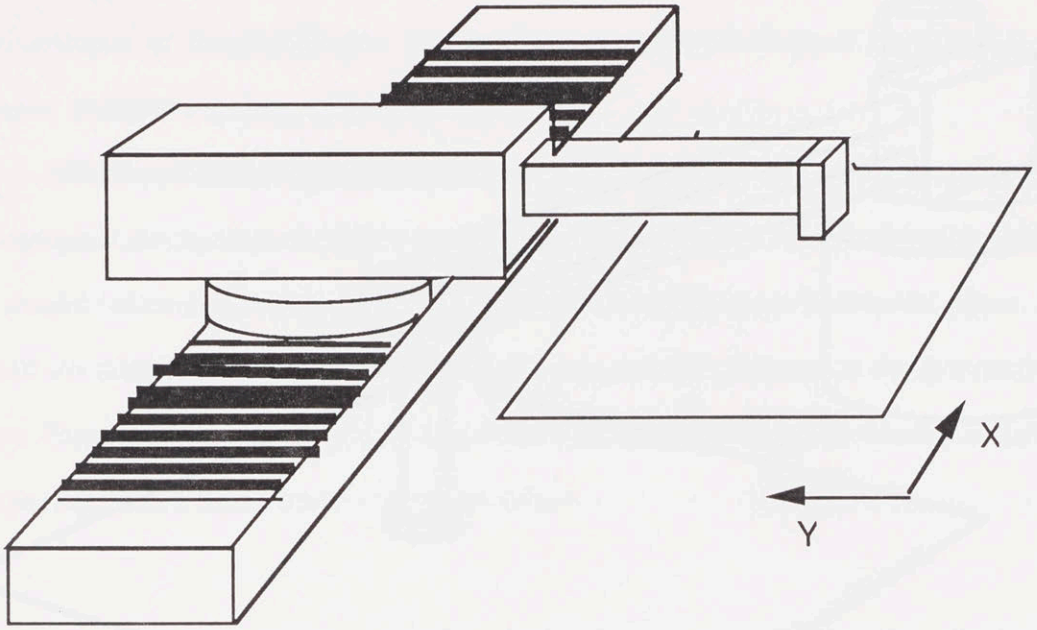

Fig. 4.1 Cartesian Configuration

4.1.2 Cylindrical Frame

The cylindrical coordinate system is used to describe movement that has one angular motion with an additional radial degree of freedom (see Fig. 4.2). Cylindrical frames require a relatively small space and a simplified layout plan, and are especially good for transferring materials from conveyor belts or handling small parts with limited horizontal motion.[19]. This type of frame is easy to program and capable of reaching into tight spaces. One disadvantage of the cylindrical frame is that the arm can not reach far enough from the vertical axis unless its structure is reinforced to support additional bending stress.

---

19 Poole, H., *Fundamentals of Robotics Engineering*, Van Nostrand Reinhold, NY, 1989

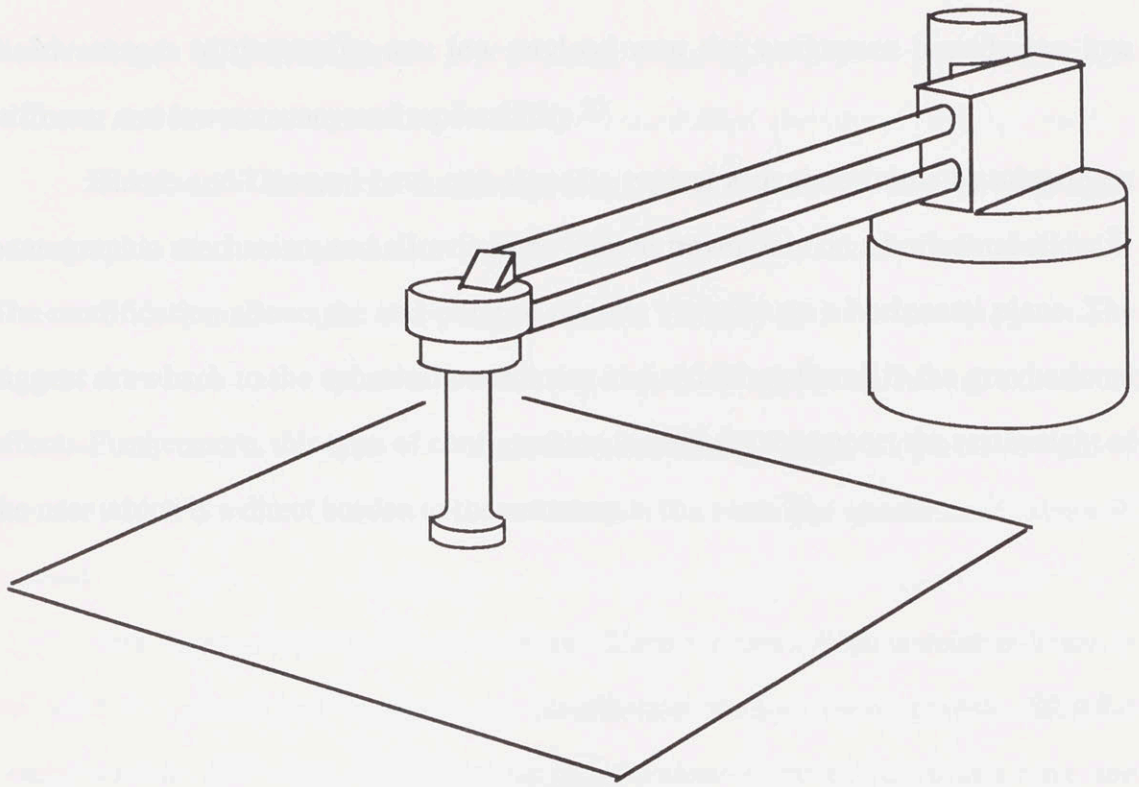

Fig. 4.2 Cylindrical Configuration

4.1.3 Spherical Coordinate Frame

Some manipulator designs use spherical coordinate frames which require a much more sophisticated control system (see Fig. 4.3). This type of frame works better for three-dimensional motion in a large service space. One modification to the spherical coordinate frame is the replacement of the prismatic joint (radial motion) with an additional revolute joint, so-called jointed or articulated frame. The main advantages of both spherical and articulated frames are the small size of hardware compared to service space and the potential to work with high degrees of accessibility. The major

disadvantages of the design are: low payload near the workspace boundaries; low stiffness; and low accuracy and repeatability.[20]

Hirose and Umetani have redesigned a typical articulate frame by adapting a pantographic mechanism and allowing one joint to travel only on a horizontal slider.[21] The modification allows the end-point to operate virtually on a horizontal plane. The biggest drawback to the spherical coordinate and articulate frame is the gravitational effect. Furthermore, this type of configuration is unlikely to support the rest weight of the user which is a direct burden to the actuators.

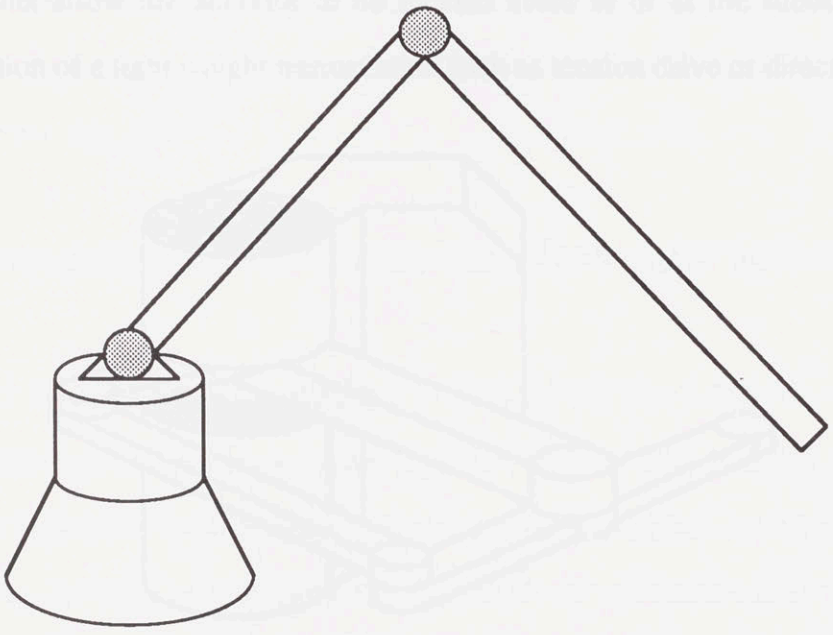

Fig. 4.3. Spherical Coordinate Configuration

20 Asada, H. and Youcef-Toumi, *K. Direct-drive robot*, MIT Press, Cambridge, 1988

21 Hirose, S. Umetani, Y., *A cartesian coordinates manipulator with articulated structure*, 11th International Symposium on Industrial Robots, Tokyo, Japan 1981

4.1.4 SCARA Frame

If articulated frames are designed to allow every joint axis to align parallel to the vertical axis, the configuration is called SCARA (Selective Compliance Assembly Robot Arm). Such designs are being used more extensively in assembly operations. The SCARA arm has at least two basic degrees of freedom. Additional degrees of freedom may be added to generate vertical motion: nevertheless, the planar movement has already covered the majority of movements in the assembly operations[22] (about 80 percent).

One important positive feature of the SCARA robot is high angular stiffness in all vertical planes and controllable compliance in horizontal planes. SCARA configurations allow the actuator to be located close to or at the robot's base and implementation of a light weight transmission such as tension drive or direct-drive.

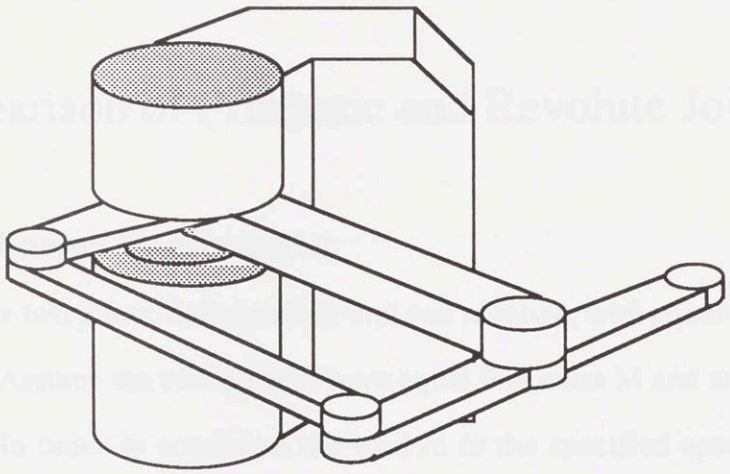

Fig. 4.4 SCARA Configuration

Since all presented configurations have the potential to satisfy our workspace requirement, other criteria is needed to justify configuration selection. According to the

---

22 Coiffet, P., Modelling and Control, *Robot Technology*, Vol.1, Prentice Hall, 1983

specifications in Chapter 3, end-point friction is the most critical parameter, while effective inertia reflected at the end-point is a less critical parameter. One approach to determine the type of configuration for the manual teaching aid is to compare their end-point friction and inertia properties. Size and weight of the system are additional criteria but are not as critical.

Each configuration consists of a series of prismatic (or translational) and revolute (or rotational) joints. Cartesian configuration has three prismatic joints perpendicularly aligned to each other. Similarly, if motion of the base joint is revolute and that of the other is prismatic, the configuration is then classified as a cylindrical frame. Articulate, pantomec,[23] and SCARA configurations consist of a pure series of revolute joints. One key approach to justify these configurations is, therefore, to investigate these fundamental prismatic and revolute joints kinematically and dynamically. In other words, how much friction and inertia do these configurations contribute to the end-point.

4.2 Comparison of Prismatic and Revolute Joints

4.2.1 Energy Consumption

Consider two joints, one prismatic and one revolute, with equal-tip speed V and acceleration a. Assume the two systems have equal link mass M and end–point load m (see Fig. 4.5). In order to accelerate the load m to the specified speed V from zero velocity, the prismatic joint requires total energy ($T_{G)}$ of

$$T_G = (M+m)V^2/2$$

---

23 Pantograph mechanism

where as the revolute joint requires total kinetic energy (T_R) of

$$T_R = ((L_2/L_1)^2 M+m)V^2/2$$

note that L_2/L_1 is less than 1

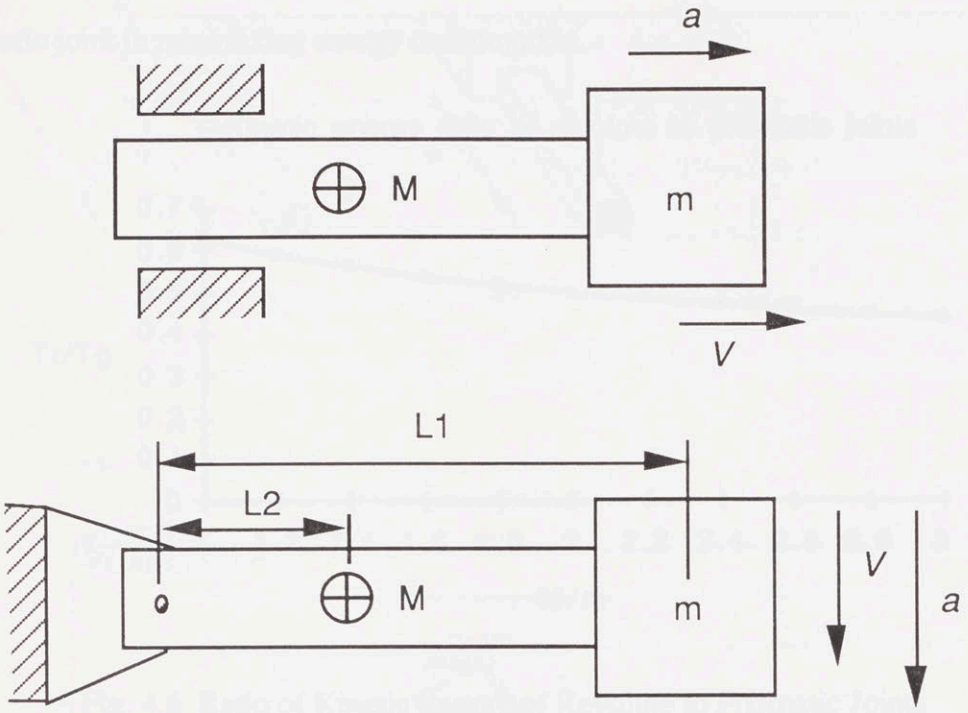

Fig. 4.5 Prismatic and Revolute Joints

From the above equations, the revolute joint definitely requires less energy than the prismatic one since ratio L_2/L_1, which multiplies M, is always less than unity.

In order to provide more practical data, suppose L1 is 21 inches. (to cover the length of 15X18 workspace) made of square aluminium tubing weight 5 pounds. The end-point load is taken to be 2-pounds. The ratio of T_R to T_G is therefore 0.48; in other words, the revolute joint requires much less power to accelerate/decelerate than the prismatic one. Practically, the final weight of the prismatic joint is quite likely to be 2.5 to 3 times greater than its payload m, thus, the energy difference is 50 to 100 percent

between the two joints.[24] Figure 4.6 illustrates the ratio of kinetic energy between revolute to prismatic joints for different mass ratios (M/m) given that the L_2/L_1 is 0.5.

In terms of energy, the revolute joint has a substantial advantage over the prismatic joint in minimizing energy consumption.

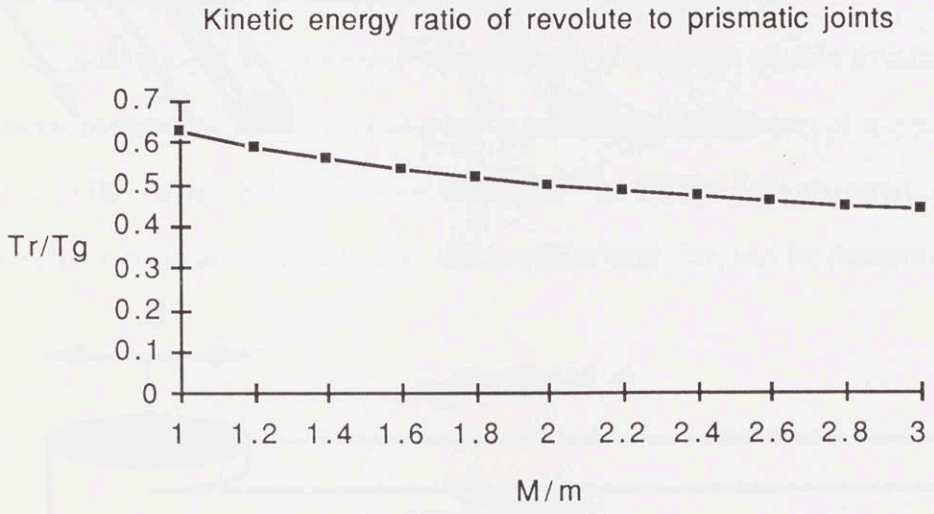

Fig. 4.6 Ratio of Kinetic Energy of Revolute to Prismatic Joints

4.2.2 End-point Static Friction

The anatomy of the prismatic joint generally combines a linear actuator (ball screw, linear motor, friction drive, etc) with a linear or sliding guideway (usually linear circulating ball bearing). Similarly, the revolute joint always consists of a rotary actuator and rotary bearings.

Aside from the friction contributed by actuators, end-point static friction is a direct effect of bearing friction combined with the kinematic or geometry effect of the mechanism. In order to obtain a clearer example, prismatic and revolute joints are constructed as shown in Fig. 4.7 a and b.

---

[24] Irvin, E.I., *Mechanical Design of Robots*, McGraw-Hill, New York, 1988.

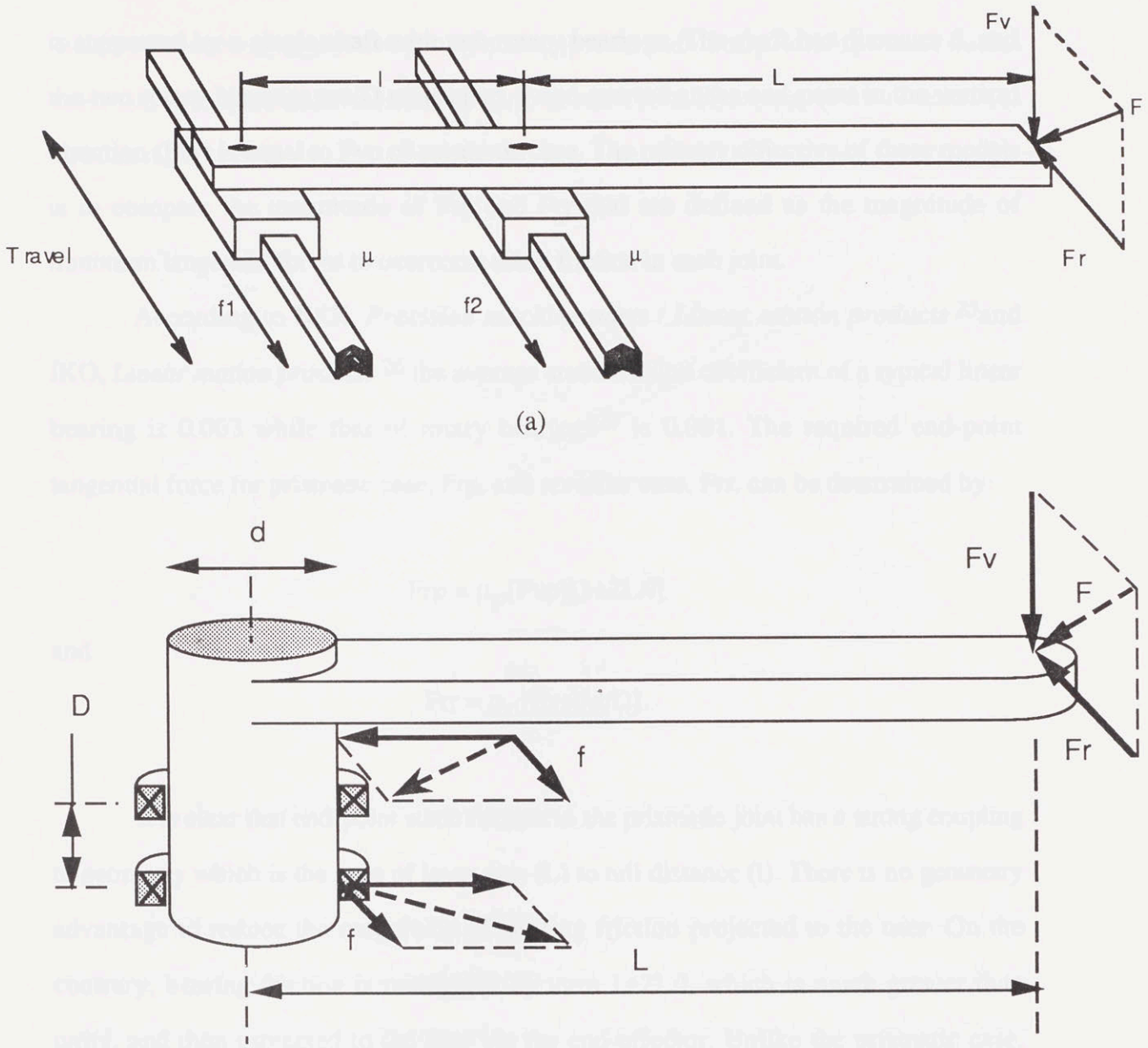

Fig. 4.7 Model of Prismatic and Revolute Joints for Friction Determination

Figure 4.7 (a) is a model of a double-row-linear-bearing prismatic joint. Payload, in terms of downward force F_v , is applied at the end-point. Fr is the minimal tangential force needed to counter joint friction. The vector of Fvp and Frp can be combined to make resultant force F. The loaded point is L units away from one of double row linear bearings, which is l unit apart. In Figure 4.7 (b), the revolute model

is supported by a single shaft with two rotary bearings. The shaft has diameter d, and the two rotary bearings are D units apart. Load exerted at the end-point in the vertical direction (Fvr) is equal to Fvp of prismatic case. The primary objective of these models is to compare the magnitude of Frp and Frr that are defined as the magnitude of minimum tangential forces to overcome static friction in each joint.

According to NSK, *Precision machine parts / Linear motion products* [25]and IKO, *Linear motion products* [26] the average static friction coefficient of a typical linear bearing is 0.003 while that of rotary bearings[27] is 0.001. The required end-point tangential force for prismatic case, Frp, and revolute case, Frr, can be determined by:

$$Frp = \mu_p[Fvp][1+2L/l]$$

and

$$Frr = \mu_r [Fvr][d/D].$$

It is clear that end-point static friction in the prismatic joint has a strong coupling to geometry which is the ratio of lever arm (L) to rail distance (l). There is no geometry advantage to reduce the magnitude of bearing friction projected to the user. On the contrary, bearing friction is multiplied by term 1+2L/l, which is much greater than unity, and then projected to the user via the end-effector. Unlike the prismatic case, end–point friction in revolute construction is factored by the ratio d/D which can certainly be designed to be much less than unity.

To give an implicit example, some practical numbers are assigned to the model. According to NSK and IKO references, μ_p and μ_r are 0.003 and 0.001, respectively. L remains as 28 inches consistent with the model in Section 4.2.1, while l is selected as 5

---

25 Nippon Seiko K.K, *Precision machine parts / Linear motion products* , Japan, 1987

26 Nippon Thomson Co.,Ltd.; *Linear motion products* ; CAT-5736, 5731, 5715, 5714, 5732, 5717, 5737; Japan.

27 Eschmann, P., *Ball and roller bearings*, 2nd.Ed., John Wiley and Sons, NY, 1985

inches to give an acceptable actuator package. The two rotary bearings are 6 inches apart (D) with 1-inch shaft diameter (d). Fvp and Fvr are set equally to represent the same end-point payload. The ratio of Frr to Frp can be seen in Fig. 4.8.

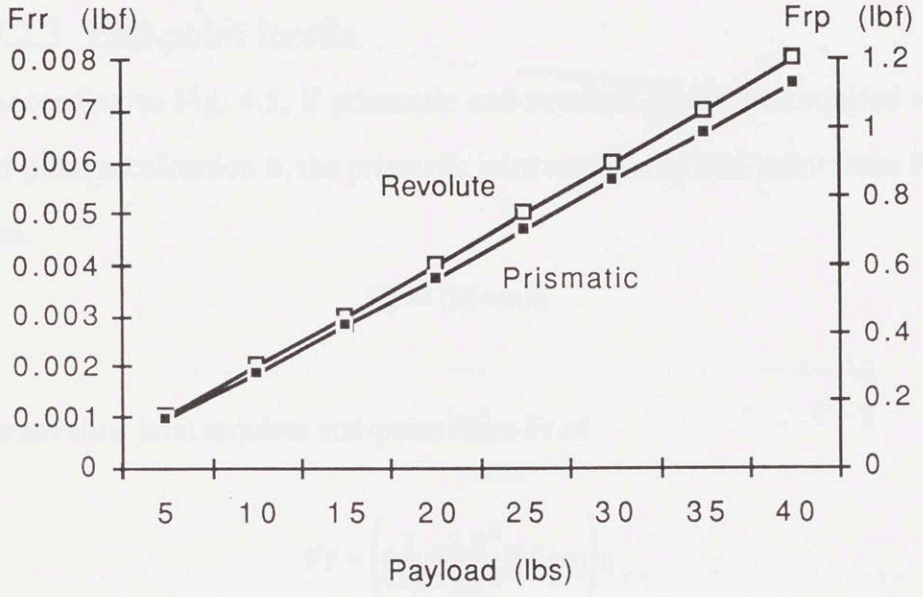

Fig. 4.8 Reflected End-Point Friction for Prismatic and Revolute Joints

According to Fig. 4.8, it is seen that the end-point friction of the revolute joint is substantially lower than that of the prismatic joint with the ratio on the order of 1:100. The prismatic joint is geometrically inferior because of the lack of the "lever effect" to factorize the bearing friction projected to the end-point. Another cause of excessive friction in the prismatic joint is caused by the construction of recirculating linear ball bearings. Non-existence of separators or cages between adjacent balls allows direct-rubbing. Friction is also initiated in the circulating path; a row of accumulated inactive balls in the recirculating path is a burden for those active balls in the track to recirculate them. Measured static friction of NSK linear bearings used in a linear

friction-drive prototype[28] shows an average friction of 2 ounces. At some random spots along the rail, however, friction rises to 5 ounces showing nonuniformity of friction.

4.2.3 End-point inertia

According to Fig. 4.5, if prismatic and revolute joints are required to obtain equal end-point acceleration a, the prismatic joint requires an end-point force Fp which is equal to.

$$Fp = (M+m)a$$

where the revolute joint requires end-point force Fr of

$$Fr = \left(\left(\frac{1}{12} + \frac{L2^2}{L1^2}\right)M+m \right)a$$

or, if link L has uniform mass distribution L2 = 0.5 L1

$$Fr = \left(\frac{1}{3}M+m\right)a$$

Again m and M are payload and mass of the joint respectively.

Figure 4.9 shows the ratio between end-point inertia of the revolute joint to that of the prismatic joint for different M/m values. The revolute joint thus shows another positive feature over the prismatic joint. End-point inertia of the revolute configuration is 50 to 55 percent of that of the prismatic one for the practical ratio of M/m of 2 to 3.

---

[28] Linear friction-drive prototype is constructed by J. Charnnarong and A. Sharon in The Newman Laboratory for Biomechanics and Human Rehabilitation, MIT, to study effectiveness and performance of friction-drive system. The prototype has a single linear bearing with a direct-drive wheel on its track.

In conclusion, the revolute joint has an advantage over the prismatic joint in terms of end-point friction, end-point inertia, and energy consumption. Consequently, the arm design of the manual teaching aid should be implemented using revolute joints.

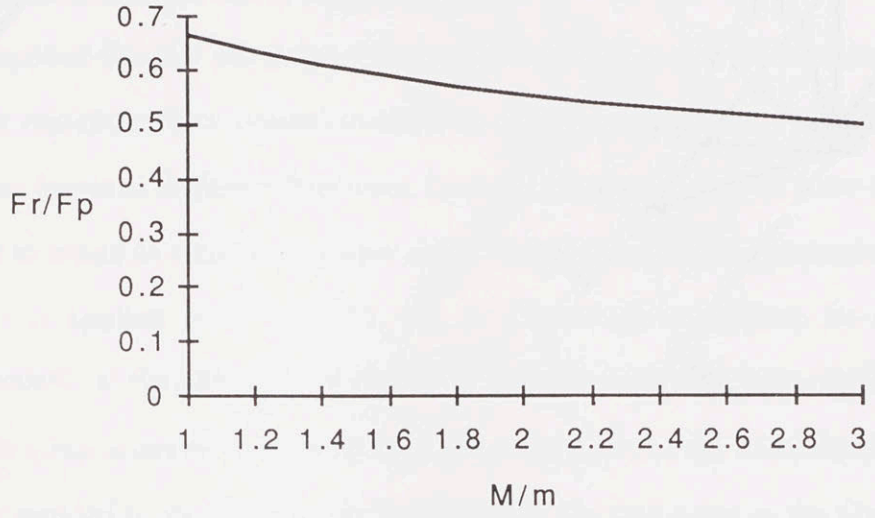

Fig. 4.9 Ratio of End-Point inertia of Revolute to Prismatic Joints

4.3 Decision on Arm Configuration

4.3.1 End-point Friction of Arms

In Section 4.2.2, friction models of single-degree-of-freedom joints have been developed; however, distribution of end-point friction of the whole arm mechanism is more interesting to quantify. As previously mentioned, prismatic and revolute joints are the most fundamental elements of any robot arm configuration. Any configuration is formed by different orders of prismatic and revolute joins, which determine the characteristics of end-point friction and inertia.

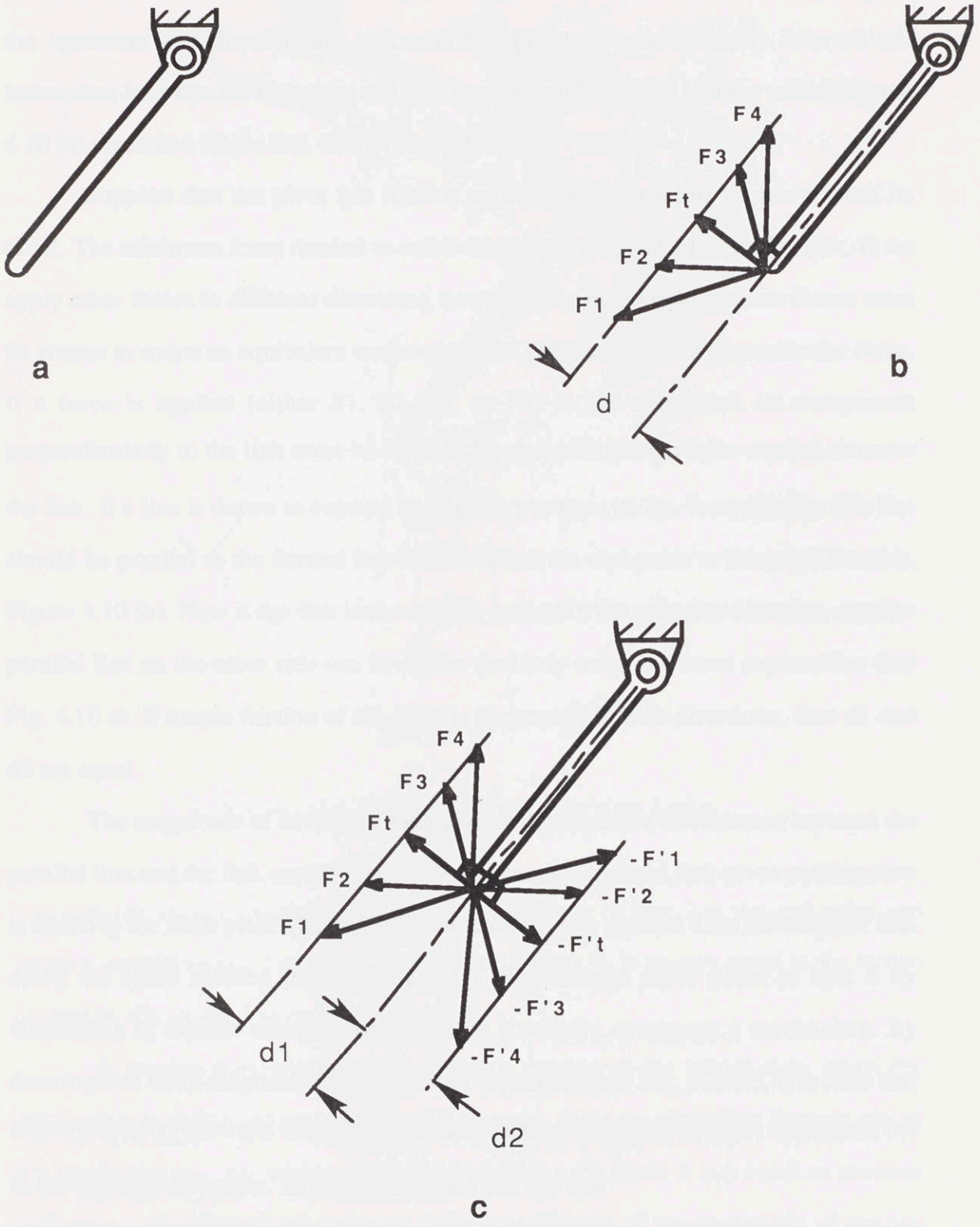

Fig. 4.10 Revolute Joint with Pivot Friction

In order to create a clear understanding of end-point friction of a SCARA mechanism, the upstream and downstream links, at this point, are individually focused on. Interaction between the upstream and the downstream links will be later added. Figure 4.10 (a) presents a single link with pivot friction.

Suppose that the pivot has friction and the link is needed to move about its pivot. The minimum force needed to rotate the link is perpendicular to this link. If we apply other forces in different directions, however, the magnitude of these forces must be greater to create an equivalent torque about the pivot as does the perpendicular force. If a force is applied (either F1, F2, F3, or F4) to the end-point, its component perpendicularly to the link must be equal to F_t, or the minimum force needed to move the link. If a line is drawn to connect each force vector at its tip, theoretically, this line should be parallel to the normal line that connects the end-point to the pivot's center, Figure 4.10 (b). Now if the link is about to be moved in the opposite direction, another parallel line on the other side can be drawn similarly using the same explanation (see Fig. 4.10 c). If torque friction of the pivot is symmetric in both directions, then d1 and d2 are equal.

The magnitude of friction in each pivot will determine the distance between the parallel line and the link centerline d. Suppose another isolated link-pivot combination is added to the same plane, we can still construct the two parallel lines for this new link using the same method (see Fig.4.11(a)). Replacing a fixed pivot of link a by connecting to another movable pivot on link b serially constructs a mechanism. By drawing free body diagrams of the each link separately (see Fig. 4.11(b), it is clear that action force F_{12} between links 1 and 2 has a reaction force F_{21} equal in magnitude but in the opposite direction . In other words, we can say that

$$F_{12} = -F_{21} = F = Fb$$

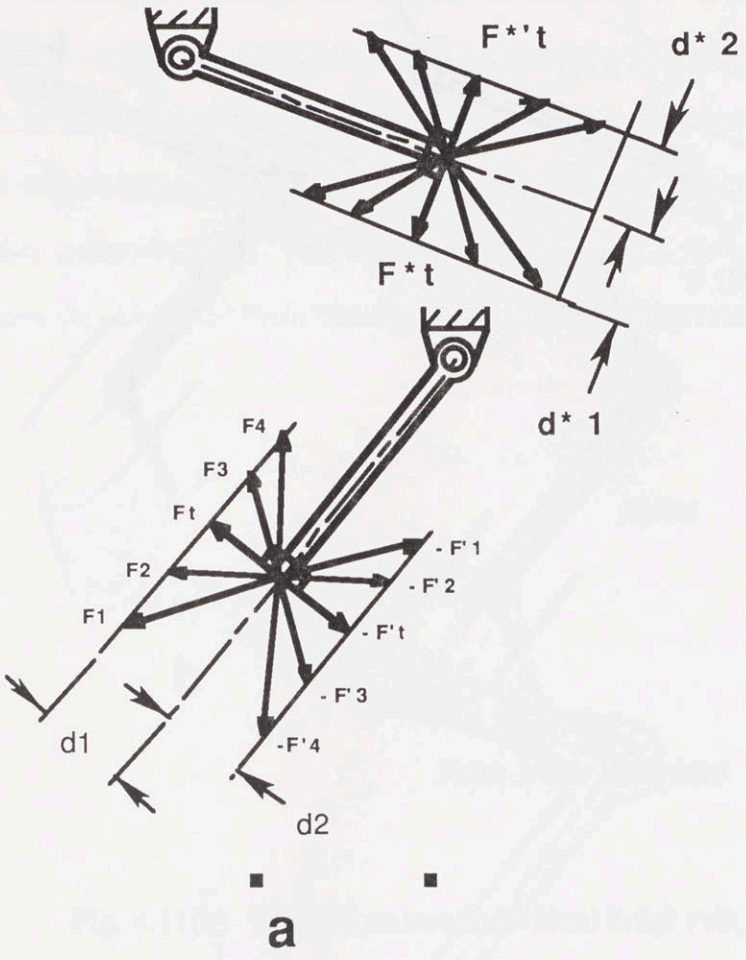

Fig. 4.11(a) Friction on Two Individual Links

The equality allows transferring the two parallel lines of link 2 to the end-point and forms a parallelogram. The introduced torque of force F_b is always equal to the torque created by the external force F (see Fig 4.12).

A friction parallelogram can describe motion at the initial state when the mechanism is at rest and just about ready to move. If the tip of applied force is still in the parallelogram, no motion is generated because the force is too small to produce sufficient torque about both pivots to overcome friction. If the magnitude of applied force increases until its tip reaches out of the parallelogram's boundary, then motion is generated, depending on which region the tip lies.

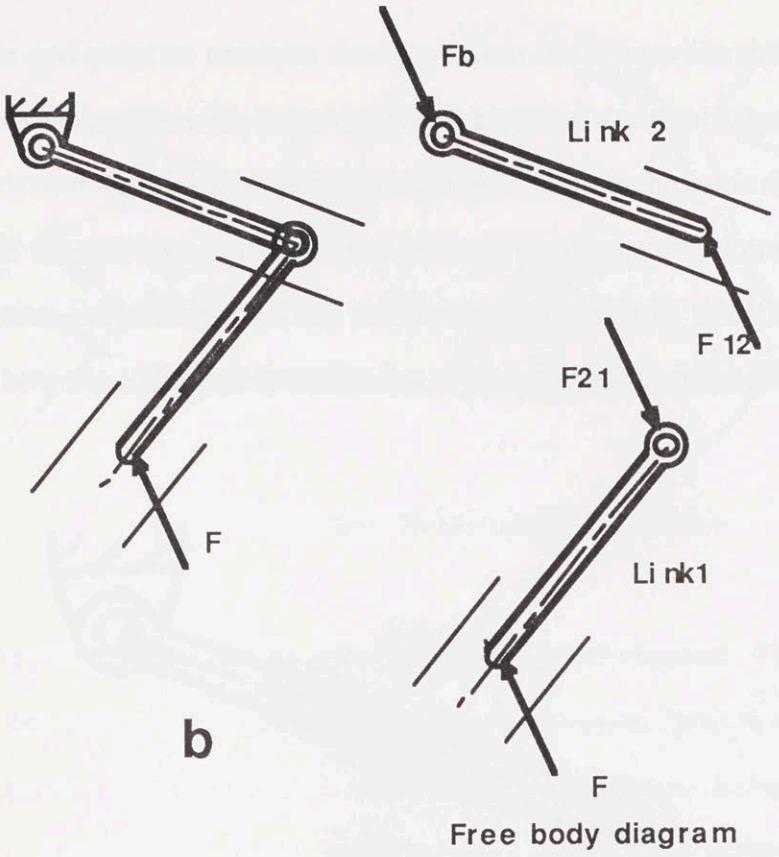

Fig. 4.11(b) Friction on two individual links

If the tip is out of the parallelogram and points into regions 1 or 2, link 1 then moves about its pivot, but no motion is generated at link 2. On the other hand, if the tip lies in region 3 or 4, only link 2 then moves about the base pivot. In this case, even though link 1 moves, there is no relative motion between the two links. Note that in the first two cases, no matter how large the force is, only one link moves at a time about its pivot. If the tip is in regions 13, 23, 14, 24, both links then start moving in the corresponding direction. The diagonals of the parallelogram represent the minimum force needed to turn both links at once.

The friction parallelogram gives some idea of the magnitude and direction of required force to compensate for friction in the SCARA mechanism. If a force sensor is

installed at the end-point to measure the interaction force between the user and the manipulator, we can compensate for joint friction by using a control algorithm. We can send commands to the actuators to produce additional force in the same direction as the user does, until the combined forces of the user and compensation command exceeds the local friction parallelogram. The whole mechanism will then make a move depending on how the combined force lies out of the parallelogram (see Fig. 4.13).

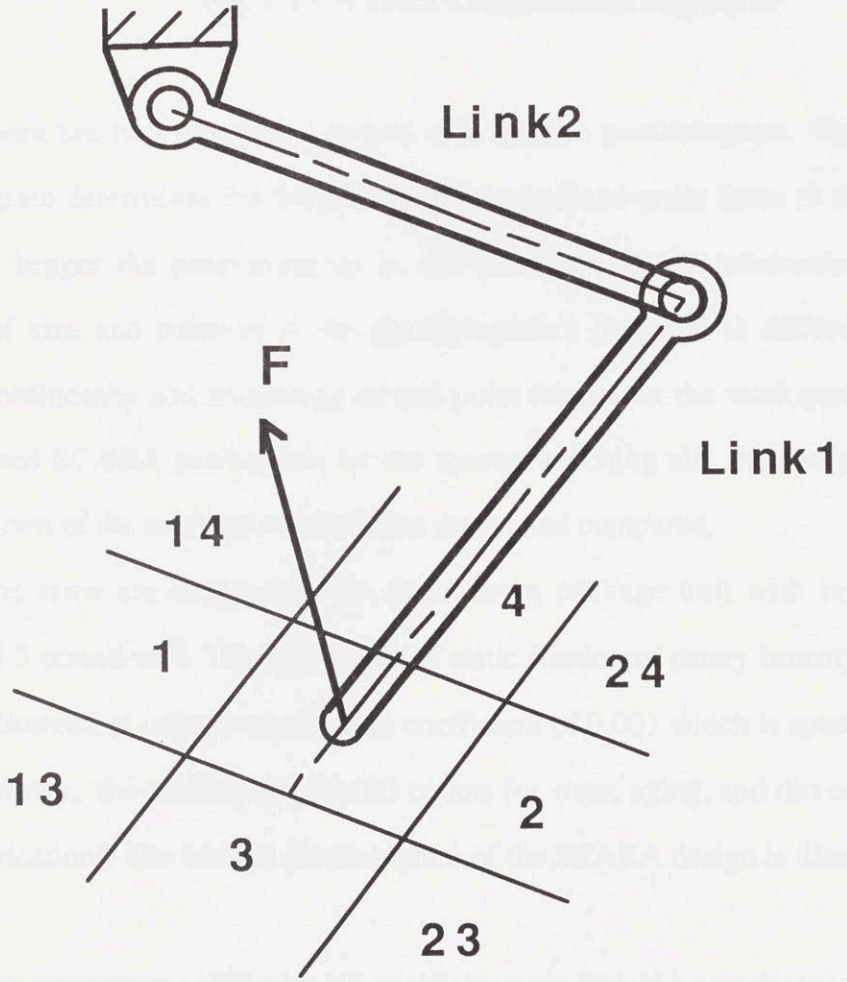

Fig. 4.12 Friction Parallelogram

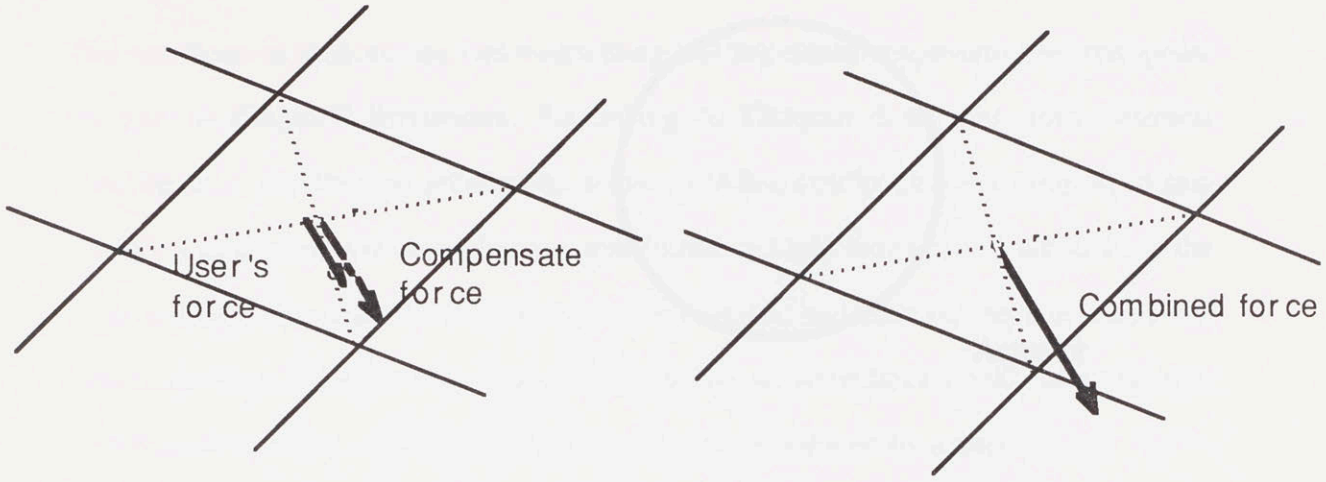

Fig. 4.13 Friction Compensation Algorithm

There are two interesting details of a friction parallelogram. The size of the parallelogram determines the magnitude of required end-point force in any direction, Thus, the bigger the parallelogram is, the more poorly the mechanism performs. Change of size and rotation of the parallelogram's diagonal in different locations reflects nonlinearity and anisotropy of end-point friction in the workspace. To justify the designed SCARA mechanism for the manual teaching aid, the end-point friction parallelogram of the mechanism should be drawn and compared.

The arms are coupled to the direct-drive package unit with internal rotary friction of 3 pound-in[29]. The coefficient of static friction of rotary bearings is taken to be 0.003 (instead of using static friction coefficient of 0.001 which is specified for new rotary bearings, the coefficient of 0.003 counts for wear, aging, and dirt contamination in the lubrication). The friction parallelogram of the SCARA design is illustrated in Fig. 4.14.

The uppermost and the lowest parallelograms should be neglected since they lie outside the selected workspace. Seven other parallelograms, which are inside the workspace, are quite uniform in terms of diagonal length and orientations.

---

29 From Inland Motor, brushless DC motor catalog

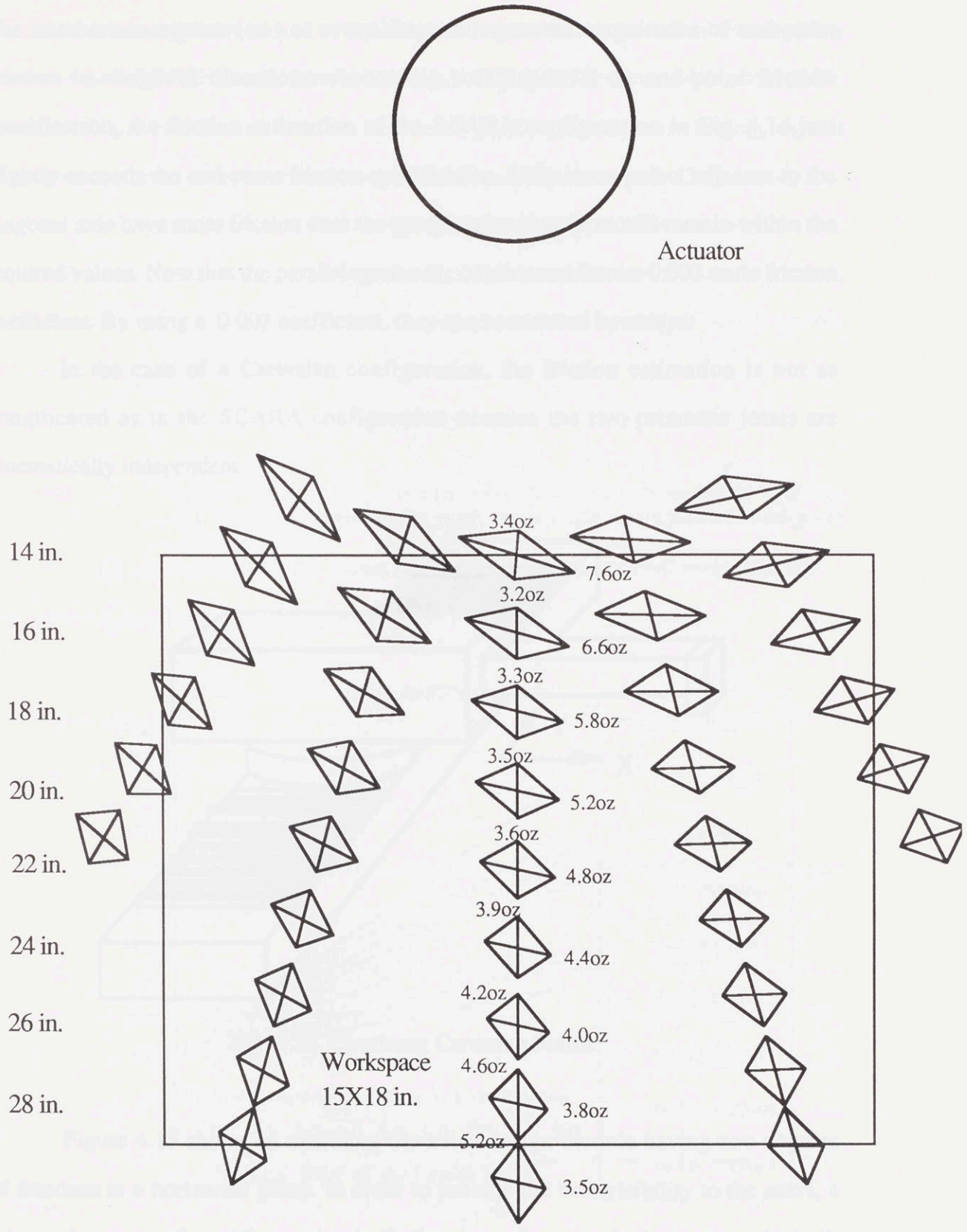

Fig. 4.14 End-Point Friction Parallelogram of Designed SCARA Arm

The numbers in ounces (oz.) at every diagonal represent magnitudes of end-point friction in diagonal directions. According to Chapter 3 on end-point friction specification, the friction estimation of the SCARA configuration in Fig. 4.14 just slightly exceeds the end-point friction specification. Only some points adjacent to the diagonal axis have more friction than the specification, but most still remain within the required values. Note that the parallelograms are constructed from a 0.003 static friction coefficient. By using a 0.001 coefficient, they can be reduced by a third.

In the case of a Cartesian configuration, the friction estimation is not as complicated as in the SCARA configuration because the two prismatic joints are kinematically independent.

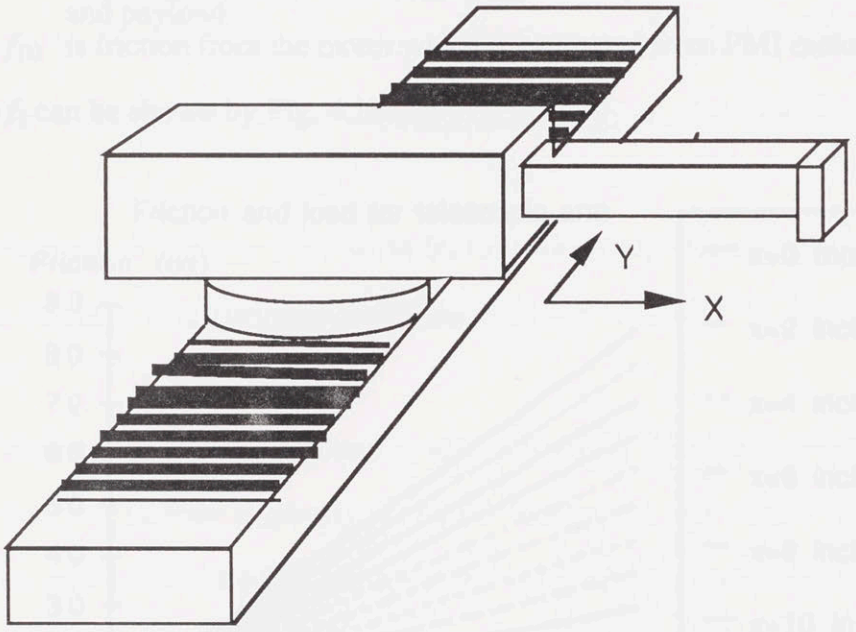

Fig. 4.15 Overhung Cartesian Frame

Figure 4.15 shows an overhung Cartesian design module having two degrees of freedom in a horizontal plane. In order to provide the best visibility to the users, a telescopic arm is selected for motion in X-direction; otherwise, both axes must be built as a gantry manipulator which is generally heavier and longer. The telescopic arm is put

on the lower carriage that moves in Y-direction. This model uses an ideal transmission system which has no transmission friction but only actuator friction. Friction of the cartesian design is estimated from the IKO bearing catalog, PMI motor catalog, and test data from the linear friction-drive prototype built by A. Sharon and J. Charnnarong.

The driving wheels with 1-inch OD are stationary but the track, which is also the design structure, moves. A special spring-loaded mechanism forces the driving wheels onto the track guided by IKO's miniature linear bearing. Friction on the telescopic arm f_t can be estimated by

$$f_t = f_b + f_m$$

where f_b is friction from bearings which combine friction from linear bearings and all rotary bearings on the shaft. f_b depends on location of end-point and payload.

f_m is friction from the motor which is estimated from PMI motor catalog.

Estimated f_t can be shown by Fig. 4.16.

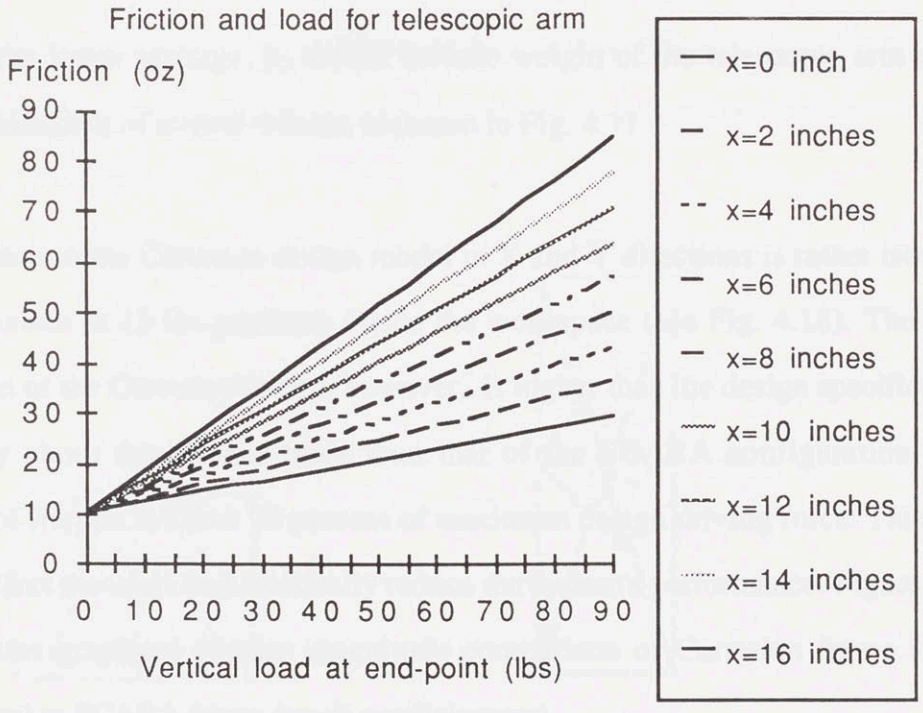

Fig. 4.16 Estimated Friction of Telescopic Arm of Cartesian Frame

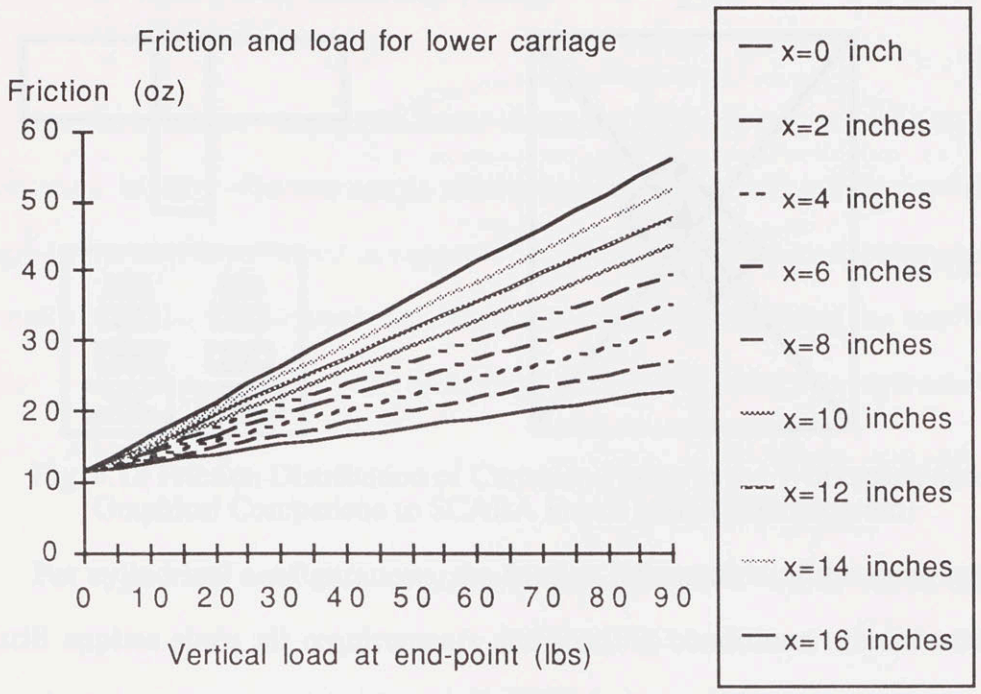

Fig. 4.17 Estimated Friction on Lower Carriage of Cartesian Frame

For the lower carriage, f_b should include weight of the telescopic arm as its payload. Estimation of overall friction is shown in Fig. 4.17.

Friction in the Cartesian design model in X and Y directions is rather isotopic (20 to 25 ounces at 15 lbs payload) inside the workspace (see Fig. 4.18). The end-point friction of the Cartesian design, however, is higher than the design specification and roughly about three times more than that of the SCARA configuration. The magnitude of friction is about 20 percent of maximum design driving force. This will definitely affect the users and drastically reduce the system's performance. Figure 4.18 also illustrates graphical friction magnitude comparison of Cartesian frame (large parallelogram) to SCARA frame (small parallelogram).

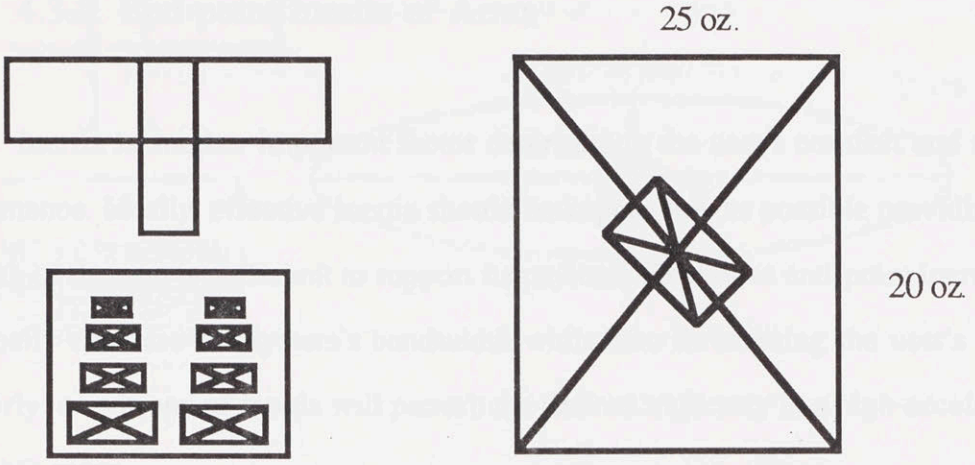

Fig. 4.18 Friction Distribution of Cartesian Frame in the Workspace and Graphical Comparison to SCARA Frame (small parallelogram)

For cylindrical configurations, the friction information of the same telescopic arm still applies since all requirements and loading conditions remain unchanged (except the lower carriage of the Cartesian design is replaced by a rotary platform). The telescopic arm contributes excessive friction (25 ounces at 15 pounds payload) violating the specification aspects (see Figure 4.19). Furthermore, directional friction distribution is not isotopic and friction in telescopic arm is about five times of that of the rotary joint. It is more comfortable for the user to move the end-point sideways than to push/pull the telescopic arm.

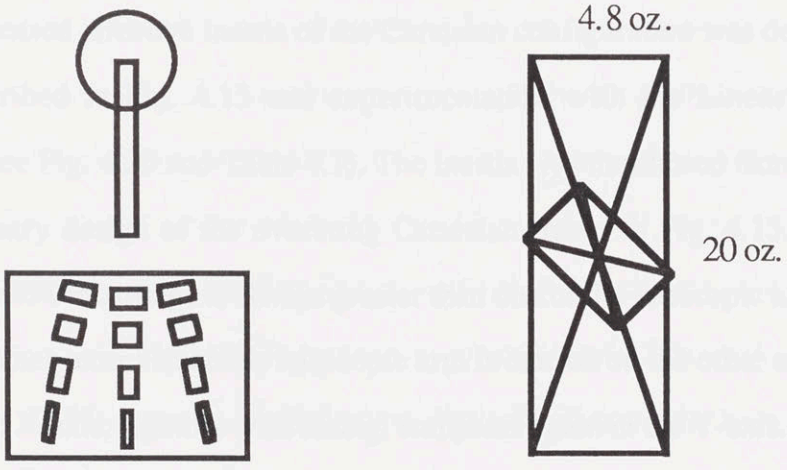

Fig. 4.19 Friction Distribution of Cylindrical Frame on the Workspace and Graphical Comparison to SCARA Frame (small parallelogram)

4.3.2 End-point Inertia of Arms

Inertia is another important factor determining the user's comfort and system performance. Ideally, effective inertia should be kept as low as possible providing that strength of the arm is sufficient to support its payload. Excessive end-point inertia will drastically decrease the system's bandwidth while also threatening the user's safety. Similarly, anisotropy of inertia will perturb the desired trajectory in a high-acceleration ("quick") move.

For Cartesian configurations, the end-point effective inertia can be calculated from

$$I_e = I_S + I_m + I_{tr}$$

where

I_S is effective inertia of structural elements.

I_m is effective inertia of motor.

I_{tr} is effective inertia of transmission systems.

Estimated effective inertia of the Cartesian configuration was derived from the model described in Fig. 4.15 and experimentation with the Linear friction-drive prototype (see Fig. 4.20 and Table 4.1). The inertia was monitored from the weight of the preliminary design of the overhung Cartesian frame in Fig. 4.15. Note that the inertia of the lower carriage is always greater than that of the telescopic arm (in this case about four times more) since the telescopic arm is carried on the other axis. The whole inertia of the X-axis, together with casing, reappears again in the Y-axis.

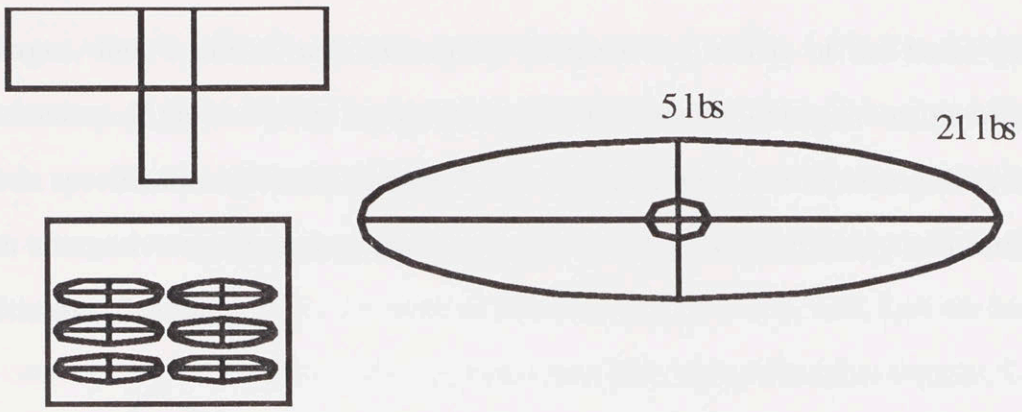

Fig. 4.20 Inertia Distribution of Cartesian Frame on the Workspace and Graphical Comparison to SCARA Frame (small ellipsoid)

Axis	Effective Inertia (lbs)
Telescopic arm (Y-axis)	5
Lower carriage (X-axis)	21

Table 4.1 Estimated Effective Inertia for a Particular Cartesian Frame

One advantage of the Cartesian design is the linearity of inertia as a function of end-point location; in other words, the inertia ellipsoid of every point in the workspace remains unchanged. The only undesirable inertia property of the Cartesian frame is directional anisotropy. Replacing the friction-drive transmission in the lower carriage would not alleviate the inertia anisotropy problem which is strongly coupled to the dynamic of Cartesian configuration. For example, implementing a cable drive in place of a friction-drive will decrease the inertia anisotropy only by 5 percent.

In the SCARA frame, the end-point inertia depends on the type of mechanism, linkage mass distribution, and location of end-point. A good reason for selecting a five-bar parallel mechanism as a model (see Fig. 4.21), is that the mechanism has two additional linkages (Link 2 and 3) to control the orientation of link 4. These additional

linkages, link 1 and 4, will essentially increase the inertia of the basic SCARA mechanism. If the end-point inertia of the five bar parallel linkage remains within the inertia specification given in Chapter 3, this will guarantee that replacing links 2 and 3 with alternative transmissions ,such as cable or band, will definitely still satisfy the inertia specification.

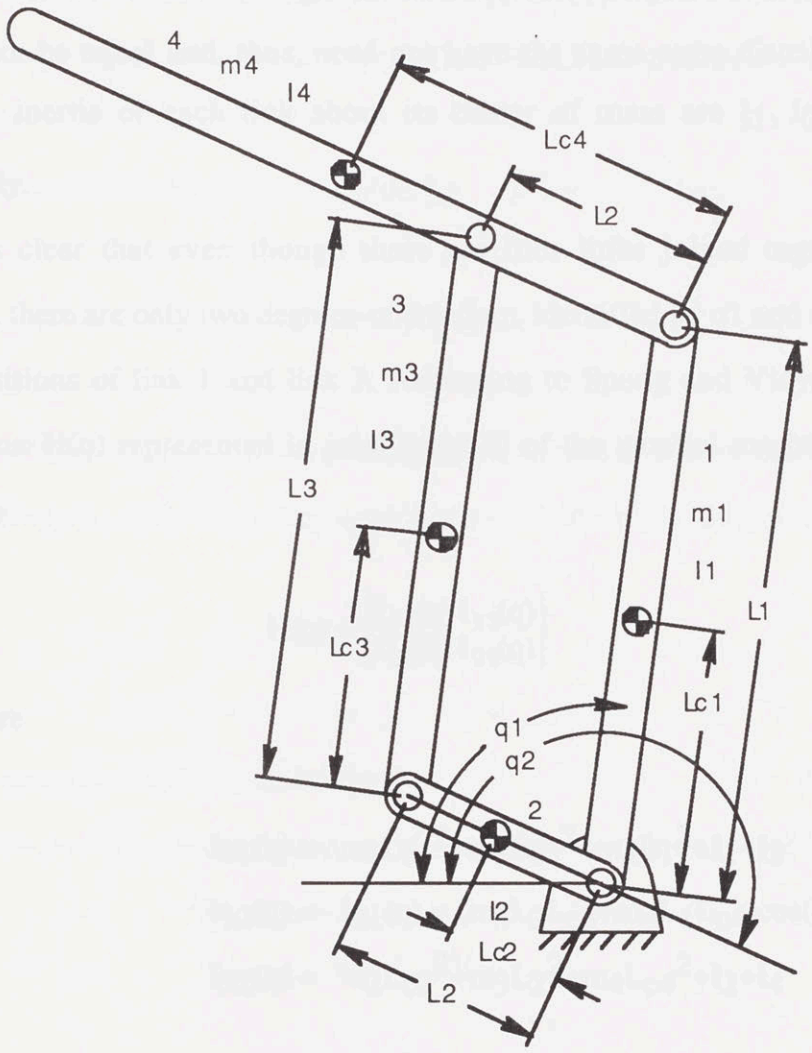

Fig. 4.21 Five-bar Parallel Mechanism

The inertia of the parallel mechanism is rather complex and strongly coupled to the posture, or joint space of the whole mechanism. q_1 and q_2 are angles of the upper

arm and forearm affixed to a stationary frame as shown in Fig. 4.21. It is assumed that the lengths of links 1 and 3 are equal and the length of L2 on links 4 and 2 are the same, forming a parallelogram. Inertia consideration on the parallelogram mechanism is much less complex than non-parallelogram since angular displacements and velocities of links 1 and 3 are always the same as link 2 and 4. Lc1, Lc2, Lc3, Lc4 are locations of center of mass. Note that although link 1 and link 3 have the same lengths, Lc1 and Lc3 need not be equal and, thus, need not have the same mass distribution. Mass moment of inertia of each link about its center of mass are I_1, I_2, I_3, and I_4 consecutively.

It is clear that even though there are four links joined together in this mechanism, there are only two degrees-of-freedom, identified by q1 and q2, which are angular positions of link 1 and link 2. According to Spong and Vidyasagar,[30] the inertia matrix H(q) represented in joint space Q of the parallel mechanism can be described by

$$H(q) = \begin{bmatrix} I_{11}(q) & I_{12}(q) \\ I_{21}(q) & I_{22}(q) \end{bmatrix}$$

where

$$I_{11}(q) = m_1L_{c1}^2+m_3L_{c3}^2+m_4L_1^2+I_1+I_3$$
$$I_{12}(q) = I_{21}(q) = (m_3L_2L_{c3}+m_4L_1L_{c4})\cos(q2-q1)$$
$$I_{22}(q) = m_2L_{c2}^2+m_3L_2^2+m_4L_{c4}^2+I_2+I_4$$

If the effective inertia of the end-point could be calculated, it would be an interesting piece of data. According to H. Asada[31] one approach for arm design is to use generalized inertia ellipsoids. The dynamics of a manipulator arm are primarily

---

30 Spong and Vidyasaga, *Robot Dynamics and Control*, John Wiley and Sons, New York, 1989

31 Asada H., *Arm Design*, 2.853 in-class document, Massachusetts Institute of Technology

dependent upon the mass properties of each member as well as the kinematic structure. In Lagrangian dynamics, the inertia matrix can be defined by

$$T = 1/2 Q'^T H(q) Q'$$

where H(q) is n x n inertia matrix represented in joint space $Q = [q1,q2,...,qn]^T$, and T is kinetic energy. Matrix H(q) is positive definite thus having all positive eigenvalues and invertible.

h is momentum of the arm described by

$$h = H(q)Q'$$

If p is the momenta of the arm reflected to the end-point, we can transform the momenta with respect to a Cartesian coordinate system fixed in space, so that

$$h = J^T p$$

where J^T is transpose of Jacobian matrix.

Now we can rewrite these equations as another expression of kinetic energy as

$$T = 1/2 p^T G p$$

where

$$G = JH^{-1}J^T$$

G is a matrix representing inertial characteristics reflected in end-point motion. Since H is invertible then G exists regardless of the dimension or singularity of the Jacobian matrices.

Since H is positive definite, H can describe a quadratic surface by $u^T Hu = 1$. It turns out that the quadratic is therefore an ellipsoid. This ellipsoid is known as Generalized Inertia Ellipsoid (GIE)[32] reflected to the origin of the Cartesian coordinate. Similarly, the inverse inertia matrix can be used to find the effective inertia reflected to the end-point represented in the form of an ellipsoid surface, so called inverse GIE. The inverse GIE has principal axes diagonally in the inverse inertia matrix. Thus the principal axes are aligned with the eigenvectors of the matrix and the length of each axis is the reciprocal of the square root of corresponding eigenvalue. Therefore, the largest eigenvalue corresponds to the minor axis of the ellipsoid in which the moment of inertia is minimized in that direction. On the other hand, the smallest eigenvalue corresponds to the major axis of the ellipsoid in which the moment of inertia is maximized in that direction.

Effective inertia changes from point to point in the workspace. Therefore, the lengths of both major and minor axes of the inertia ellipsoids, as well as the direction of each axis, keep changing as the arm moves from one point to another. Rate of change of directions of principle axes can be described as the non linearity of effective inertia.

In the above method, Jacobian matrix J of the five-bar mechanism in Fig. 4.21. is

$$J = \begin{bmatrix} -L_1 \sin q_1 & L_2 \sin q_2 \\ L_1 \cos q_1 & -L_2 \cos q_2 \end{bmatrix}$$

$H^{-1}(q)$ is inverse matrix of H(q)

---

32 Paul, R. P., Stevenson, C. N., *Kinematics of Robot Wrists*, Int. J. of Robotics Research, 2-1, 31/38, 1983

$$H^{-1} = \frac{1}{(I_{11}I_{22}-I_{12}^2)}\begin{bmatrix} I_{22} & -I_{12} \\ -I_{12} & I_{11} \end{bmatrix}$$

Now we can compute G as $G = JH^{-1}J^T$ as

$$G = \frac{1}{(I_{11}I_{22}-I_{12}^2)}\begin{bmatrix} h_{11} & h_{12} \\ h_{21} & h_{22} \end{bmatrix}$$

where

$$h_{11} = L_1^2 I_{22}\sin^2 q_1 + 2L_1L_2I_{12}\sin q_1 \sin q_2 + L_2^2 I_{11}\sin^2 q_2$$

$$h_{12} = h_{21} = -L_1^2 I_{22}\sin q_1 \cos q_1 - L_1L_2I_{12}\cos q_1 \sin q_2 - L_1L_2I_{12}\sin q_1 \cos q_2 - L_2^2 I_{11}\sin q_2 \cos q_2$$

$$h_{22} = L_1^2 I_{22}\cos^2 q_1 + 2L_1L_2I_{12}\cos q_1 \cos q_2 + L_2^2 I_{11}\cos^2 q_2$$

The estimated lengths for each link to cover 15X18 inches workspace are:

L_1 =	16 in.	L_{c1} =	8 in.
L_2 =	6 in.	L_{c2} =	3 in.
L_3 =	16 in.	L_{c3} =	8 in.
L_4 =	20 in.	L_{c4} =	15 in.

Mass and moment of inertia of each link at its center of gravity is estimated based on using 1.5X1.5-inch aluminium-alloy square tube on all links including joints and weight of bearings.

M_1 =	2 lbs.	I_1 =	1.32 lb-in^2
M_2 =	1 lbs.	I_2 =	0.13 lb-in^2
M_3 =	2 lbs.	I_3 =	1.32 lb-in^2
M_4 =	4 lbs.	I_4 =	4.56 lb-in^2

Effective end-point inertia of the mechanism is presented in Fig. 4.22 (a) and (b). The ellipsoids in Fig. 4.22 (a) are drawn at different radii from the manipulator base at 2 inch interval from 14 to 26 inches. The ellipsoids at 18 inch radii, which are in

t

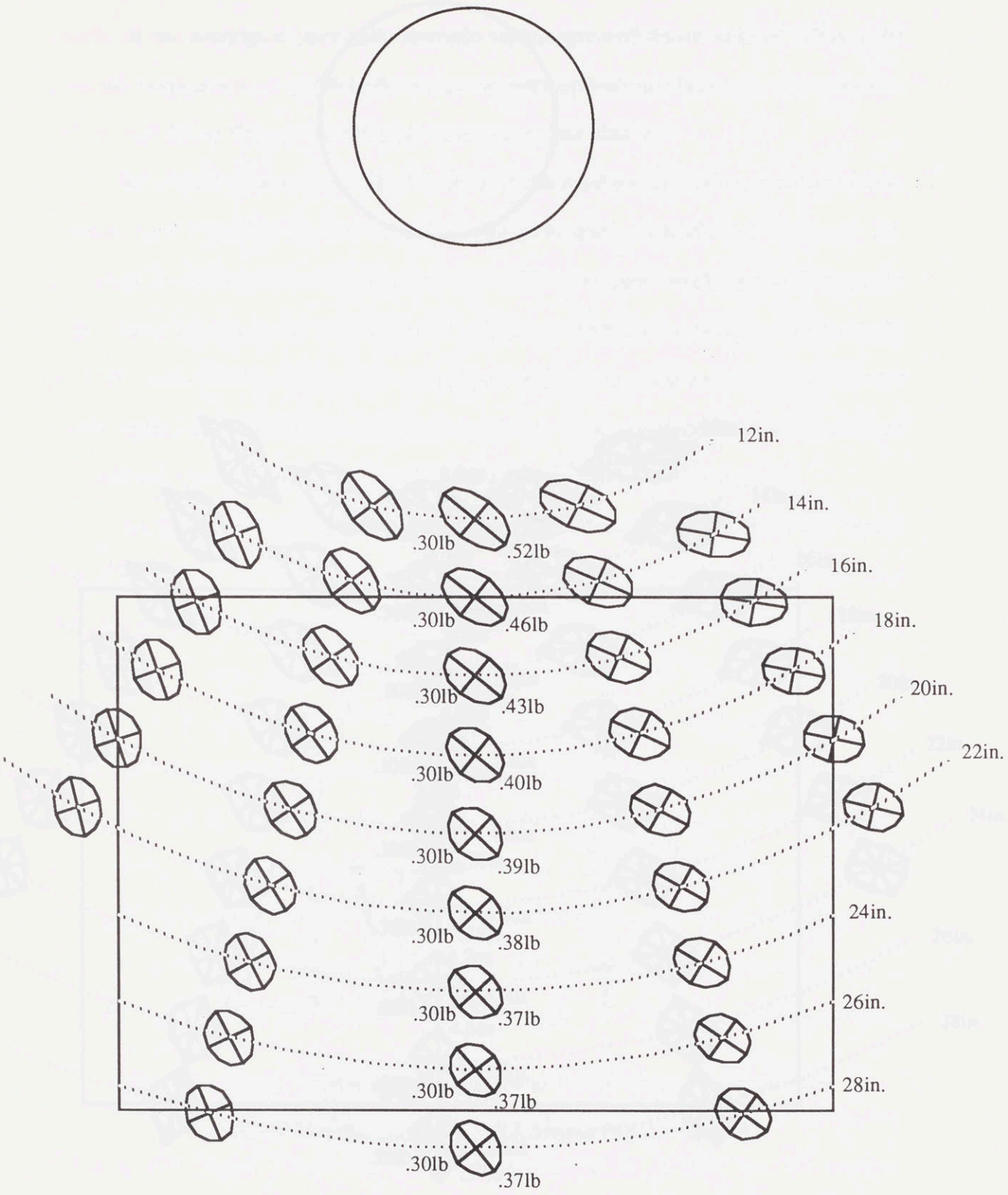

Fig. 4.22 (a) End-Point Inertia Ellipsoids of Designed Parallel Mechanism

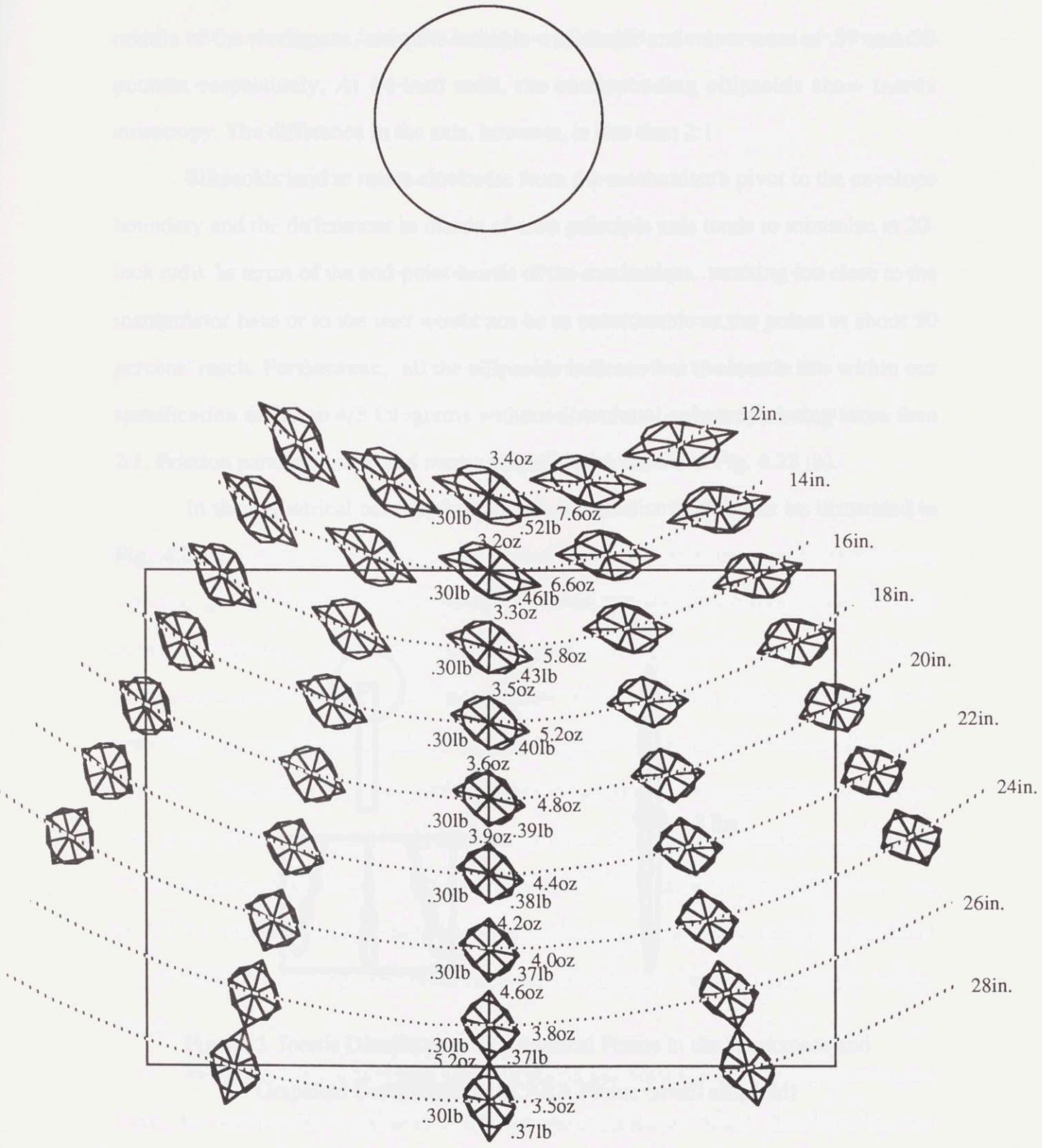

Fig. 4.22 (b) Friction Parallelograms and Inertia Ellipsoids of Designed Parallel Mechanism

middle of the workspace, are quite isotopic with major and minor axes of .39 and .30 pounds, respectively. At 14-inch radii, the corresponding ellipsoids show inertia anisotropy. The difference in the axis, however, is less than 2:1.

Ellipsoids tend to rotate clockwise from the mechanism's pivot to the envelope boundary and the differences in inertia of each principle axis tends to minimize at 20-inch radii. In terms of the end-point inertia of the mechanism, working too close to the manipulator base or to the user would not be as comfortable as the points at about 50 percent reach. Furthermore, all the ellipsoids indicate that the inertia lies within our specification of 2/3 to 4/3 kilograms without directional anisotropy being more than 2:1. Friction parallelograms and inertia ellipsoids are shown in Fig. 4.22 (b).

In the cylindrical case, end-point inertia and distribution can be illustrated in Fig. 4.23.

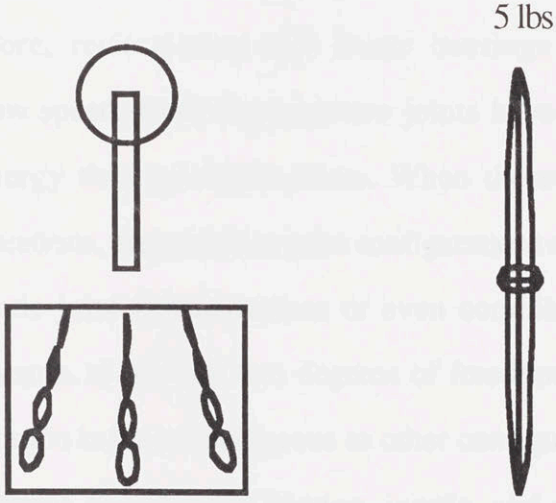

Fig. 4.23 Inertia Distribution of Cylindrical Frame in the Workspace and Graphical Comparison to SCARA Frame (small ellipsoid)

The ratio of directional inertia anisotropy is found to be 1:15 with some degrees of nonlinearity resulting from rotating motion of base joint. As a consequence, in terms of

inertia, the cylindrical frame is not appropriate for the manual teaching aid's configuration.

4.3.3 Chapter conclusion

In this Chapter, we discussed many important things about friction and inertia in mechanisms. All the configurations proposed in the beginning of this Chapter have potential, in terms of kinematics, to operate and provide motion inside the selected therapy workspace. If, however, we focus more closely on the end-point friction and inertia, we can justify and properly select the right configuration.

All configurations are formed with either prismatic or revolute joints. We found that a prismatic joint has substantially more friction than a revolute joint because the latter has geometrical advantage to reduce the actual bearing friction reflected to the end-point. Furthermore, recirculating ball linear bearings are sensitive to friction fluctuations at low speed. Basically, revolute joints have less end-point inertia and consume less energy than prismatic joints. When these joints are combined into kinematic configurations, pure revolute joint configurations still project their advantages over pure prismatic joint configurations or even combined prismatic-and-revolute joints. In other words, to provide two degrees of freedom in a horizontal plane, the SCARA configuration is far advantageous to other configurations, such as cylindrical or Cartesian, in terms of end-point friction, inertia, and motion smoothness at low speed.

Pantomec and articulated configurations are strongly coupled to gravitation force. An active motor command or counter-weight scheme should, therefore, be used to compensate for gravitational effect in order that the configurations do not collapse. This is considered unsuitable for a backdrivable system.

In conclusion, the SCARA configuration has been shown to be the superior mechanism over other configurations, such as Cartesian, cylindrical, articulate, and Pantomec for this particular therapeutic application.

Chapter 5

Transmission and Actuator Selection

5 Transmission and Actuator Selection

According to Chapter 3 on configuration selection, the most promising configuration, having low and uniform end-point friction and inertia for our therapeutic applications, is the SCARA frame. In this Chapter, the selection and design of the transmission and actuator is discussed. According to the specifications in Chapter 3, the electromagnetic actuator is selected as the primary power source since electrical energy is the most easily available source in hospitals. Although pneumatic and hydraulic power supplies are obtainable from electricity, they still have unacceptable levels of noise and vibration. Furthermore, pneumatic and hydraulic systems are generally massive and "dirty" compared to "clean" electromagnetic actuators. In this Chapter, various types of electrical actuators and transmission systems are evaluated using the end-point specification in Chapter 3.

5.1 Linear and Rotary Drives

Electromagnetic drives are produced in both linear and rotary constructions. For example: linear motors, linear ball screws, friction/traction drives, rack-and-pinions, direct–drives, cable/band drives, and rotary speed reducer drives. Again, for our therapeutic application, we have a very strict requirement that the manipulator should be backdrivable. In other words, the actuator system *must* comply to the user. This requirement makes this manipulator design far different from any industrial robots. Only a few existing transmission systems are applicable. High reduction ratio speed reducers with high impedance, or mechanisms with high mechanical advantage such as low-lead linear screws or worm gears are disqualified for this therapeutic robot as they reflect high resistance in terms of friction and inertia to the user.

5.1.1 Linear Actuators

Applicable linear actuator systems that meet the backdrivable requirement are linear motors, friction/traction drives, and rack-and-pinions. Generally, backdrivable linear actuators are quite massive and space consuming compared to backdrivable rotary actuators for the same output. For example, a linear motor package which stalls at ten pound-force weighs thirty to forty pounds[33]. The heaviest part of a linear motor is the stator where wires are wound in a slotted bar. Unlike the rotary construction where the commutation circulates around a ring-shape stator, the linear motor's stator must be as long as the actuator's "stroke," resulting in excessive weight. Overheating is another problem for linear motors, a forty pound linear motor can only produce 2 pound-force for a few seconds before getting overheated.

Rack–and-pinion and friction/traction drives transform rotary motion into linear motion. Basically, rack-and-pinion systems have a pinion running on a gear-cut bar, called a rack. If the rack is stationary, the pinion must rotate and translate on the track. On the other hand, if the pinion is stationary but rotates, the rack with linear guide (linear bearings) must travel. In either case, rack-and-pinion drives still contribute high output inertia. For instance, in the case of a pinion pitch diameter of two inches, in order to produce thirty pound-force, a five to eight pound motor is required. In addition, precision racks are usually made of hardened stainless steel which, together with the linear guide, contribute substantial amount of output inertia. Another negative feature of rack-and-pinion systems is "backlash" or free clearance between two adjacent gear teeth. Backlash reduces the performance of the control system and degrades the user's comfort.

---

33 Northern Magnetic

In traction and friction drives, power is transmitted between two elements which are driving and driven by means of a friction force. According to Rivin,[34] the transmission approach is called "friction drive" if no lubricant is applied between the two elements (e.g. steel-rubber), while, on the other hand, if lubrication is applied and power is transmitted through fluid layers, then the drive is called "traction drive." Typically, both surfaces of friction and traction drives are pressed together with a force Q by preloading mechanisms to produce friction force fQ between contact bodies as shown in Fig.5.1.

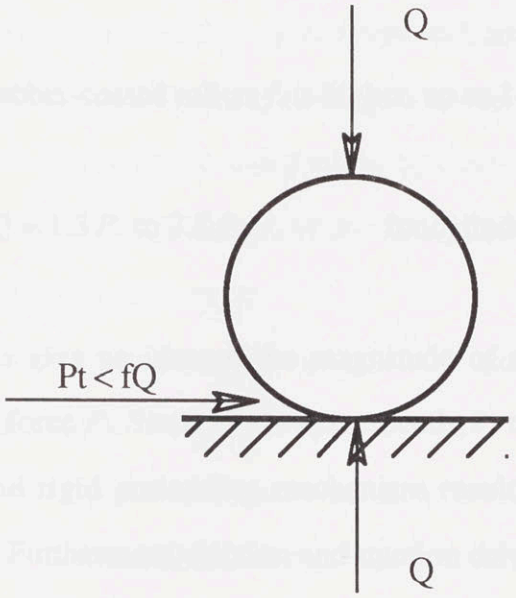

Fig. 5.1 Contact Condition of Friction/Traction Drive

In friction and traction drives, sliding *always occurs* as a natural phenomena between the two elements. Sliding can be reduced by introducing a preloading factor m at rated tangential force P

$$P < fQ/m$$

---

[34] Rivin, E. I., *Mechanical Design of Robots*, McGraw-Hill, New York, 1988

where m is normally 1.5 for industrial applications and 2.5 for servodrives. Since preload Q determines the tangential force, increasing Q will result in higher traction force, causing more structural stress, and also requiring a more powerful preloading mechanism. It is recommended that f be 0.2 for dry steel-to-steel or steel-to-cast iron applications and m be 2.5 for servodrive applications.

Q relates to P as

$$Q = 7.5\,P \text{ to } 12.5\,P \qquad \text{for cylindrical rollers}$$

For special rubber-coated rollers f is higher, up to 1, which gives

$$Q = 1.5\,P \text{ to } 2.5\,P \qquad \text{for cylindrical rollers}$$

These equations give an idea of the magnitude of the preloading force Q required for tangential force P. Since Q always exceeds P, the transmission always requires a powerful and rigid preloading mechanism resulting in high inertia and occupying large space. Furthermore, friction and traction drives are very sensitive to dirt, contaminations, and nonuniform wearing of contact surfaces. Initially, friction and traction drives may provide "backlash free and smooth motion;" however, aging and nonuniform wear will gradually degrade effectiveness and the motion's quality. In addition, the linear drive approach suggest the use of linear bearings that have unfavorable characteristics as described earlier in Section 4.2.2.

In conclusion, we have reviewed several demerits of linear drives such as high inertia, backlash phenomena, and unsmoothed motion.

5.1.2 Rotary Actuators

Rotary drives have been developed and used much more than linear drives. Rotary drives are currently considered "standard" in most applications since there is more knowledge, experience, and technology available for this type of actuator. Instead of producing force and translational displacement as in the linear case, rotary drives produce torque and angular displacement as outputs. Generally, rotary drives have infinite travel as shafts can be kept rotating. However, in the linear drive case, mechanical travel is limited by the "stroke" or the length of linear travel. If a mechanism is not fully confined to linear motion, implementing rotary drives usually requires less space. Rotary drives can be categorized into 2 types: 1) Direct and 2) Reduced. Speed reducers bring down output angular speeds of the actuator, while enhancing output torque as a reciprocal of the reduction ratio.

For our application with the SCARA mechanism, rotary actuators have some advantages over linear actuators:

1. The only moving part in a rotary actuator is the shaft which turns and supplies torque into the system. Hence, when compared to a linear actuator, the rotary actuator has less reflected end-point inertia due to transmission.
2. Rotary actuators consume less space for this therapeutic application. All the rotary sensors can be simply installed inside a nice and clean cylindrical package, unlike linear actuator construction where protrusion of linear rods increases the package's volume and space.

In conclusion, rotary drives show significant merits over linear drives in terms of inertia reflected at end-point, space utilization, and potential to provide smooth and low friction motion. As a consequence, the design of the manipulator should be focused on implementing rotary actuators instead of linear ones.

5.2 Impact of Speed Reducer on Transmission Systems

In general, speed reducers are transformers, reducing the speed of prime movers or actuators into proper speed ranges for the outputs. According to the law of conservation of energy, output torque from speed reducers will be increased as the reciprocal of the reduction ratio. For example, internal combustion engine automobiles, require at least 3 different reduction ratios to allow engines to operate, most of the time, at maximum torque ranges over wide ranges of output shaft velocities. In other words, speed reducers extend output shaft speed and torque ranges while allowing its upstream actuator to operate at a proper angular velocity. Speed reducers also increase output torque and allow actuators to be smaller and lighter than non-reduced types.

Considering our therapeutic application where the required stall torque is estimated at 1300 ounce-inch at both shoulder and elbow pivots, both non-reduced actuators and actuators with various speed reduction ratios are applicable. However, we need to investigate static friction, effective inertia reflected to the user, together with weight and ease of actuator's controllability. Table 5.1 compares weight, output rotor inertia, and static friction due to different "ideal" speed reduction ratios given that each of the speed reducers, bearings, attached sensors, and any rotating elements in the transmission system contribute no friction, weight, and inertia to the output shaft. In other words, Table 5.1 displays each motor's weight, static friction, and the rotor inertia of the motor reflected to the output shaft of the speed reducer.

In order to give a clearer point of view, Figure 5.2 represents a diagram of the motor and an "ideal" speed reducer set. The term "ideal" indicates zero weight and friction contribution from the drive train with a hundred percent transmission efficiency. The objectives for this Section are to compare impacts of different reduction ratios from 1:1 to 1:10 on friction, inertia, and weight properties of the motor reflected to the output shaft.

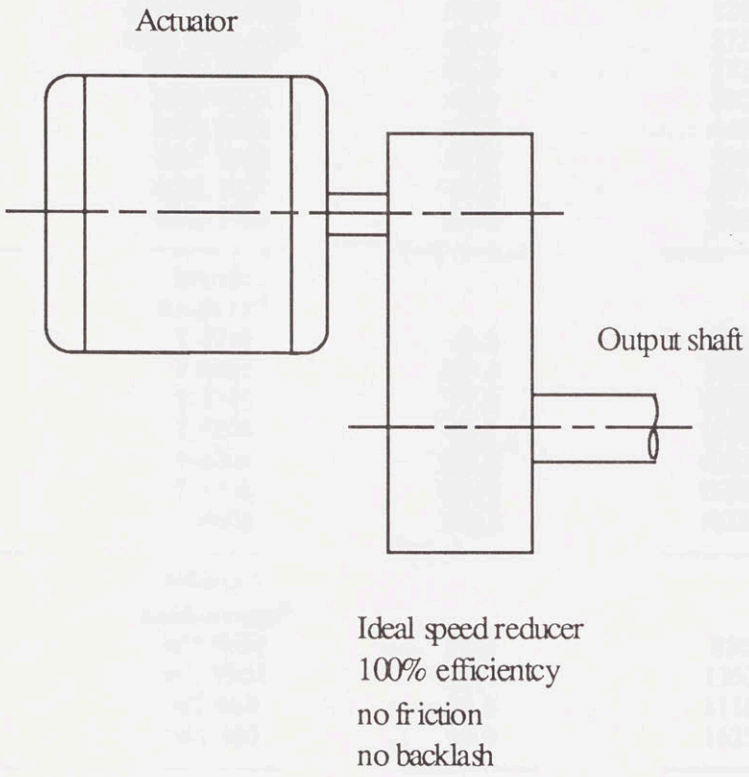

Fig. 5.2 Actuator and Ideal Speed Reducer

In addition to the above assumptions for "ideal" speed reducers and transmission elements, we pin down the electromagnetic rotary actuator to some commercially available brands which only differ in technology. Inland Motor provides both high performance Brushed and Brushless DC motors. These two motors use conventional construction (radial air-gap). providing low static friction and high torque-to-weight ratio.

Reduction ratio[1]	Motor model	Static friction[3] oz-in	Rotor inertia[4] 10^{-3} oz-in-sec^2	Weight[5] oz
	Inland's Brushless DC			
1	RBE 3003-A50	32.0	128	123
2	RBE 3001-A50	51.0	272	66.4
2	RBE 3002	36.0	372	92.3
3	RBE 2103	42.0	320	64.3
4	RBE 2102	46.0	440	50.0
5	RBE 1805	47.0	558	48
6	RBE 1804	49.8	677	40
10	RBE 1505	64.0	911	24.5
	Inland's Brush DC			
1	T-7250	40.3	4416	360
2	T-6205	134.4	1728	160
	T-5745	57.6	6144	240
3	T-6204	86.4	11232	112
	T-6202	138.2	10022	99
4	T-5730	69.12	15360	116
6	T-5406	138.2	10368	48
	Infranor's Axial air-gap[6]			
1	MT-2000	15.2	850	705.6
2	MT-1000	17.0	1360	424.0
3	MT-600	16.6	1116	246.4
5	MT-300	12.0	1625	193.6
Reduction ratio[1]	Motor model	Static friction[3] oz-in	Rotor inertia[4] 10^{-3} oz-in-sec^2	Weight[5] oz
	PMI's Axial air-gap[7]			
1	JR25M8CH	25.0	700	1120
3	JR16M4CH	33.0	756	280
6	JR16M4C	66.0	756	216
10	U12M4HA	65.0	1000	176

Note
1. Ideal reducers which introduce no friction with 100% power efficiency
2. Motor makers, types, and models
3. Only motors' static friction reflected to output side
4. Motors' rotor inertia only reflected to output shaft
5. Only motor's weight without the reducer
6. Infranor's Mavilor® DC Servo motors
7. PMI Motion Technologies JR and U Series

Table 5.1 Reflected Static Fiction, Rotor inertia, and Actuator Weight for Different speed Reducer Ratios

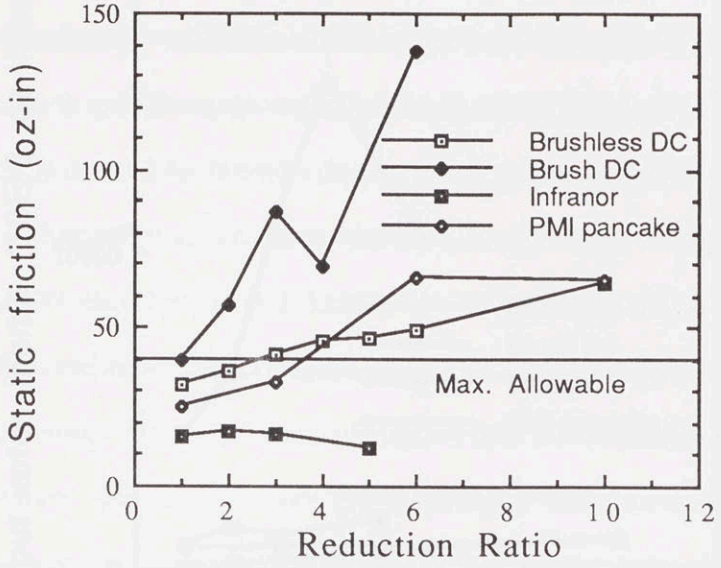
Static friction (oz-in)
150
100
50
0
0
2
4
6
8
10
12
Reduction Ratio
Brushless DC
Brush DC
Infranor
PMI pancake
Max. Allowable

(a)

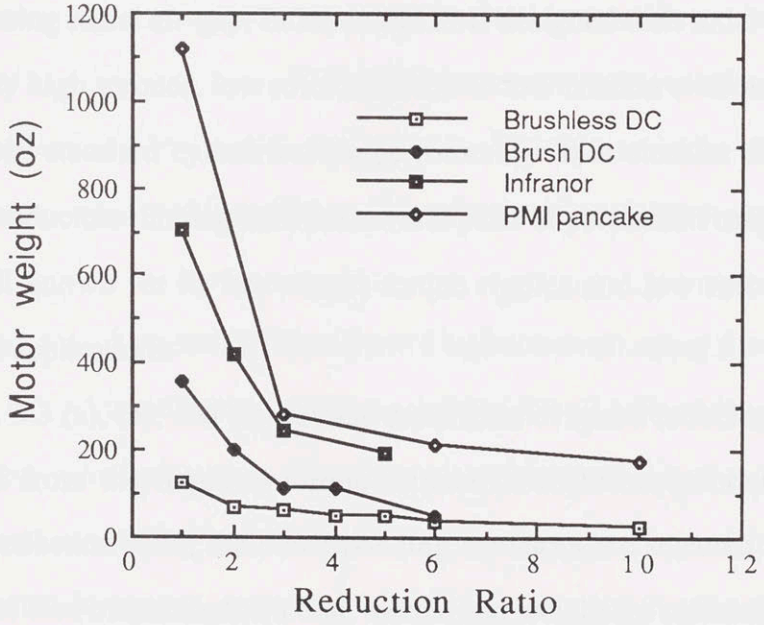
Motor weight (oz)
1200
1000
800
600
400
200
0
0
2
4
6
8
10
12
Reduction Ratio
Brushless DC
Brush DC
Infranor
PMI pancake

(b)

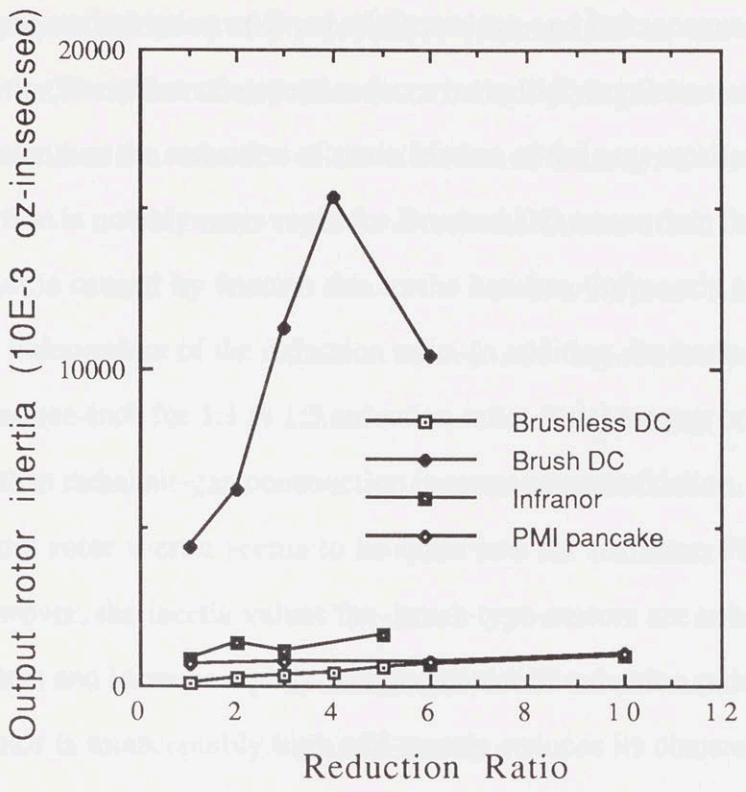

(c)

Fig 5.3 (a), (b), (c) Friction, Weight, Output Rotor Inertia for Different Reduction Ratio

Instead of using radial air-gap, Infranor and PMI designed their axial air-gap motors to provide very high torques, low rotor inertia, and low friction without torque cogging. PMI replaced standard cylindrical shape rotors by thin circular disks with built in electrical conductors running between several pairs of permanent magnets. This design is very well known for its low output torque ripples and low rotor inertia for high acceleration applications.

Fig. 5.3 (a), (b), and (c) review the effects of speed reducing. The figures are constructed from the required torque criteria of 1300 oz.-in continuous. For one particular reduction ratio, the corresponding actuators are selected from each motor construction, then output shaft friction, inertia, and weight are calculated and plotted for each construction category.

Output static friction of Brushed, Brushless, and Infranor motors increases with reduction ratio. The effect of a speed reducer in multiplying the actuator's static friction is much greater than the reduction of static friction of the next smaller actuator. Increase in static friction is notably more rapid for Brushed DC motor than for any other type of motor, which is caused by friction due to the brushes. Infranor's axial air-gap motor seems to be independent of the reduction ratio. In addition, its static friction is constant at about 15 ounce-inch for 1:1 to 1:5 reduction ratio. Axial air-gap construction tends to be superior than radial air-gap construction in terms of static friction.

Output rotor inertia seems to be quite low for Infranor, PMI, and Brushless motors. However, the inertia values for brush type motors are substantially different from the others and increase rapidly with increment of reduction ratio. In fact, inertia of Brushed motor is unacceptably high and greatly reduces its chances for the proposed actuator and transmission for the designed robot.

Motor weight seems to be another interesting parameter. Both Infranor and PMI axial-air-gap have high weight because their constructions require several pairs of strong and massive magnets to compensate for field losses. If we compare the weights of motors with a 1:1 reduction, PMI and Infranor's weight are nine and seven times larger than Brushless DC motors, respectively. Excessive weight of the axial air-gap design restricts mobility of the robot and impedes its adaptability to the manual teaching aid.

Brushless DC motors seem to have a higher overall rating than any other motor in terms of the reflected inertia, friction, and weight. In a Brushless DC motor, ideal speed reducers have tremendous effects on the weight and sizes of motors. Direct-drive or 1:1 reduction requires a 123 ounces motor for our toque requirement. As the reduction ratio increases, weight is drastically reduced by three times with 6:1 reduction. In case of rotor inertia, increasing the reduction ratio brings up the reflected rotor inertia of output shaft. The 6:1 reducer increases the output inertia by almost

seven times that of the direct-drive configuration because the square of reduction ratio is multiplied by the motor's output inertia (see Fig 5.3 (c)). However, static friction increases only slightly over a 1:1 to 10:1 reduction ratio range (see Fig. 5.3 (a)).

Considering that actual reducers always contribute static friction, inertia, and weight to a transmission system, it is not clear that use of speed reducers may be more beneficial than a direct-drive approach. Reducer's weight is substantial and may be much more than the difference in weight between a large motor and its next smaller size. In other words, it might not be true that a speed reducer can decrease overall transmission weight and, in fact, may worsen the situation. Additional inertia contributed by a speed reducer will increase the output shaft's inertia. If we consider the fact that reducers always introduce static friction and inertia, we can simply conclude that we do not gain any benefit by using a speed reducer for our application. Furthermore, speed reducers generally introduce undesirable characteristics such as backlash, and cogging. These problems are very difficult to overcome with the existing technology.

In terms of reflected output inertia, friction, and weight, DC Brushless motors have higher overall ratings than any other motor types. Instead of the typical wound rotor, Brushless motors have a wound stator which surrounds permanent magnet elements on the rotor, an inverse arrangement from that of brushed motors. Stator windings are electronically commutated instead of using conventional brushes and commutators. Disappearance of brushes and commutators eliminates brush friction and improves torque response characteristics. In addition, heat can dissipate away more quickly from coils in the stator than from rotor coils, thus, for a given continuous torque rating, a Brushless motor requires less winding space than a corresponding brushed motor, resulting in smaller package with higher efficiency. Replacing rotor coils, brushes, and commutators with high performance magnets eliminates arc problem, thus, decreasing maintenance and downtime cost.

Brushless motors offer several advantages of the Pulse Width Modulation (PWM) technique that allows the motors to be operated very efficiently. One drawback of Brushless motors is its slightly higher cost than brushed motors due to the presence of complex solid-state power switches in amplifiers. However, if accounted for energy, maintenance, and downtime costs, Brushless motors may even cost less than conventional Brushed types. Furthermore, switch cost continues to drop, in part because of increased use of MOSFET technology and insulated gate type switches. Costs are also dropping for ICs used in commutation, feedback interpreting, and PWM circuits.

Brushless motors have proven their effectiveness in several robotic applications. One major concern of Brushless motors in a direct-drive system is torque ripple or cogging. However, several robotic researchers have successfully reduced torque ripple to 1.5 percent[35] to 0.1 percent[36].

In conclusion, Brushless DC motors have shown their advantages over Brushed motors in terms of reflected friction, inertia, weight, efficiency, and size of package. In practice, Brushless motors have successfully been implemented on various robotic applications especially on direct–drive platforms. Therefore, our design decision should be made towards adopting Brushless motors as primary actuators with non-reducer transmission approach.

5.3 Direct-Drive Versus Cable drive

Up to this point, direct-drive actuation is the leading contend. It is crucial that a direct-drive design be effectively implemented at the shoulder joint of the selected five bar parallelogram mechanism. However, implementing a direct-drive actuator on the

---

35 Paul, B. J., *A Systems Approach to the Torque Control of a Permanent Magnet Brushless Motor*, MIT SM Thesis (Artificial Intelligence Laboratory), 1987.

36 Levin, M. D., *Design and Control of a Closed-Loop Brushless Torque Actuator*, MIT SM Thesis (Artificial Intelligence Laboratory), 1990.

elbow joint is questionable as it substantially increases effective inertia of the end-point. Furthermore, it is not preferable that the upper arm should support the moment caused by the weight of the elbow actuator as well as the payload at the end–point.

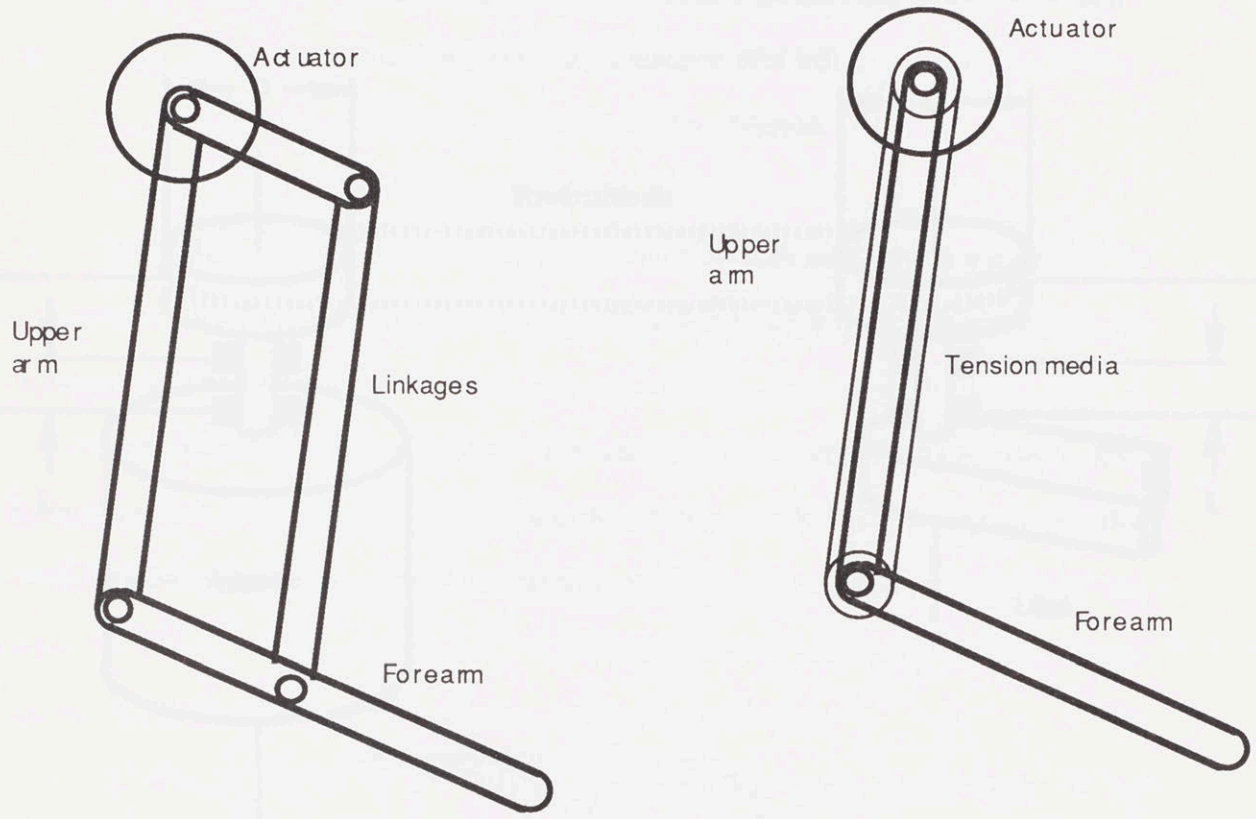

Fig. 5.4 Five-Bar-Linkage and Cable Drive for Forearm

It is advantageous that the elbow actuator be stationary, while transmitting torque to the output through some kind of 1:1 transmission such as as shown in Fig. 5.4. The task is now to evaluate the two methods to actuate the forearm.

Light weight linkages, which induce low friction, are achievable. Tension drives prove their effectiveness in various applications such as the Salisbury hand[37] and WAM[38] (Whole Arm Manipulator). However, these robotic applications are far

---

[37] Three finger hand developed by Prof. Kenneth Salisbury, Artificial Intelligence Laboratory, Massachusetts Institute of Technology.

[38] Four degrees of freedom articulated configuration built by William Townsend, Massachusetts Institute of Technology.

different from that of the manual teaching aid. One good idea is to make a preliminary design of a cable drive and five-bar-linkage for the elbow joint then compare their friction and inertia.

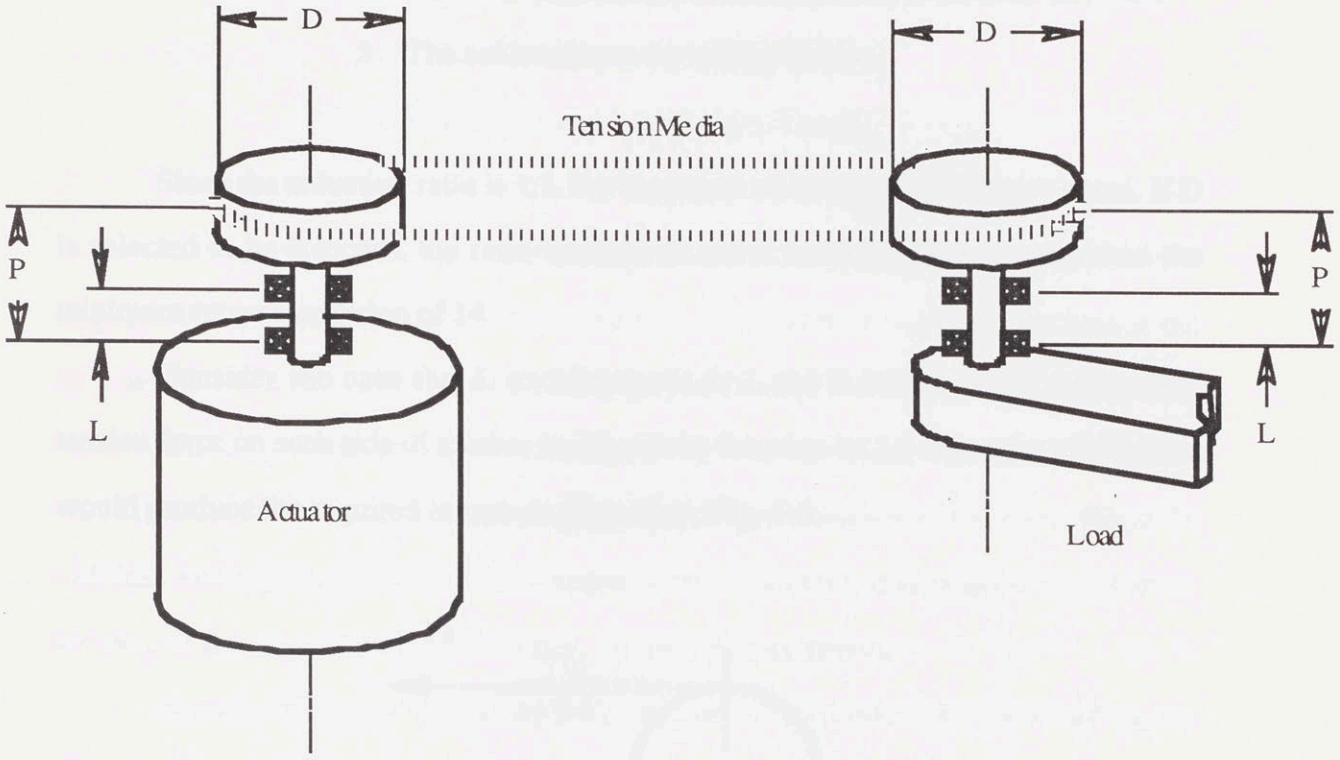

Fig. 5.5 Preliminary Design of Tension Drive for Forearm

Figure 5.5 illustrates a preliminary design of a cable drive model. The tension media needs pre-tension before being subjected to load. Pre-tension stress on the media must be more than the necessary tension. When one side of the media is subjected to load,the other side still must have sufficient tension to prevent slip. According to Townsend[39], it is recommended that pre-tension be set at 1.5 times the rated torque tension.

---

39 Townsend W.T., *The Effect of Transmission Design on Force-Controlled Manipulator Performance*,MIT PH.D. Thesis, 1984

Assumptions
1. Required torque is 1300 ounce-inch or 81.25 inch-pound
2. Pretension at 1.5 times the required torque
3. Static friction coefficient μ of each bearing is 0.003
4. Cable: AB092 aircraft cable with diameter (d) = .094 inches diameter (Maximum tension 960 lbf)
5. The cable induces no rolling friction

Since the reduction ratio is 1:1, the diameters of both pulleys (D) are equal. If D is selected to be 2 inches, the ratio between D and d is 21.3 which is more than the minimum recommendation of 14.

Consider the case that L and P are set to 1 and 2 inches respectively. Pre-tension force on each side of tension media can be found to be 1.5 times the tension that would produce the required torque on the pulley, Fig. 5.6.

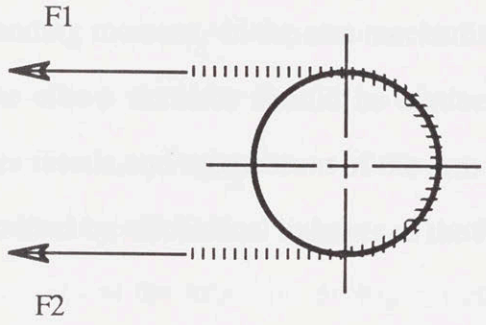

Fig. 5.6 Pre-Tension Force on Cable

Therefore pre-tension forces F1 and F2 are

$$F_1 = F_2 = 1.5(\frac{81.25X2}{2}) = 121.9 \text{ lbf.}$$

Bearing load on each pulley would generate friction f of

$$f = 2\mu F_1(\frac{2P}{L}-1) = 2.2 \text{ lbf.}$$

Where P/L is set at 2.

If the bearing pitch diameter is 1 inch then the generated friction on the pulleys (τ) are:

$$\tau = 2(f)(0.5) = 2.2 \text{ in-lb} = 35.2 \text{ oz-in.}$$

As compared to the motor friction of 0.44 inch-pound, cable drive contributed a large portion of friction torque of d 2.2 inch-pound which is considerably higher (or 83.3 percent of overall friction) compared to the linkage approach. High pre-tension force is the most negative feature of cable drive. The pre-tension introduces bearing load which induces friction torque, degrading the performance of the cable drive. In addition, not only does pre-tension increase internal friction, it also generates internal stresses, in the form of bending moment, in the arm mechanism.

In conclusion, the elbow actuator should be stationary and installed at the shoulder joint to minimize inertia and momentum of the arm mechanism. Power from the actuator is to be transmitted by mechanical linkages to the forearm.

5.4 Bearing Selection

Bearings play an important role in low friction and low speed applications. Linear speeds at pitch lines of each bearing determine speed classes. Low speed bearings have a pitch line speed lower than 500 feet per minute. Pitch speeds between 500 and 3,000 fpm (feet per minute) are generally considered to be mid-range bearings. Bearings with pitchline speeds of 3,000 fpm or more are considered to be high speed

bearings[40]. In general, larger pitchline diameter bearings are allowed to turn at lower angular velocity than those of smaller pitchline diameter bearings. Performance requirements for low speed bearings can be defined by ten basic bearing parameters. The parameters are: rotational accuracy; stiffness; load capacity; resistance to vibration and shock; resistance to hostile environments; frictional torque characteristics; maintenance; service life; motion characteristics; and reliability.

The manual teaching aid's therapeutic tasks can be categorized as a low speed where friction torque characteristics, rotational accuracy, and motion characteristics are the primary concerns.

5.4.1 Bearing Friction

Roller bearings generally have low friction. However, the friction varies from one type to another due to different degrees of sliding and rolling. Major rotational resistance in roller bearings is caused by rolling, sliding, and lubricant friction. Rolling friction occurs when the rolling elements (balls or rollers) roll over the race way. Sliding friction is a result of the guiding mechanism between the race way's lips and the rolling elements' surface. Lubricant friction is internal friction caused by hydrodynamic and shear stress of the lubricant during action. For most applications, bearing friction is negligible compared to the transferred torque. However, in our application, friction is a key parameter to determine the system's performance. Ideally, the device should have as low friction as possible, low magnetic cogging, and low drag torque. Wise bearing selection will definitely improve the system's performance and eventually the interaction between the manual teaching aid and the users.

---

40 Eschmann, P., *Ball and Roller Bearings*, 2nd. Ed., John Wiley and Sons, New York, 1985

Rolling contact friction is a complex phenomenon resulting from elastic hysterisis and associated sliding resistances. Deformation of the raceway and a rolling element are shown in Fig. 5.7. Both bodies are deformed due to load concentration at the contact area. The roller is depressed while the raceway is stretched. The deformation difference in each body causes sliding, thus creating friction during rolling motion.

Another important component of rolling friction originates from hysterisis of the material. During the rolling friction movement, the section ahead of the material are deformed. Part of the energy required in the deformation process is only recovered behind the rolling element - the rest transforms to heat. Ball bearings with three or four-point contacts exhibit greater friction than typical two-point contacts. Moreover, a ball bearing with closer curvature-conformity of balls and groove introduces higher friction than a looser curvature-conformity. The size of the contact angle also determines the friction since the spinning friction grows with larger contact angles.

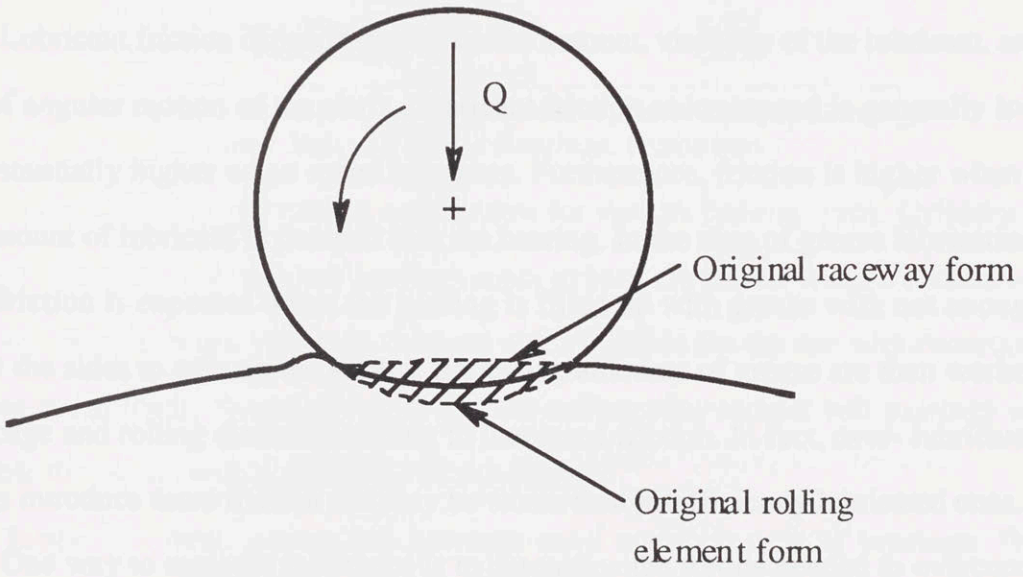

Fig. 5.7 Deformation of a Rolling Element and the Raceway
in the Direction of Rolling Motion

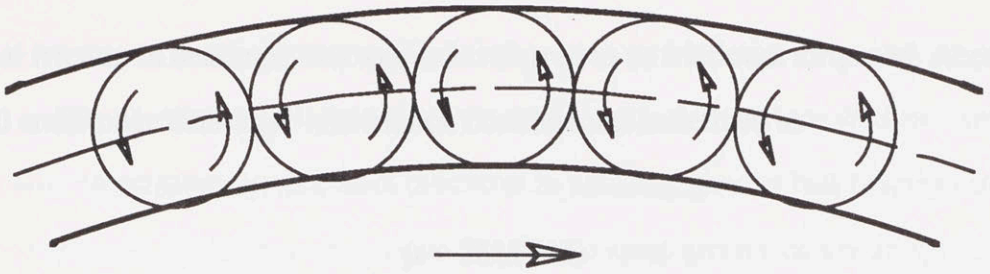

Fig. 5.8 Motion in cageless bearings

Sliding friction occurs at guiding surfaces of the cage, the raceway lips, and between adjacent rolling elements in a cageless design (see Fig. 5.8). Roller bearings always introduce more sliding friction from the raceway's lips than deep groove ball bearings. Nevertheless, sliding friction is generally small under normal operating conditions with good lubrication. However, friction considerably increases with poor lubrication and contamination. Cageless designs normally have more sliding friction than caged bearings since each rolling element rubs its adjacent elements which are rotating in opposite directions.

Lubricant friction depends mostly on the amount, viscosity of the lubricant, and speed of angular motion of the shaft. Lubricant friction at low speed is generally low but substantially higher when speed increases. Furthermore, friction is higher when a large amount of lubricant is pumped into the bearing. In the case of grease lubrication, higher friction is expected when the bearing is filled up with grease with not enough room at the sides to take up the excess. Excessive amounts of grease are then worked by the cage and rolling elements leading to increased friction. In fact, over- lubricated bearings introduce more friction and may be worse than insufficiently lubricated ones.

One way to measure resistance is to determine the torque needed to overcome

internal friction in bearings. The torque is referred to as frictional torque M. According to Ball and Roller Bearings[41] the friction coefficient μ is defined as

$$\mu = 2M/(F*d)$$

where

M = total friction torque of bearing (N-mm)

F = resultant bearing load (N)

d = bore diameter (mm)

Bearing type	Friction coefficient μ
Deep groove ball bearings	0.0015-0.003
Self-aligning ball bearings	0.001-0.003
Angular contact ball bearings, Single row	0.0015-0.003
Angular contact ball bearings, Double row	0.0024-0.003
Cylindrical roller bearings	0.001-0.003
Needle roller bearings	0.002
Spherical roller bearings	0.002-0.003
Tapered roller bearings	0.002-0.005
Thrust ball bearings	0.0012
Spherical roller thrust bearings	0.003
Cylindrical roller thrust bearings	0.004
Needle roller thrust bearings	0.004

Table 5.2 Friction Coefficient μ for Various Rolling Bearings
Source: Ball and Roller Bearings, Eschmann

Table 5.2 represents friction coefficients for various bearing types. Cylindrical roller, self-aligning, and trust ball bearings seem to have the lowest friction coefficient among all other bearings. However, they are not applicable for the use with combined axial and radial loads. Single row deep groove and angular contact ball bearings are applicable for the use with both radial and axial forces.

Single row deep groove ball bearings are a common type of bearings. The raceway grooves on both the inner and outer rings have circular arcs of slightly larger radius than that of the balls. The bearings can sustain both radial and axial loads. In

---

[41] Eschmann, P., *Ball and Roller Bearings*, 2nd. Ed., John Wiley and Sons, New York, 1985

general, single row deep groove ball bearing have low frictional torque since their design minimizes the contact areas and allows the balls to wade into the lubricant more efficiently. In addition, geometrical precision in the deep groove ball bearings is much easier to achieve than in any other type. Single row deep groove ball bearings are more suitable for low friction, low vibration, and low noise.

In single row angular contact bearings, the raceways are arranged such that the forces from one side of the raceway are transmitted to the other in a certain contact angle (commonly available at 40 degrees). Due to the greater contact angle, single row angular contact bearings are better qualified to sustain high axial force than single row deep groove ball bearings. However, they can sustain radial loads only when simultaneously subjected to axial loads. If axial load is not constantly applied or the ratio between radial and axial loads exceeds the limit allowed by the contact angle, two angular contact bearings need to be arranged in opposite orientations for mutual axial support.

Features	Deep groove ball bearings	Angular contact ball bearings
Radial load	Good	Good
Axial load	Fair	Good
Combined load	Good	Very good
High speeds	Excellent	Excellent
High accuracy	Excellent	Excellent
Low noise	Excellent	Fair
Low friction	Excellent	Good
Angular mis-alignment	Good	Poor

Table 5.3 Comparison of Deep Groove and Angular Contact Ball Bearings
Source: NSK ball and roller bearings

In addition, an axial preload must be implemented to obtain satisfactory load distribution and rolling conditions. Practically, single row angular contact ball bearings

are suitable mainly for carrying high axial loads at high speeds with minimum radial forces such as spindle applications.

Table 5.3 compares deep groove and angular contact ball bearings in terms of various features. If we look into our application, the radial load for bearings is estimated to be much more than the axial load (30 times). Furthermore, what we really need to have is low friction and low angular misalignment with high accuracy.

According to SKF's engineering data, an accurate estimation of bearing friction torque at slow speed can be obtained using equation

$$M = 0.083 f_1 P_\beta d_m + 1.88 \times 10^{-4} f_0 d_m^3$$

Where

M is friction torque in foot-pounds

$f_1 = z\left[\frac{P_0}{C_0}\right]^y$

P_0 is static equivalent load, C_0 is basic static load rating

z and y are obtained from table 5.4

$P_\beta = F_r$ or $0.9F_a \cot \alpha - 0.1F_r$ whichever value is greater

α is the bearing contact angle

F_a is thrust load, F_r is radial load

f_0 is obtained from Table 5.5

d_m is the bearing mean diameter

Ball bearing type	contact angle α	z	y
Deep groove	10	0.0009	0.55
Angular contact	40	0.0013	0.33

Table 5.4 Load Torque Values, z and y, for Ball Bearings
Source: SKF Engineering Data, SKF Industries, Inc., 1973

Bearing type	Vertical Mounting
Single row deep groove ball bearing	3.0-4.0
Single row angular contact ball bearing	4.0

Table 5.5 Viscous Torque Factors
Source: SKF Engineering Data, SKF Industries, Inc., 1973

Consider a case where d_m, f_0, Fr, and Fa of deep groove and angular contact ball bearings are equal while both bearings have a static load rating ($P_0 = C_0$). As mentioned earlier that, in our application, Fr is 30 times F_a , so P_β must be equal to F_r. Therefore, M depends only on the value of z which is less for deep groove ball bearings. We can conclude from the SKF's bearing friction torque that single row deep groove ball bearings have less friction than angular contact ones in our application.

Therefore, single row deep groove ball bearing seem to be more favorable than single row angular contact ball bearings.

5.4.2 Lubricant Selection

In most applications, a standard lubricant, grease, or oil of various consistency or viscosity provides a reliable lubrication. However, there are some applications where a special lubricant is necessary. Grease-lubrication is more common for simple applications since it does not require special sealing and is applicable to both the vertical and horizontal axes. Grease also provides protection against contamination into bearings. Grease is classified by the grease thickener and the base oil used. The amount of grease thickener and the base oil determine the consistency of the lubricants. Oil-lubrication is always used when bearings are subjected to high temperature since oil is capable of transferring heat from the bearings through forced circulation. However, even under normal load and temperature, bearings are often lubricated with oil. Frequently, lubricant selection depends on the bearings' environment. For example, bearings in a gear train are lubricated with oil because gearwheels require oil lubricant. If oil is used for lubrication, special sealing and an oil circulation system must be considered, especially with vertical and inclined shafts.

In general, when bearings are not subjected to vital temperatures and speed, grease lubrication is preferable. For our robotic application, grease lubrication has

substantial advantages over oil lubrication since it does not require complicated sealing as oil-lubrication does. However, there are many different types and classes of grease lubricants available for different purposes. Properly selected grease will not only reduce static friction but also provide smooth motion.

It is recommended that a low friction running condition be achieved by using low viscosity, synthetic base oil, with penetration number 2. This special grease is soft providing the lowest internal lubricant friction. Some criteria for grease selection as shown in Table 5.6 and 5.7.

Some criteria for grease selection		Grease characteristics
Running properties	Low friction	Grease with low viscosity synthetic base oil; penetration number 2
	Low noise level	Filtered grease with high viscosity base oil
Operating conditions	Inclined or vertical axis	Grease of penetration number 3; grease thermal stability must exceed operating temperature
	For-life lubrication	Grease retaining its consistency; grease thermal stability must exceed operating temperature

Table 5.6 Criteria for Grease Selection[42]

Grease thickener	Base oil	Temperature range	Resistant to to ageing	Anticorrosive properties	Water resistance	Remarks
Lithium oil	Diester	-50/+120	Very good	Good with additive	stable upto approx. 90C	low-temp. grease; also good for high speed;low friction

Table 5.7 Properties of Recommended Grease for Low Friction Running Applications (NSK Ball and roller bearings catalog)[43]

---

42 Deutshchman, A., Micheals, W., Wilson, C., *Machinery-Design*, Macmillan Publishing Co., Inc. New York, 1975

43 *NSK Ball and roller bearings*, Nippon Seiko K.K., Japan, 1986

In conclusion, single row deep groove ball bearings were selected for the proposed machine, while a lithium thickener synthetic oil base with low viscosity was chosen as the lubricant.

5.5 Chapter Conclusion

In this Chapter, we found that brushless DC motors with direct-drive transmission are promising for our therapy application in term of end-point reflected friction, inertia, and overall weight of the system. In addition, single row deep groove ball bearings with lithium oil base will facilitate low friction joints.

Chapter 6

Sensor Selection

6 Sensor selection

6.1 Position Sensors

Position sensors are extremely important for the functioning of the robotic aid. The servo controller requires position information to properly commutate each phase of the stator winding corresponding to the rotor's position. Perfect synchronous commutation sequence results in minimum torque ripple of the Brushless motors. The controller also needs precise position information, velocity, and force feedback for its control algorithm. However, our experience with a similar robot[44] shows that a resolution of at least 16 bits is required to correctly determine the interaction force between a human and a machine.

Our criteria for choosing a position sensor are: 1) Low friction 2) Light weight (less than 2 pounds) with acceptable dimensions (less than 4 in. OD and 3 in. thick) 3) At least 16 bit resolution with high accuracy 4) Absolute position information 5) Good repeatability 6) Compatibility with brushless DC motor controller.

6.1.1 Position Resolutions

Table 6.1 illustrates position resolutions in terms of binary bits, angles, and minimum end-point resolution based on a 30 inch arm length.

13 binary bits of information is not sufficient to determine the directions of force at the manipulandum end-point. Therefore, we should consider a position sensor which is, at least 16 bits.

---

[44] Ernie Fasse and his work in Bizzi Lab, Massachusetts Institute of Technology

No. of bits (N)	Resolution (2^N) / rev.	Arc minutes / bit	Arc. seconds / bit	End-point resolution (inches)
10	1024	21.09375	1265.625	0.1841
11	2048	10.54688	632.8125	0.0920
12	4096	5.273438	316.40625	0.0460
13	8192	2.636719	158.20313	0.0230
14	16384	1.318359	79.10156	0.0115
15	32768	0.659180	39.55078	0.0058
16	65536	0.329590	19.77539	0.0029
17	131072	0.164795	9.88770	0.0014
18	262144	0.0823997	4.94385	0.00072
19	524288	0.041199	2.47192	0.00036
20	1048576	0.020599	1.23569	0.00018

Table 6.1 Resolutions of Position Sensors

Table 6.2 lists commercially available absolute position sensors with their resolutions and price ranges. Only high-accuracy absolute optical encoders and high-accuracy resolvers or synchros meet our resolution requirements.

Position sensor type	Absolute resolution	Remarks
High-accuracy abs. optical encoders	1.2 arc. sec.	Very expensive
High-accuracy resolvers/synchros	7 arc. sec.	$2,000
Medium-accuracy optical encoders	23 arc. sec.	$2,500/bin output
Selected resolvers/synchros	3 arc. min.	$425 with $225 R/D
Standard resolvers	7 arc. min.	$340 with $225 R/D
Typical absolute optical encoders	11 arc. min.	$400 / bin output
Typical Incremental optical encoders	11 arc. min.	$200 / bin output
Absolute contact encoders	26 arc. min.	$675 / bin output
Incremental contact encoders	26 arc. min.	Pulse output

Note: For all resolvers, absolute resolution also depends on resolver-to-digital converter

Table 6.2 Comparison of Position Sensors
Source: Machine Design, *1990 Systems Design Reference Volume*, Penton, 1990

6.1.2 High-Accuracy Optical Shaft Encoders

Rotary optical encoders are very common for position and motion sensing. Encoders have discs or plates containing slots or transparent segments moving between LED's or detectors (see Fig 6.1). Code discs are usually made from glass and thus are

not likely to operate in a harsh environment or on a mobile system with high acceleration and/or vibration.

Position information is derived from the number of light pulses or light pulse codes. There are two basic encoder styles: absolute and incremental.

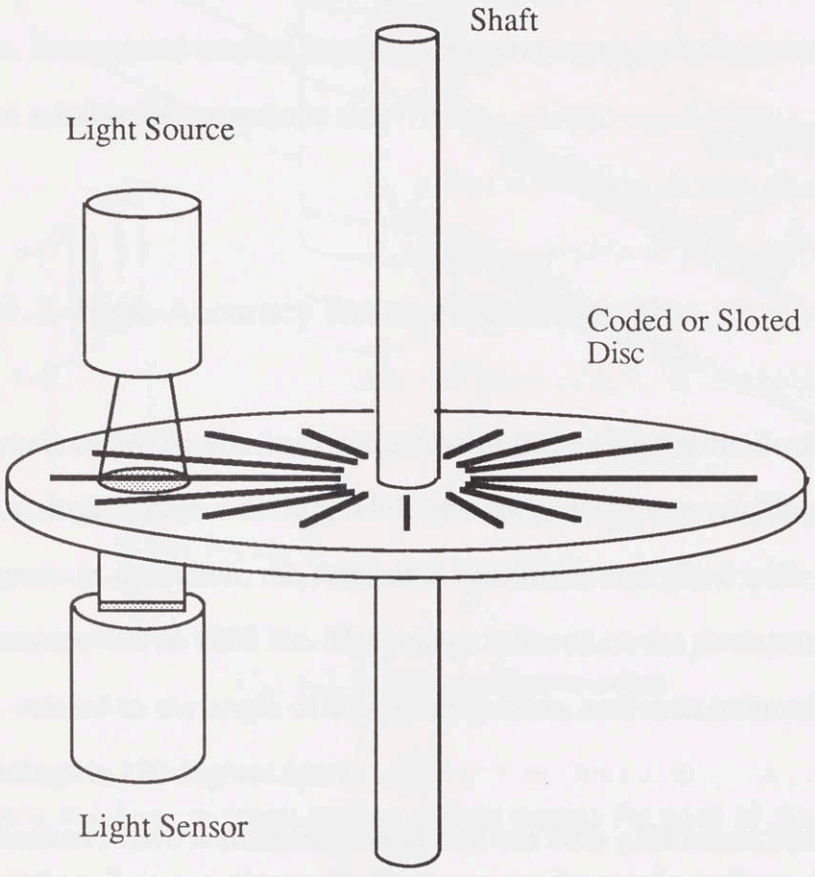

Fig. 6.1 Optical Encoder Construction

An absolute encoder contains multiple light sources and detectors, sensing a disc of multiple tracks of slots. For each position, the detectors sense a unique set of codes so that the shaft position could be absolutely determined. Tracks on absolute encoders are generally arranged to give out a binary output called Gray Code as a single bit changes at a time. Therefore, the maximum error of the encoder is only 0.5 bit.

Absolute encoders will provide information even if power to the encoder is interrupted and then restored.

Incremental encoders determine the angular position by using a datum from a particular slot as a reference and measuring the number of counts away from that slot. The reference information is kept in a RAM unit, which vanishes if the encoders are shut down. Incremental sensors require calibration every time the system is started up, and are not suitable for our robotic aid.

6.1.3 High-Accuracy Resolvers and Synchros

Synchros are similar in construction to three-phase wound-rotor motors. The rotor has a single phase winding, while the stator has three windings arranged 120 degrees apart. In operation, the rotor of a synchro is energized with an AC voltage, usually between 400 to 1200 Hz. The voltage induced on the three stator windings are precisely related to the angle of the synchro rotor, and each induced voltage on the stator windings is 120 degrees apart.

Resolvers have a similar construction but with a different stator offset angle. The resolver's rotor has a single winding while the stator has two windings at a 90 degrees offset. When the rotor is excited with an AC reference signal, the stator windings produce AC voltage outputs that vary in amplitude according to the rotor position. Since the two stator windings are 90 degrees apart, the output phase difference between each winding is also 90 degrees. In other words, resolvers produce sine and cosine outputs in which amplitudes vary according to the rotor position (see Fig. 6.2).

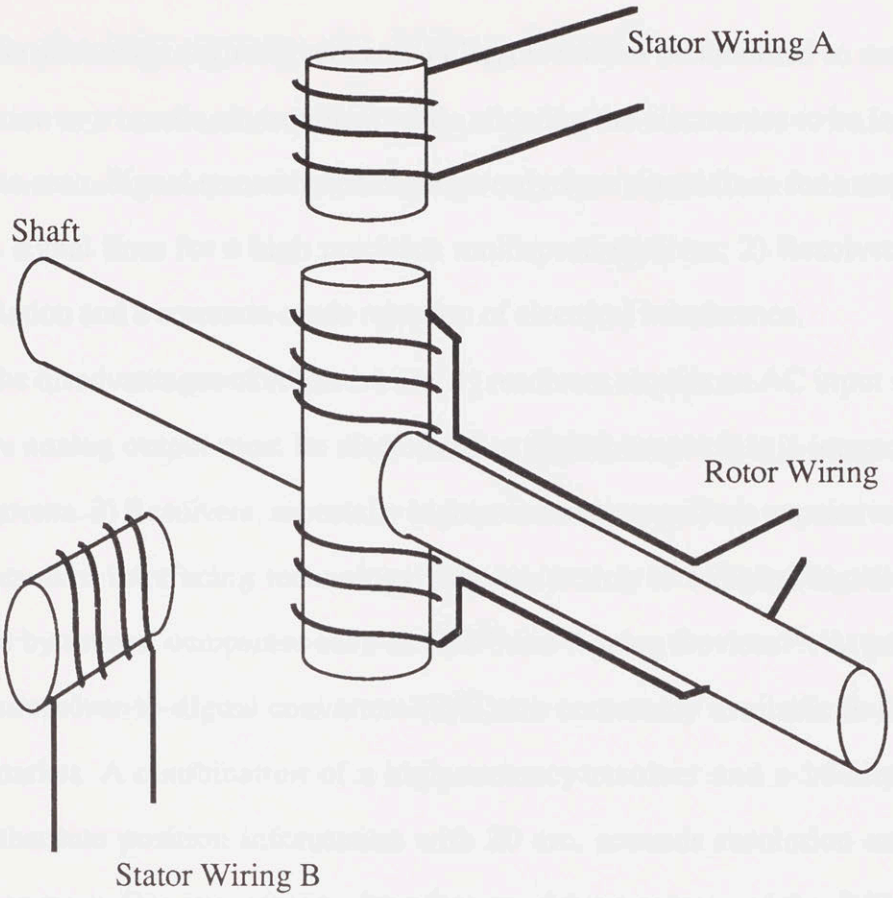

Fig. 6.2 Resolvers Construction

Most resolvers generate unique output signals for each of the 360 degrees of rotor revolution. These resolvers are known as single speed resolvers. If the number of pairs of stator windings is increased, the electrical output cycles per mechanical revolution will be increased, and then they are called multispeed resolvers. For example, a two speed resolver has two pairs of stator windings and there are two output cycles for each rotor revolution. Multispeed resolvers are more accurate than single speed ones for the same outside dimensions. Therefore, multispeed resolvers are always used in high resolution and accuracy applications. Typical accuracy for existing multispeed units is 20 arc. seconds for 36- and 64-speed, 30 arc. seconds for 16-speed, and 60 arc. seconds for 8-speed.

The advantages of resolvers are: 1) Resolvers can be mounted to measure the shaft rotation in a hostile environment while allowing the electronics to be located in a less hostile area. Signal transmission requires only four signal lines for a single speed and eight signal lines for a high precision multispeed resolver; 2) Resolvers provide signal isolation and a common-mode rejection of electrical interference.

The disadvantages of resolvers are: 1) resolvers require an AC input signal. 2) Resolver's analog output must be discretized to digital output if it is interacting with digital systems. 3) Resolvers, especially higher-accuracy types, are expensive.

Resolver interfacing technology from an analog to a digital signal has been developed by several companies such as CSI[45] and Analog Devices[46]. At present, 12- to 20-bits resolver-to-digital converters (R/D) are commonly available in the motion control market. A combination of a high-accuracy resolver and a 16-bits R/D can provide absolute position information with 20 arc. seconds resolution and 30 arc. seconds accuracy. One important positive feature of this resolver and the R/D converter is that velocity is measured as a by-product. If this velocity signal is clean and reliable, then there will be no need for a tachometer, thus, reducing the package size and complexity of both the hardware and software of the manual teaching aid.

In conclusion, high-resolution resolvers have shown positive features over high-resolution encoders in terms of a robust working environment, and velocity measurement as a by-product. The life time of resolvers is also much greater than that of encoders.

---

45 Control Sciences Incorporated, 9509 Vassar Ave., Chatsworth, CA 91311, U.S.A.

46 Analog Devices, Motion Control Group, Central Avenue, East Molesey, Surrey, KT8 0SN, England

6.2 Angle Measurement Using Resolvers

There are several methods of using a resolver to obtain precise shaft angle positions.

6.2.1 Direct Angle Technique

In this method, the rotor winding is excited by an alternating signal and the output signals are taken from the two windings in the stator. Both outputs have nearly the same time-phase angle as the original signal. However, their amplitudes differ by sine and cosine modulation caused by the position. These outputs can be fed into any R/D converter or an analog device such as a resolver chain. Nevertheless, the error sources from direct angle technique depend on the resolver's accuracy and the converter's accuracy and resolution.

6.2.2 Phase Analog Technique

In this method, the two stator windings are excited by signals that are in phase quadrature to each other. This induces a voltage in the rotor winding with an amplitude and a frequency that are fixed and a time-phase that varies with the shaft angle. The method is referred to as the "phase analog technique." This method has been widely used since it can be easily converted to produce a digital signal by measuring the change in phase shift with respect to the reference signal.

However, the accuracy of this method depends on where the crossover (where the sine signal changes from positive to negative) takes place. A source of error for this method is the noise generated by the environment. This affects the point where the crossover occurs resulting in wrong shaft angle position.

6.2.3 Sampling Technique

The sampling technique takes a sample from both sine and cosine signals at the point where the peak reference input occurs. The signals are then converted to digital signals by an analog to digital converter. The resulting digital words are used as a memory address to "look up" the shaft angle.

However, the technique is unable to deal with noise. If noise is picked up in the signal lines during the sampling period, the resulting shaft position reading will be wrong.

6.2.4 Tracking Resolver-to-Digital Converter

The tracking conversion technique overcomes all the difficulties of every technique described above. Modern resolver-to-digital converters are now cost-competitive with other methods and provide superior accuracy and noise-immunity. A tracking converter works ratiometrically. It uses only the ratio of the sine to cosine outputs of an excited resolver rotor. Since resolvers work like transformers, any excitation waveform distortion or amplitude variation appears in both sine and cosine output in the correct ratio and has little effect on the accuracy. A tracking converter contains a phase modulator. Therefore, frequency variation and incoherent noise do not affect accuracy.

Some of the resolver-to-digital converters are more sophisticated. Instead of using a single resolver, they combine a "virtual" resolver to help track position data (see Fig. 6.3). Figure 6.4 illustrates two resolvers (A and B). Resolver A will act as a transmitter. The resolver is excited and produces sine and cosine outputs as usual.

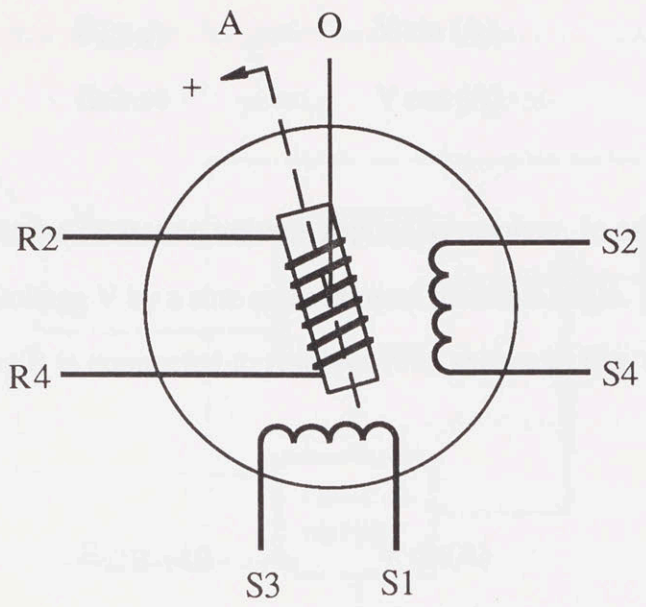

Fig. 6.3 Equivalent Resolver Schematics

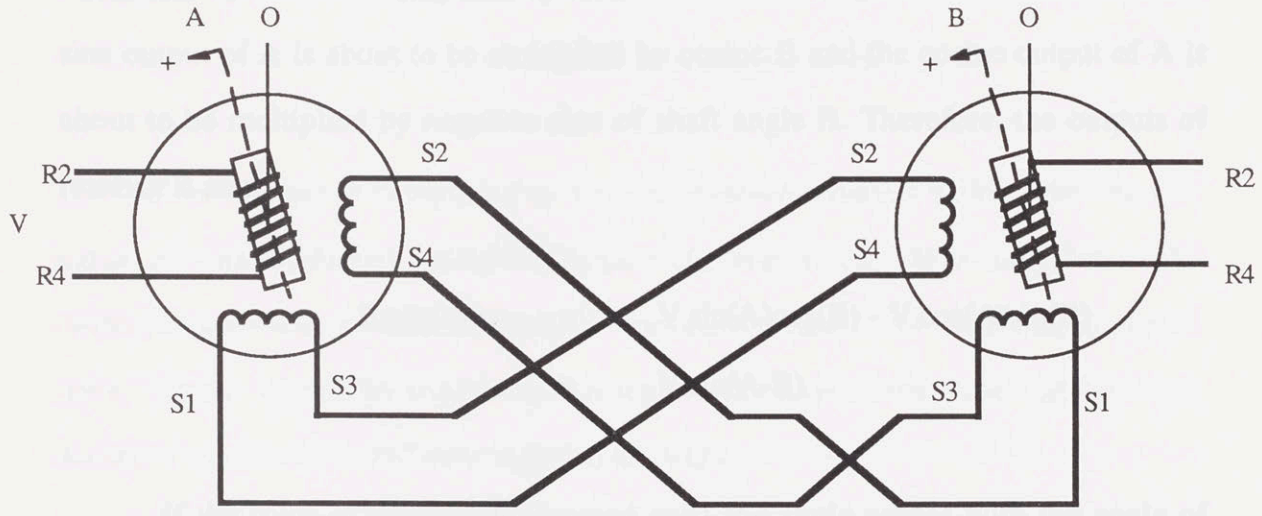

Fig. 6.4 Basic Resolver Tracking System

If the transformation ratios of resolver A and B are equal to 1.0 then the output to input signal amplitude of each resolver are equal. The output of resolver A is:

$$E_{s3\text{-}s1} = V \sin(A)$$

$$E_{s2\text{-}s4} = V \cos(A)$$

where V is the excitation voltage applied to resolver. In other words, resolver A multiplies input voltage V by a sine and cosine of the shaft angle.

If resolver B is connected to resolver A as shown in Fig. 6.4, then the resolver B's inputs are:

$$E_{s2B\text{-}s4B} = V \sin(A)$$

$$E_{s1B\text{-}s3B} = V \cos(A)$$

Resolver B is now acting as a control transformer resolver, multiplying the $E_{s1B\text{-}s3B}$ by sine and $E_{s2B\text{-}s4B}$ by cosine of its shaft angle B. In other words, the sine output of A is about to be multiplied by cosine B and the cosine output of A is about to be multiplied by negative sine of shaft angle B. Therefore, the outputs of resolver B are:

$$E_{R2B\text{-}R4B} = V \sin(A)\cos(B) - V \cos(A)\sin(B)$$

$$= V \sin(A\text{-}B)$$

If the rotor of resolver B is tuned until the angle agrees with the angle of resolver A, it may be seen that the output of resolver B would go to zero. Even if the amplifier's error is added to both resolvers A and B, the position of shaft B would be driven continually to agree with the position of shaft A.

However, if resolver B is replaced by an electronic resolver which performs sine and cosine multiplication with 'tracking' unit for the shaft angle difference, then its scheme can be illustrated as in Fig. 6.5.

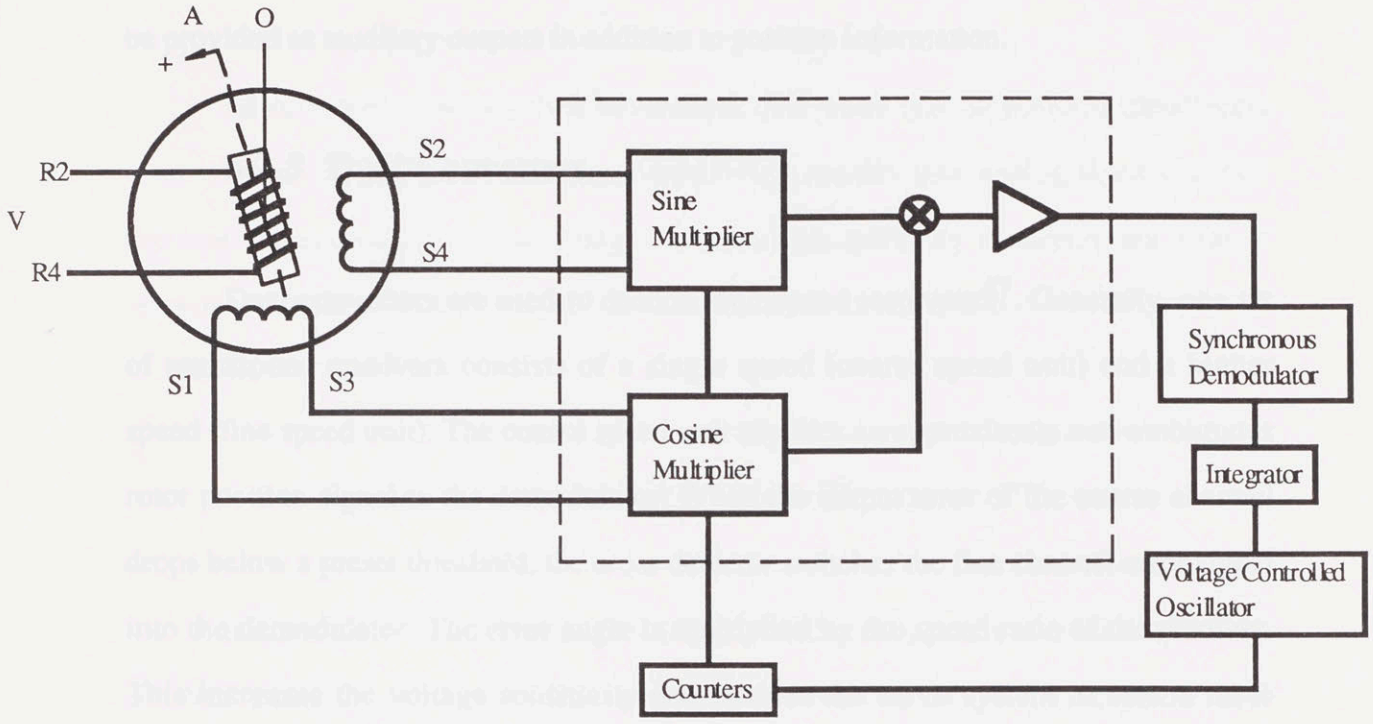

Fig. 6.5 Solid State Tracking Resolver

The shaft of resolver B is replaced by a set of up/down counters which store angle B and control the sine/cosine multipliers in the solid state circuit. The output of the VCO (Voltage Controlled Oscillator) "drives" the counters until input and output angles agree. The servo amplifier in resolver B is replaced by a synchronous demodulator and integrator that provide a DC error signal to the VCO.

A tracking converter contains two integrators. The first is a conventional analog integrator, and the second is an incremental integrator implemented by the up/down counters. Since the tracking converter consists of a closed loop system with two lags, it forms a type II servo system. The converter system exhibits negligible delays with velocity and only minor delays with acceleration. The input to the VCO is proportional

to velocity, and the input to the integrator is proportional to acceleration. Both may also be provided as auxiliary outputs in addition to position information.

6.2.5 Dual Converters

Dual converters are used to decode multispeed resolvers[47]. Generally, one set of multispeed resolvers consists of a single speed (coarse speed unit) and a higher speed (fine speed unit). The coarse speed unit supplies an approximate non-ambiguous rotor position signal to the demodulator. When the output error of the coarse channel drops below a preset threshold, the cross detector switches the fine channel error signal into the demodulator. The error angle is multiplied by the speed ratio of the resolver. This increases the voltage sensitivity and enables the servo system to seek a more accurate null. The converter continues to use the fine error signal for continuous tracking.

In conclusion, for sampling methods of the resolver, the tracking-resolver-to-digital-converter has more advantages in terms of accuracy, noise immunity, and capability to provide both velocity and acceleration among all the methods described above. In addition, the sampling method is now commercially available with 10 to 20 bit information that is adequate for the robotic aid application. Some of the resolver-to-digital converters also provide dual tracking together with tracking resolver-to-digital converter method, thus, providing much higher accuracy for position information.

---

[47] Resolver construction which has two different speed resolvers in one unit

6.3 Position Sensor Selection

Resolvers have shown their advantages over other type of position transducers since most of the DC Brushless motor controllers usually take analog signals from a resolver for commutation switching. Further, high-accuracy resolvers are able to provide sufficient *absolute* position data in terms of accuracy and resolution up to 20 arc. seconds (16 bits).

6.3.1 Resolver-to-Digital Converters Selection

Before we select a resolver, we have to investigate the availability of the resolver-to-digital converter (R/D converter). Two common high accuracy R/D converters are produced by Analog Devices and Control Sciences Incorporated (CSI). However, there are some substantial differences in detail between the two brands. Analog Devices produces several models of single chip R/D converter ranging from 10 to 16 bits. Each model differs in accuracy grades from 29.22 to 2.33 arc. min. with a tracking resolver-to-digital converter scheme. Similarly, Control Sciences Incorporated supplies families of high accuracy R/D converters with single speed and two speed resolvers (Dual tracking). The families provide a range of 10 to 20 bit resolution with 7 arc. seconds to 30 arc. min. accuracy. CSI's dual tracking R/D converter can increase the output accuracy substantially (see Table 6.3).

Table 6.3 presents the comparison of various models of resolver-to-digital converter produced by Analog Devices and CSI. A single speed resolver cannot give an accuracy better than 1.3 arc min. as our requirement. However, by implementing 2-speed tracking (Dual tracking with 2-speed resolver), the accuracy can be substantially increased to 20 arc. second which corresponds to the least significant bit (LSB) of 16-bit information.

Maker	Model	Resolution (Bits)	Accuracy	Tracking rate (rps)	Remark
Analog Devices	AD2S80	16	2 arc min	0.51	Single speed
	AD2S82	16	2 arc min	0.51	Single speed
	AD2S83	16	8 arc min	0.51	Single speed
CSI	168H100	16	1.3 arc min	3	Single speed
	168H200	16	3.5 arc min	5	Single speed
	168H800	16	1.3 arc min	8	Single speed
	168F500	16	24 arc min	2	2-speed
	168H503	16	20 arc sec	3	2-speed
	168K400	16	20 arc sec	5	2-speed
	168K500	20	7 arc sec	0.33	2-speed
	168M500	16	20 arc sec	3	2-speed

Table 6.3 Resolver-to-Digital Converter Performance

Even though CSI produces several models of 2-speed R/D converters, there are 5 models likely to be applicable to our machine. The 168F500, 168H500, 168K400 series provide 16 bit information with roughly 20 arc seconds accuracy, but differ in tracking rates. Both 168H500 and 168K400 series supply 20 arc seconds accuracy with sufficient tracking rate (236% for H500 and 394% for K400 of the required tracking rate). Between H500 and K400 series, the 168K400 series is more attractive because of the high speed tracking potential which might be necessary in the future.

6.3.2 Resolver Selection

At this stage, we have decided to use a tracking resolver-to-digital converter and two-speed tracking as the position tracking scheme. Thus we should look into two-speed resolvers that would be applicable to the selected R/D converter. The 168K400 R/D converter is applicable to 1:32, 1:36 dual-speed resolver with 20 arc seconds accuracy.

Maker	Model	Speed	Input V/Hz	Output V	Accuracy Arc min	Dimension OD	ID	OAW	Weight oz
Vernitron[48]	VRP36-10	1/32	5/2048	2.23	30/.16	2.598	1.112	.200	N/A
	VSP37-7	1/36	26/400	15.6	90/.5	3.500	2.080	.777	N/A
	VSP37-8	1/36	11.8	15.3	90/.5	3.500	2.080	.750	N/A
Harowe[49]	31RCX-300	1/32	26/1200	4.5/8.4	30/1	3.030	1.200	.600	12
Clifton[50]	SSJH19B1	1/36	10/1200	6.4/1.8	20/.5	1.840	.840	.525	3
	SSJH23A1	1/36	7/1000	3.4/1.6	6/.33	2.250	1.000	.437	4
	SSJH27B1	1/36	26/400	11.8/11.8	15/.25	2.630	1.220	.620	8.2
	SSJH31S6	1/36	26/400	3.51/3.51	5/.5	3.030	1.200	.530	5.7
	SSJH44B2	1/36	28/800	28/5.04	8/.13	4.400	3.000	.636	14
	SSJH50A1	1/36	28/800	28/5.04	12/.13	5.000	3.46	.750	18.7

Table. 6.4 Profiles of Potentially Applicable Resolvers

Table 6.4 lists the selected resolvers that are applicable to the selected R/D converter (168K400 series). Note that we prefer to have a resolver which has an accuracy higher than 0.33 arc seconds (for fine-speed) corresponding to the least significant bit of the 168K400 R/D converter. Therefore, the choice has been narrowed to VRP36-10, SSJH23A1, SSJH27B1, SSJH44B2, and SSJH50A1. The VRP36-10 is only 32-speed compared to 36-speed of the others. Thus, it will provide less accuracy with the selected R/D converter. Among the SSJH models, the 27B1 needs lower input frequency limiting the tracking rate of the R/D converter to 1000° per second. The 50A1 is quite heavy and space consuming. If we compare the accuracy of the 23A1 and 44B2, the 44B2 is 3 times more accurate than the 23A1 with acceptable weight and size.

---

48 Vernitron controls, 1601 Precision park Lane, San Diego, California 92073

49 Harowe Servo Controls, Inc. A Fasco Company, 500 Chesterfield Center, Suite 200, St. Louis, MO 63017

50 Litton Clifton Precision, Marple at Broadway, Clifton Heights, PA 79018

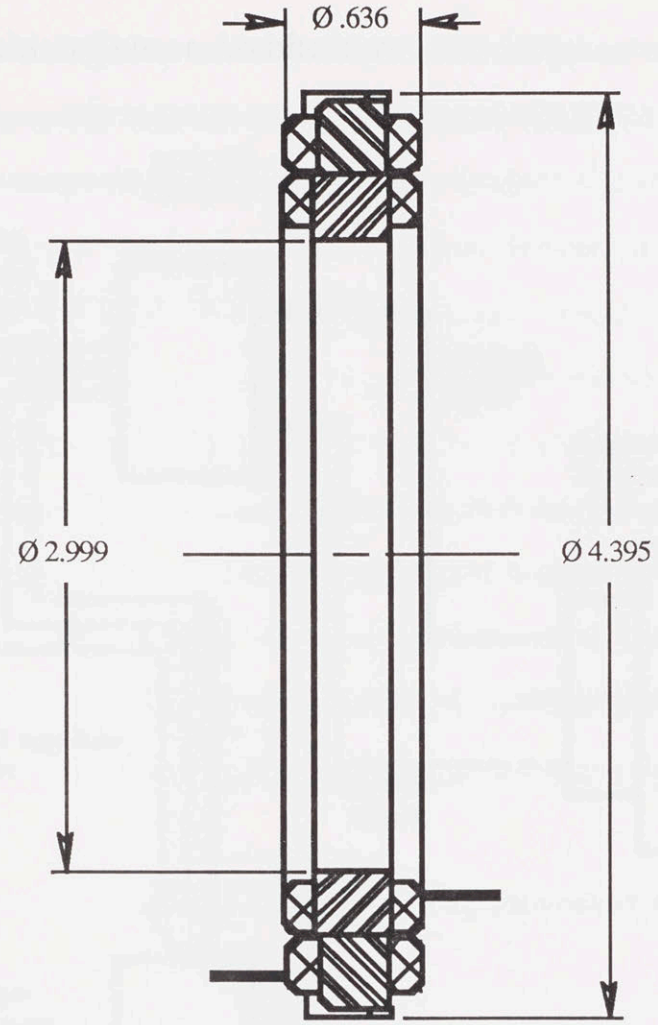

Fig. 6.6 True Size Cross Section of SSJH44B2 Multi Speed Resolver

In conclusion, Clifton precision's SSJH-44-B-2 2-speed resolver was selected as our position transducer. If the resolver is connected to CSI's 168K400 series R/D converter, the system will provide 16-bit angular position information with 0.35 arc min (root-mean-square) error and 0.46 arc min worst case. Furthermore, the system should permit 1800° per second tracking rate which is 394 percent higher than the requirement. True size cross-section of the SSJH44B2 is presented in Fig. 6.6.

6.3.3 Position Sensor Architecture

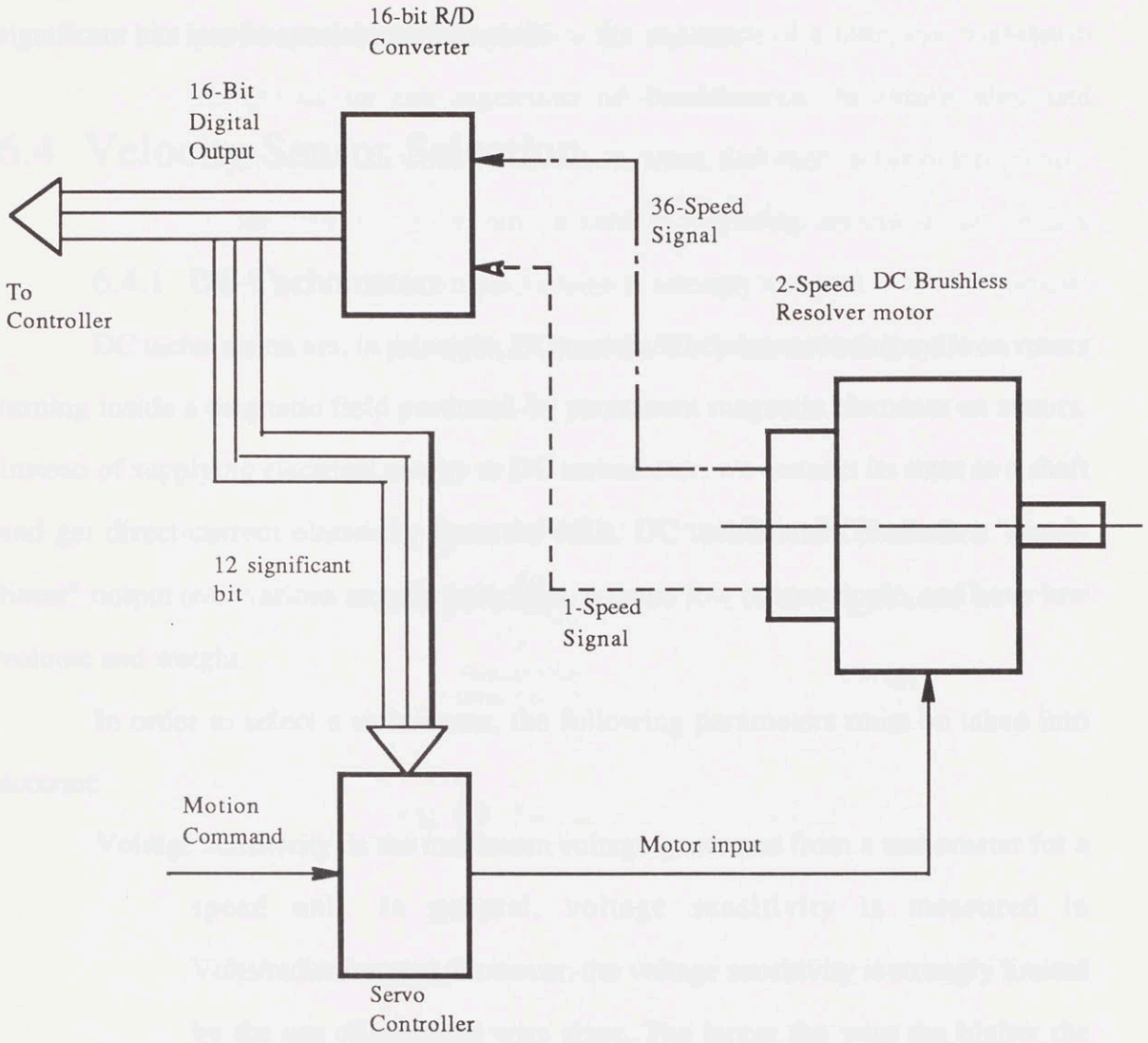

Fig. 6.7 Architecture of Position Measurement Interfacing

The robotic aid's controller requires more than 13-bit position information, while a typical DC Brushless motor controller needs only 12-bit for commutation. The position signal from the SSJH44B2 resolver is transmitted to the 168K400 high-accuracy R/D converter. The converter will convert the resolver's analog signal into a 16-bit digital output. This digital output will be used by: 1) the motion controller 2) the

servo controller to manage the commutation for the Brushless motor (see Fig. 6.7). Since the servo controller requires a lower resolution signal, we can send only 12 significant bits into its special interface card.

6.4 Velocity Sensor Selection

6.4.1 DC Tachometers

DC tachometers are, in principle, DC motors. They have rotating coils on rotors turning inside a magnetic field produced by permanent magnetic elements on stators. Instead of supplying electrical energy to DC tachometer, we connect its rotor to a shaft and get direct-current electricity from the coils. DC tachometers produce a "quasi-linear" output over various angular velocities, possess low output ripple, and have low volume and weight.

In order to select a tachometer, the following parameters must be taken into account:

Voltage sensitivity is the maximum voltage generated from a tachometer for a speed unit. In general, voltage sensitivity is measured in Volts/radian/second. However, the voltage sensitivity is strongly limited by the use of practical wire sizes. The larger the wire the higher the sensitivity of the tachometer. For low speed applications, the output voltage should be at least 20 milliVolts/rad/sec in order to get a good signal to noise ratio[51].

Ripple voltage is the voltage variation superimposed on the DC output voltage. This voltage variation is due to the fact that commutation is done in discrete steps (see Fig. 6.8).

---

51 According to Craig Bernick, Inland Motor Inc.,

The lowest frequency of ripple cycles per revolution is numerically equal to the number of rotor slots used in the design. The pattern of output in Fig. 6.8 is the signature of a complete waveform composed of the signature of fundamental armature slot and commutation frequencies and harmonics, and high frequency inductive spikes resulting from circuit switching during commutation. In low speed applications, ripple voltage is strongly coupled to the tachometer construction such as number of poles, internal windings, and slot / brush design.

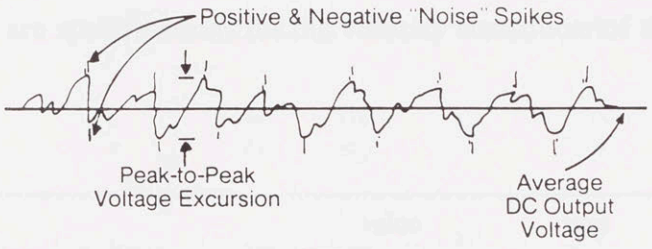

Fig. 6.8 Tachometer Output Waveform
Source: Inland Motor

Thus, proper selection is recommended for low speed tasks. However, for high speed applications, a low pass filter can be implemented to remove high frequency "noise" from the output and get a smoother signal.

Ripple frequency is the number of ripple cycles in one revolution of the armature. The low frequency ripple is numerically equal to the number of robot slots of the tachometer. The high frequency ripple is fundamentally equal to the number of commutator bars for each particular tachometer design.

Static friction is the friction torque created by the brush-commutators and magnetic field friction. However, static friction of this type is quite small compared to that of a motor.

Maximum output voltage is the maximum output voltage of a tachometer measured at the output terminals. For the robotic aid application, the number should be in the range of +/- 10 Volts since it is fed to a standard analog to digital converter.

6.4.2 Tachometer Selection

Listed in Table 6.5 are specifications for the velocity transducer of the manual teaching aid.

specification	value	unit
Output voltage at 0.008 rad/sec (min)	20	mV.
Output voltage at 8 rad/sec (max)	+/- 10	V.
Inside diameter	1-3	inches
Outside diameter	3-5	inches
Thickness	1-1.5	inches
Weight (max)	2	pound
Friction (max)	2	oz-in
Ripple voltage (max)	5%[52]	

Table 6.5 Tachometer Specifications

Table 6.6 lists some interesting tachometers which are commercially available. The performance of each tachometer is calculated from Inland Motor's catalog. Note that the outputs are estimated at two different angular velocities. The maximum speed of 8 radian/second is estimated from the necessary speed of the end-point given that the

52 Percent of rated output voltage

end-point must move with 9 inches amplitude at a frequency of 2 hertz. Similarly, the minimum speed of 0.008 radian/second is also estimated from the criteria that the end-point must move 0.5 inches in 1 second with worst arm orientation[53].

model Voltage Sensitivity V/rad/s	Output @ 8 rad/s V	Output @ 0.008rad/s mV	Ripple voltage %	Ripple freq. cy/rev	Ripple@8rad/s Voltage mV	Ripple@8rad/s Freq. Hz	Ripple@0.008rad/s Voltage mV	Ripple@0.008rad/s Freq. Hz
TG-2936								
1.1	8.8	8.8	0.5	91	44	116	.02	.06
1.4	11.2	11.2	0.5	91	56	116	.03	.06
1.75	14	14	0.5	91	70	116	.04	.06
2.2	17.6	17.6	0.5	91	88	116	.04	.06
TG-2939								
2	16	16	4	41	640	52	.32	.03
TG-2913								
1.3	10.4	10.4	4	41	416	52	.21	.03
1.6	12.8	12.8	4	41	512	52	.26	.03
TG-2169								
1.38	11.04	11.04	5	33	552	42	.28	.02
1.75	14	14	5	33	700	42	.35	.02
TG-2138								
1.02	8.16	8.16	5	33	408	42	.20	.02
1.38	11.04	11.04	5	33	552	42	.28	.02

Table 6.6 Tachometer Performances

All the tachometers meet most of the specifications except for output voltage which is an extremely important parameter. The operation speed range of the manual teaching aid is much wider than that of the practical limitation. For example, if a tachometer outputs 20 milliVolts at 0.008 radians/second, it is supposed to give 20 Volts at 8 radian/second. On the other hand, if a tachometer gives 10 Volts at 8 radians/second, it should produce 10 milliVolts at 0.008 radians/second. However, if

53 Full extended arm and the end-point is at the farthest point from its pivot

we focus on ripple voltage and frequency, the TG-2936 model has lower ripple amplitude than any other tachometer. Since the number of slots and phases on TG-2936 is higher than the others, it yields out higher ripple frequency that enhances implementation of a low pass filter. In other words, the TG-2936 DC tachometer has shown it's advantage over other models in terms of ripple voltage and frequency.

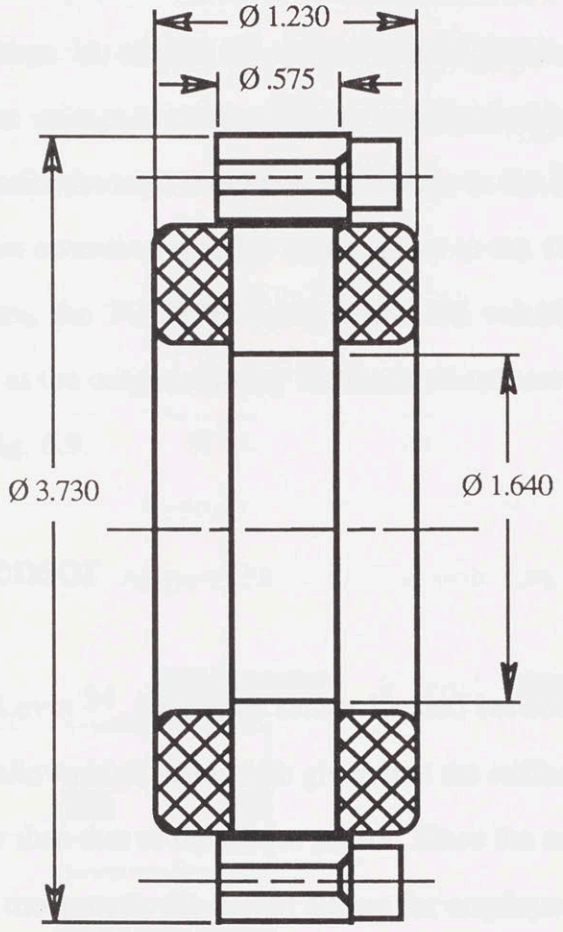

Fig. 6.9 True Size Cross Section of TG-2936 Tachometer

Furthermore, the TG-2936 still has various windings available ranging from 1.1 to 2.2 Volts/radian/second. Since the output voltage specification is not consistent between maximum and minimum operating speed, none of the TG-2936 windings can

perfectly match the specification. In order to determine the suitable winding we have to decide on the primary operating speeds.

Observations at the Spaulding Rehabilitation Hospital indicate that most of the patients are so weak and the chance that they would be able to make high speed moves is low. Furthermore, the duration in which any patient can conduct high speed motion is much shorter than that of the low speed motion. Inland Motor has suggested that the minimum output voltage be around 20 mV to obtain good signal to noise ratio. Considering the output voltage corresponding to maximum operating speed, the TG-2936 with 1.75 volt/radian/second should be preferable to the 2.2 version because its output at the maximum operating speed is much closer to the 10 Volts A/D converter requirement. Therefore, the TG-2936 model with 1.75 volt/radian/second voltage sensitivity is selected as the output velocity feedback transducer. The actual size cross section is shown in Fig. 6.9.

6.5 Torque Sensor

According to Levin [54], the torque sensor located between the actuator and the output shaft (in-line) allows high bandwidth given that the stiffness of the transmission system is much higher than that of the torque sensor. Since the actuators operate within 270 degree rotational movement, the design allows for employment of reaction torque sensors instead of more complex rotating types. Reaction torque sensors basically use a strain gage without slip rings, a torsional variable differential transformer (TVDT), or a phase shift device as in rotating types which always introduce noise and brush friction. Reaction torque sensors are generally much more compact than rotating torque sensors. They can be located inside the actuator housing, producing a clean compact package. In

---

54 Levin, M.D., *Design and Control of a Closed-Loop Brushless Torque Actuator*, MIT SM Thesis, 1990.

addition, the simple strain gage beam will not be affected by the high magnetic field inside the motor allowing the actuator and torque sensor to be installed side-by-side to give a compact actuator package.

Reaction torque sensors are commonly available ranging from a few ounce-inch to several hundred thousand pound-inch. A nice reaction torque sensor should have high stiffness, compact size, low nonlinearity, low hysteresis, and low temperature effect. For our robotic aid application, the selected Brushless actuator produces 3502 ounce-inch rated torque with 1165 ounce-inch continuous torque, therefore, the torque sensors should operate in this torque region.

Make	Model	Rated Output (oz-in)	torsional Stiffness (in–lb/rad)	Nonlinearity % of R.O[55].	Hysterisis % of R.O.	Temp eff. % of Load/F
Transducer Techniques	TRT-200	3200	20,375	0.1	0.1	0.005

Table 6.7 Performance of TRT-200 Reaction Torque Sensor

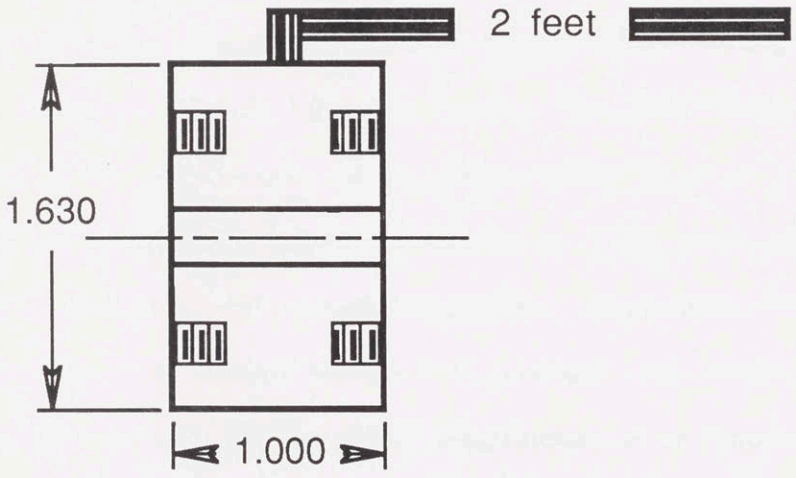

Fig. 6.10 True Size Cross Section of TRT-200 Reaction Torque Sensor

55 Rated Output

Transducer Techniques produces a light and small high performance reaction torque sensor (1.5 in. OD and 1 in. OAW) which is very suitable for our application. One nice feature is its small size which permit this torque sensor to be installed *inside* the actuator package. The performance and true size cross-section of the TRT-200 reaction torque sensor from Transducer Techniques are shown in Table 6.7 and Fig. 6.10.

Chapter 7

Actuator and Arm Design

7 Actuator and Arm Design

7.1 Installation Requirements for Actuator Package Design

7.1.1 RBE-3003-AOX Brushless DC Motor

Basic elements of the actuator package are 1) Inland Motor's RBE-3003-AOX[56] Brushless DC motor 2) Clifton Precision's high accuracy two speed resolver model SSJH44B2, 3) Transducer Techniques' TRT-200 reaction torque transducer, and 4) Inland's TG-2936-B high performance tachometer. Ideally, they should be aligned on a single motor shaft that is directly coupled to the arm's shoulder joint. However, packaging design of the drive unit is strongly dependent on special requirements of each element. For example, easy accessibility must be arranged for a unit which requires frequent maintenance.

Since there is no contact between stator and rotor, RBE-3003-AOX Brushless DC motor requires no mechanical maintenance. Hence, both the rotor and the stator are sensitive to stress, it is recommended that they be retained by two separate retainer rings bolted externally to the shaft and motor housing. The stator housing bore should should extend to a depth slightly less than the stack length of the stator. A shoulder for the stator to bank against should be placed inside the bore. The inside diameter of the shoulder should be slightly greater than the maximum dimension shown over the windings and encapsulation. A small portion of the laminated stack should pilot into the counterbore of the stator's retainer ring. The inside diameter of the retainer ring should be the same as the inside diameter of the banking shoulder in the stator housing. The

---

56 Suffix A means 100 V. line-to-line motor wiring, OX means a special model for this particular therapy application where key arrangements are required. All other performances is the same as Inland's RBE-3003-A.

outside diameter of the clamp ring must be large enough to accommodate the clamping screws. These screws should pass through the clamp ring and thread into the tapped holes in the stator housing, axially clamping the stator in place. Figure 7.1 and 7.2 illustrates an mounting arrangement of a rotor and a stator.

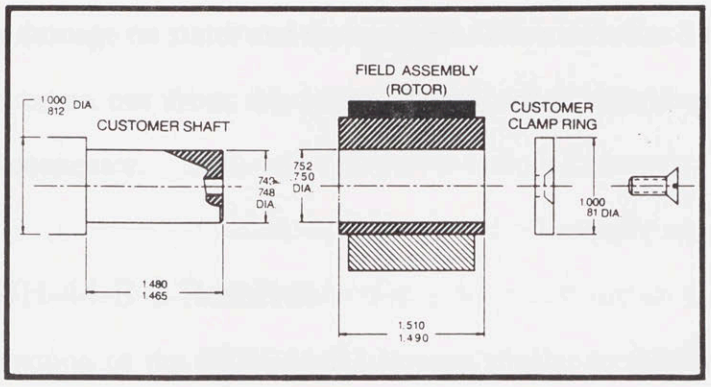

Fig. 7.1 Example of Stator Mounting
Source: Inland Motor, DC Brushless Motors and Servo Amplifier

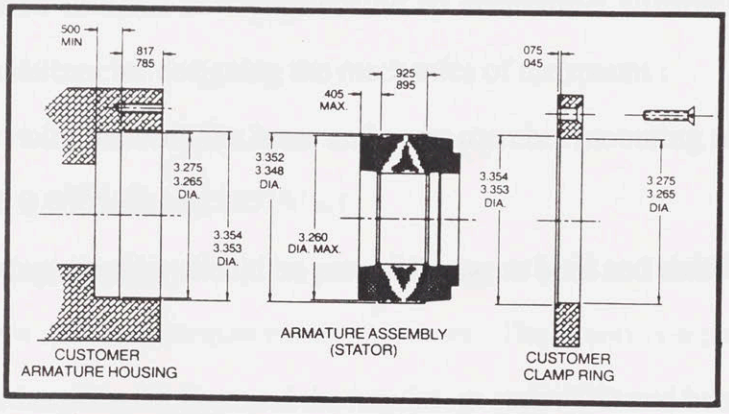

Fig. 7.2 Example of Rotor Mounting
Source: Inland Motor, DC Brushless Motors and Servo Amplifier

Another retainer ring is also recommended for the rotor. The rotor should bank against a shoulder on the shaft when mounted and should not cover the magnet

surfaces. The concentricity of the rotor and the stator *must be within 0.004 inches* when mounted.

When installing the rotor into the stator's bore, the powerful rotor magnets can create unmanageable forces colliding the rotor into the stator. Therefore, a sheet of mylar slightly thinner than the clearance between the rotor and the stator may be inserted to prevent damage on stator and the magnets. The motor has 3 teflon-coated, 6 inch wires which come out from the stator. These wires should go directly to a specially arranged connector.

7.1.2 SSJH-44-B-2 Resolver

The construction of the SSJH-44-B2 is very similar to the Brushless motor. Here again, the rotor and stator are sensitive to the mounting stress, and the same retainer arrangement as the motor installation, is used. Since the resolver construction has no mechanical contact, no mechanical maintenance is required. This allows the sensor to be located in areas that may not be so accessible. Clifton Precision has provided some guidelines for designing the mechanics of the mount :

1. Eccentricity between the inner and outer member mounting surfaces should not exceed 0.0005 inches.
2. Mounting shoulder should be perpendicular to bore and shaft within 0.0005 inches.
3. The fit between the bore and the maximum stator OD and between the shaft and the minimum rotor ID should be from 0.0002 to 0.0005 inches. This will assure that there is no line-to-line or interference fit.
4. Axial misalignment or variation in mounting dimensions between the rotor and the stator mounting surfaces should not exceed 2 percent of the stack height. For example, if the stack height is 0.250 inches the axial misalignment should not exceed 0.005 inches.

Due to defective hardware or buildup tolerance violating the above guidelines, some deviation and change in electrical characteristics is anticipated. The degree of deviation depends on the air gap clearance and the number of poles in the resolver. Axial offset results in a slight decrease in accuracy, deviation of null voltage which is usually used as an index point, decrease of the ratio between the resolver's output and input (transformation ratio), slight shifting of phase, and increase of input current and power. Radial offset has a similar impact as axial offset, but differs in severity. Accuracy will decrease proportionally to radial offset, but the degree of severity on transformation ratio, phase shift, and input power and current is lower. Rotor or stator tilt within 0.001 to 0.002 inches with respect to each other will have very little effect on any parameter. However, greater tilt must be avoided to prevent rotor and stator from making contact.

Note that there are seven wires coming out of the rotor. These wires must rotate with the shaft before reaching the connectors. Eight additional wires come out of the stator.

7.1.3 TG-2936-B Tachometer

Due to the existence of a brush arrangement, the TG-2936-B tachometer's construction differs from the resolver and the motor. The brush is a set of electrical contacts bridging the induced current on the rotating shaft (rotor) to a stationary part (stator), and thus, requires service, maintenance, and occasional replacement. As a consequence, the tachometer should be installed at a location that permits easier accessibility. The tachometer stator has built-in bores allowing the stator to be mounted on the housing shoulder directly with countersunk flat head socket cap screws. The rotor may be installed on the motor's shaft with a retainer ring. The TG-2936-B tachometer has only 2 wires coming out from the stator.

7.1.4 TRT-200 Torque Sensor

The TRT-200 reaction torque sensor is the smallest transducer in the system. Its 1.630 in. OD is smaller than the ID of motor and resolver rotors, therefore, allowing the torque sensor to be installed concentrically within the Brushless motor or the resolver rotor bores. Since the torque sensor acts as a coupling unit, it can be used as a coupling between the drive unit and the shoulder joint to account for slight misalignment of installation and bending due to load. The TRT-200 has two 0.25 in. pilot bores on each side that help align the motor shaft with the shoulder joint connector. Here again, there are four 28-AWG wires coming out from the torque transducer, and these wires must rotate with the motor's shaft before reaching their connectors, just as the resolver rotor's wires do.

7.2 Actuator Design

7.2.1 Actuator Package

According to all installation requirements, the actuator package was mechanically designed as shown in Fig. 7.3. The tachometer is mounted behind to permit accessibility by opening the rear cover plate (no.26). Radially around and back of the tachometer is a chamber where all the wires from the motor and sensors gather. These wires are sectioned to the connectors along the circumference of the rear housing (no.21). Similarly to the tachometer, the accessibility to these wires and connectors is through the rear cover plate. The tachometer's stator is mounted against the special shoulder and bore arrangement on the rear housing. The tachometer's rotor is clamped on the motor's shaft with a retainer ring. The rear housing has one low friction deep groove ball bearing (no.22) supporting the motor's shaft (This is made possible by designing a shoulder step or lip where the rear and mid housings join to provide

alignment and concentricity). The bearing's housing also acts as a "magnet shield wall" preventing the motor's high magnetic field from interfering with the the tachometer's function and operation.

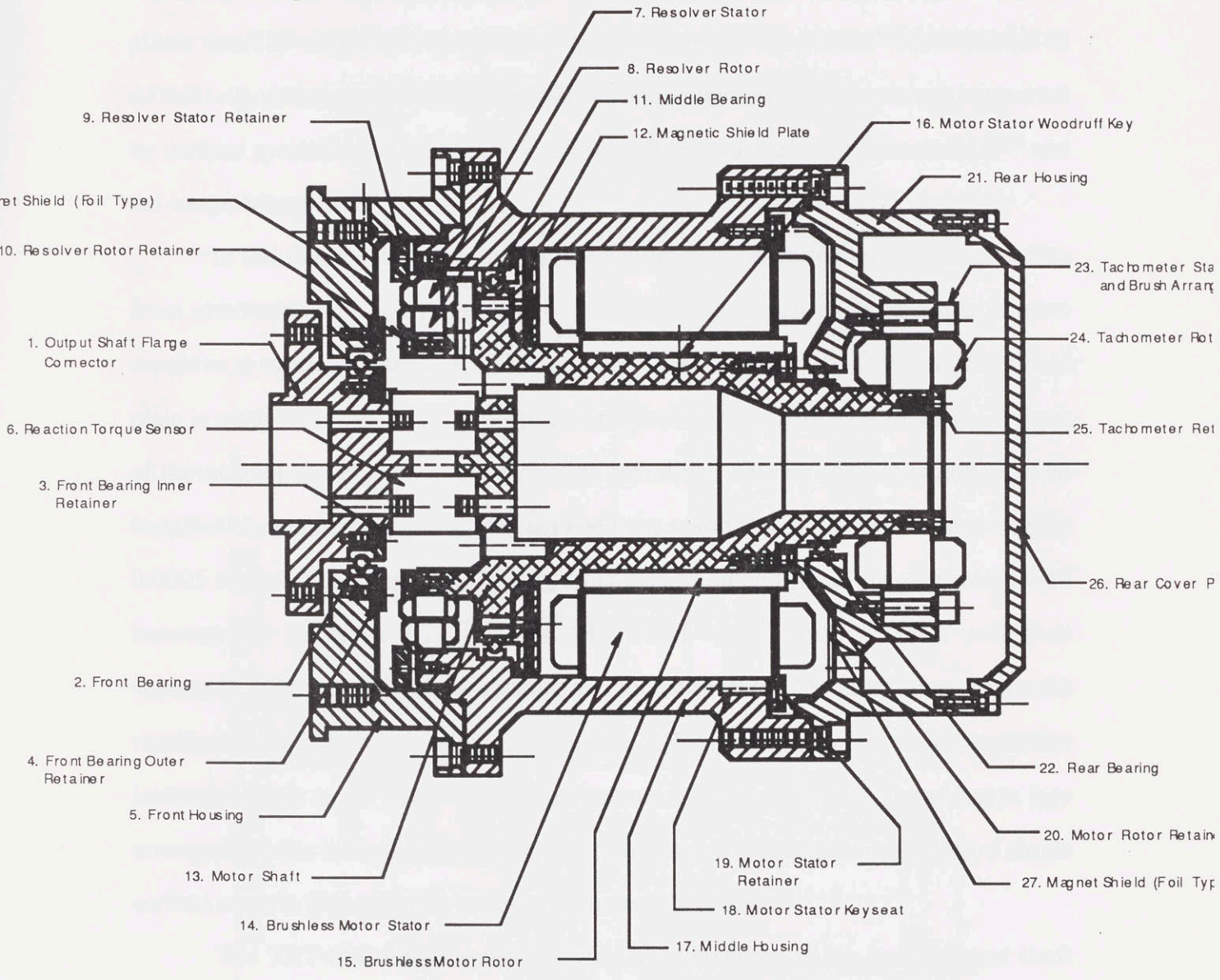

Fig. 7.3 Cross Section of Designed Actuator Package (scale 1:2)

Adjacent to the rear housing is the mid housing on which the Brushless motor is mounted. Both the motor's stator (no.14) and rotor (no.15) are clamped by two

separated retainer rings (no. 19 and 20) before the housing is put in place. Note that both the stator and rotor have individual key arrangements (no.16 and 18) to index relative position for reassembly procedure. In front of the motor are magnetic shield plates (no.12) which are compressed of one sheet of coro-steel[57], two sheets of ADMU-48, and two sheets of ADMU-80[58]. This shield arrangement is recommended by various specialists in the magnetic shield industry such as Vacuumschmelze[59] and Ad-vance Magnetics[60], Inc.

In this design, the motor has its own chamber to keep the motor's magnet flux from interfering with the resolver and the tachometer. Because the resolver is more sensitive to electromagnetic interference than the tachometer, the front magnet shield plate is made of several high-performance magnetic shield materials in series. In front of the magnet shield plate is a low friction radial ball bearing (no.11) which must be installed to maintain concentricity between the resolver's stator and rotor to within 0.0005 inches. The housing for this bearing acts as an additional magnet shield wall between the motor and the resolver. The SSJH-44-B-2 resolver (no.7 and 8) is separately clamped on the mid housing and motor shaft by 2 retainer rings. Since the resolver is ultimately sensitive to geometric offset, tolerances at these particular locations have to be very critical and accurate. The resolver's stator has a key arrangement for indexing. However, the rotor has no mechanical index but a single scribed mark to help align the stator in the assembly process.

The TRT-200 torque transducer (no.6) is installed in the bored motor shaft concentrically with the resolver's rotor. Note the hollow bore arrangement in the motor shaft to reduce moment of inertia and weight. TRT-200 is bolted to the motor shaft with four socket cap screws inserted inside the shaft's hollow bore.

---

57 100% iron

58 Soft magnetic materials from Ad-vance Magnetics Inc.

59 Vacuumschmelze GmbH, Werk Hanau, Gruner Weg 37, 6450 Hanau, Germany

60 Ad-vance Magnetics Inc., 625 Monroe St., Rochester, IN 46975

7.2.2 Transmission Design

According to Chapter 4, the direct-drive concept was selected for the manual teaching aid. The design incorporates a rigid shaft supported by several bearings. One

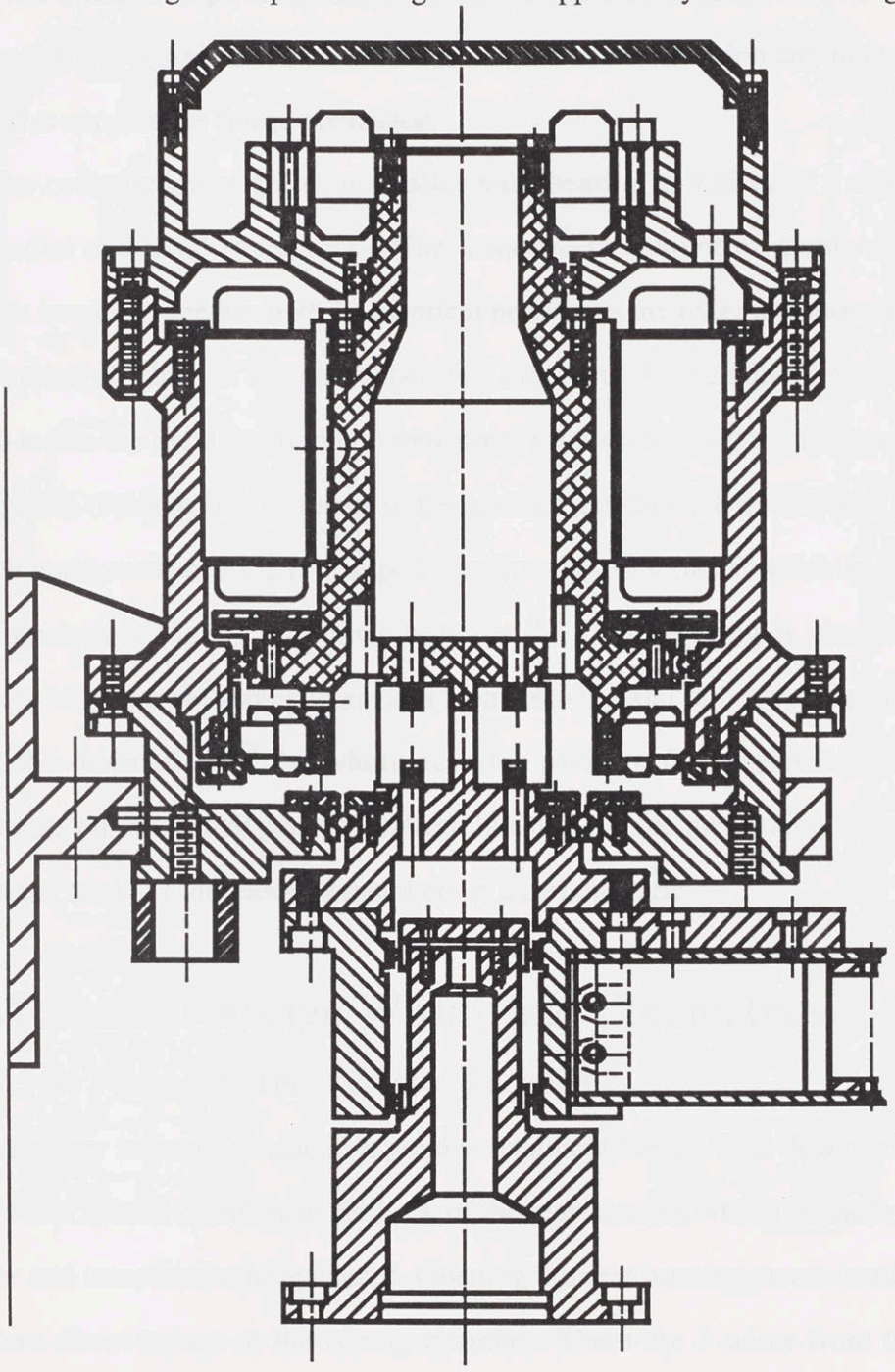

Fig. 7.4 Cross Section of Designed Actuator Package with Shoulder Joint (scale 1:2)

way to achieve transmission rigidity and light weight is to minimize the shaft length. Referring to Fig. 7.3 and 7.4, the output shaft flange connector (no.1) is designed as the transmission shaft connecting the torque transducer to the shoulder joint. The flange is made with a step to align the shoulder joint concentrically with the motor's shaft. One four-point-contact (gothic arch) ball bearing (no.2) with low friction and high accuracy is installed to support the flange connector.

The construction of gothic-arch allows the bearing to withstand a combination of both radial and axial forces, including a moderate amount of moment. In other words, this bearing, together with its identical bearing in the other actuator package, is used to support all kinds of forces and bending moments. At the same time the bearing is used to locate the axial location between every rotor on the motor's shaft to its stator on the housing (bearing arrangements in the actuator package are float-type). The outer ring of the gothic-arch bearing is clamped into front housing (no.5) which is part of the robot's foundation. Figure 7.4 shows how the the front housing is clamped to the foundation. Note the pin arrangements on front housing and the clamping mechanism to index the orientation of the whole actuator package for reassembly. Threaded arrangements on the frontal part of the front housing are for mechanical stops to limit the rotational travel of the shoulder members to a certain angle.

7.3 Actuator Package Wiring and Connections

7.3.1 Wiring in The Actuator Package

Wiring is a very important issue in a good mechanical design. The designed actuator package has a special chamber in the back of the rear housing where all the wires from the motor and transducers are gathered. Opening the rear housing cover (no.26 in Fig. 6.1) allows direct access to the wiring chamber. There are 3 wires from the motor stator. These wires get in the wiring chamber through a special hole just on the right and top of the motor's stator (see Fig. 7.5). These wires need a separate connector as

they transmit high power and are likely to generate electromagnetic flux. The resolver's stator is located far from the wiring chamber, and there is no internal path for the wires to get to the chamber except externally.

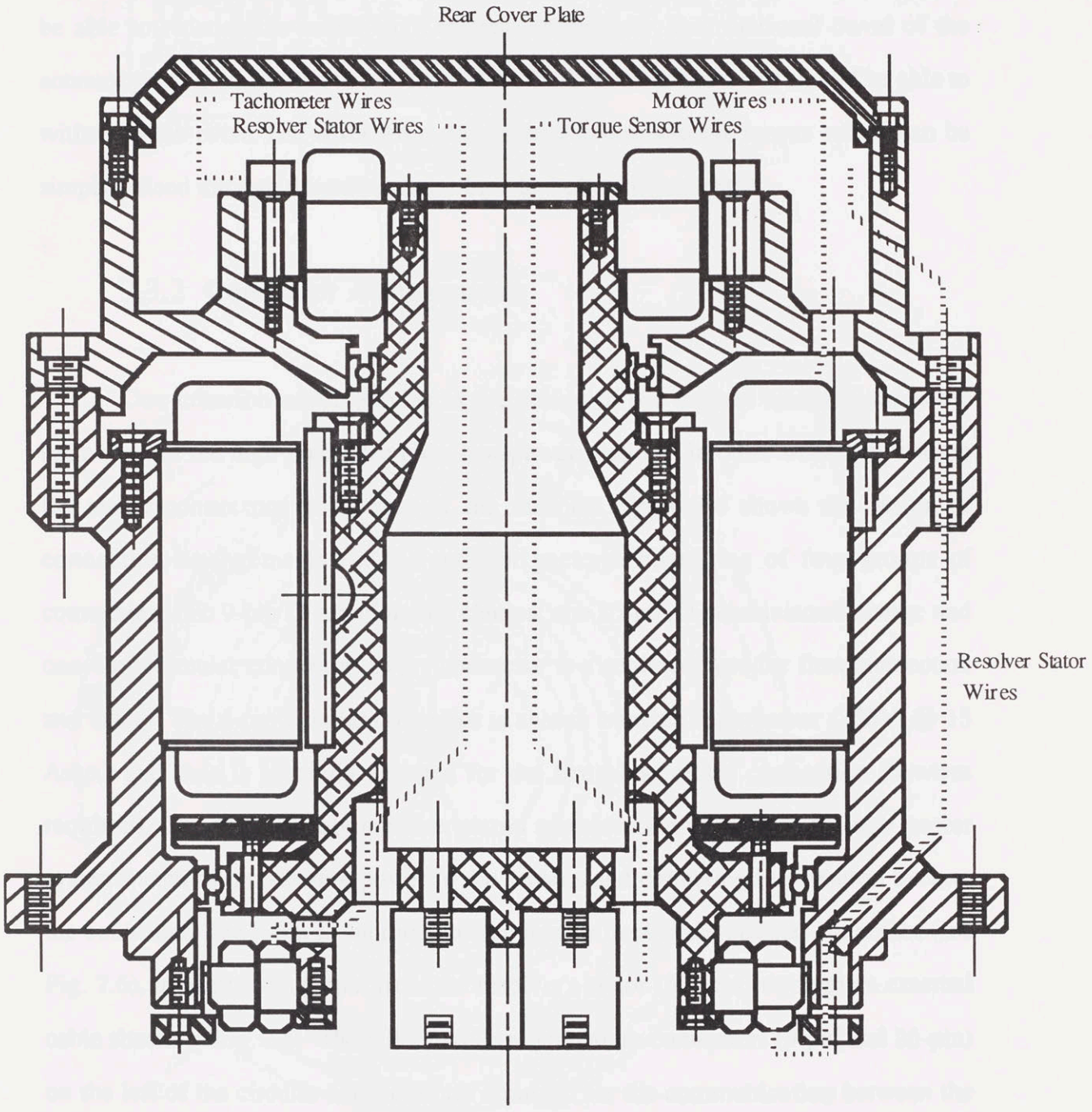

Fig. 7.5 Wiring Routes of Actuator Package (scale 1: 1.25)

This group of wires goes out of the mid housing body through a special bore to be clamped along the housing body and enters inside the wiring chamber through a connector. The wiring from the rotating sensors is more complicated as the wires must be able to twist as the motor shaft rotates. Fortunately, the rotational travel of the actuator package is limited to less than 270°. Thus, most of the wires should be able to withstand the twist. The wires from the resolver's rotor and the torque sensor can be simply passed through the wiring holes into the hollow motor shaft.

7.3.2 Connector Arrangements

One criterion which applies to the design of the manual teaching aid is the separation of the high-power from the low-power sections. In other words, separating the motor connectors from those of the sensors. Figure 7.6 shows the design of connection arrangements for the actuator package consisting of four groups of connectors: two 9-pin D-subminiature clamps; one 25-pin D-subminiature clamp; and one 4-pin circular connector. Every connector is a soldered type for firm connection and safety. The 4-pin circular connector is able to transmit high-power (250V. @ 13 Amp.) and thus is specially selected for the Brushless motor connection (3 wires required). The other D-subminiature clamp connectors are used for the low power systems such as transferring power to the sensors and collecting information back to the controller. The 9-pin D-subminiature connector next to the circular connector (see Fig. 7.6), transmits the output from the resolver's stator (8 wires) through an external cable shown in Fig. 7.5. The other two D-subminiature connectors (9-pin and 25-pin) on the left of the circular connector are arranged for the communication between the controller and the actuator package. The 9-pin connector is used for transferring the resolver's rotor signals to the R/D converter in the controller unit where the 25-pin-

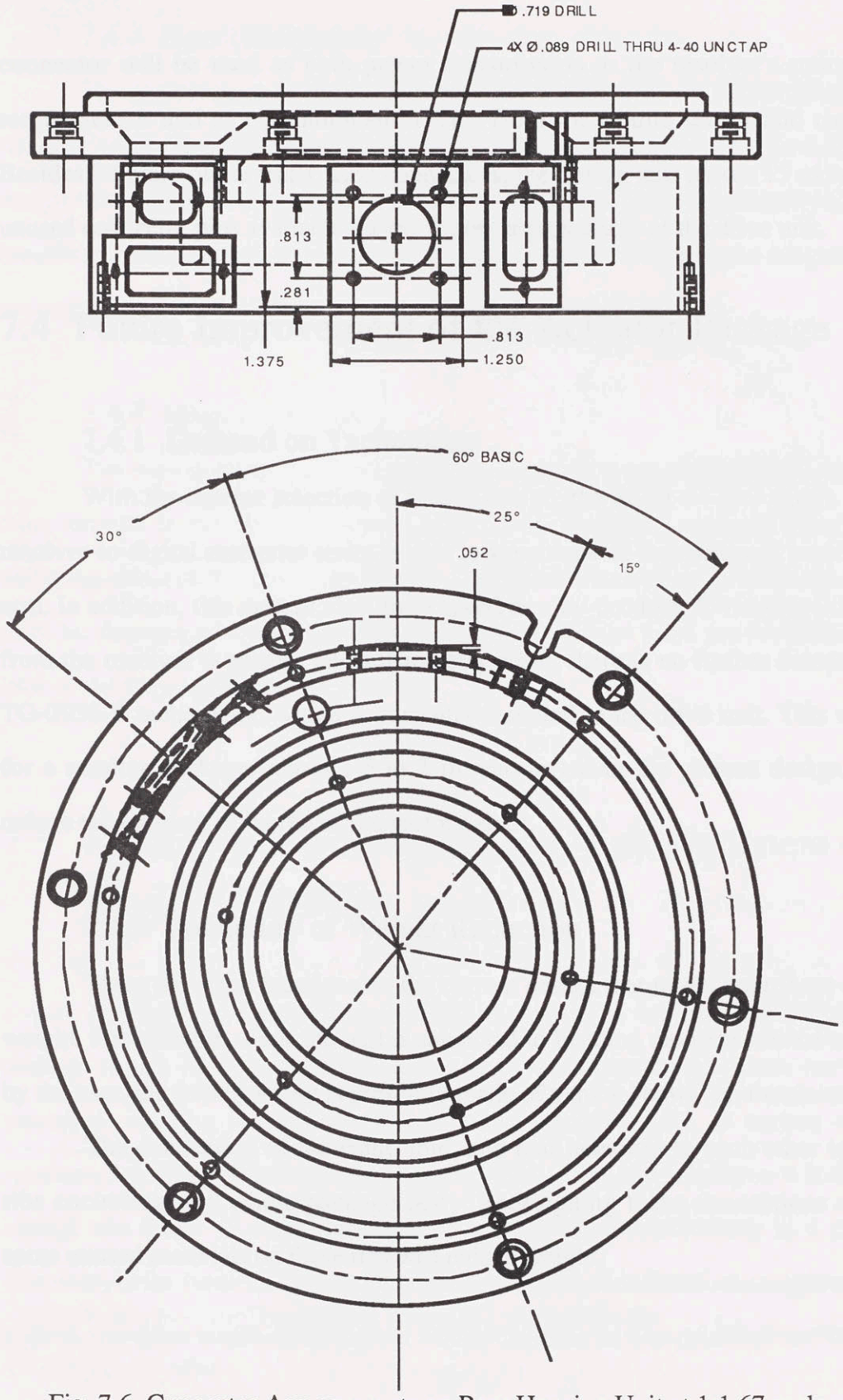

Fig. 7.6 Connector Arrangements on Rear Housing Unit at 1:1.67 scale
(Detail in DWG#M09B)

connector will be used as both power transmission to the resolver's stator and the torque sensor and as communication lines from the torque sensor and tachometer. Besides 24 pairs of currently used connectors, the design still leaves 15 more pairs of unused connector pins available for the future improvement of the drive unit.

7.4 Future Improvement of the Actuator Package

7.4.1 Demand on Tachometer

With the current selection of sensor design, the SSJH-44-B-2 with a 168K400 resolver-to-digital converter series is able to keep track of the rotational position of the arm. In addition, this system also gives speed as a by-product. If velocity information from the resolver is precise and sufficiently clean, there is no further demand for the TG-2936-B tachometer, which is currently installed in the drive unit. This will allow for a smaller package (about 1.5 to 2 in. shorter) than the present design and will reduce the moment of inertia of the motor's shaft.

7.4.2 Possibility of Weight Reduction

There are some locations on the current design that might contribute excessive weight. For example, since the part is subjected to bending moment created on the arm by the user, the front housing is presently made of a thick "bowl" of aluminium.

The connection of the front, mid, and rear housings to each other is made of ribs encircling the whole package body. Redesigning these connections or cutting some unused materials on these ribs will reduce weight.

7.4.3 Heat Dissipation

The performance of the Brushless motor is dependent on the rated temp of the winding which is always specified at 155°C. At present, the current heat dissipation design of the drive unit depends on natural convection. If natural convention is proven insufficient, forced convection, either by axial or cross flow, must be adapted into the actuator package to cool down the overheating stator winding.

7.4.4 Magnet Shields

The current design of the magnet shield uses recommendations and experiences from experts in the field. However, there is no analytical analysis describing the shielding effect of this particular design. The effectiveness of the current shield design must be determined experimentally. If the shield fails to work successfully, a closer look at the magnet shield must be taken.

7.5 Determination of Profile and Wall Thickness of the Arm Members

The choice of materials to be used as the robot's arm is quite important. The material should be light, rigid and easy to be formed or machined. Since our robot is a prototype, looking into advanced composite materials such as carbon epoxy, or reinforced plastic structure may not be beneficial at this stage, because it is difficult to change the shape of these materials as is undoubtedly necessary in a prototype. However, in the future, a composite material might be considered as a replacement. For a given end-point inertia specification, aluminium alloy is well qualified for the arm.

7.5.1 Cross Section Profiles of Arm Members

The most common cross section profiles of robot arms are rectangular and circular tubes. We can treat square tubes as a special case of rectangular tubes where all sides are equal.

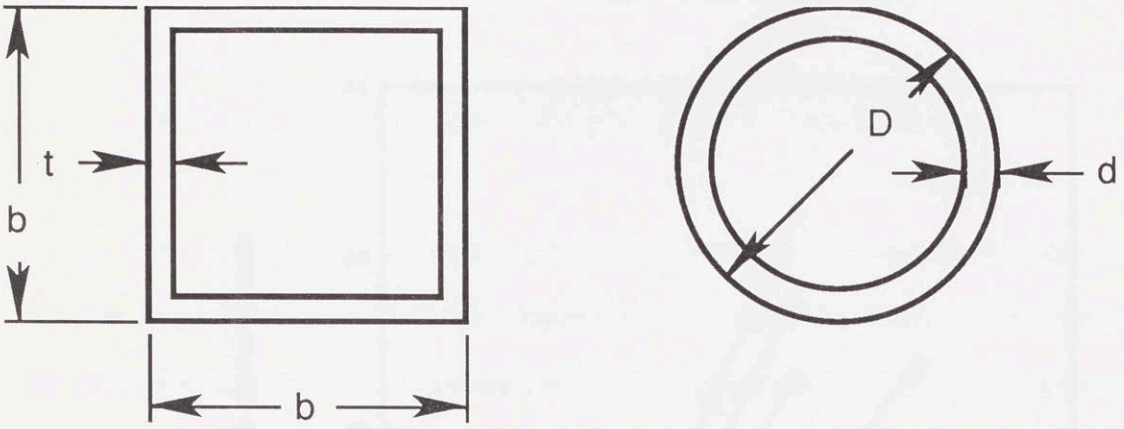

b	Outside width/height of square structure
t	Thickness, square structure
D	Outside diameter, circular tube
d	Thickness, circular tube

Fig. 7.7 Square and Circular Tube Structures

Consider the square and circular tubes in Fig. 7.7. Given that they both have the same mass per unit length (M_{sq} for square tube and M_{cir} for circular tube) and outside dimension (b = D), where

$$M_{sq} = b^2-(b-2t)^2 = M_{cir} = \frac{\pi}{4}(b^2-(b-2d)^2)$$

therefore, d can be determined from

$$d = 0.5\left(b-\sqrt{b^2-16(b-t)t/\pi}\right)$$

Consider the mass moment of area (I) of both cross-sections.

For the square tube,

$$I_{sq} = \frac{1}{12}\left(b^4-(b-2t)^4\right)$$

and for the circular tube:

$$I_{cir} = \pi/64\left(b^4 - (b-2d)^4\right)$$

The product of E and I determines the stiffness of the structural member due to external forces where E is the modulus of elasticity and I is the moment of area of the cross section about a horizontal line which passes through its center of area. Increasing the

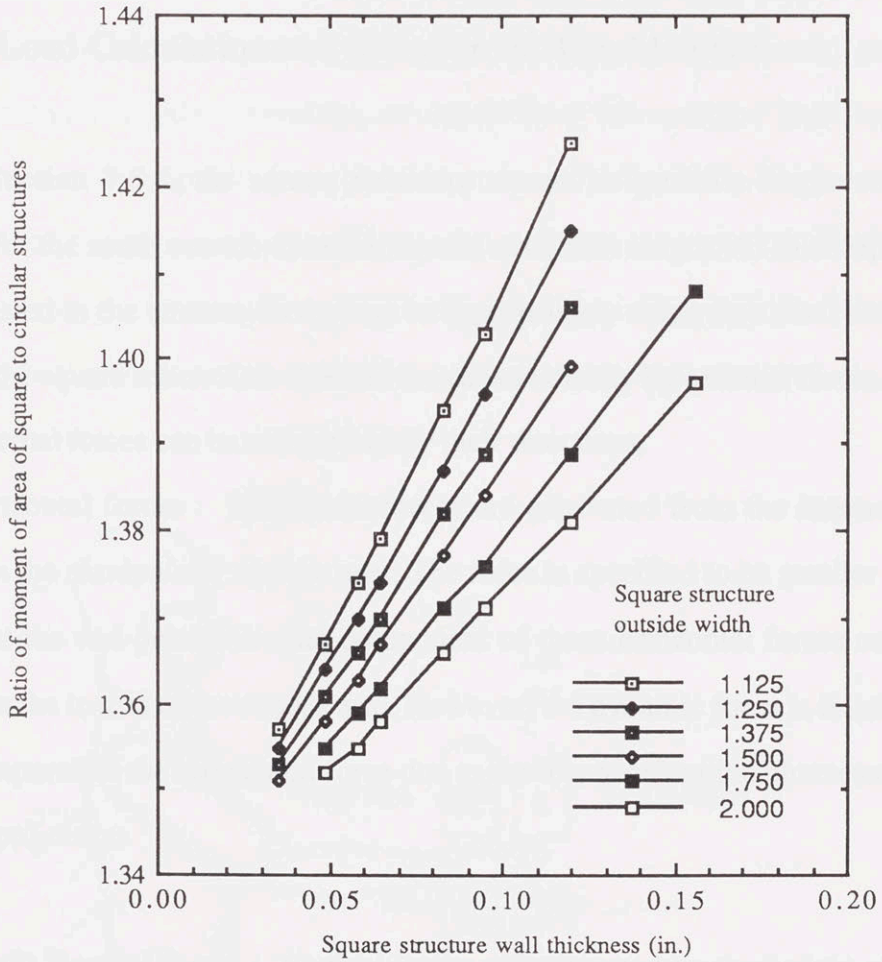

Fig. 7.8 Ratio of Moment of Area of Square to Circular Tubes

product of EI means the system is stiffer, resulting in a higher structural natural frequency. Therefore, the idea is to select the structural member, between square and circular tubes, which provides the highest moment of area (I) given the same mass per

unit length, acceptable outside dimension, and same type of material. Figure 7.8 illustrates the computed ratio of I_{sq} and I_{cir} numerically based on the standard square structures and the corresponding circular tubes. The ratios of moment of area of square to circular structures, (see Fig 7.8), are in the range of 1.35 to 1.42. Therefore, implementing a square structure instead of a circular structure will yield a higher structural natural frequency by roughly the square root of 1.4 or 20 percent.

7.5.2 Load Calculation and Selection of Arm Member

From Section 7.5.1, the square structure shows its positive features over circular tubes for the same outside dimensions and mass/unit length. At this step, we are more interested in the stresses on the arm to appropriately determine cross section dimensions of the square tubes. Arm Stresses are caused mostly by external forces.

The external forces can be categorized by their directions,

(1) Horizontal forces : Horizontal forces are generated from the interaction between the manipulator and the user. The force is specified to be smaller than 10 lbf at the end-point. Another component of these horizontal forces comes from the the inertia of the robot's arm. However, the dynamic force is relatively low compared to the interaction force due to the low acceleration characteristic of the application.

(2) Vertical forces : Vertical forces are generated by the weight of the arm members and rest weight of the user. Since the arm is designed to be light-weight, the majority of the vertical load is caused by the rest-weight of the user. The design should take into account that the arm should withstand this weight for a short interval of time. Since the effects of both horizontal and vertical forces on each arm member and joint depend on the location of loading points,

the design should be based on "the most critical posture" which corresponds to the maximum bending stress on the arm.

In general, the vertical downward load is more critical than the interaction load to the structural design for 2 reasons:

(1) In terms of magnitude, the user's rest weight is much greater than the interaction force.

(2) The arm has been designed to have variable stiffness in the horizontal plane and to be backdrivable. Therefore, no matter how the machine and human interact, the reaction/action force should not exceed 10 pounds. On the other hand, the high stiffness of SCARA configuration in the vertical direction requires the arm to support all vertical loads, regardless of magnitude. In other words, every arm member will share the bending stress caused be the downward force.

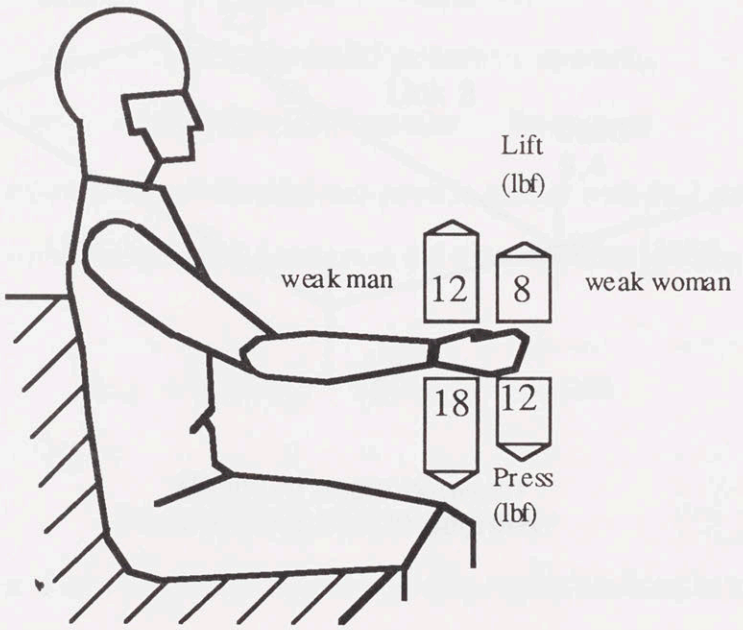

Fig. 7.9 Human Strength in Lift and Press of Weak Man and Woman

According to *Humanscale7*[61], the maximum lift and press strength of typical weak man and woman in seated posture are shown in Fig. 7.9. The robot's arm must be able to sustain the bending stress generated by the lift/press forces at the end-point. Note that the data in Fig. 7.9 does not represent rest weight, but only human strength. Therefore, it is better to compensate for these unpredictable forces by introducing a safety factor to multiply the lift/press data in Fig. 7.9. Using a safety factor of 2.5, we will get a press force of 50 pounds (more than a strength of an average man to press), which is quite "acceptable," to be used as the maximum end-point payload before the permanent deformation occurs.

Figure 7.10 presents end-point load diagram when the selected SCARA arm is loaded with 50 lbf. at the end-point.

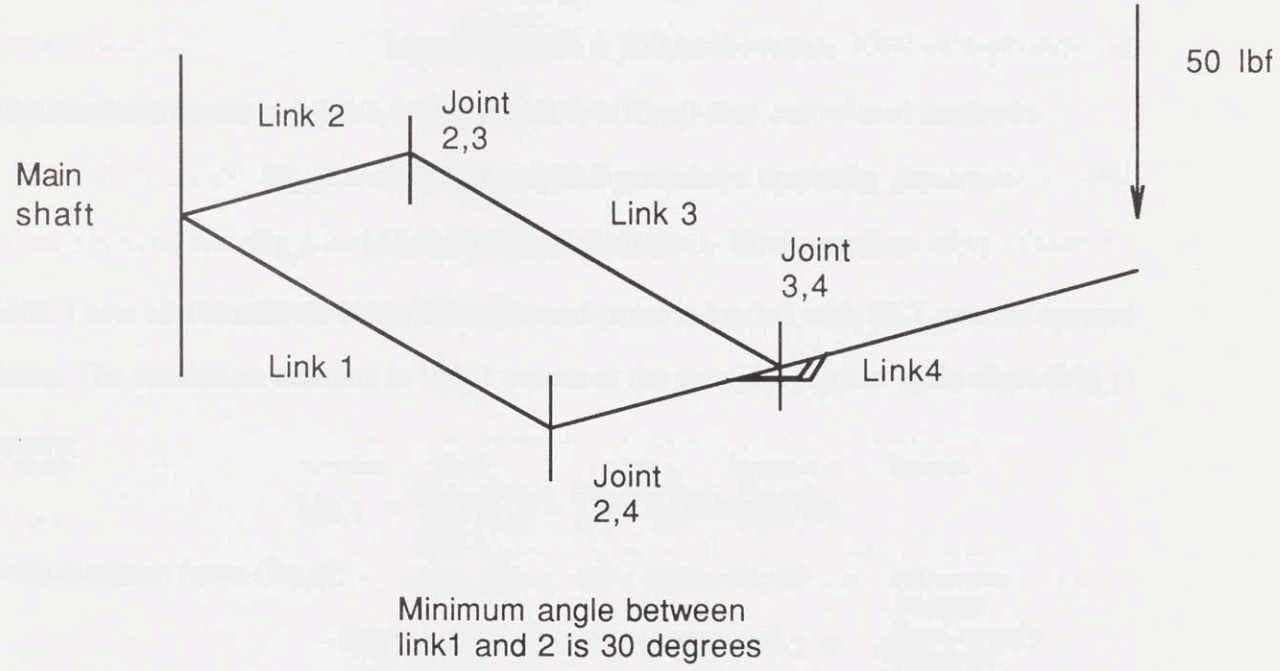

Fig 7.10 SCARA Arm with Vertical End-Point Load

---

61 Differient, Tilley, Harman, *Humanscale 7*, MIT Press, Cambridge, 1981

To calculate the stress in the arm members and in the joints, some assumptions have to be made to simplify the calculation:

1) Each arm member dimensions are taken as follows:

L_1 = 16 in.

L_2 = 6 in.

L_3 = 16 in.

L_4 = 20 in.

2) Torsional stress is small and, therefore, negligible for the calculation. Only longitudinal bending stresses and resultant forces are to be counted.

Link 4 is a double supported overhung beam, where maximum bending moment occurs at joint 3,4 ($M_{3,4}$)

$$M_{3,4} = 50X14 = 700 \text{ in-lb}$$

The resultant forces at joint 3,4 ($R_{3,4}$) and 1,4 ($R_{1,4}$) are,

$R_{3,4}$ = 50X20/6 = 166.7 pounds upward

$R_{1,4}$ = 166.7-80 = 86.7 pounds downward

Link 1 acts as a cantilever beam where its end-point is loaded with 86.7 pounds upward force. The maximum moment in link 1 occurs at the shoulder joint or main shaft ($M_{0,1}$) where:

$$M_{0,1} = 86.7X16 = 1387.2 \text{ inch-pounds}$$

with resultant force ($R_{0,1}$):

$R_{0,1}$ = 86.7 pounds downward

Similarly, link 3 acts as a cantilever beam, where its end-point load is 166.7 pounds downward. The maximum bending moment on link 3 occurs at joint 2,3 ($M_{2,3}$)

$$M_{2,3} = 166.7X16 = 2667.2 \text{ inch-pounds}$$

with resultant force ($R_{2,3}$):

$$R_{2,3} = 166.7 \text{ pounds upward}$$

At link 2, the stress in this member is quite complex with the maximum bending moment ($M_{0,2}$):

$$M_{0,2} = 166.7X21.4 = 3567.38 \text{ lb-in}$$

($M_{0,2}$) occurs when link 1 and 2 are at 30° apart. $M_{0,2}$ is perpendicular to the line between the main shaft of joint 3,4 at this posture.

The resultant force on link 2 ($R_{0,2}$) is:

$$R_{0,2} = 166.7 \text{ pounds upward}$$

The main shaft counters the bending moment (M_0) which is:

$$M_0 = 50X35.8 = 1790 \text{ inch-pounds}$$

with the resultant force (R_0):

$$R_0 = 50 \text{ pounds downward}$$

In conclusion for the stress analysis, the bending moment resulting from 50 pound payload at the end-point occurs at link 2 at approximately 3500 inch-pounds. All shear stresses in each member are quite small, and are thus considered negligible.

A standard and commonly used aluminium for building structures is 6061 aluminium alloy with T6 heat treatment, called 6061-T6 aluminium alloy. Table 7.1 lists the mechanical properties of the alloy.

Density	Tension		Compression	Shear		Bearing		Modulus of	Remark
	Ultimate	Yield		Ultimate	Yield	Ultimate	Yield	Elasticity	
lb/cu.in	ksi	ksi	ksi	ksi	ksi	ksi	ksi	E, ksi	
0.098	42	35	35	27	20	88	56	10,100	Heavy-duty Structure Good corrosion resistance

Table 7.1 Minimum Expected Mechanical Properties of 6061-T6 Aluminium Alloy

Standard 1.5 inch square hollow tubing is selected as a fundamental material for the arm structure as it would not interfere much with visibility. However, thickness of the tube is still a variable to provide different arm strength. Table 7.2 shows the estimated safety factor of different wall thicknesses of the member when subjected to 3500 inch-pound bending moment.

Material : 6061-T6 Aluminium alloy (hot roll type)

Thickness in.	Moment of area $in.^4$	c in	Load stress ksi	Yield stress ksi	Safety factor
.035	.0734	.75	35,763	35,000	.979
.049	.0999	.75	26,276	35,000	1.332
.058	.1162	.75	22,590	35,000	1.549
.065	.1283	.75	20,460	35,000	1.711
.083	.1580	.75	16,614	35,000	2.107
.095	.1865	.75	14,075	35,000	2.487
.120	.2119	.75	12,388	35,000	2.825

Table 7.2 Comparison of Safety Factor of 1.5 inches Square Tube With Various Thickness

According to Table 7.2, we select 1.5 inches square tube with 0.120 inches thickness as arm member material. When subjected to a 3500 inch-pound bending moment, the tube still provides an adequate safety factor of 2.825.

7.6 Arm Design

Figure 7.11 illustrates the arm assembly from the top view. The actuators are located face-to-face on the shoulder joint (left most joint). The upper actuator drives link 2 (the shortest link) and link 3 (right pair of the parallel links) while the lower actuator drives link 1 (left pair of parallel links). Both links 1 and 3 determine the orientation and position of link 4 (the longest link), where the end-effector is installed.

All the arm members are made of 1.5 inch 6061-T6 aluminium alloy square tubing with 0.120 inch wall thickness.

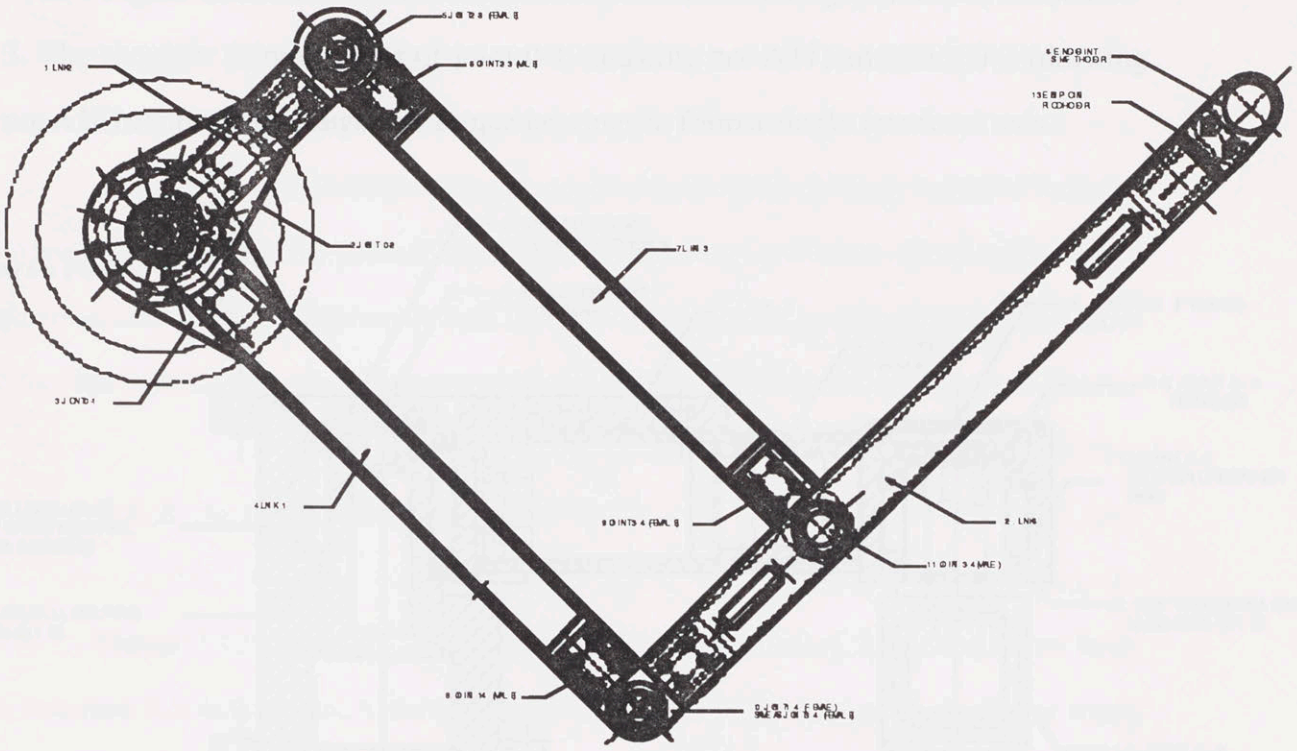

Fig. 7.11 Top View of Arm Assembly (scale 1:5)

According to the load calculation in Section 7.5.2, the maximum stress occurs on link 2. Therefore, the design has to employ a reinforced aluminium plate extended from joint 0-2 (Drawing no. A16) to increase strength and stiffness. Joint 2-3 (the joint that connects link 2 and link 3 together) is also exposed to a high bending moment. Therefore, the bearing housing, joint shaft, and size of bearings are chosen to be larger than the others in the mechanism. The whole arm is constructed with 2 levels to maximize the relative rotational travel between each link pair. Link 2 and 4 are on the upper level while link 1 and 3 are on the lower layer. Details of arm subassemblies will be described in the further sections

7.6.1 Shoulder Joint and Joint 2-3

Figure 7.12 illustrates the cross section of the shoulder joint, link 2, and joint 2-3. The shoulder joint consists of joint 0-1 (drawing no. A17) and joint 0-2 (drawing no. A16) connected through low torque bearings to form a single rotational axis.

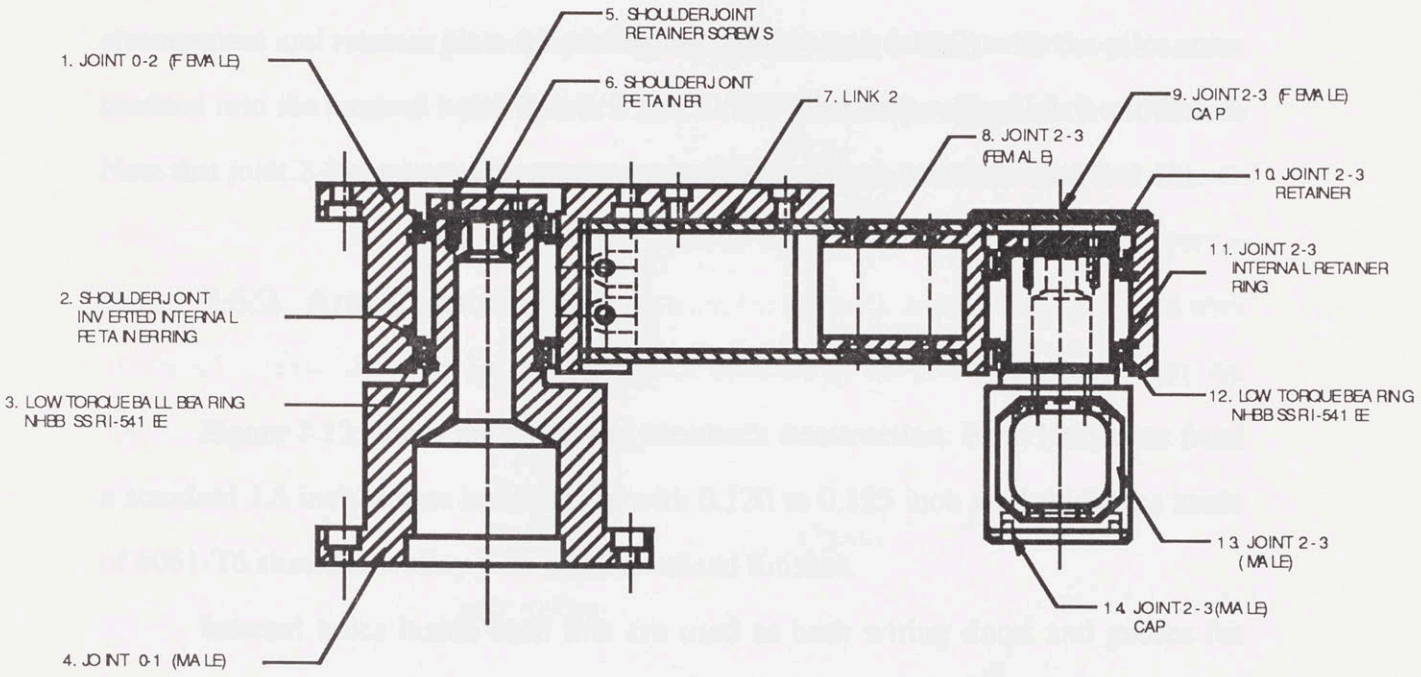

Fig. 7.12 Cross Section of Shoulder Joint (scale 1:2.2)

Experience with a similar robot at MIT has indicated that if the shoulder members are not perfectly aligned, the misalignment stress during the actuator installation will create a large amount of friction in the mechanism. However, the manual aid construction has a different approach by allowing the shoulder members to align on a single axis with the actuators (forming a single rotational axis). The installation of the motor to the machine's foundation is adjustable in several degrees of freedom which can minimize the misalignment-induced friction in the arm mechanism. Note that each joint has a

retainer plate which can be tightened to adjust the axial play and the friction in the joint's bearings.

Joint 0-1 and 0-2 have special plates which extend to support and reinforce the connected links. These plates help increase the link's strength and stiffness, especially in link 2 in which the highest stress occurs.

Joint 2-3 has a similar construction as the shoulder joint in terms of bearing arrangement and retainer plate for preloading. However, it is built with the pilot cores inserted into the internal holes in link 2 and 3. The pilot helps align link 2 and link 3. Note that joint 2-3 employs caps to protect the bearings from contamination and dirt.

7.6.2 Arm Construction

Figure 7.13 shows the basic arm member's construction. Each link is cut from a standard 1.5 inch square hollow tube with 0.120 to 0.125 inch wall thickness made of 6061-T6 aluminium alloy with black anodized finishes.

Internal holes inside each link are used as both wiring ducts and guides for pilot cores of joints. Note that the right end of link 2 has an internal cut to allow a tight tolerance fit with the pilot core of joint 2-3.

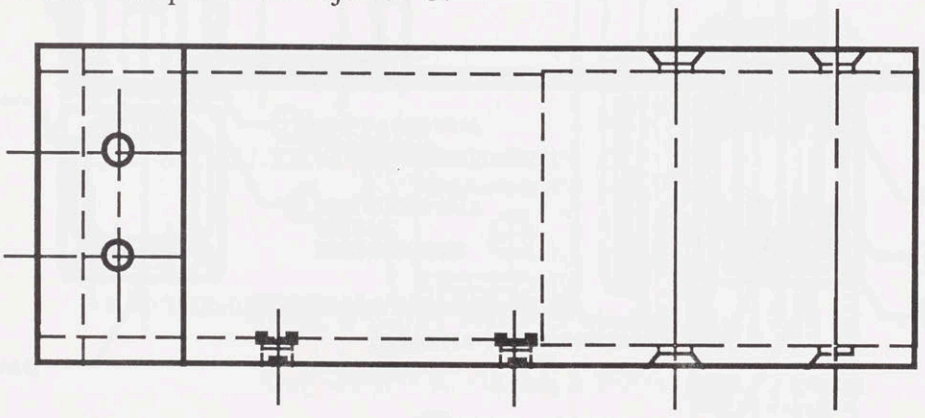

Fig. 7.13 Front View of Link 2 (scale 1:1)

7.6.3 Construction of Link 4 Joints

There are two joints on link 4 (see Fig. 7.14). The left most connects link 1 to link 4, so called joint 1-4. This joint has a very similar construction to joint 2-3, but differs in the bearing's size, bearing's housing, and joint's shaft since it is subjected to a lighter load. The joint on the right connects link 3 to link 4, so called joint 3-4. It has almost the same construction as joint 1-4, except it has a reverse posture and the joint shaft has no pilot core and is instead bolted on the top side of link 4. Link 4 has a number of wires inside allowing for the communication between the controller and end-effector. As a consequence, joint 3-4's shaft is cut in the middle to provide wiring clearance. Again, both joints in Fig. 7.14 have the retainer plates to adjust axial play and bearing preload stress. Similarly, they are covered by the joint caps that protect the low friction bearings from dirt and contaminations.

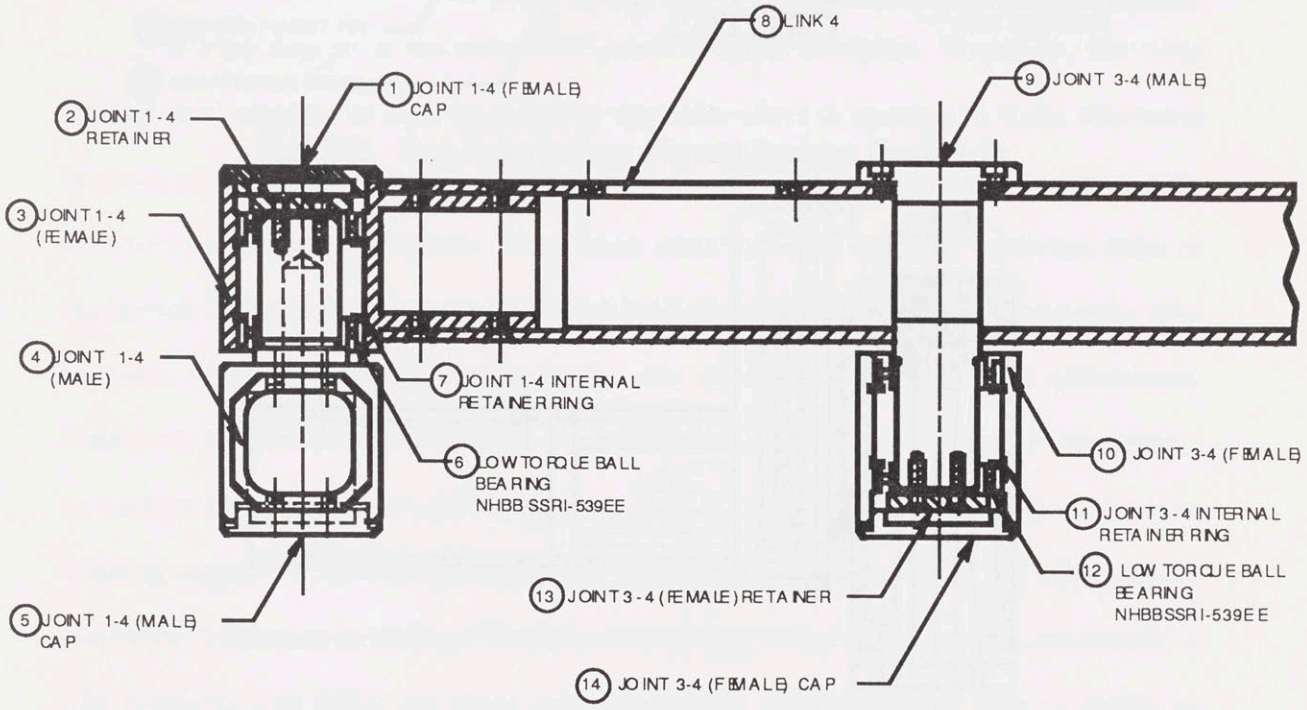

Fig. 7.14 Joint Constructions of link 4 (scale 1:2)

7.6.4 End-Point Joint

Figure 7.15 illustrates the end-point joint that is designed as a connector for the end-effector and the overload mechanism. The end-effector is connected to the end-point joint via a bearing arrangement allowing one rotational degree of freedom. This rotation is then monitored by a high accuracy potentiometer (no. 26) installed above the end-point joint cap (no. 21). The end-point joint consists of 2 basic assembly parts.

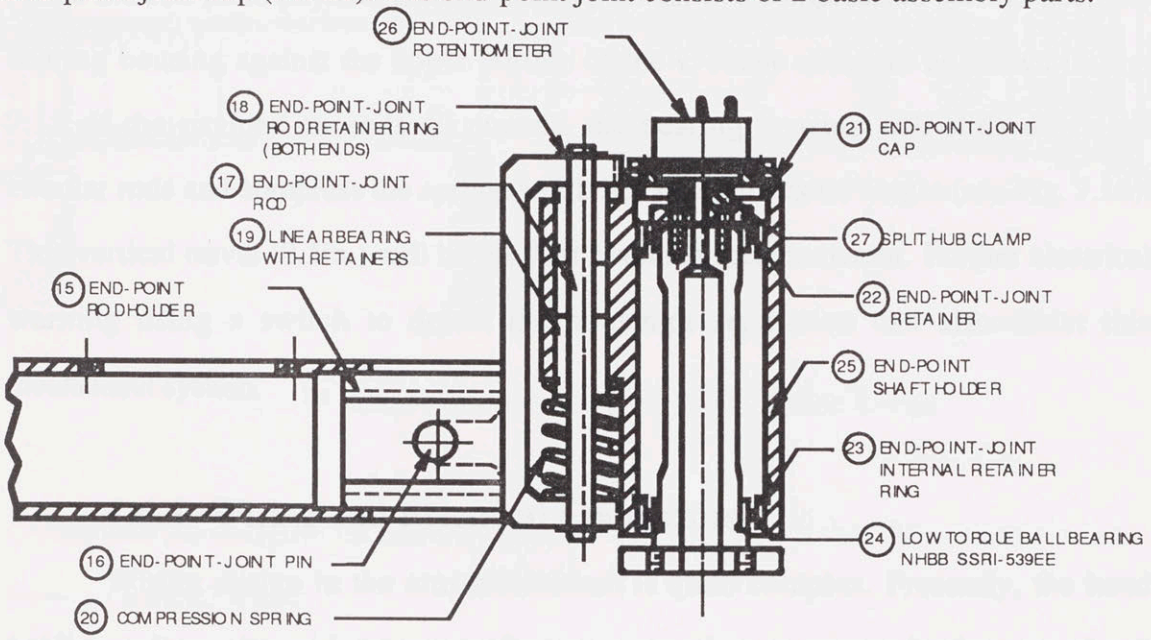

Fig. 7.15 End-Point Joint at Normal Position (scale 1:2)

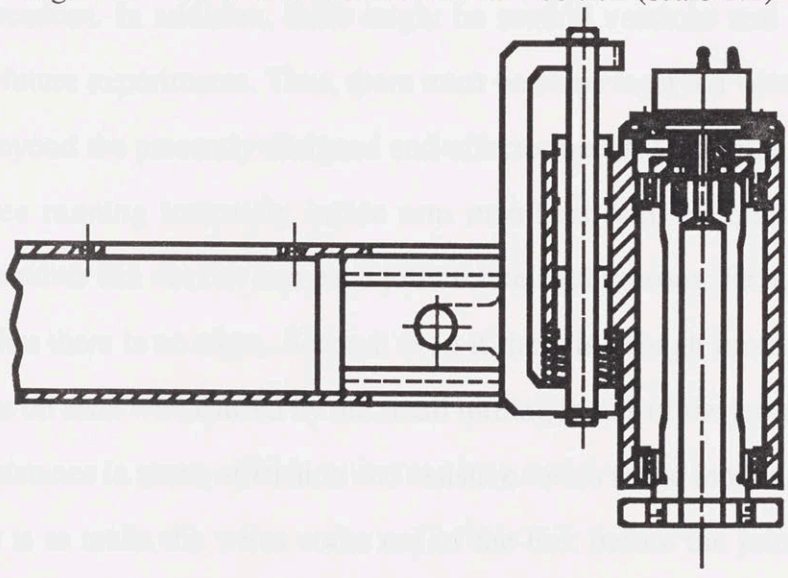

Fig. 7.16 End-Point Joint at Overloaded Condition (scale 1:2)

The first part is a C-shape structure with a pilot bore that plugs into link 4 (no. 15). This C-shape frame is locked to link 4 by two knobs on the pilot bore. The second part is a rotary bearing housing with a linear bearing arrangement (no. 25) allowing this whole part to slide down along the circular rods (no. 17) held by the C-shape frame. When the end-point payload is less than 40 pounds, two compression springs keep the bearing housing against the upper portion of the C-shape structure as shown in Fig. 7.15. If the payload exceeds 40 pounds, the bearing housing will slide down the circular rods and compress the springs until they reach the solid height (see Fig. 7.16). This vertical travel (0.5in.) will be the first overload state indicator. Further electrical warning using a switch to detect the housing's separation can also assist this mechanical system.

7.6.5 Wiring and Electrical Connectors

Wiring design in the arm mechanism is quite complex. Presently, the hand holding unit requires at least twenty-four separate wires to operate its three rotational degrees of freedom. In addition, there might be several versions and types of end-effectors for future experiments. Thus, there must be some reserved wires and pairs of connectors beyond the presently designed end-effector needs. Currently, we have fifty separate wires running internally inside arm members with adequate connectors. However, the wires can not run into each joint for several reasons. First, every joint is so compact that there is no room. Second, even if there is enough room for the wires, bending stress on each wire caused by the small turning radius of the joint will certainly contribute resistance in terms of friction and resistive forces to the motion. A solution to this problem is to make the wires come out of the link before the joint to create an outside loop to get into another joint pair (see Fig. 7.15).

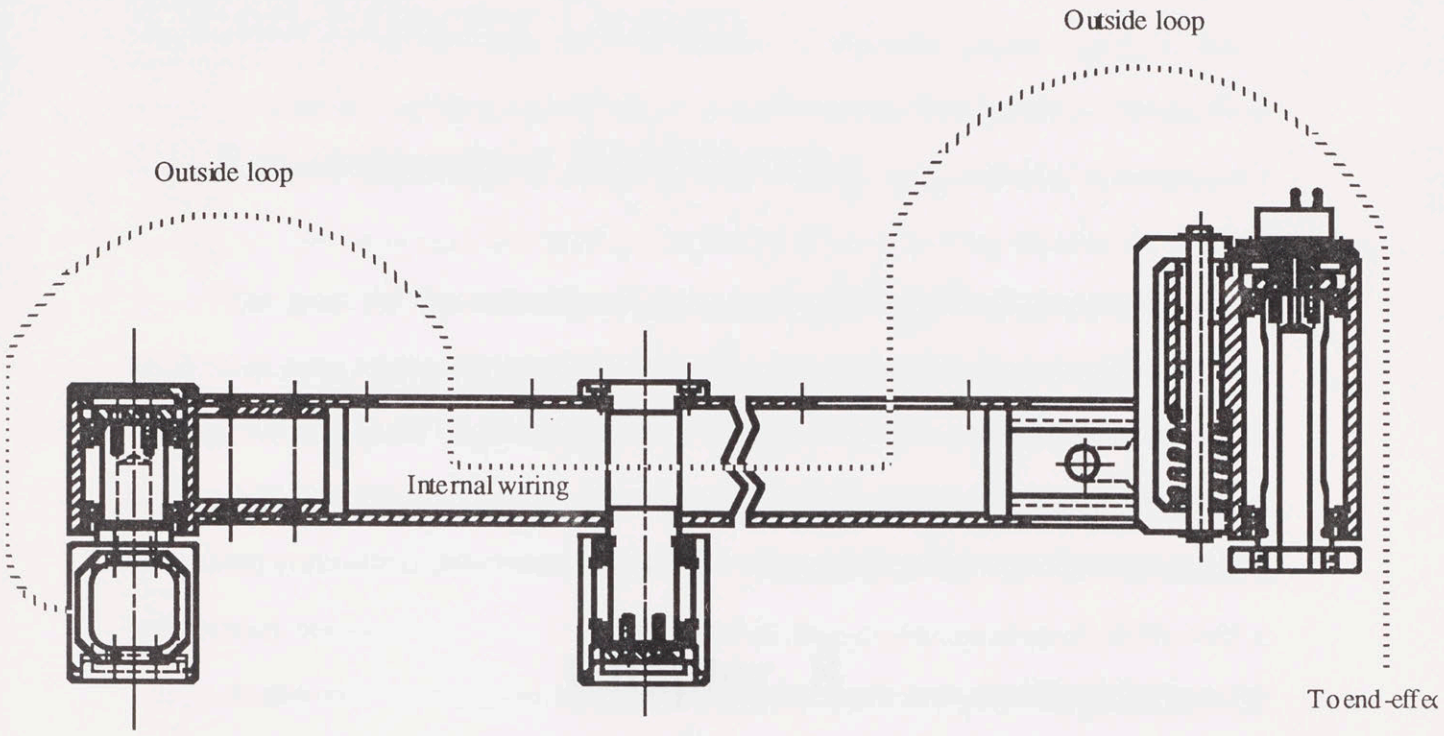

Fig. 7.15 Internal Electrical Wiring and Outside Loops

Connectors are designed on one side of link 1 and link 4 such that they connect outside loops to internal wires.

Chapter 8

End-Effector Design

8 End-Effector Design

8.1 Requirements on End-Effector

The goal for the end-effector design is to achieve 2 rotational degrees of freedom of wrist motion (flexion/extension and abduction/adduction (see Fig. 2.6 and 2.7) and an additional degree of freedom for the forearm's rotation (pronation and supination). If possible, it is preferable that all the three rotational degrees of freedom be actively controlled. Otherwise, they should be passive and be monitored by position and velocity sensors.

As presently envisioned, actuators, and sensors are to be installed locally at the end-point. Therefore, weight and size of the end-effector unit must be kept as low as possible to minimize the reflected friction and inertia of the arm and to provide maximum visibility to the user.

In terms of safety, the user should be able to pull free from the hand holding unit without assistance.

8.2 Choices of Supporting Point

There are many ways of attaching the user's hand to the machine. Figure 8.1 illustrates possible holding points labeled as A, B, and C. Point A holds the user on the back of his/her palm where points B and C support under his/her forearm at different locations. B is approximately under the user's wrist and C is further upstream on the forearm.

The fact that humans tend to lean or rest their arms against the robot helps determine a suitable holding point. If point A is selected, resting against the machine

tends to lift the palm up, while the wrist is lowered. Since the whole wrist is locked in extension position, this position inhibits any wrist motion . Changing the wrist position will affect the levitation of the center of gravity of the forearm, and thus will consume a substantial amount of muscular energy. On the other hand, holding the arm at point C is a different issue. The design needs to allow small degrees of free rotation at the holding point to account for the user's changing of elbow level at different arm postures in the workspace. If point C is allowed to hold the user's arm, the vertical position of the user's finger tips can not be accurately determined since the system is not overconstrained (both the holding point's rotation and wrist's flexion/extension determine the position of finger tips). In addition, this might not enhance wrist motion because the user may choose to use the holding point (C) as a pivot instead of moving his/her wrist to lower his/her palm.

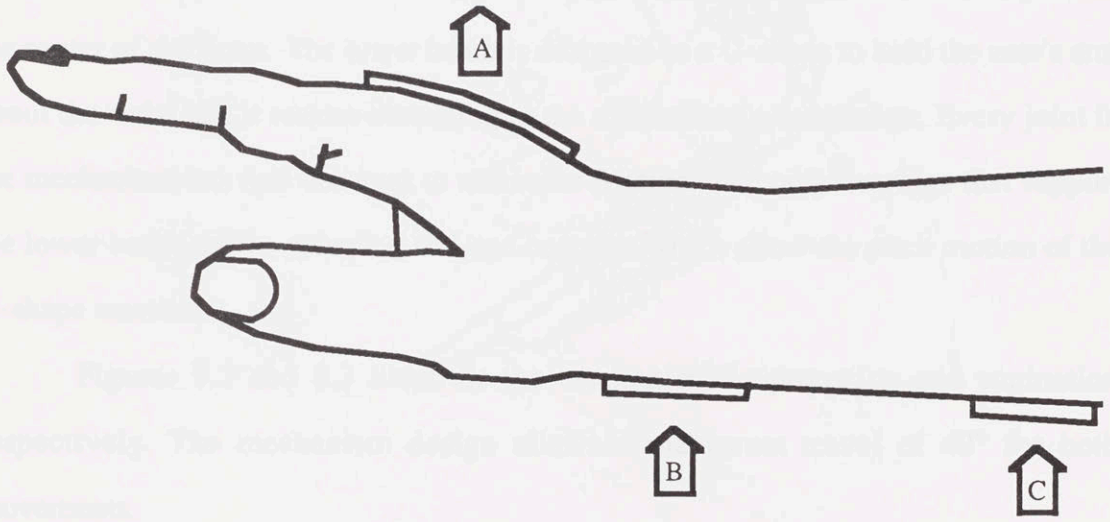

Fig. 8.1 Choices of Supporting Point

The most suitable holding point is point B which is roughly under the user wrist. This arrangement allows the leaning or resting weight (up to 50 pounds) to be supported by the hand holding unit and be transferred to the robot arm while flexion/extension and abduction/adduction are independently permitted. However, the

holding mechanism at point B should allow pronation/supination. In other words, the mechanism component which attaches to the user's arm must rotate co-axially with the user's forearm to permit pronation/supination.

8.3 Pronation/Supination

8.3.1 Mechanism

Figures 8.2 and 8.3 show the designed mechanism for pronation/supination consisting of several linkages. A high torque motor with a built-in potentiometer and tachometer is on the top of the mechanism which drive an eccentric crank. The crank is then connected to a four-bar mechanism which has 2 vertical rods and 2 horizontal beams. One of the vertical rods is longer and connects the crank to this mechanism; the other rod is shorter and holds the 2 beams in place. The upper beam has a fixed pivot at the center of the beam. The lower beam is designed as a U-shape to hold the user's arm about the wrist and it rotates according to the mechanism's constraints. Every joint in the mechanism has ball bearings to minimize friction. The only bearings that support the lower beam are the spherical rod-end bearings which allow the pitch motion of the U-shape member.

Figures 8.2 and 8.3 illustrate the mechanism in pronation and supination respectively. The mechanism design allows a maximum travel of 40° for both movements.

Note that when the user rests his/her arm against the hand holding unit, the load will be supported by the U-shape lower beam, and then be transferred to the vertical rods and to the upper beam, which are supported by the SCARA arm. In other words, the rest weight of the user will have no effect on the pronation/supination mechanism which allows the use of a small actuator.

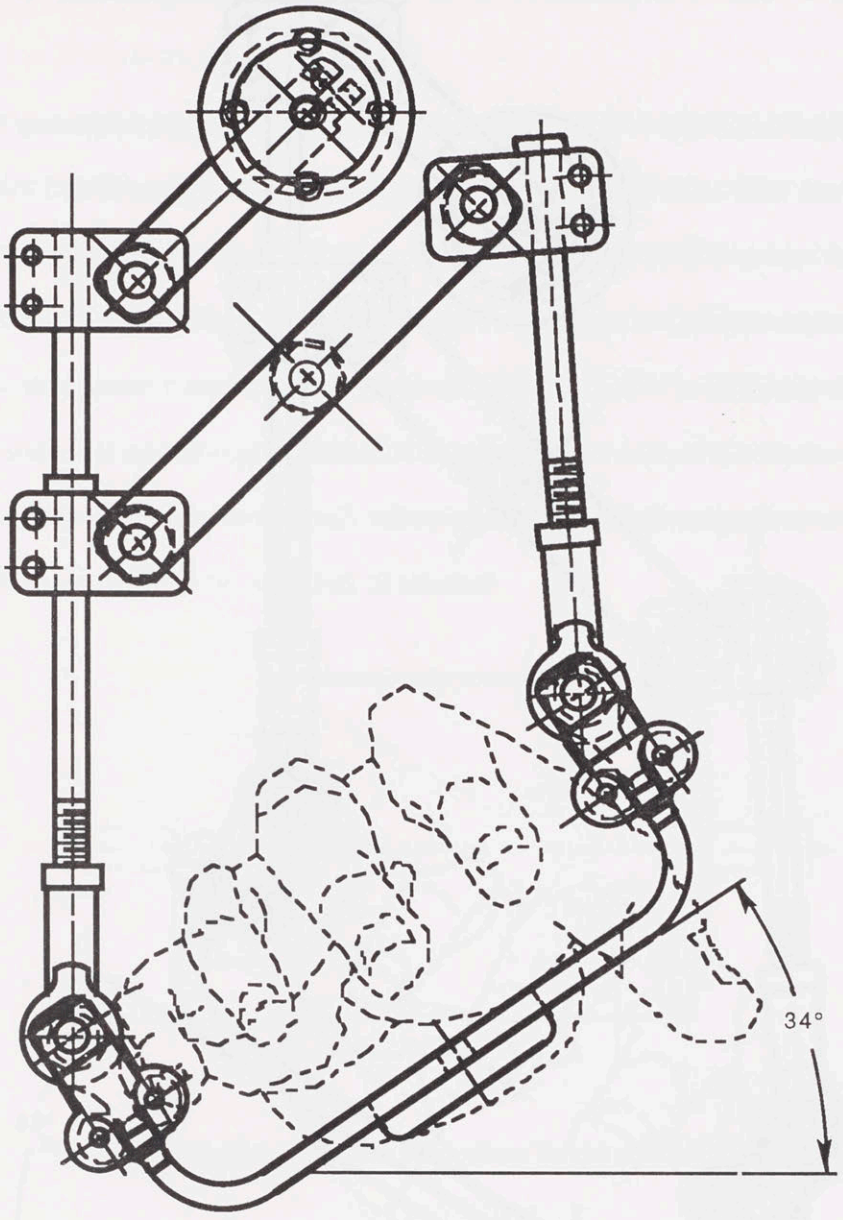

Fig. 8.2 Posture of Mechanism in Forearm Pronation

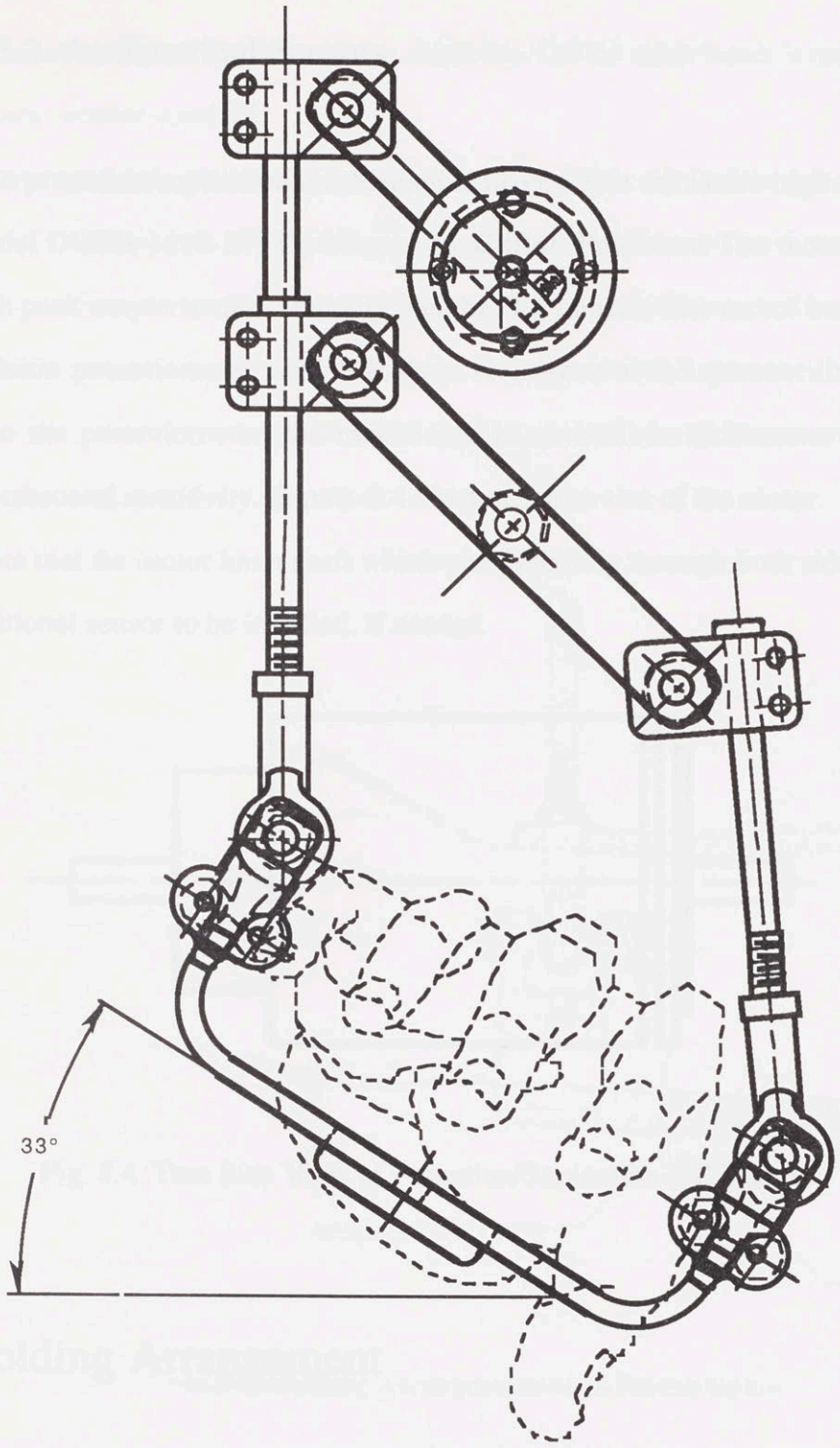

Fig. 8.3 Posture of Mechanism in Forearm Supination

8.3.2 Actuator and Sensors

The pronation/supination mechanism is driven by a miniature high torque DC motor model DGPH-1610-B-1T produced by Clifton Precision. The motor has 15.4 ounce-inch peak output torque, and only weighs 9.2 ounces. The motor has a built-in high-precision potentiometer with 5 Kohms resistance at 0.5 percent linearity. In addition to the potentiometer, the motor also has a built-in tachometer with 0.07 volts/radian/second sensitivity. Figure. 8.4 illustrates true size of the motor.

Note that the motor has a shaft which passes axially through both sides to allow for an additional sensor to be installed, if needed.

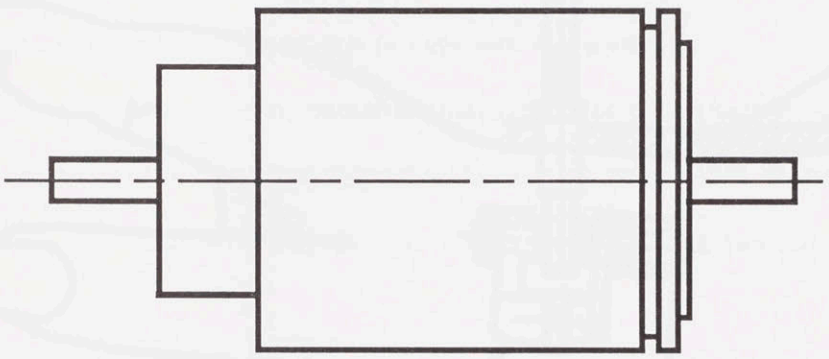

Fig. 8.4 True Size View of Pronation/Supination DC Motor

8.4 Holding Arrangement

The method of the arm holding is another interesting problem. The fact that the human skin tissue has a substantial degree of deformation when subjected to external force tends to degrade the position accuracy. Excessive holding force will only have

insignificant improvement on the position accuracy. On the other hand, it may hurt the user and lower his/her comfort.

At this stage, we have little knowledge of a suitable arm holding method. The current design uses several sizes of light-weight plastic splints as the holding media between the machine and patient. An appropriate splint must be worn by the user before the splint is tightened to the U-shape structure in the pronation/supination mechanism (see Fig. 8.5). However, fore and aft adjustments are still available to set the hand forward or backward relative to the beam.

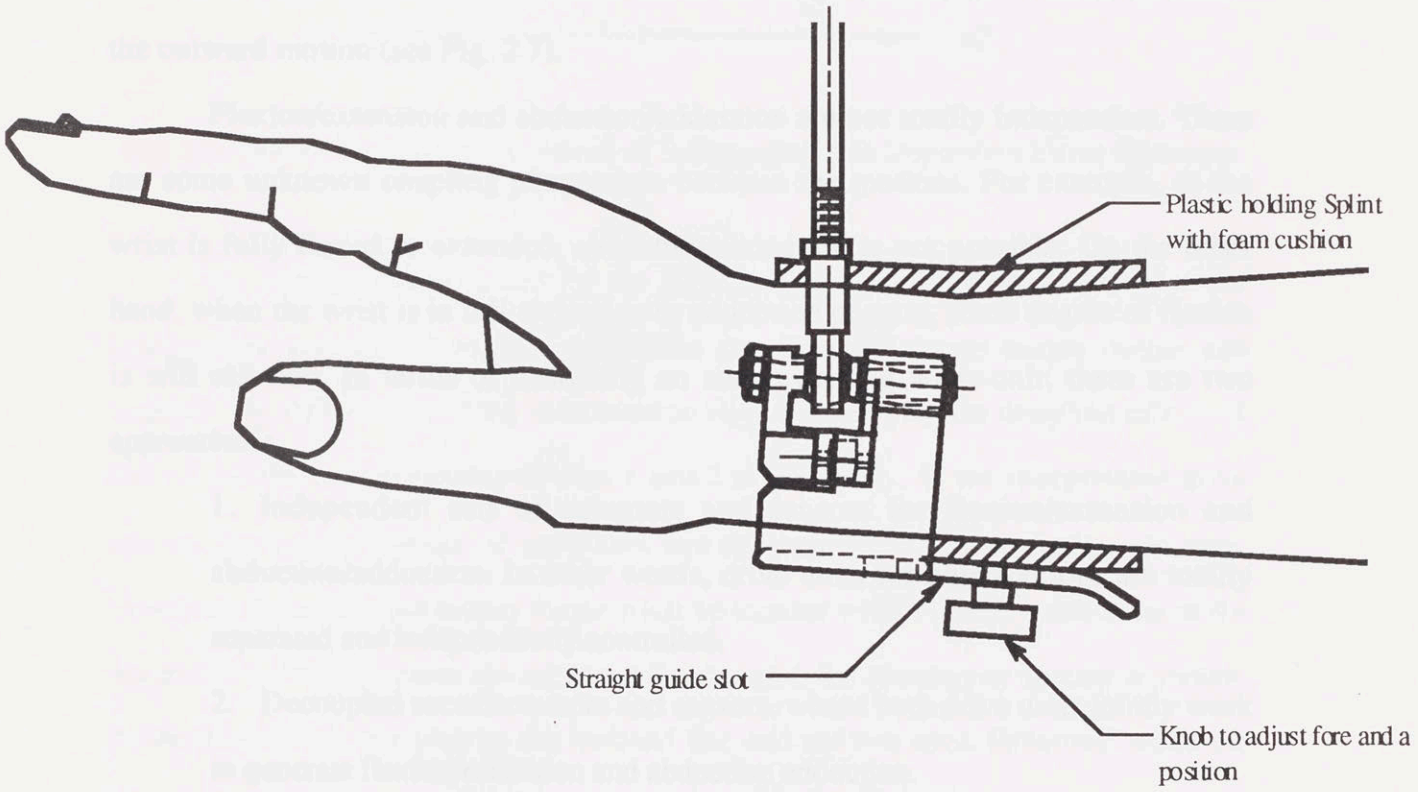

Fig. 8.5 Forearm Holding Arrangement with Plastic Splint

If this current method is shown to be ineffective, a special holding mechanism to the user's elbow and upper arm can be arranged, or a new hand holding unit design must be considered.

8.5 Flexion/Extension and Abduction/Adduction

8.5.1 Mechanism

There are two types of wrist motions relative to the forearm: flexion/extension and abduction/adduction. When an arm is extended in front of the body, flexion is the rotation of the wrist caused by a flexion muscle. In this case, the hand is moving toward the ground. Extension is the reverse motion of flexion in which the hand is lifting up (see Fig. 2.6). Abduction and adduction are sideways movements. Abduction is the motion of the hand towards the body's centerline where adduction is the outward motion (see Fig. 2.7).

Flexion/extension and abduction/adduction are not totally independent. There are some unknown coupling phenomena between the motions. For example, as the wrist is fully flexed or extended, abduction/adduction is not possible. On the other hand, when the wrist is in full abduction or adduction posture, some degree of flexion is still allowed. In terms of designing an active driving wrist unit, there are two approaches :

1. Independent sets of actuators and sensors for flexion/extension and abduction/adduction. In other words, drive units for both motions are totally separated and independently controlled.
2. Decoupled set of actuators and sensors, where both drive units jointly work to generate flexion/extension and abduction adduction.

There are benefits and drawback to each approach. Independent drives are less complex to control and it is easier to measure kinematic parameters. A lower degree of computation is required, whereas the decoupled drive is much more complex and requires more computation.

Figure 8.6 illustrates output torque characteristics of the two approaches.

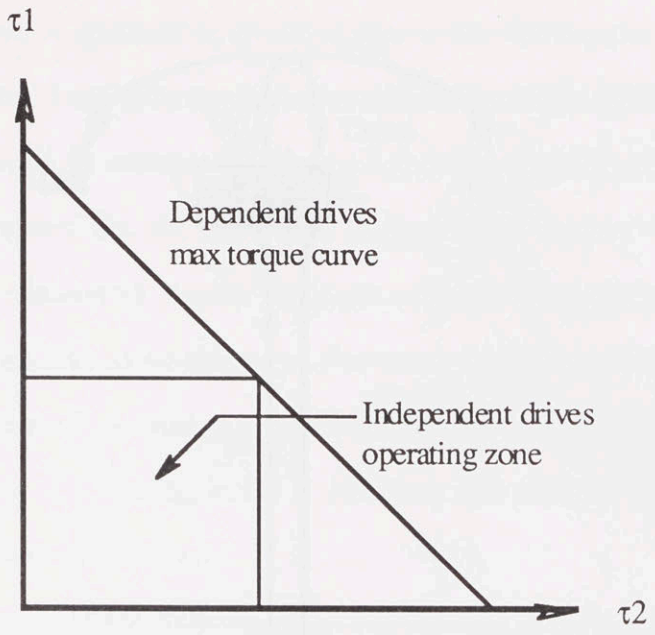

Fig. 8.6 Output Torque Characteristic of Independent and Dependent Drive Concepts

An important assumption for the curve in Fig. 8.6 is that the actuators of the independent and the decoupled approaches are the same (same torque output and weight). The differences of the transmission layout determine the coupling effect. $\tau 1$ and $\tau 2$ are the output torques of axes 1 and 2 respectively. In the independent drive system, the output torque of each axis can fall anywhere inside the square area. However, the maximum output torque must be located within the bounded lines of the square area. If the actuators are dependently arranged, the system can operate anywhere inside the triangle bounded by the inclined line and the two axes. However, when the maximum torque is needed, the operating point will shift up and run along the inclined line. Note that the maximum output torque of one particular axis can be substantially increased to about twice the original value. For the reasons that the maximum output torque to weight ratio is important and computation speed has been improving, the coupled drive concept was chosen.

A light-weight and simple mechanism is a differential drive(see Fig. 8.7).

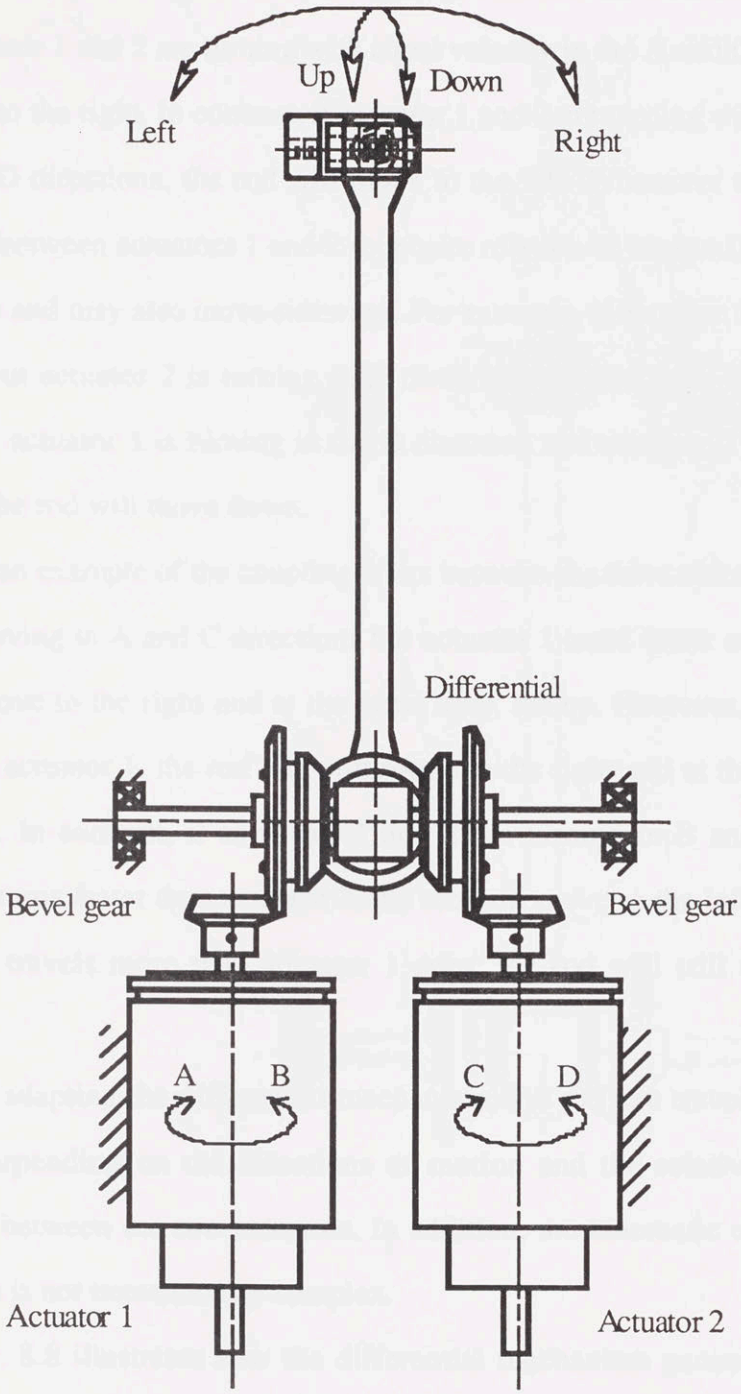

Fig. 8.7 Differential Mechanism for Flexion/Extension and Abduction/Adduction

The system in Fig 8.7 has two actuators driving through two sets of bevel gears. Each bevel gear is then connected to a differential that consists of 3 identical gears. Two of these gears have a face-to-face arrangement and are joined by the third

one. Note that a rod is attached to the third gear in the differential. According to Fig. 8.7, if actuator 1 and 2 are turning with equal velocity in the A and C directions, the rod will rotate to the right. In contrast, if actuator 1 and 2 are turning with equal velocity in the B and D directions, the rod will move to the left. Whenever there is a rotational difference between actuators 1 and 2 (opposite rotation or unequal), the rod will move up or down and may also move sideways. For example, if actuator 1 is turning in the A direction but actuator 2 is turning in D direction, the rod will lift up vertically. In contrast, if actuator 1 is turning in the B direction and actuator 2 is turning in the C direction, the rod will move down.

As an example of the coupling effect between the drive units, consider actuators 1 and 2 moving in A and C directions but actuator 1 turns faster actuator 2 does. The rod will move to the right and at the same time, lift up. However, if actuator 2 turns faster than actuator 1, the rod will still rotate to the right and at the same time, move downward. In contrast, if actuators 1 and 2 are turning in B and D directions but actuator 1 turns faster than actuator 2, the rod will move to the left and downward. If actuator 2 travels more than actuator 1 does, the rod will still move left but also upward.

By adapting the differential mechanism, the rod can travel in two degrees of freedom depending on the directions of motion and the relative rotational speed difference between the two actuators. In addition, the kinematic computation of this mechanism is not tremendously complex.

Fig. 8.8 illustrates how the differential mechanism generates abduction and adduction if the end-point of the rod is connected to the user's hand (providing his/her forearm is aligned perpendicularly to the differential's shaft). Note that the actuators and bevel gears are not shown.

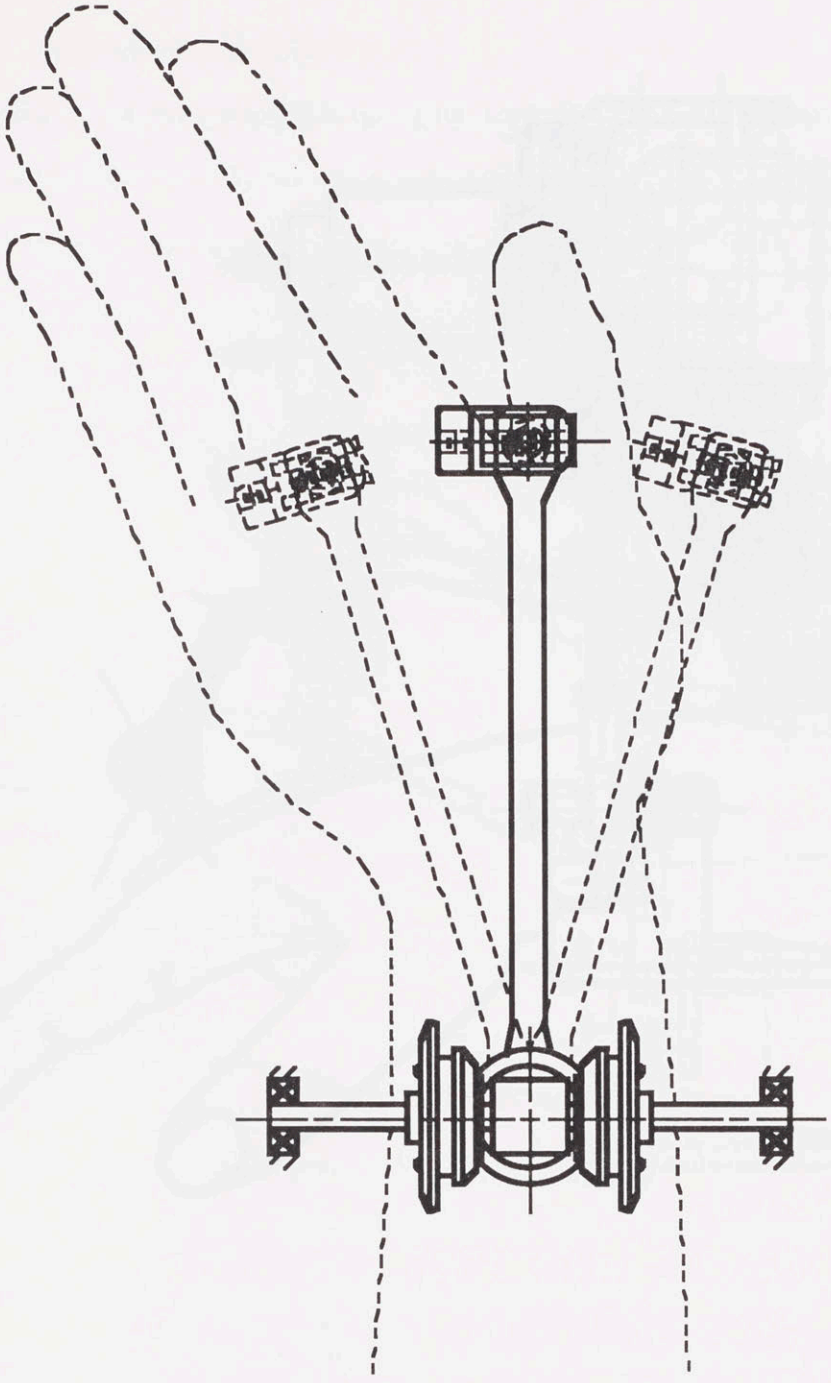

Fig. 8.8 Differential Mechanism in Wrist Abduction/Adduction Posture

Figures 8.9 and 8.10 illustrate how to generate flexion and extension with the differential mechanism. Currently the differential is placed above the user's forearm about 1 to 2 in. behind the wrist proximal joint.

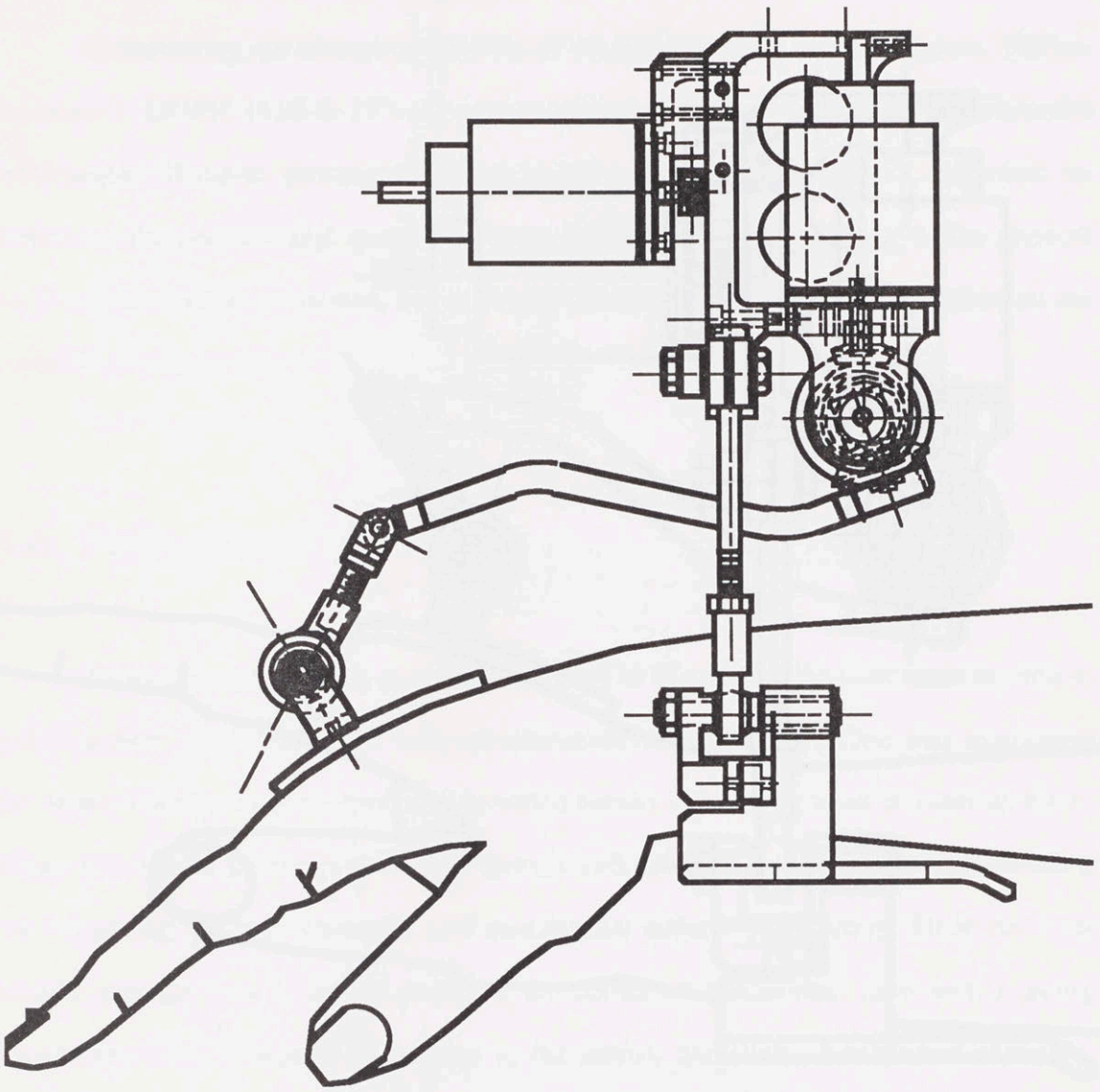

Fig. 8.9 Differential Mechanism in Wrist Flexion Posture

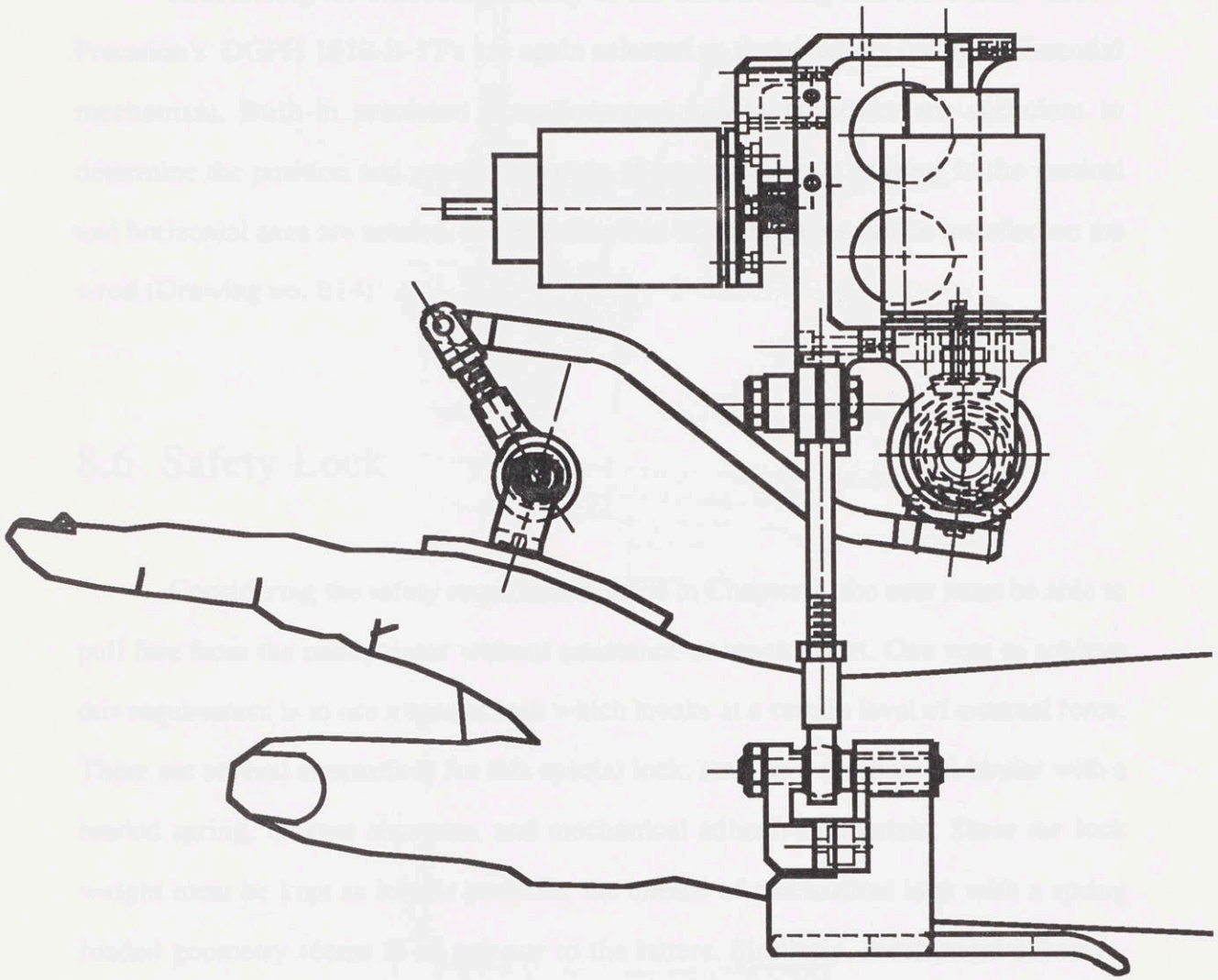

Fig. 8.10 Differential Mechanism in Wrist Extension Posture

8.5.2 Actuators and sensors

Considering the interchangeability of the hand holding unit's actuators, Clifton Precision's DGPH 1610-B-1T's are again selected as the actuators for the differential mechanism. Built-in precision potentiometers and tachometers are sufficient to determine the position and speed. However, if accurate torque or force in the vertical and horizontal axes are needed, two separate sets of strain gages can be installed on the s-rod (Drawing no. E14)

8.6 Safety Lock

Considering the safety requirement listed in Chapter 2, the user must be able to pull free from the manipulator without assistance or much effort. One way to achieve this requirement is to use a special lock which breaks at a certain level of external force. There are several alternatives for this special lock, such as a mechanical binder with a loaded spring, magnet elements, and mechanical adhesive materials. Since the lock weight must be kept as low as possible, the choice of mechanical lock with a spring loaded geometry seems to be inferior to the latters. Similarly, mechanical adhesive, such as velcro, has an unpredictable separation force due to contamination and aging. The most elegant lock with light weight characteristics is the magnetic one where basically, two pieces of magnet are attracting each other. Separation force is determined by gauss strength of the magnetic field which has proven reliability and predictability. Recently, strong magnets have been made of advanced materials such as rare-earth cobolt, alnico, and neodymium-iron-boron, resulting in yet lighter weight. The strongest commercially compact magnet is made of neodymium-iron-boron with energy density of 27 to 35 million gauss oersteds.

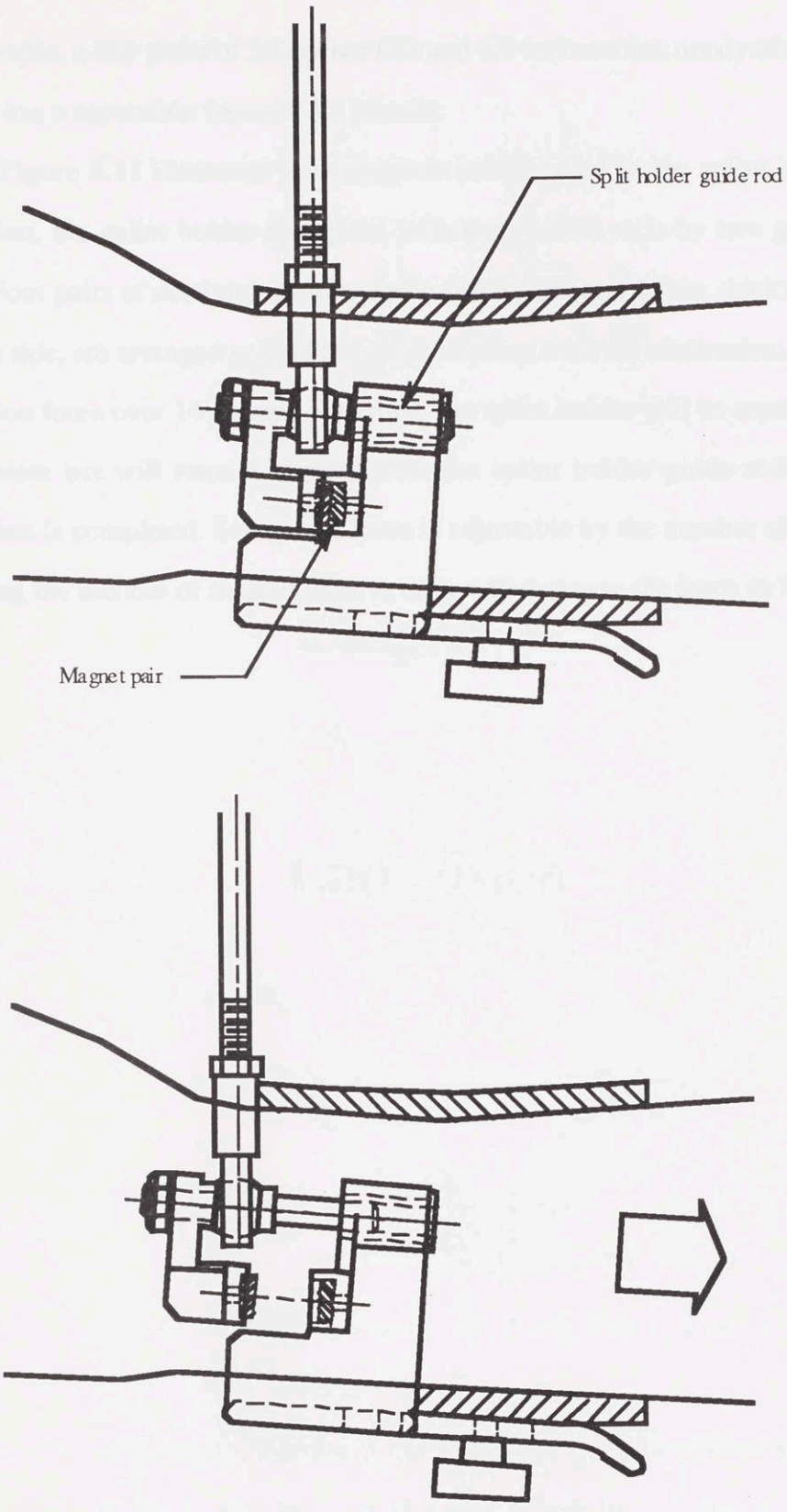

Fig. 8.11 Separation of Splint Holder with Magnet Lock

For example, a tiny piece of 3/8 inches OD and 1/8 inches thick neodymium-iron-boron magnet has a separation force of 3.5 pounds.

Figure 8.11 illustrates how magnets are installed in the splint holder. Before separation, the splint holder is aligned with the vertical rods by two guide rods and bores. Four pairs of neodymium-iron-boron (3/8in. OD and 1/8 in. thick) magnets, two on each side, are arranged to hold the splint in place with the mechanism. If an external separation force over 14 pounds is applied, the splint holder will be separated from the mechanism but will remain aligned with the splint holder guide rod until the full separation is completed. Separation force is adjustable by the number of magnet pairs. Reducing the number of magnet pairs to three will decrease the force to 10.5 pounds.

Chapter 9

Conclusion

9 Conclusion

9.1 Design of Manual Teaching Aid

At this stage, the manual teaching aid has been designed with five degrees of freedom, two in translation of the end–point and three in the wrist's rotation. The translation is achieved via a SCARA arm (see Fig. 9.1), where low end-point friction of 3 to 6 ounces and reflected inertia of 0.3 to 0.6 pounds are achieved. The friction and reflected inertia are smaller than in any other configuration such as Cartesian or cylindrical.

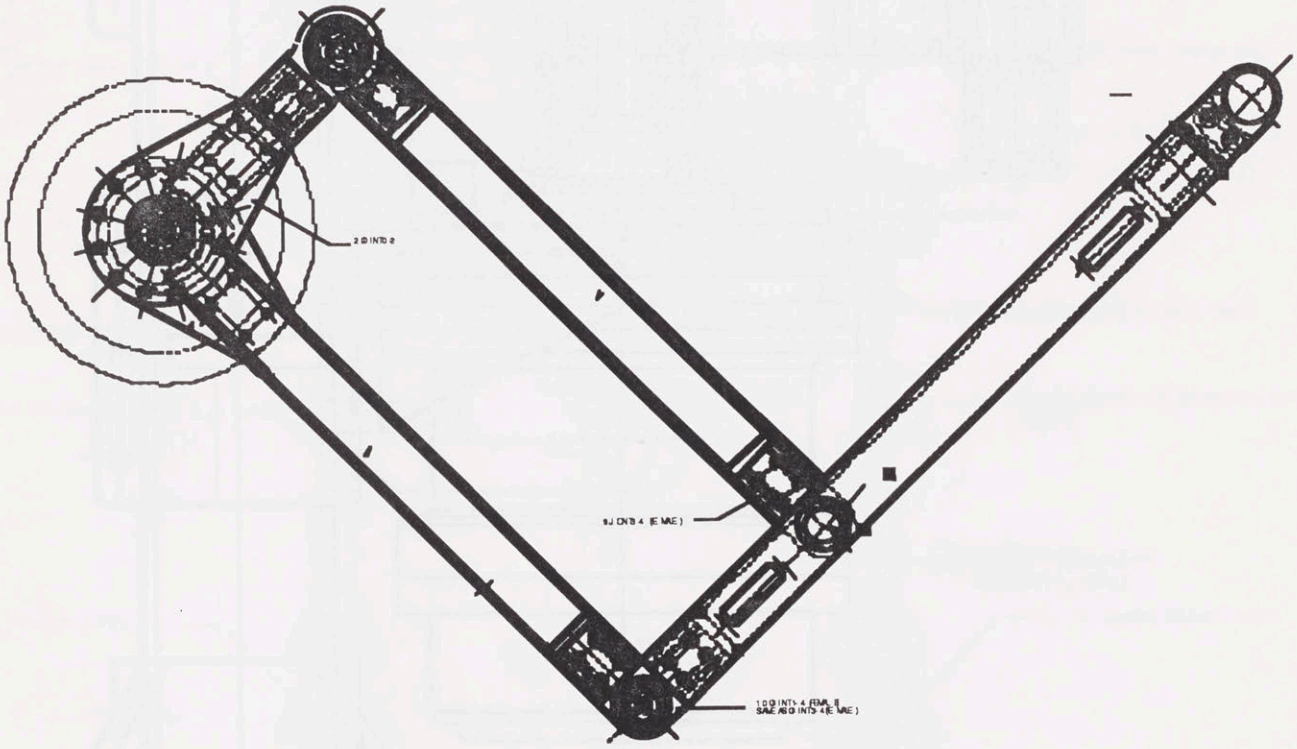

Fig. 9.1 The Designed SCARA Arm (scale 1:5 see detail in drawing ASB A03)

The details drawings of each element of the SCARA arm are included in appendix A

The direct-drive approach, together with Brushless DC motors, results in low friction, high stiffness, and low inertia properties reflected to the user. Each actuator

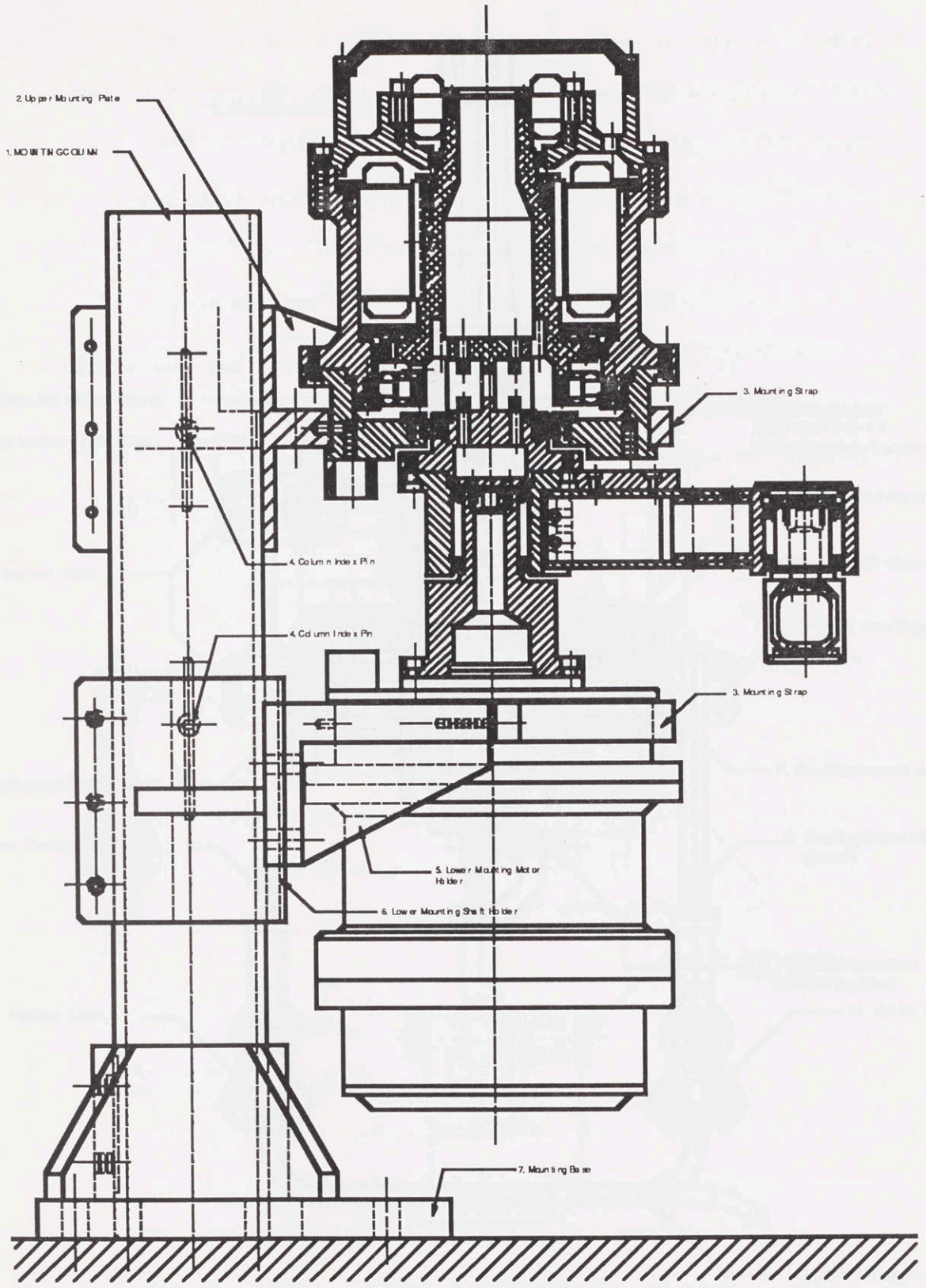

Fig. 9.2 Cross Section View of the Manual Teaching Aid (drawing ASB B01)

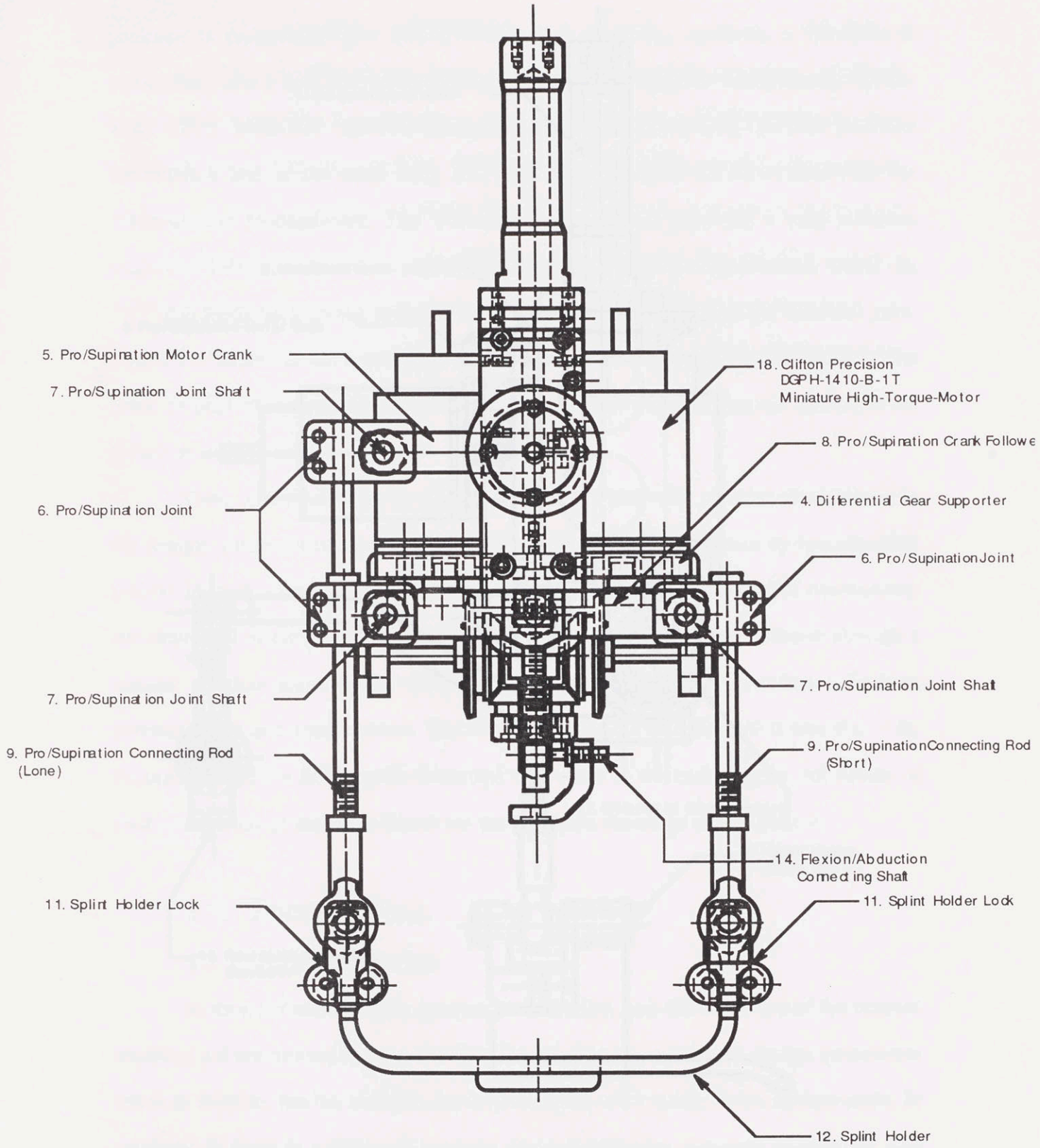

Fig. 9.3 Front View of the End-Effector (scale 1: 1.8, drawing ASB E01)

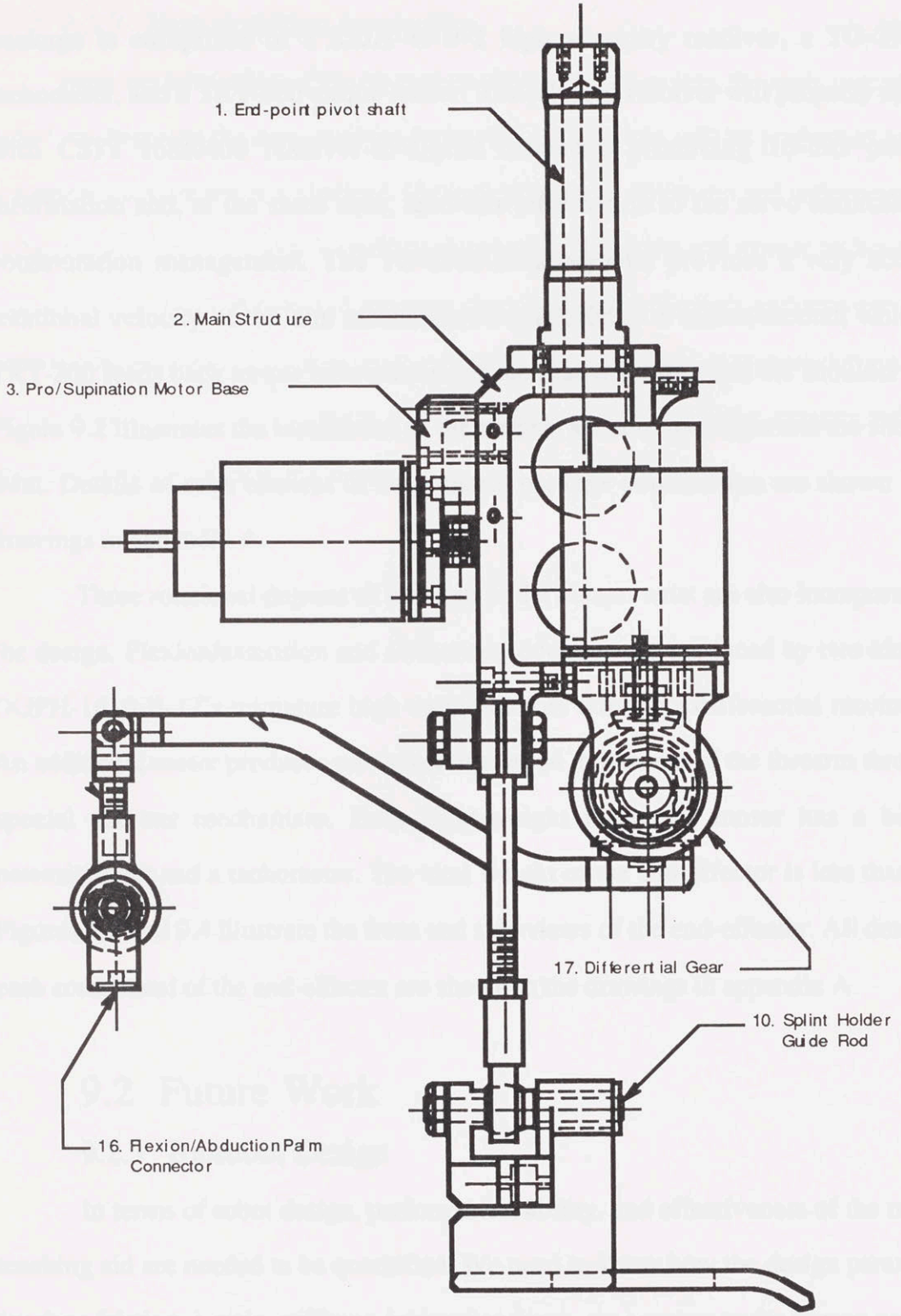

Fig. 9.4 Side View of the End-Effector (scale 1:1.81, drawing ASB E01)

package is comprised of a SSJH-44-B-2 high accuracy resolver, a TG-2936-B tachometer, and a TRT-200 torque sensor. The selected resolver will properly operate with CSI's 168K400 resolver-to-digital converter producing 16-bits position information and, at the same time, feed this information to the servo controller for commutation management. The TG-2936-B tachometer provides a very accurate rotational velocity of the arm mechanism from 0.008 to 8 radian/second, while the TRT-200 feeds back torque information between the drive unit and the shoulder joint. Figure 9.2 illustrates the installation of the tandem actuator packages and the shoulder joint. Details of each element in the actuator package construction are shown in the drawings in appendix A.

Three rotational degrees of freedom of the human wrist are also incorporated in the design. Flexion/extension and abduction/adduction are produced by two identical DGPH-1610-B-1T's miniature high torque motors through a differential mechanism. An additional motor produces pronation/supination movement of the forearm through a special six bar mechanism. Each light-weight miniature motor has a built-in potentiometer and a tachometer. The total weight of the end-effector is less than 3 lb. Figures 9.3 and 9.4 illustrate the front and side views of the end-effector. All details of each component of the end-effector are shown in the drawings in appendix A.

9.2 Future Work

9.2.1 Biorobot Design

In terms of robot design, performance, ability, and effectiveness of the manual teaching aid are needed to be quantified. We need to know how the design parameters (such as friction, inertia, stiffness, interaction force, etc.) matter to the human users. In addition, if there is a trade-off between these parameters, we need to find the cost function in order to be able to find the optimum for the next biorobot design versions.

9.2.2 Man-machine Interaction

Once the fabrication of the manual teaching aid is complete, the main part of the project can begin on the man-machine interaction. This study will be performed using the manual teaching aid as a platform. Using this platform, hardware and software tools in physical therapy applications could be developed. Computer and robotic technology might facilitate a new method of physical therapy, such as therapy performance and progress measurement (implies having a quantification method) or remote therapy. If this machine is successful, perhaps various other machines could be constructed for therapy of different parts of the body.

Bibliography

Bibliography

[1] Abul-Haj C.J., Hogan N., *Functional Assessment of Control Systems for Cybernetic Elbow Prostheses*, IEEE Transactions on Biomedical Engineering, 1990

[2] Asada, H. and Youcef-Toumi, K., *Direct-drive robot*, MIT Press, Cambridge, 1988

[3] Asada H., *Arm Design*, 2.853 in-class document, Massachusetts Institute of Technology

[4] The American National Standards Institute ANSI Pub. A117-1961, Revalidated 1971

[5] Campbell C.L., *Introduction: Robotics and the Disabled*, Occupational Therapeutic Health Care 3, 1986

[6] Coiffet, P., Modelling and Control, *Robot Technology*, Vol.1, Prentice Hall, 1983

[7] Craig, J.J., Raibert, M.H., *Hybrid Position/Force Control of Manipulators*, ASME Journal of Dynamic Systems, Measurement and control, Vol. 102, June 1981, pp. 126-133

[8] Department of the Air Force,*AFSC Design Handbook 1-3*, Jan 1977, Headquarters Air Force Systems Command, Andrews AFB, DC 20334, pp. 16-17

[9] Dept. of Health and Human Service, *Disability Survey 72*, Research report no. 56, April 1981

[10] Deutshchman, A., Micheals, W., Wilson, C., *Machinery-Design*, Macmillan Publishing Co., Inc. New York, 1975

[11] Diffrient, Tilley, Harman, *Humanscale 1/2/3* , MIT press, Cambridge, 1981

[12] Diffrient, Tilley, Harman, *Humanscale 7/8/9*, MIT press, Cambridge, 1981

[13] Dijkers M.P., Geer D.M., *Patient and Staff Acceptance of Robotic Technology in Occupational Therapy: A pilot study*, Journal of Rehabilitation Research and Development Vol. 28 No. 2, 1991

[14] Eschmann, P., *Ball and roller bearings*, 2nd.Ed., John Wiley and Sons, NY, 1985

[15] Faye I. C., *An Impedance Controlled Manipulandum For Human Movement Studies*, MIT SM Thesis, 1986

[16] Harwin W.S., Ginige A., Jackson R.D., *A Robot Workstation for Use in education of the Physically Handicapped*. IEEE Trans Biomed End 35(2), 1987

[17] Hogan, N., *Impedance Control: An Approach to Manipulation: Part 1- Theory Implementation, and Application*, Journal of Dynamic Systems, Measurement, and Control, Vol. 107, March 1985

[18] Hogan, N., *Stable Execution of Contact Tasks Using Impedance Control*, Proceedings of IEEE International Conference on Robotics and Automation, 1987

[19] Khalili D, Zomlefer, *An intelligent Robotic System for Rehabilitation of Joints and Extimation of Body Segment Parameters*. IEEE Trans Biomed Eng 35(2), 1988

[20] Levin, M. D., *Design and Control of a Closed-Loop Brushless Torque Actuator*, MIT SM Thesis (Artificial Intelligence Laboratory), 1990.

[21] Machine Design, *1990 Systems Design Reference Volume*, Penton, 1990

[22] Makino, H. and Furuya, N., *Selective compliance assembly robot arm*, Proc. 1st Int. Conf. on Assembly Automation, Brighton, IFS, Kempston, UK, 1980

[23] Michigan Center for a Barrier-Free Environment by Salem, *Barrier Free Design*, 1977.

[24] Mortensen A., *Automatic Grinding*, Preceedings of the 13th International Symposium on Industrial Robots, 1983

[25] Nippon Seiko K.K, *Precision machine parts / Linear motion products* , Japan, 1987

[26] Nippon Seiko K.K.,*NSK Ball and roller bearings*, Japan, 1986

[27] Nippon Thomson Co.,Ltd.; *Linear motion products* ; CAT-5736, 5731, 5715, 5714, 5732, 5717, 5737; Japan.

[28] Hirose, S. Umetani, Y. *A Cartesian coordinates manipulator with articulated structure*, 11th International Symposium on Industrial Robots, Tokyo, Japan 1981

[29] Paul, B. J., *A Systems Approach to the Torque Control of a Permanent Magnet Brushless Motor*, MIT SM Thesis (Artificial Intelligence Laboratory), 1987.

[30] Paul, R. P., Stevenson, C. N., *Kinematics of Robot Wrists*, Int. J. of Robotics Research, 2-1, 31/38, 1983

[31] Poole, H., *Fundamentals of Robotics Engineering*, Van Nostrand Reinhold, NY, 1989

[32] Rivin, E.I. *Mechanical Design of Robots*, New York, McGraw-Hill, 1988.

[33] Seamone, W., G. Schmeisser, *Evaluation of the APL/JHU Robot Arm Work Station, Interactive robotic Aids - One Option for Independent Living World Rehabilitation Fund*, New York, 1986

[34] *SKF Engineering Data*, SKF Industries, Inc., 1973

[35] Spong and Vidyasaga, *Robot Dynamics and Control*, John Wiley and Sons, New York, 1989

[36] Van Cott, Kinkade, *Human Engineering Guide to Equipment Design*, McGraw-Hill, 1963

[37] Whitney D.E., *Historical Perspective and State of Art in Robot Force Control*, International Journal of Robotics Research Vol.6, No. 1, Spring 1987

Appendices

Appendix A: Detail Drawings

Appendix A contains detail drawings of manual teaching aid. These drawings are not drawn to scale but shrinking down from 22X34 in. vellums to US letter papers. If exact dimension are to be used, please see full scale drawing at Newman Laboratory for Biomechanics and Rehabilitation, Massachusetts Institute of Technology.

Appendix A.1: Arm Subassembly

Drawing No.	Name	Page No.
ASB A01	Shoulder Joint Assembly	201
ASB A02	Arm Assembly, Front View	202
ASB A03	Arm Assembly, Top View	203
A01	Link 1	204
A02	Link 2	205
A03	Link 3	206
A04	Link 4	207
A05	Joint 3-4 (Male)	208
A06	Joint 1-4 (Male)	209
A07	Joint 1-4, 3-4 (Female)	210
A08	Joint 1-4, 3-4 Retainer	211
A09	Joint 1-4, 3-4 Cap	212
A10	Joint 2-3 (Female)	213
A11	Joint 2-3 (Male)	214
A12	Joint 2-3 Cap	215
A13A	End-Point Rod Holder	216
A13B	End-Point Shaft Holder	217
A13C	End-Point Joint Rod	218
A13D	Joint 3-4 Retainer	219
A13E	End-Point Joint Cap	220
A14	End-Point Joint Pin	221
A15	Joint 2-3 Retainer	222
A16	Joint 0-2	223
A17	Joint 0-1	224

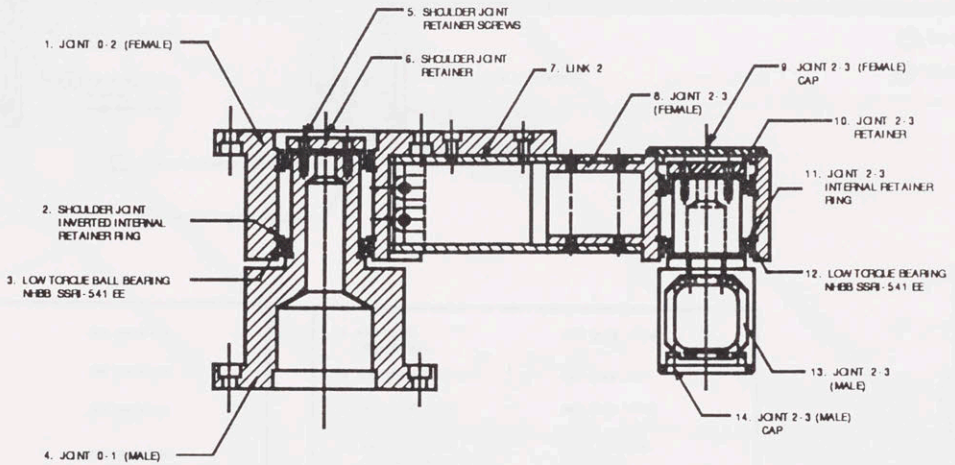

1. JOINT 0-2 (FEMALE)	SEE DWG# A16
2. SHOULDER JOINT INVERTED INTERNAL RETAINER RING	WALDES TRUARC 5008-150
3. LOW TORQUE BALL BEARING NHBB SSR1-541 EE	
4. JOINT 0-1 (MALE)	SEE DWG# A17
5. SHOULDER JOINT RETAINER SCREW	
6. SHOULDER JOINT RETAINER	SEE DWG# A15
7. LINK 2	SEE DWG# A02
8. JOINT 2-3 (FEMALE)	SEE DWG# A10
9. JOINT 2-3 (FEMALE) CAP	SEE DWG# A12
10. JOINT 2-3 RETAINER	SEE DWG# A15
11. JOINT 2-3 INTERNAL RETAINER RING	WALDES TRUARC 5008-118
12. LOW TORQUE BEARING NHBB SSR1-541 EE	
13. JOINT 2-3 (MALE)	SEE DWG# A11
14. JOINT 2-3 (MALE) CAP	SEE DWG# A12

Tolerances X ±.xx XX ±.xx XXX ±.xxx Unless specified	Manual Teaching Aid Shoulder Joint Assembly		
Scale 1 : 1	ASB A01	Drw. by Jen Charnnarong	App by Dr. Andre Sharon
	1/24/91	Massachusetts Institute of Technology	

DWG# ASB A02

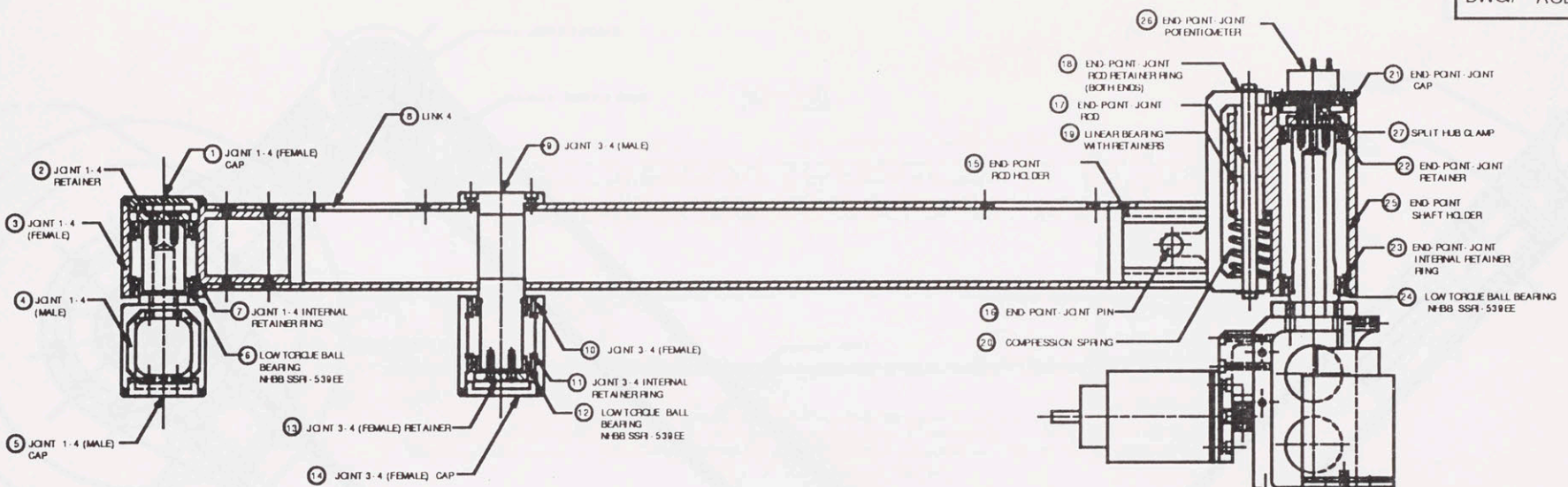

1	JOINT 1-4 (FEMALE) CAP	SEE DWG# A09
2	JOINT 1-4 RETAINER	SEE DWG# A08
3	JOINT 1-4 (FEMALE)	SEE DWG# A07
4	JOINT 1-4 (MALE)	SEE DWG# A06
5	JOINT 1-4 (MALE) CAP	SEE DWG# A09
6	LOW TORQUE BALL BEARING NHBB SSR1-539EE	
7	JOINT 1-4 INTERNAL RETAINER RING	WALDES TRUARC 5008-118
8	LINK 4	SEE DWG# A04
9	JOINT 3-4 (MALE)	SEE DWG# A05
10	JOINT 3-4 (FEMALE)	SEE DWG# A07
11	JOINT 3-4 INTERNAL RETAINER RING	WALDES TRUARC 5008-118
12	LOW TORQUE BALL BEARING NHBB SSR1-539EE	
13	JOINT 3-4 (FEMALE) RETAINER	SEE DWG# A08
14	JOINT 3-4 (FEMALE) CAP	SEE DWG# A09

15	END-POINT ROD HOLDER	SEE DWG# A13A
16	END-POINT-JOINT PIN	SEE DWG# A14
17	END-POINT JOINT ROD	SEE DWG# A14C
18	END-POINT-JOINT ROD RETAINER RING (BOTH ENDS)	BERG RETAINER RING CQ2-25
19	LINEAR BEARING WITH RETAINERS	BERG LMB-1
20	COMPRESSION SPRING	SPEC STOCK COMPRESSION SPRING
21	END-POINT-JOINT CAP	SEE DWG# A13E
22	END-POINT-JOINT RETAINER	SEE DWG# A13D
23	END-POINT-JOINT INTERNAL RETAINER RING	WALDES TRUARC 5008-118
24	LOW TORQUE BALL BEARING NHBB SSR1-539EE	
25	END-POINT SHAFT HOLDER	SEE DWG# A13B
26	END-POINT-JOINT POTENTIOMETER	NEWENGLAND INSTRUMENT 78ESC502
27	SPLIT HUB CLAMP	BERGS CG1-27-A

Tolerances
X ±.xx
XX ±.xx
XXX ±.xxx
Unless specified

Scale 1 : 1

Manual Teaching Aid

Arm Assembly, Front view

ASB A02	Drw by Jen Chermerang	App by Dr. Angela Sharon
1/24/91	Massachusetts Institute of Technology	

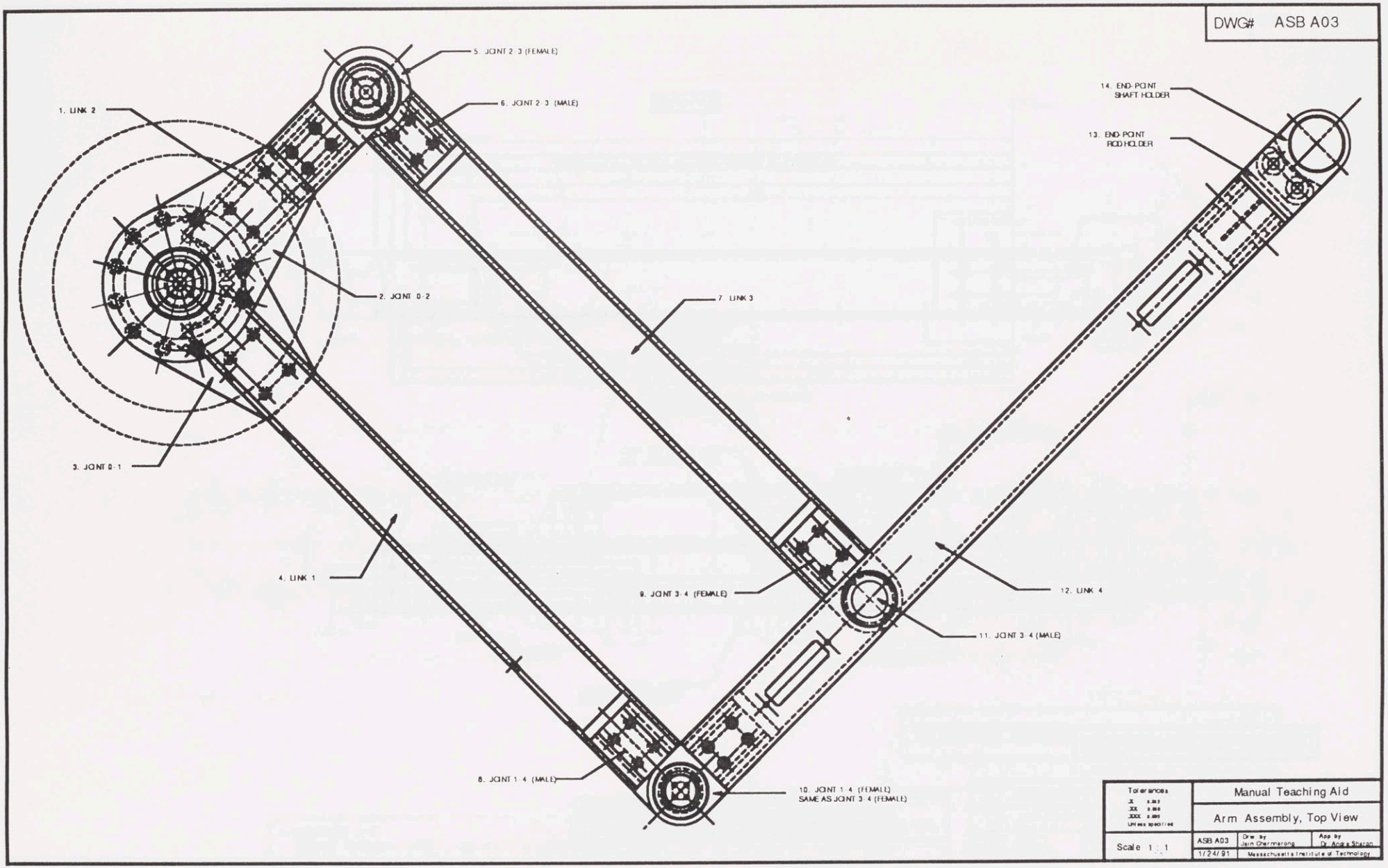
DWG# ASB A03
1. LINK 2
2. JOINT 0-2
3. JOINT 0-1
4. LINK 1
5. JOINT 2-3 (FEMALE)
6. JOINT 2-3 (MALE)
7. LINK 3
8. JOINT 1-4 (MALE)
9. JOINT 3-4 (FEMALE)
10. JOINT 1-4 (FEMALE)
SAME AS JOINT 3-4 (FEMALE)
11. JOINT 3-4 (MALE)
12. LINK 4
13. END-POINT ROD HOLDER
14. END-POINT SHAFT HOLDER
Tolerances
.X ±.xx
.XX ±.xx
.XXX ±.xxx
Unless specified
Scale 1 : 1
Manual Teaching Aid
Arm Assembly, Top View
ASB A03
Drw by Jain Chermarong
App by Dr. Anita Sharan
1/24/91
Massachusetts Institute of Technology

DWG# A01

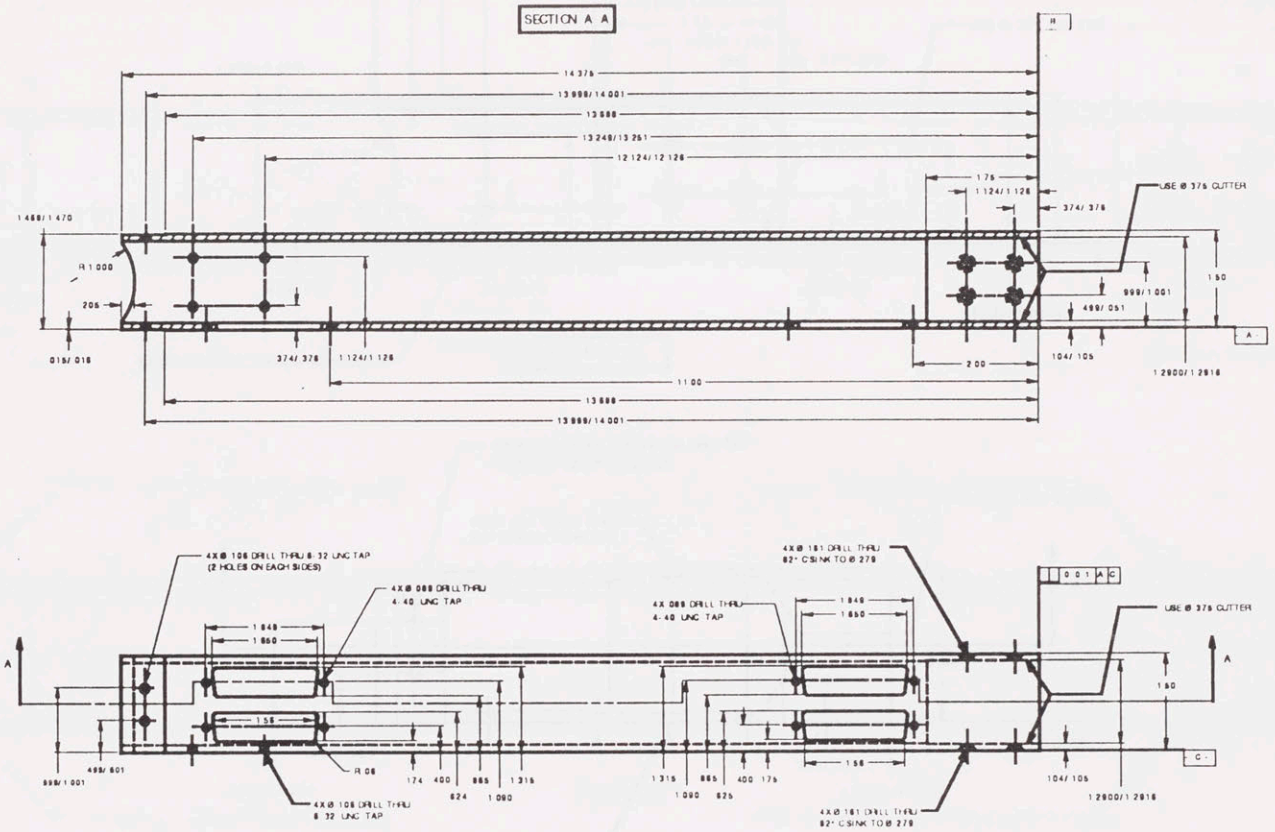

CUT FROM STANDARD SQUARE 6061-T6 ALUMINUM ALLOY STRUCTURE
1.50 X 1.50 WITH .120/.125 WALL THICKNESS

ACCESORIES LIST
1. SOCKET HEAD CAP SCREW 6-32 UNC 3/8" UNDER HEAD LENGTH 4 REQ.
2. AMP AMPLIMITE D-SUBMINIATURE CABLE CLAMP 25-PIN TYPE 747913-2 RECEPTCLE 2 REQ.
3. AMP AMPLIMITE D-SUBMINIATURE CABLE CLAMP 25-PIN TYPE 747912-2 PLUG 2 REQ.

Material: SEE ABOVE NOTE	Tolerances: X ±.xx, XX ±.xxx, XXX ±.xxx Unless specified	Manual Teaching Aid	
Finish: Black Anodize		Link 1	
Quantity Req.: 1	Scale 1 : 1	A01	Drw. by: Jean Charnnarong / App. by: Dr. Andrew Sharon
		1/24/91	Massachusetts Institute of Technology

DWG# A02

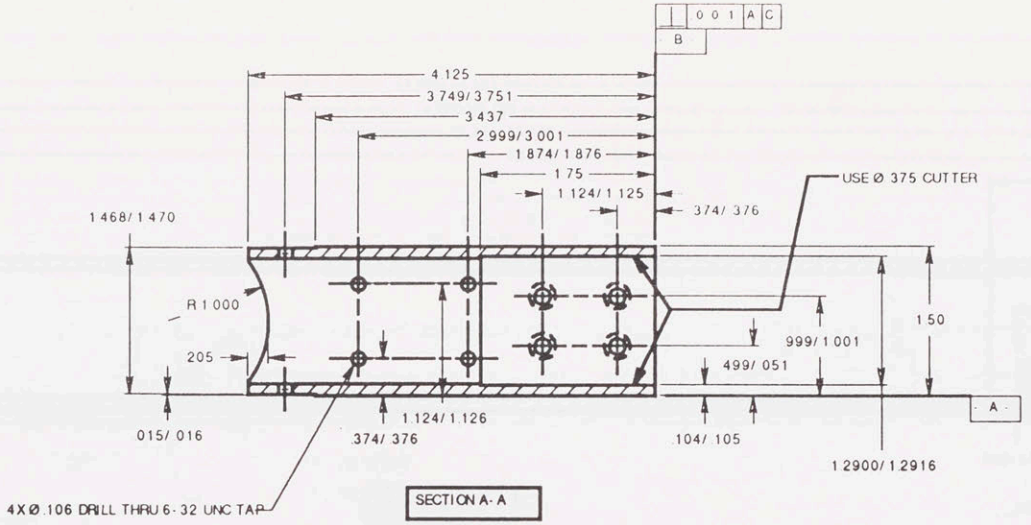

SECTION A-A

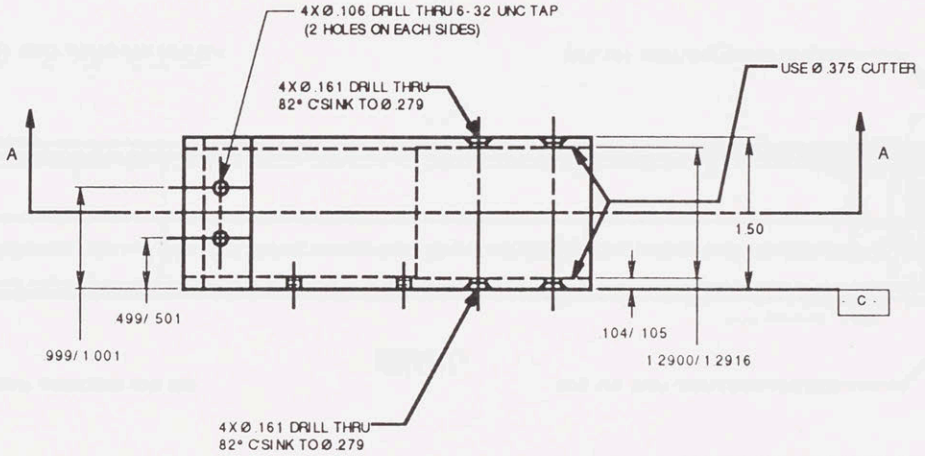

CUT FROM STANDARD SQUARE 6061-T6 ALUMINIUM ALLOY STRUCTURE
1.50 X 1.50 WITH .120/.125 WALL THICKNESS

ACCESORIES LIST
1. SOCKET HEAD CAP SCREW 6-32 UNC 3/8" UNDER HEAD LENGTH 4 REQ.
2. SOCKET HEAD CAP SCREW 6-32 UNC 1/2" UNDER HEAD LENGTH 4 REQ.

Material: See above note	Tolerances: X ±.015, XX ±.010, XXX ±.005, Unless specified	Manual Teaching Aid	
Finish: Black Anodize		Link 2	
Quantity Req.: 1	Scale 1 : 1	A02	Drw. by: Jain Charnnarong / App. by: Dr. Andre Sharon
		1/24/91	Massachusetts Institute of Technology

DWG# A03

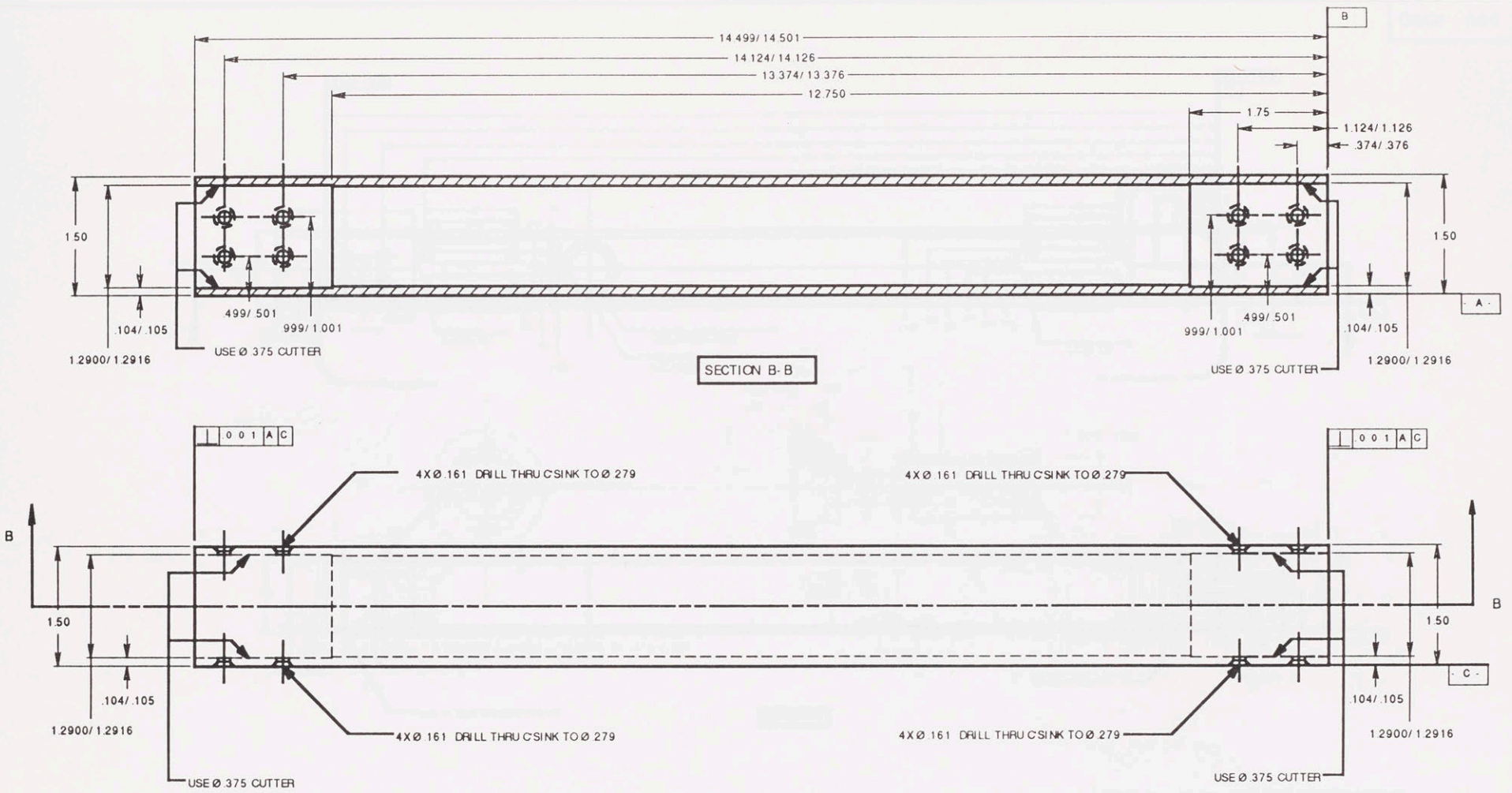

CUT FROM STANDARD SQUARE 6061-T6 ALUMINIUM ALLOY STRUCTURE
1.50 X 1.50 WITH .120/.125 WALL THICKNESS

Material: See above note	Tolerances: X ±.015, XX ±.010, XXX ±.005 Unless specified	Manual Teaching Aid	
Finish: Black Anodize		Link 3	
Quantity Req.: 1	Scale 1 : 1	A03	Drw. by: Jain Charnnarong; App. by: Dr. Andre Sharon
		1/24/91	Massachusetts Institute of Technology

DWG# A04

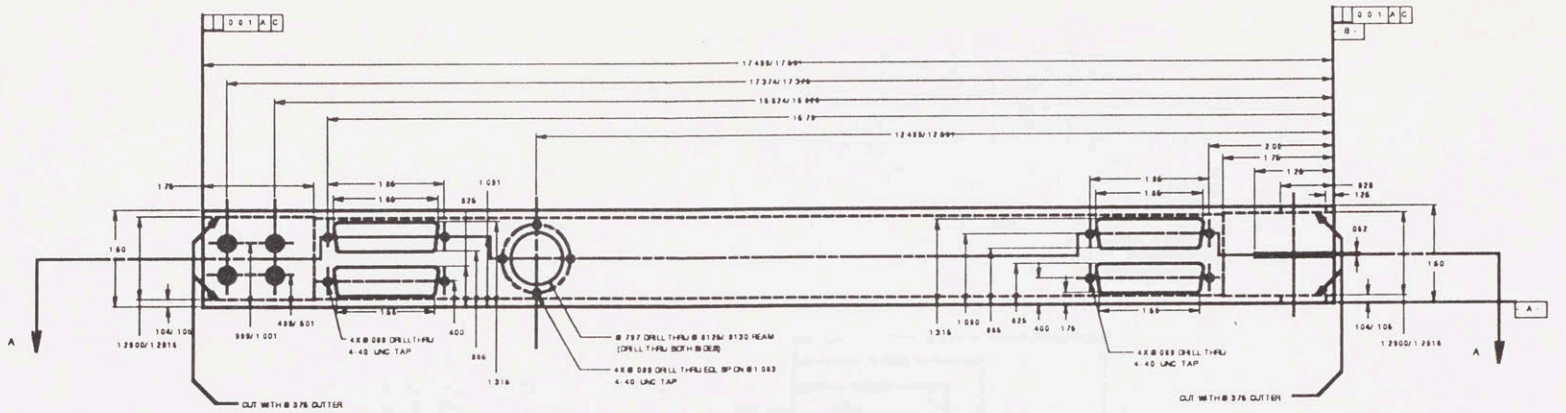

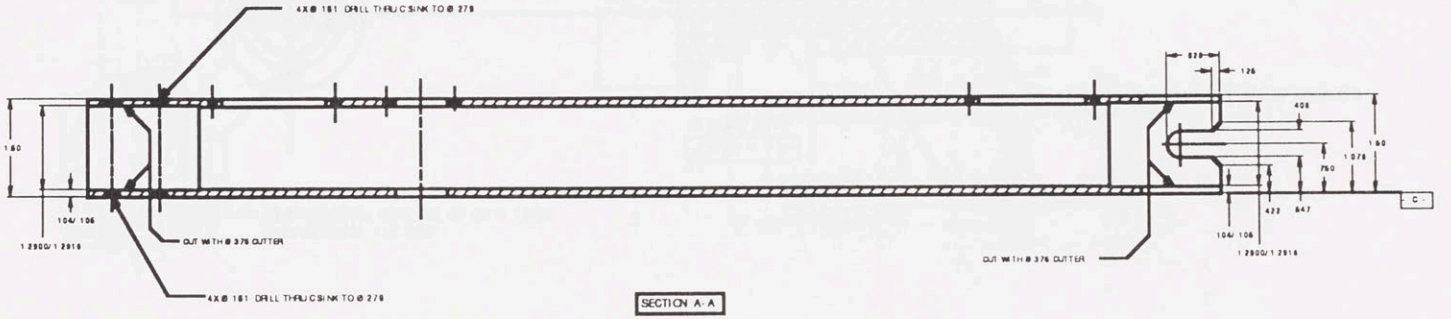

SECTION A-A

CUT FROM STANDARD SQUARE 6061-T6 ALUMINUM ALLOY STRUCTURE
1.50 X 1.50 WITH .120/.125 WALL THICKNESS

ACCESSORIES LIST
1. AMP AMPLIMITE D-SUBMINIATURE CABLE CLAMP 25-PIN TYPE 747913-2 RECEPTACLE 1 REQ.
2. AMP AMPLIMITE D-SUBMINIATURE CABLE CLAMP 25-PIN TYPE 747912-2 PLUG 2 REQ.
3. SOCKET HEAD CAP SCREW 4-40 UNC 5/16" UNDER HEAD LENGTH 4 REQ.

Material: See above note	Tolerances: .X ±.xxx, .XX ±.xxx, .XXX ±.xxx unless specified	Manual Teaching Aid	
Finish: Black Anodize		Link 4	
Quantity Req.: 1	Scale 1 : 1	A04	Drw by: Jain Charmnarong; App by: Dr. Angus Shaw
		1/24/91	Massachusetts Institute of Technology

DWG# A05

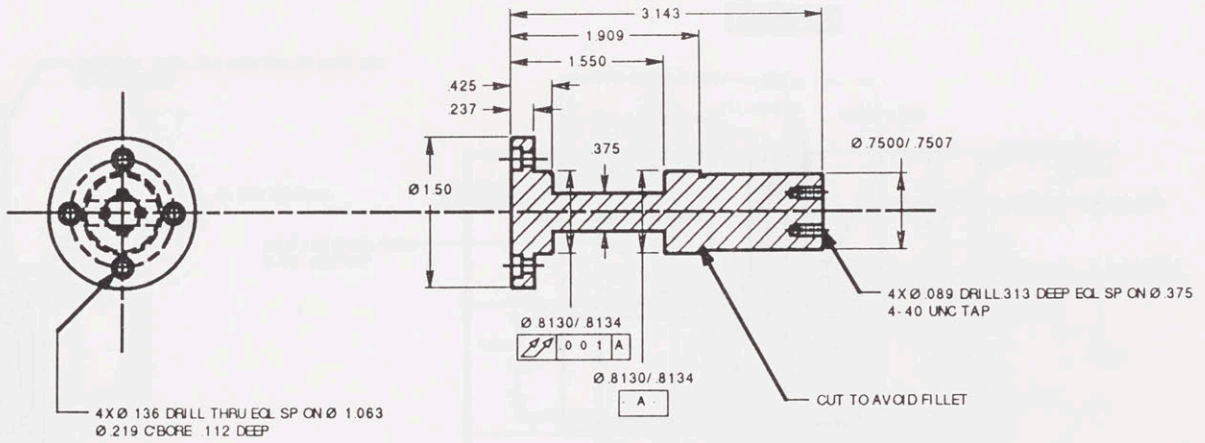

NOTE

1. R.030 FOR ALL FILLETS AND CHAMFERS UNLESS SPECIFIED

ACCESSORIES LIST

1. SOCKET HEAD CAP SCREW 4-40 UNC 3/8" UNDER HEAD LENGTH 4 REQ.

Material 6061-T6 Aluminium Alloy	Tolerances X ±.015 XX ±.010 XXX ±.005 Unless specified	Manual Teaching Aid	
Finish Black Anodize		Joint 3-4,(Male)	
Quantity Req. 1	Scale 1 : 1	A05	Drw. by Jain Charnnarong / App. by Dr. Andre Sharon
		1/24/91	Massachusetts Institute of Technology

DWG# A06

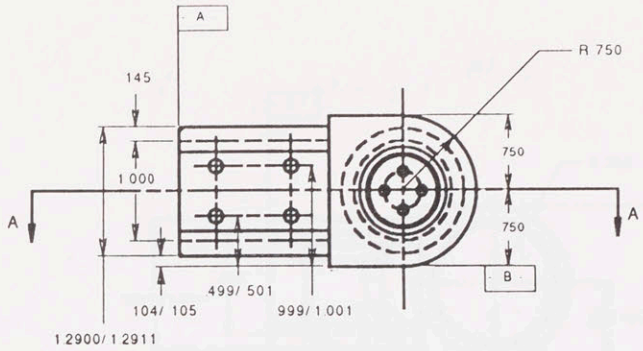

SECTION A-A

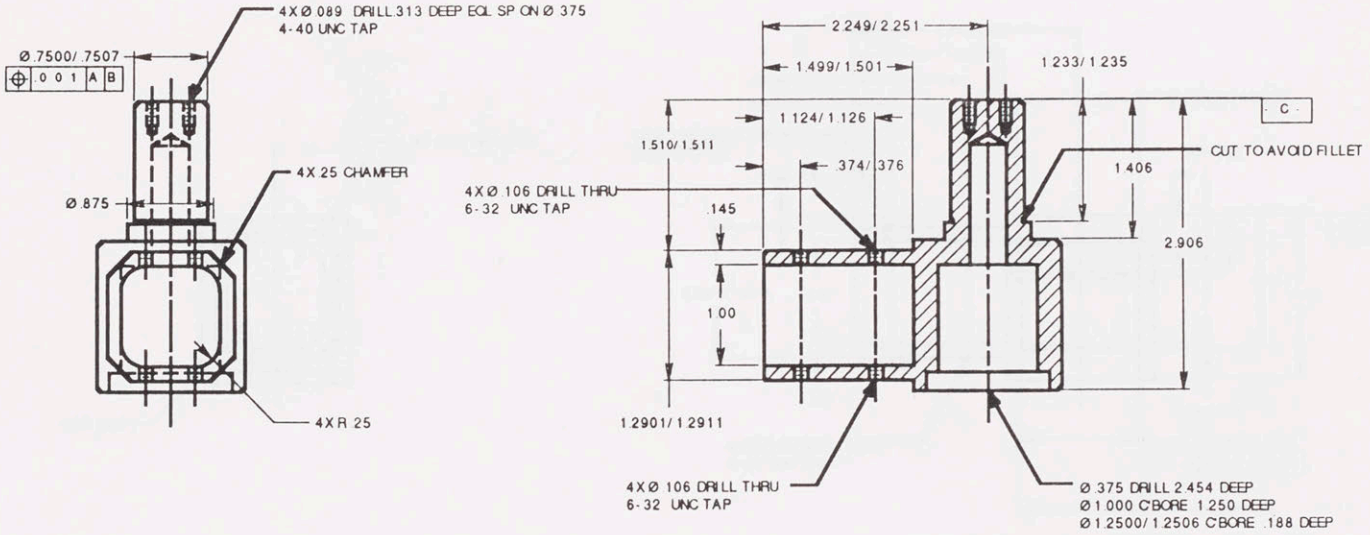

NOTE
1. R.030 FOR ALL FILLETS AND CHAMFERS UNLESS SPECIFIED

ACCESSORIES LIST
1. FLAT HEAD SOCKET HEAD CAP SCREW 4-40 UNC 5/8" OVERALL LENGTH 4 REQ.
2. FLAT HEAD SOCKET HEAD CAP SCREW 6-32 UNC 5/16" OVERALL LENGTH 8 REQ.

Material: 6061-T6 Aluminium Alloy	Tolerances: X ±.015, XX ±.010, XXX ±.005 Unless specified	Manual Teaching Aid	
Finish: Black Anodize		Joint 1-4 (Male)	
Quantity Req.: 1	Scale 1 : 1	A06	Drw. by: Jain Charnnarong; App. by: Dr. Andre Sharon
		1/24/91	Massachusetts Institute of Technology

DWG# A07

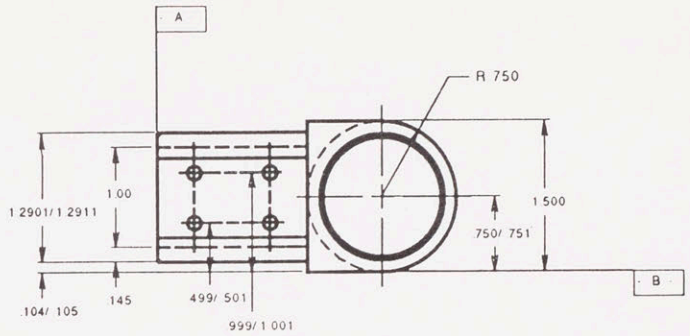

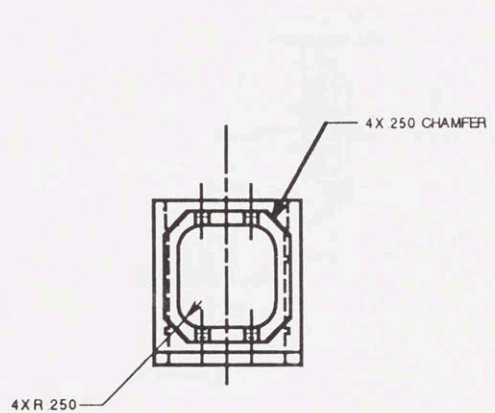

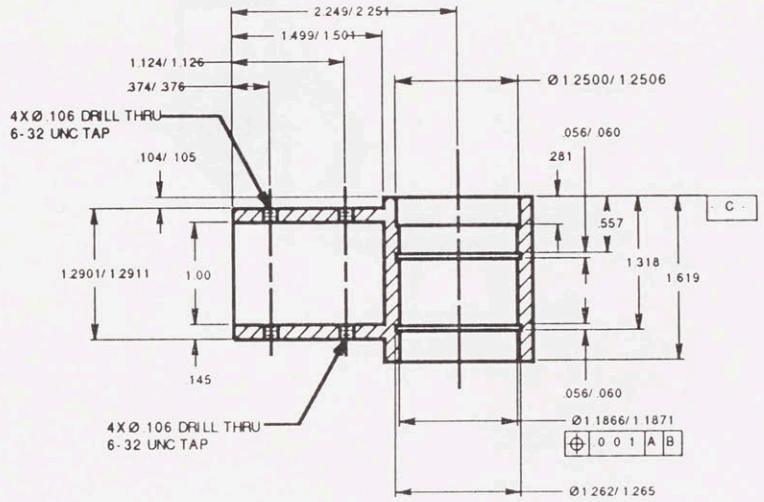

NOTE

1. R.030 FOR ALL FILLETS AND CHAMFERS UNLESS SPECIFIED

ACCESSORIES LIST

1. FLAT HEAD SOCKET HEAD CAP SCREW 6-32 UNC 5/16" UNDER HEAD LENGTH 16 REQ.
2. WALDES TRUARC INVERTED RETAINER RING 5008-118 4 REQ.
3. LOW FRICTION BALL BEARING NHBB SSRI-539EE 4 REQ.

Material: 6061-T6 Aluminium Alloy	Tolerances: X ±.015, XX ±.010, XXX ±.005 Unless specified	Manual Teaching Aid	
Finish: Black Anodize		Joint 1-4, 3-4 (Female)	
Quantity Req.: 2	Scale 1 : 1	A07	Drw. by: Jain Charnnarong / App. by: Dr. Andre Sharon
		1/24/91	Massachusetts Institute of Technology

DWG# A08

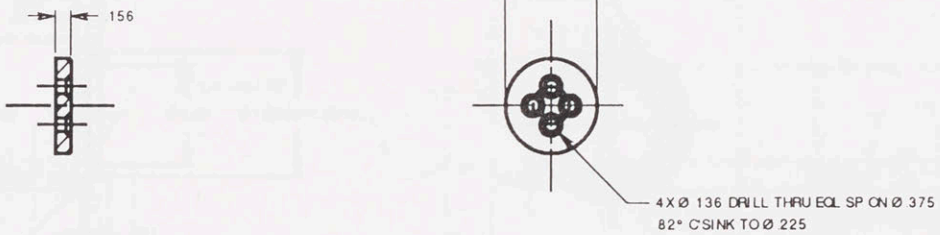

NOTE

1. R.030 FOR ALL FILLETS AND CHAMFERS UNLESS SPECIFIED

Material: 6061-T6 Aluminium Alloy	Tolerances: X ±.015, XX ±.010, XXX ±.005 Unless specified	Manual Teaching Aid	
Finish: Black Anodize		Joint 1-4, 3-4 Retainer	
Quantity Req.: 2	Scale 1 : 1	A08	Drw. by Jain Charnnarong / App. by Dr. Andre Sharon
		1/24/91	Massachusetts Institute of Technology

DWG# A09

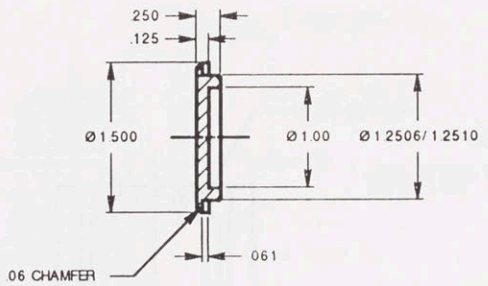

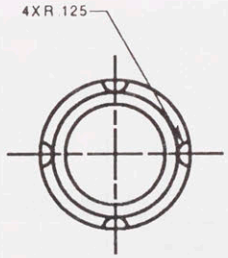

NOTE

1. .030 FOR ALL FILLETS AND CHAMFERS UNLESS SPECIFIED

Material: 6061-t6 Aluminium Alloy	Tolerances: X ±.015, XX ±.010, XXX ±.005, Unless specified	Manual Teaching Aid	
Finish: Black Anodize		Joint 1-4, 3-4 Cap	
Quantity Req.: 4	Scale 1 : 1	A09	Drw. by: Jain Charnnarong; App. by: Dr. Andre Sharon
		1/24/91	Massachusetts Institute of Technology

DWG# A10

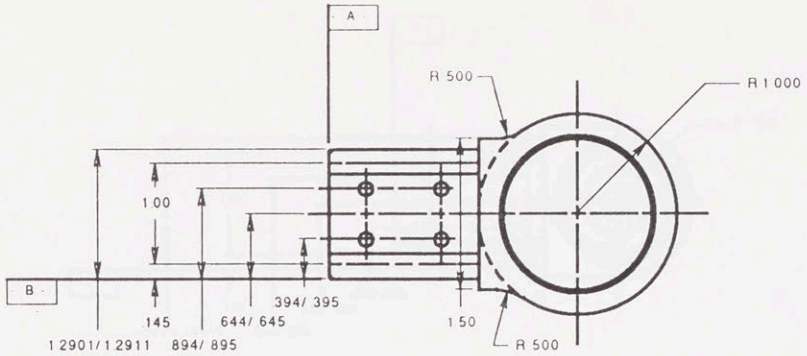

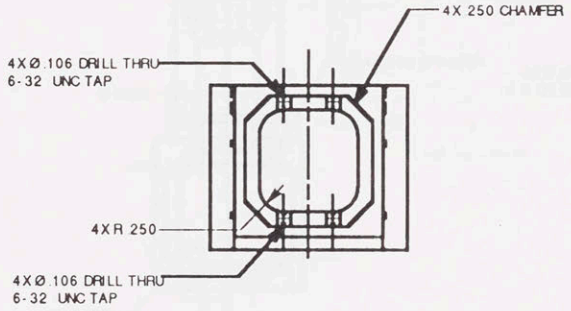

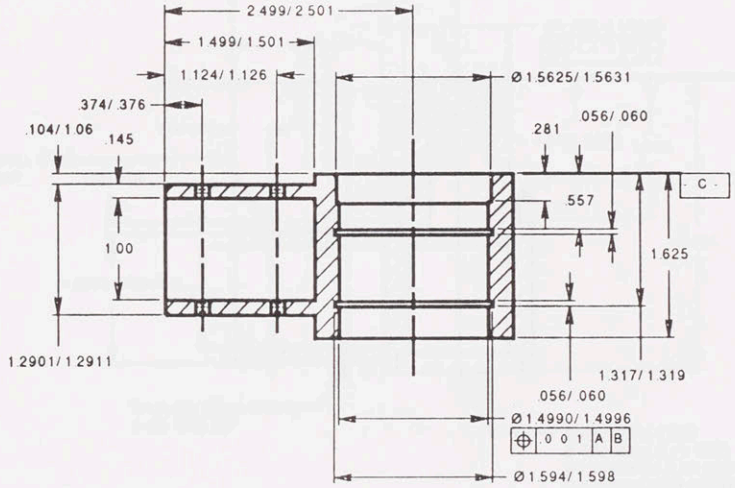

NOTE
1. .030 FOR ALL FILLETS AND CHAMFERS UNLESS SPECIFIED

ACCESSORIES LIST
1. WALDES TRUARC INVERTED INTERNAL RETAINER RING 5008-150 2 REQ.
2. LOW TORQUE BALL BEARING NHBB SSRI-541 EE 2 REQ.
3. FLAT HEAD SOCKET HEAD CAP SCREW 6-32 UNC 5/16" OVERALL LENGTH 8 REQ.

Material: 6061-T6 Aluminium Alloy	Tolerances: X ±.015, XX ±.010, XXX ±.005 Unless specified	Manual Teaching Aid	
Finish: Black Anodize		Joint 2-3 (Female)	
Quantity Req.: 1	Scale 1 : 1	A10	Drw. by: Jain Charnnarong; App. by: Dr. Andre Sharon
		1/24/91	Massachusetts Institute of Technology

DWG# A11

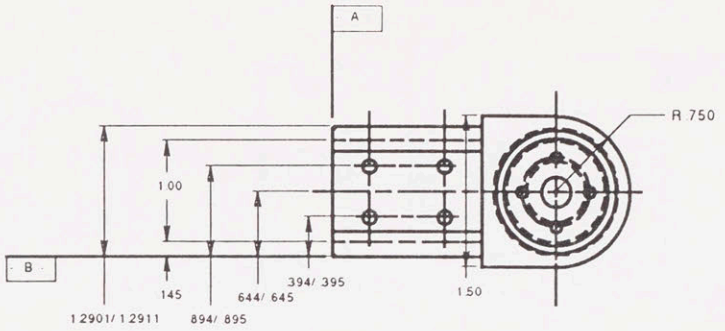

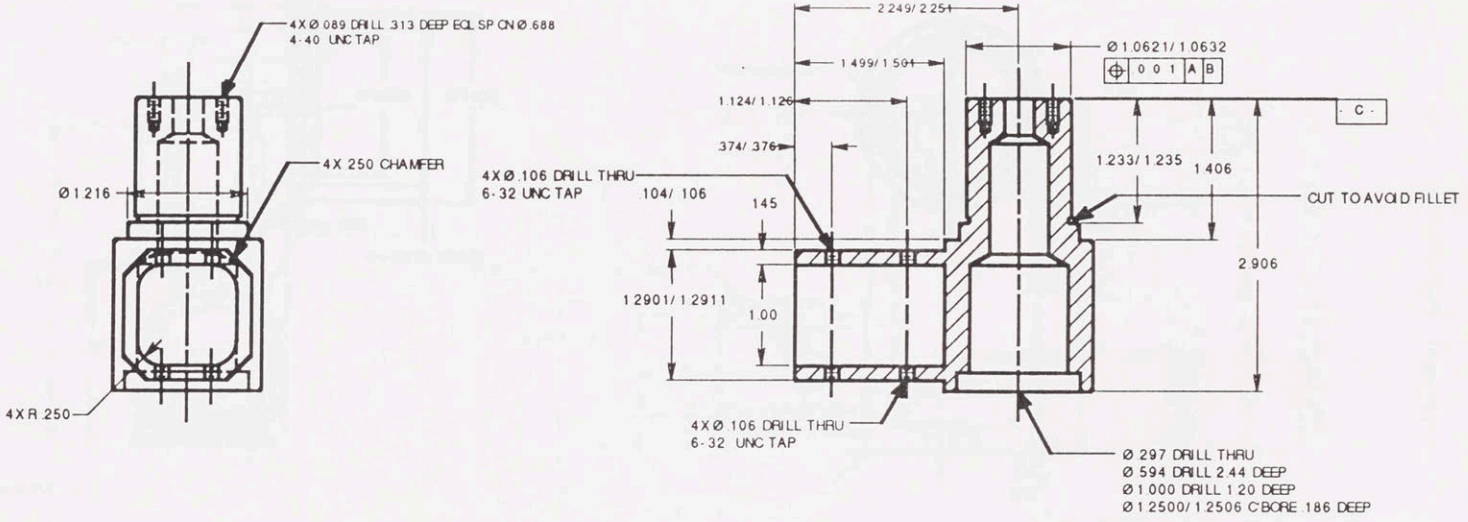

NOTE

1. R.030 FOR ALL FILLETS AND CHAMFERS UNLESS SPECIFIED

ACCESSORIES LIST
1. FLAT HEAD SOCKET HEAD CAP SCREW 6-32 UNC 5/16" OVERALL LENGTH 8 REQ.
2. FLAT HEAD SOCKET HEAD CAP SCREW 4-40 UNC 1/2" OVERALL LENGTH 4 REQ.

Material: 7075-T6 Aluminium Alloy	Tolerances: X ±.015, .XX ±.010, .XXX ±.005 Unless specified	Manual Teaching Aid	
Finish: Black Anodize		Joint 2-3 (Male)	
Quantity Req.: 1	Scale 1 : 1	A11	Drw. by Jain Charnnarong / App. by Dr. Andre Sharon
		1/24/91	Massachusetts Institute of Technology

DWG# A12

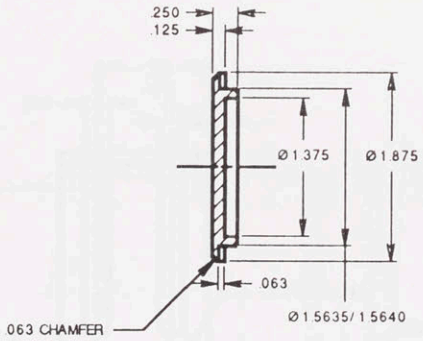

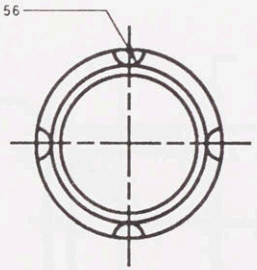

NOTE

1. R.030 FOR ALL FILLETS AND CHAMFERS UNLESS SPECIFIED

Material: 6061-T6 Aluminium Alloy	Tolerances: X ±.015, XX ±.010, XXX ±.005, Unless specified	Manual Teaching Aid	
Finish: Black Anodize		Joint 2-3 Cap	
Quantity Req.: 1	Scale 1 : 1	A12	Drw. by Jairn Charnnarong / App. by Dr. Andre Sharon
		1/24/91	Massachusetts Institute of Technology

DWG# A13A

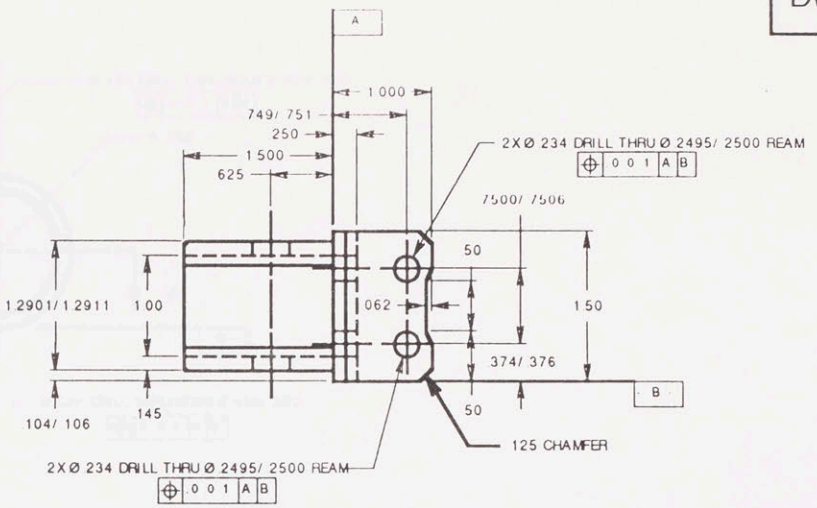

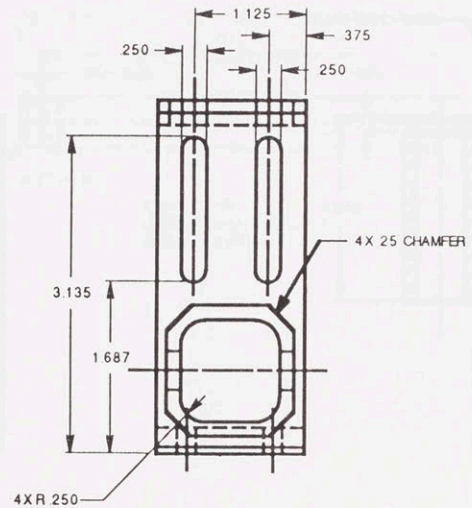

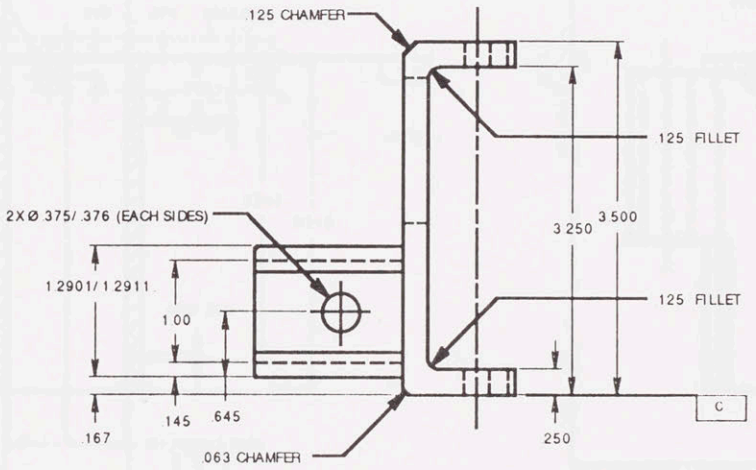

NOTE

1. R.030 FOR ALL FILLETS AND CHAMFERS UNLESS SPECIFIED

Material: 6061-T6 Aluminium Alloy	Tolerances: X ±.015, XX ±.010, XXX ±.005 Unless specified	Manual Teaching Aid	
Finish: Black Anodize		End-Point Rod Holder	
Quantity Req.: 1	Scale 1 : 1	A13A	Drw. by: Jain Charnnarong / App. by: Dr. Andre Sharon
		1/24/91	Massachusetts Institute of Technology

DWG# A13B

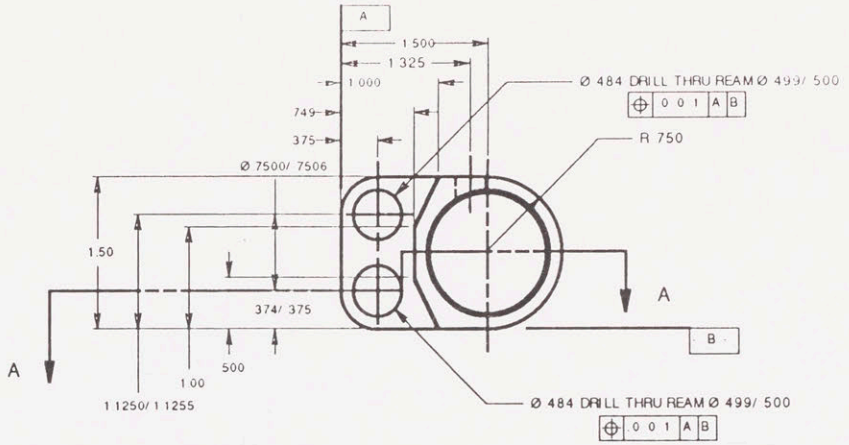

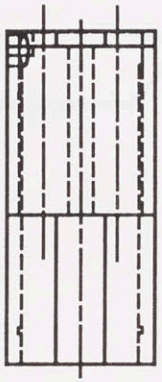

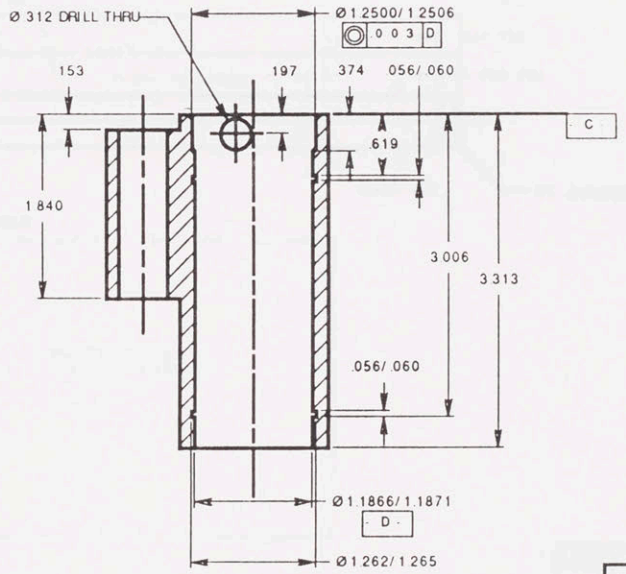

SECTION A-A

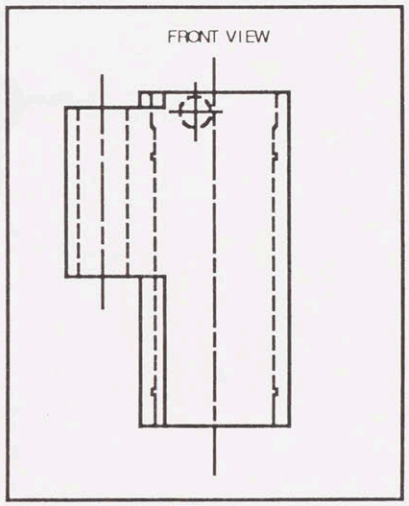

NOTE

1. .030 FOR ALL FILLETS AND CHAMFERS UNLESS SPECIFIED

ACCESSORIES LIST

1. WALDES TRUARC INVERTED INTERNAL RETAINER RING 5008-118 2 REQ.
2. BERG'S LINEAR BALL BEARING LMB-1 4 REQ.
3. BERG'S C6-50-CP RETAINER RING 4 REQ.
4. SPEC'S STOCK COMPRESSION SPRING STAINLESS STEEL C072-081-1500 2 REQ.

Material: 6061-T6 Aluminium Alloy	Tolerances: X ±.015, XX ±.010, XXX ±.005 Unless specified	Manual Teaching Aid	
Finish: Black Anodize		End-Point Shaft Holder	
Quantity Req.: 1	Scale 1 : 1	A13B	Drw. by Jain Charnnarong / App. by Dr. Andre Sharon
		1/24/91	Massachusetts Institute of Technology

DWG# A13C

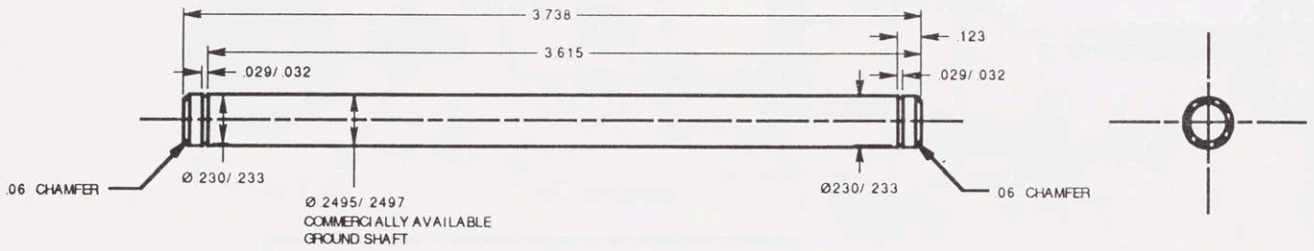

NOTE

1. R.030 FOR ALL FILLETS AND CHAMFERS UNLESS SPECIFIED

ACCESSORIES LIST

1. BERGS RETAINER RING C2-25 4 REQ.

Material	AISI 303 Stainless steel	Tolerances X ±.015 XX ±.010 XXX ±.005 Unless specified	Manual Teaching Aid	
Finish	Black Oxide		End-Point-Joint Rod	
Quantity Req.	2	Scale 2 : 1	A13C	Drw. by Jain Charnnarong / App. by Dr. Andre Sharon
			1/24/91	Massachusetts Institute of Technology

DWG# A13D

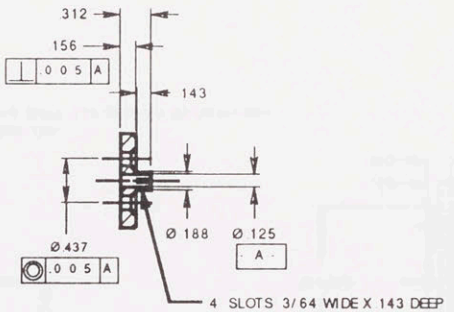

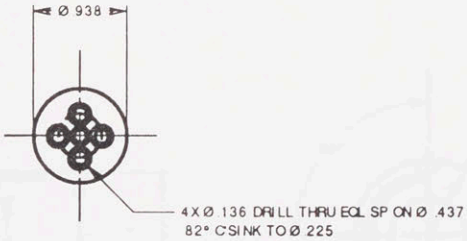

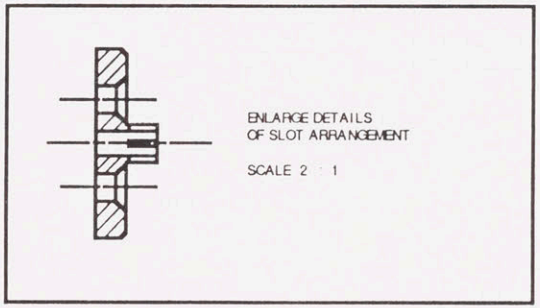

NOTE

1. .030 FOR ALL FILLETS AND CHAMFERS UNLESS SPECIFIED

ACCESSORIES LIST
1. BERG'S CG1-7-2 SPLIT HUMP CLAMP 1 REQ

Material 6061-T6 Aluminium Alloy	Tolerances X ±.015 XX ±.010 XXX ±.005 Unless specified	Manual Teaching Aid	
Finish Black Anodize		Joint 3-4 Retainer	
Quantity Req. 1	Scale 1 : 1	A13D	Drw. by Jain Charnnarong / App. by Dr. Andre Sharon
		1/24/91	Massachusetts Institute of Technology

DWG# A13E

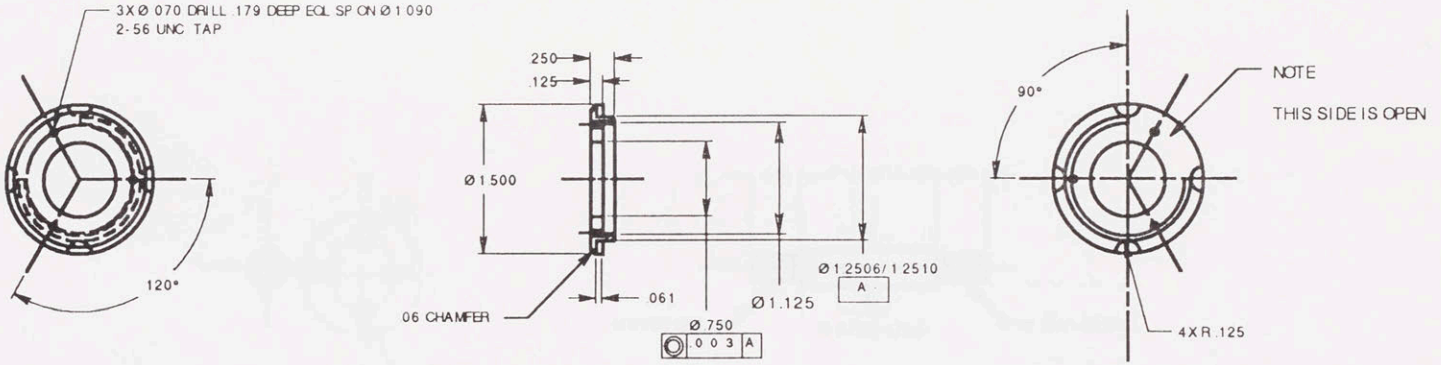

NOTE

1. .030 FOR ALL FILLETS AND CHAMFERS UNLESS SPECIFIED

ACCESSORIES LIST

1. BERG'S SQ 3 SYNCHRO CLAMP CLEAT 3 REQ

Material: 6061-T6 Aluminium Alloy	Tolerances: X ±.015, XX ±.010, XXX ±.005, Unless specified	Manual Teaching Aid	
Finish: Black Anodize		End-point join cap	
Quantity Req.: 1	Scale 1 : 1	A13E	Drw. by: Jain Charnnarong; App. by: Dr. Andre Sharon
		1/24/91	Massachusetts Institute of Technology

DWG# A14

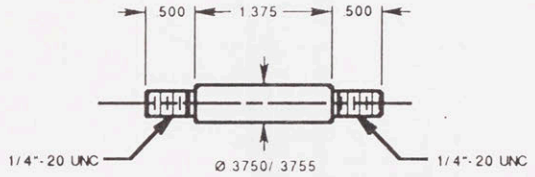

NOTE

1. R.030 FOR ALL FILLETS AND CHAMFERS UNLESS SPECIFIED

ACCESSORIES LIST
1. SMALL PARTS' THREE-ARM KNOB (TAK SERIES) C-TAK-3 2 REQ.

Material: 6061-T6 Aluminium Alloy	Tolerances: X ±.015, XX ±.010, XXX ±.005, Unless specified	Manual Teaching Aid	
Finish: Black Anodize		End-point joint pin	
Quantity Req.: 1	Scale 1 : 1	A14	Drw. by: Jairn Charnnarong; App. by: Dr. Andre Sharon
		1/24/91	Massachusetts Institute of Technology

DWG# A15

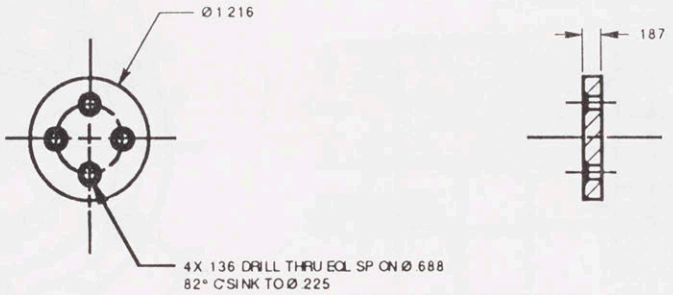

NOTE

1. R.030 FOR ALL FILLETS AND CHAMFERS UNLESS SPECIFIED

Material: 6061-T6 Aluminium Alloy	Tolerances: X ±.015, XX ±.010, XXX ±.005, Unless specified	Manual Teaching Aid	
Finish: Black Anodize		Joint 2-3 Retainer	
Quantity Req.: 2	Scale 1 : 1	A15	Drw. by: Jain Charnnarong; App. by: Dr. Andre Sharon
		1/24/91	Massachusetts Institute of Technology

DWG# A16

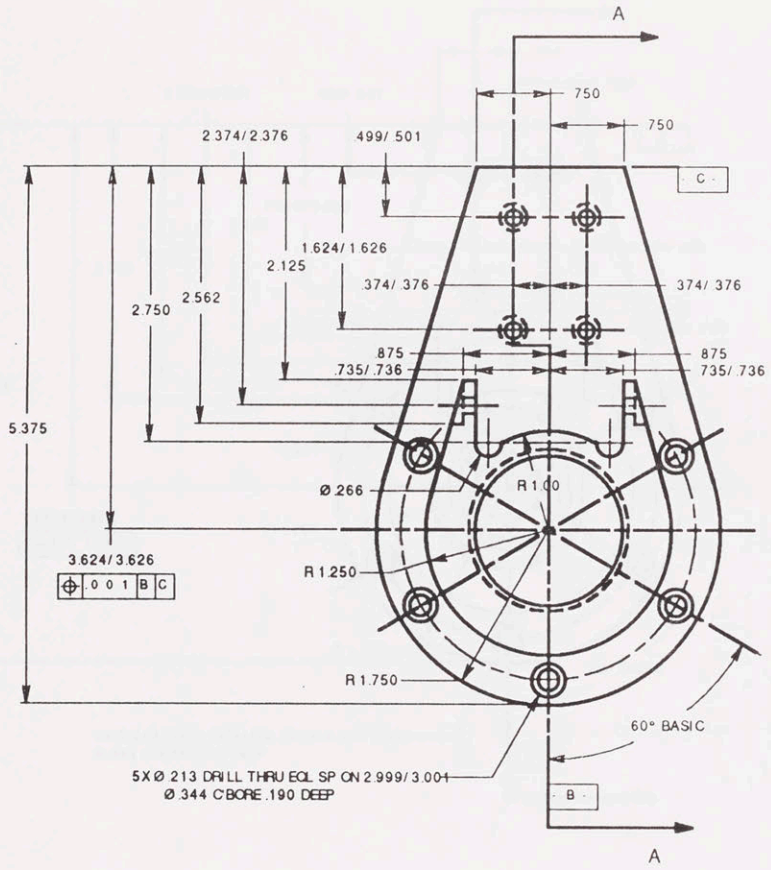

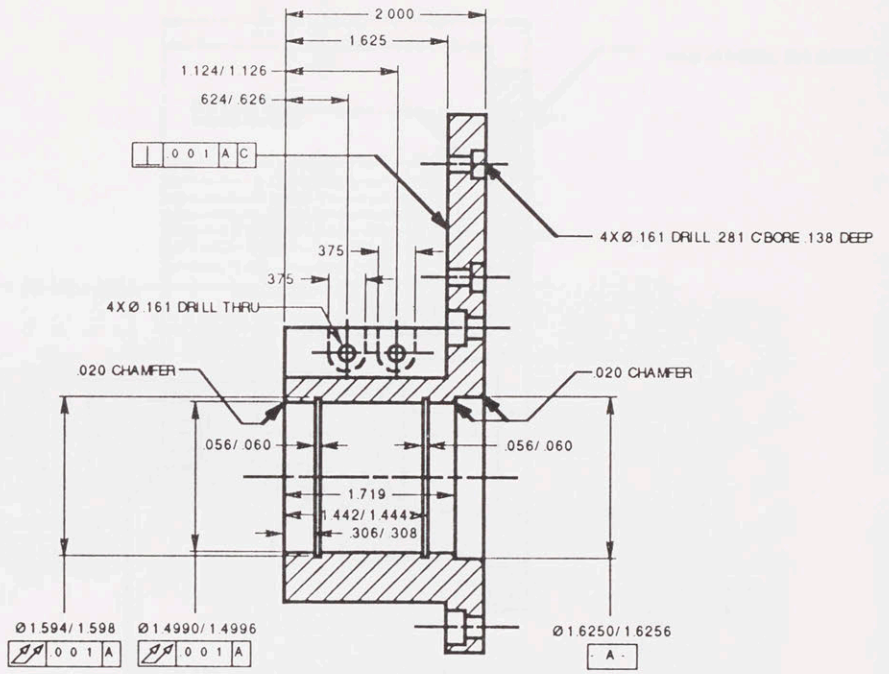

SECTION A-A

NOTE
1. .030 FOR ALL CHAMFERS AND FILLETS UNLESS SPECIFIED

ACCESSORIES LIST
1. LOW TORQUE BALL BEARING NHBB SSRI-541EE 2 REQ.
2. WALDES TRUARC INVERTED INTERNAL RETAINER RING 5008-150 2 REQ.

Material: 6061-T6 Aluminium Alloy	Tolerances: X ±.015, XX ±.010, XXX ±.005 Unless specified	Manual Teaching Aid	
Finish: Black Anodize		Joint 0-2	
Quantity Req.: 1	Scale 1 : 1	A16	Drw. by: Jain Charnnarong / App. by: Dr. Andre Sharon
		1/24/91	Massachusetts Institute of Technology

DWG# A17

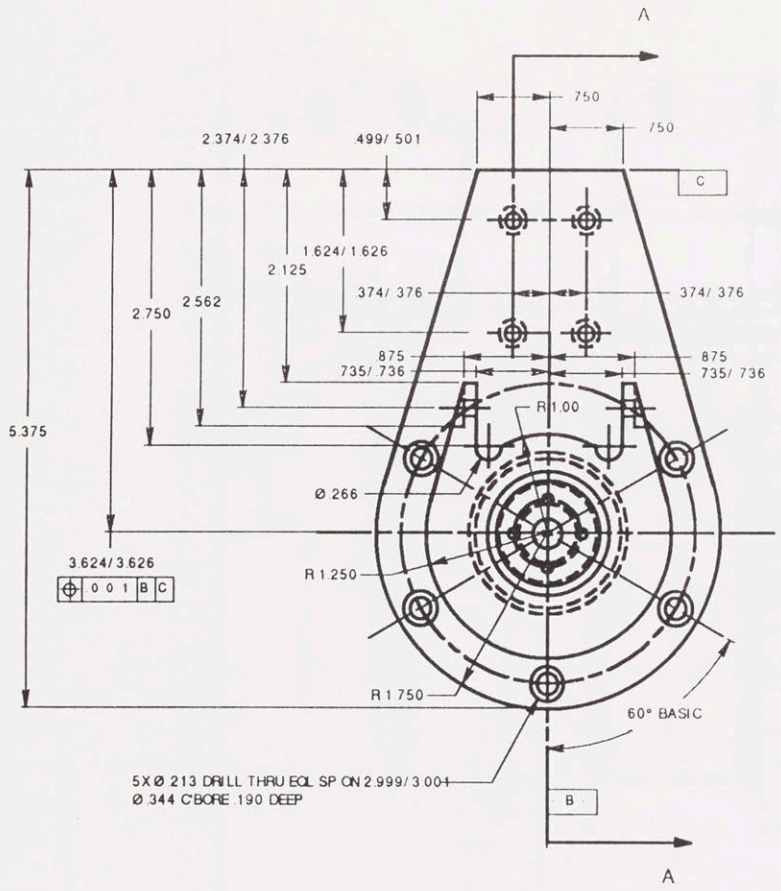

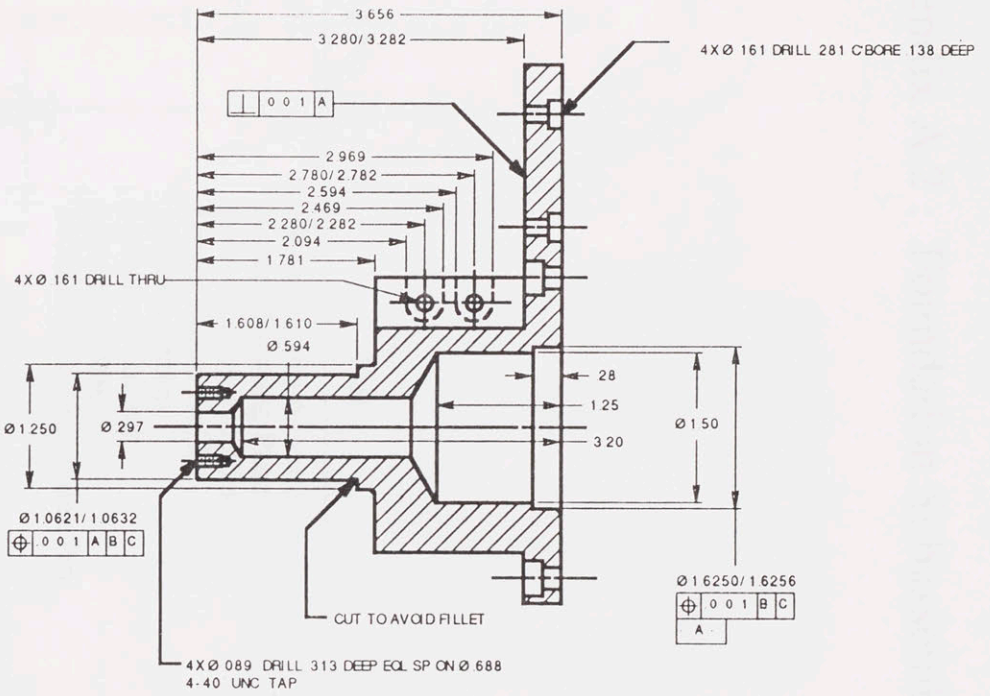

SECTION A-A

Note

1. 0.030 FOR ALL FILLETS AND CHAMFERS UNLESS SPECIFIED

ACCESORIES LIST
1. FLAT HEAD SOCKET HEAD CAP SCREW 4-40 UNC 1/2" OVERALL LENGTH 4 REQ.

Material: 6061-T6 Aluminium Alloy	Tolerances: X ±.015, XX ±.010, XXX ±.005 Unless specified	Manual Teaching Aid	
Finish: Black Anodize		Joint 0-1	
Quantity Req.: 1	Scale 1 : 1	A17	Drw. by Jairn Charnnarong / App. by Dr. Andre Sharon
		1/24/91	Massachusetts Institute of Technology

Appendix A.2 : Foundation Subassembly

Drawing No.	Name	Page No.
ASB B01	Mounting and Assembly	226
B01A	Upper Mounting Plate	227
B01B	Lower Column Holder	228
B01C	Lower Motor Holder	229
B02	Mounting Strap	230
B03	Mounting Column	231
B04A	Mounting Base	232
B05	Mounting Column Index Pin	233

DWG# ASB B01

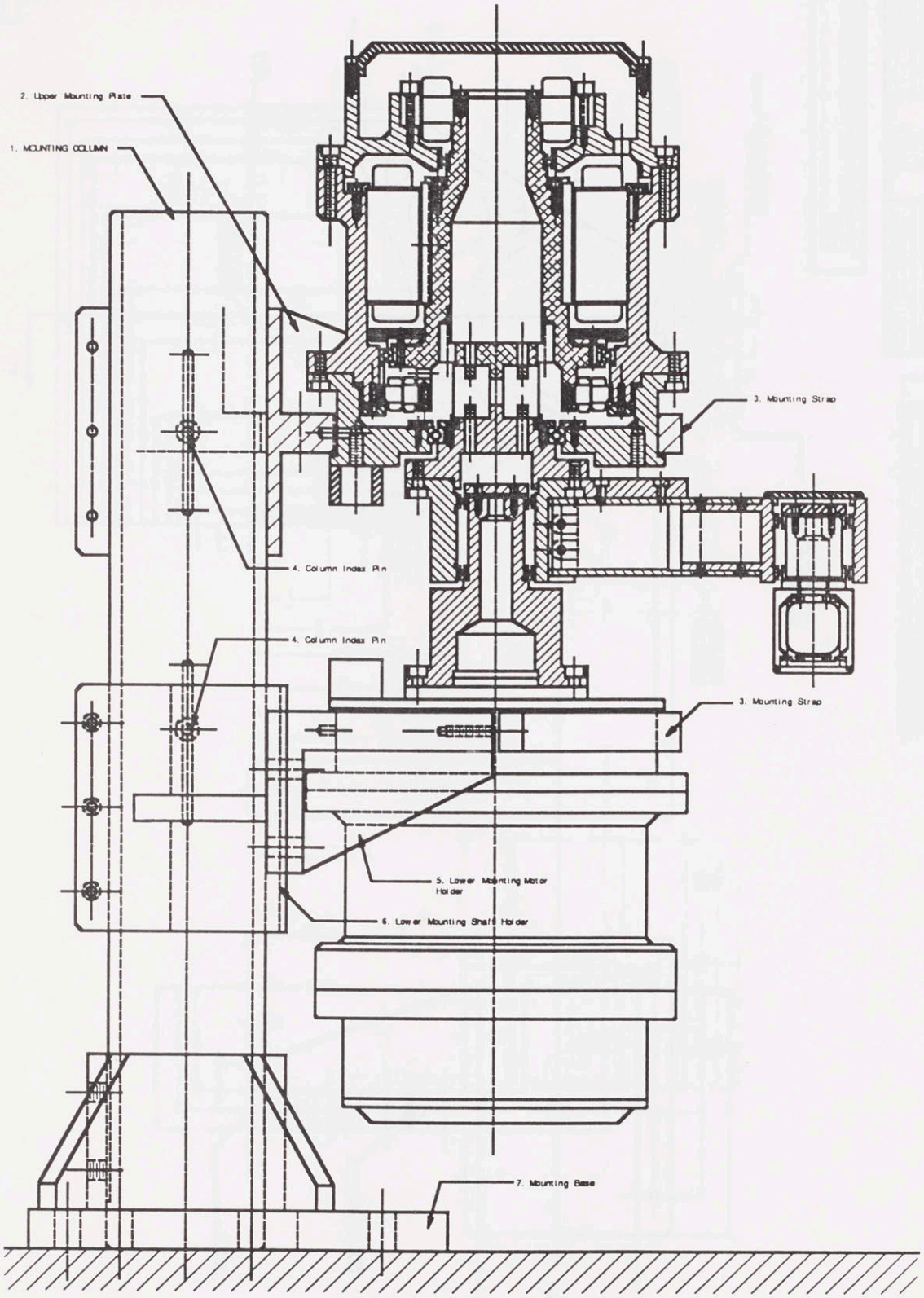

Tolerances .X ±.xxx .XX ±.xx .XXX ±.xxx Unless specified	Manual Teaching Aid	
	Mouting and Motor Assembly	
Scale 1 : 1	ASB B01	Drawn by Jain Charmerang / Approved by Dr. Andrew Sharon
	1/24/91	Massachusetts Institute of Technology

DWG# B01A

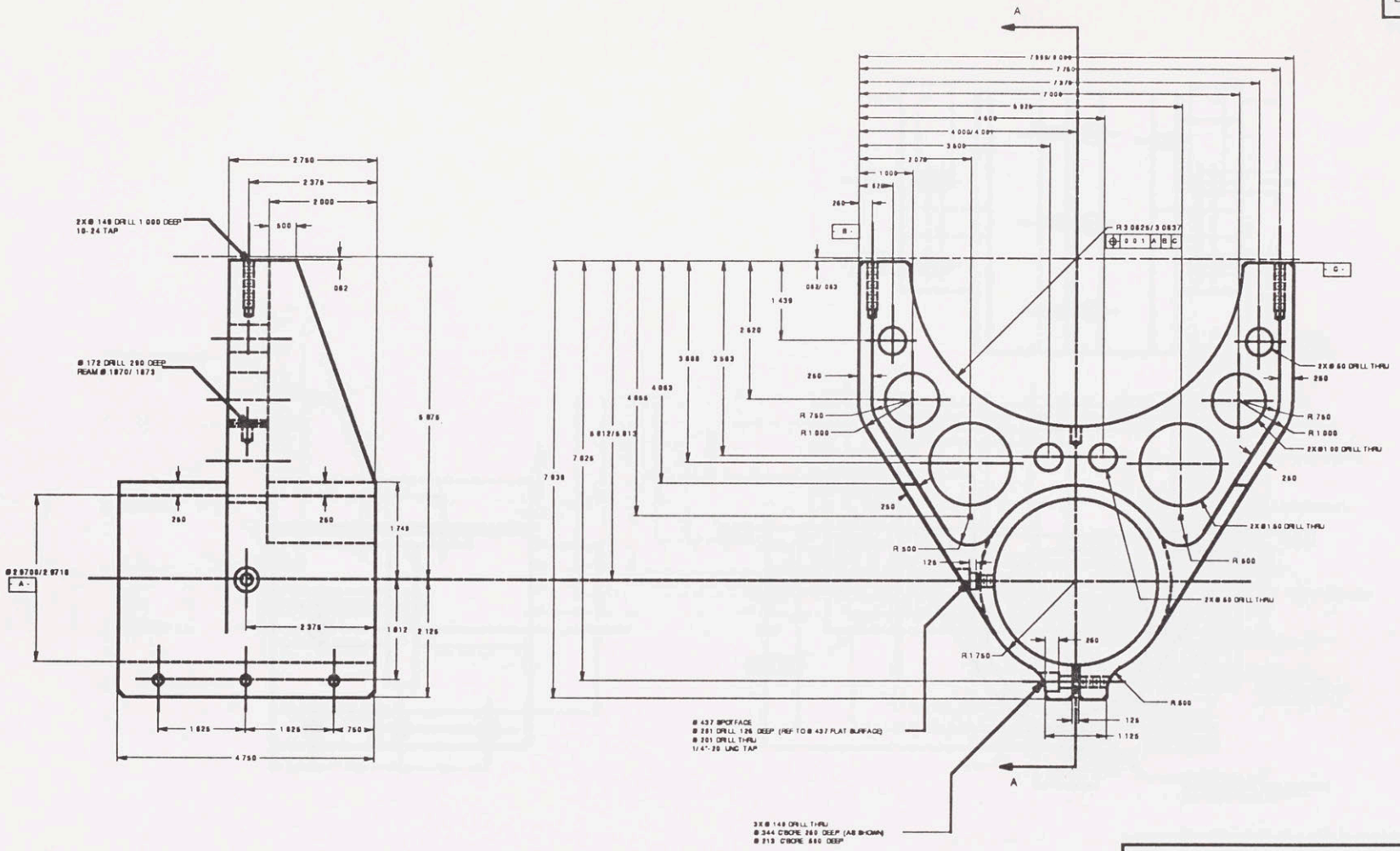

Note

1. R.06 FOR ALL FILLETS AND CHAMFERS UNLESS SPECIFIED

ACCESSORIES LIST
1. SOCKET HEAD CAP SCREW 10-24 UNC 1" UNDER HEAD LENGTH 2 REQ.
2. SOCKET HEAD CAP SCREW 10-24 UNC 3/4" UNDER HEAD LENGTH 3 REQ.

Material: 6061-T6 Aluminum Alloy	Tolerances: X ±.015, XX ±.010, XXX ±.005 Unless specified	Manual Teaching Aid	
Finish: Black Anodize		Upper Mounting Plate	
Quantity Req.: 1	Scale 1 : 1	B01A	Drw. by: Jack Chanmerang; App. by: Dr. Andris Skaugen
		1/24/91	Massachusetts Institute of Technology

DWG# B01B

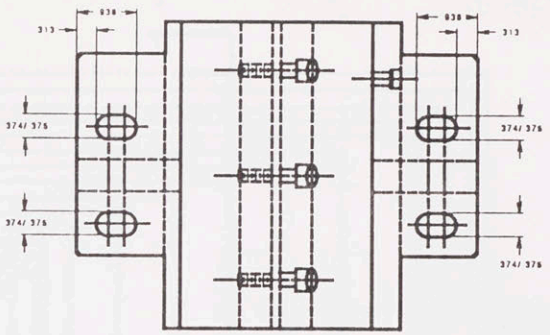

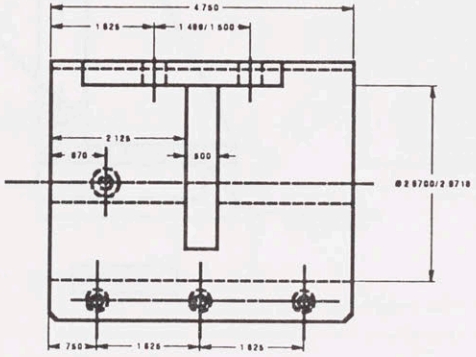

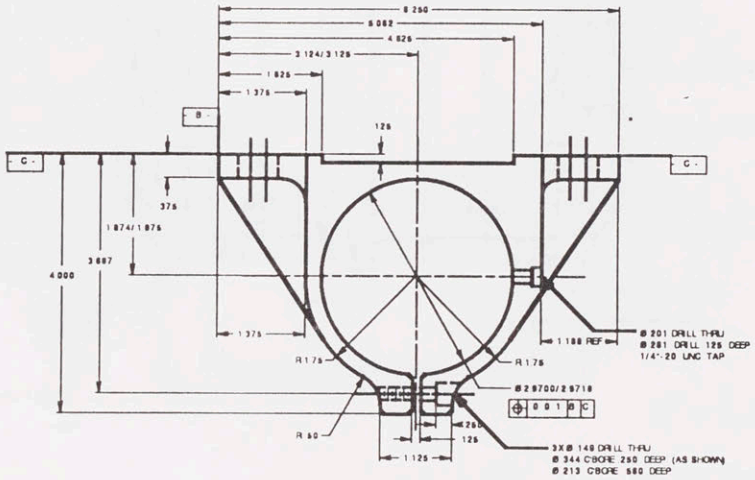

NOTE
1. .063 FOR ALL FILLETS AND CHAMFERS UNLESS SPECIFIED

ACCESSORIES LIST
1. SOCKET HEAD CAP SCREW 10-24 UNC 3/4" UNDER HEAD LENGTH 3 REQ.
2. BERGS PZ-37 SHOULDER SCREW 4 REQ.

Material: 6061-T6 Aluminium Alloy	Tolerances: X ±.xx, XX ±.xxx, XXX ±.xxx, Unless specified	Manual Teaching Aid	
Finish: Black Anodize		Lower Column Holder	
Quantity Req.: 1	Scale 1 : 1	B01B	Drw by: Jain Channarong / App by: Dr. Agung Sharon
		1/24/91	Massachusetts Institute of Technology

DWG# B01C

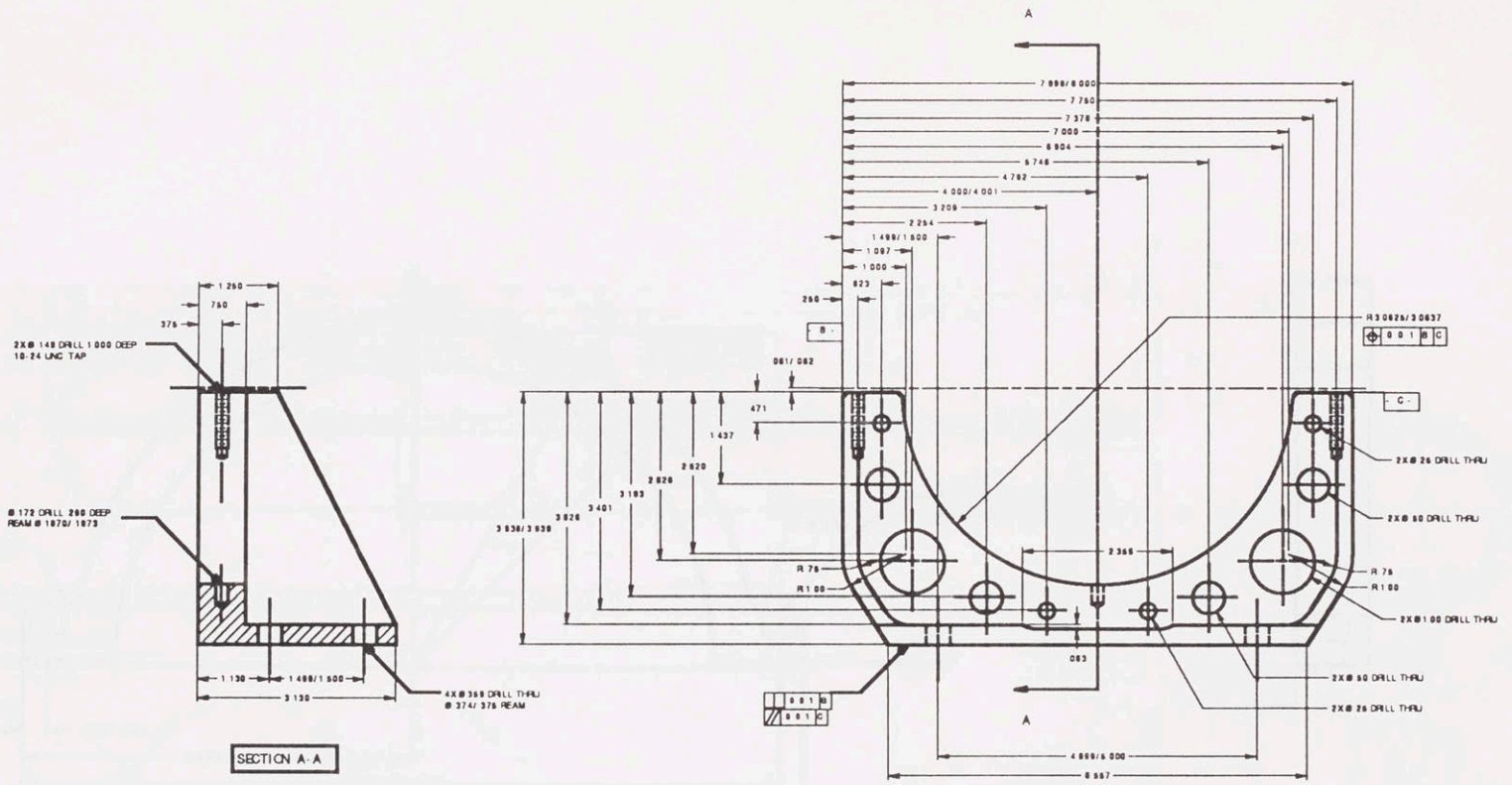

SECTION A-A

NOTE

1. .06 FOR ALL FILLETS AND CHAMFERS UNLESS SPECIFIED

ACCESSORIES LIST
1. SOCKET HEAD CAP SCREW 10-24 UNC 1" UNDER HEAD LENGTH 2 REQ.

Material: 6061-T6 Aluminum Alloy	Tolerances: X .xx, XX .xxx, XXX .xxx Unless specified	Manual Teaching Aid	
Finish: Black Anodize		Lower Motor Holder	
Quantity Req.: 1	Scale 1 : 1	B01C	Drw by Jack Chenoweth / App by Dr. Andris Sharon
		1/24/91	Massachusetts Institute of Technology

DWG# B02

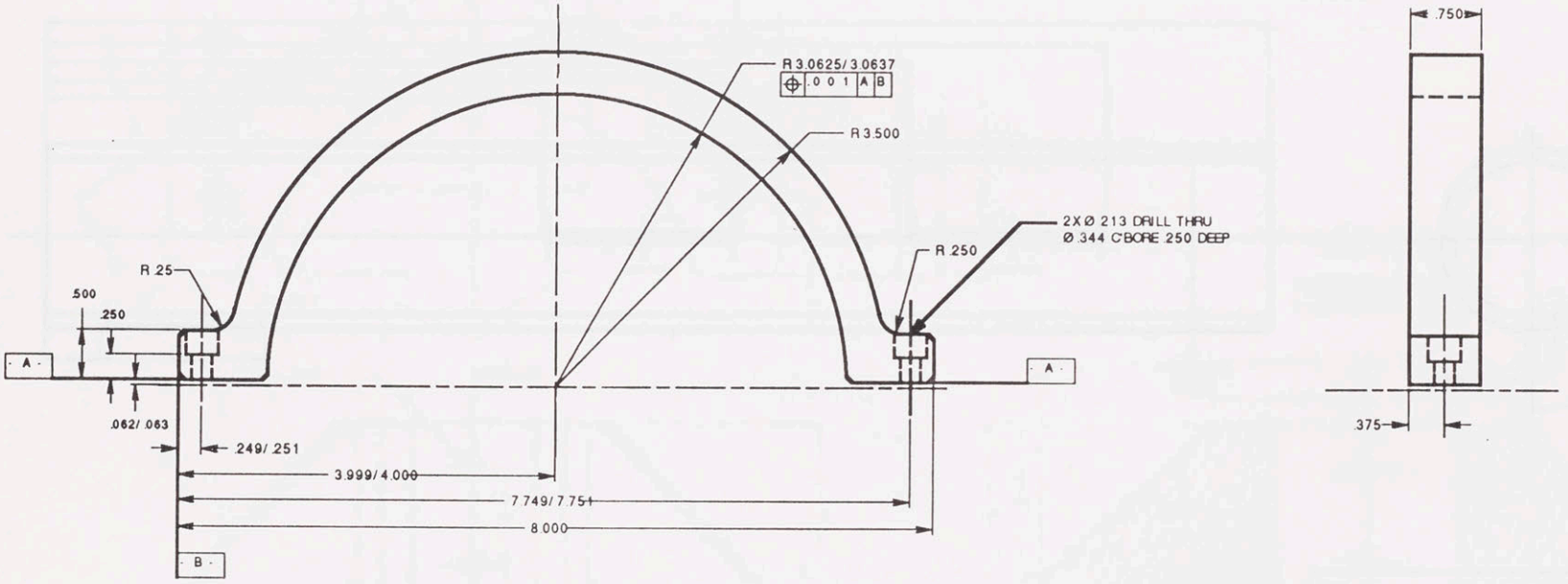

NOTE
1. .063 FOR ALL FILLETS AND CHAMFERS UNLESS SPECIFIED

Material: 6061-T6 Aluminium Alloy	Tolerances: .X ±.015, .XX ±.010, .XXX ±.005, Unless specified	Manual Teaching Aid	
Finish: Black Anodize		Mounting Strap	
Quantity Req.: 2	Scale 1 : 1	B02	Drw. by: Jain Charnnarong / App. by: Dr. Andre Sharon
		1/24/91	Massachusetts Institute of Technology

DWG# B03

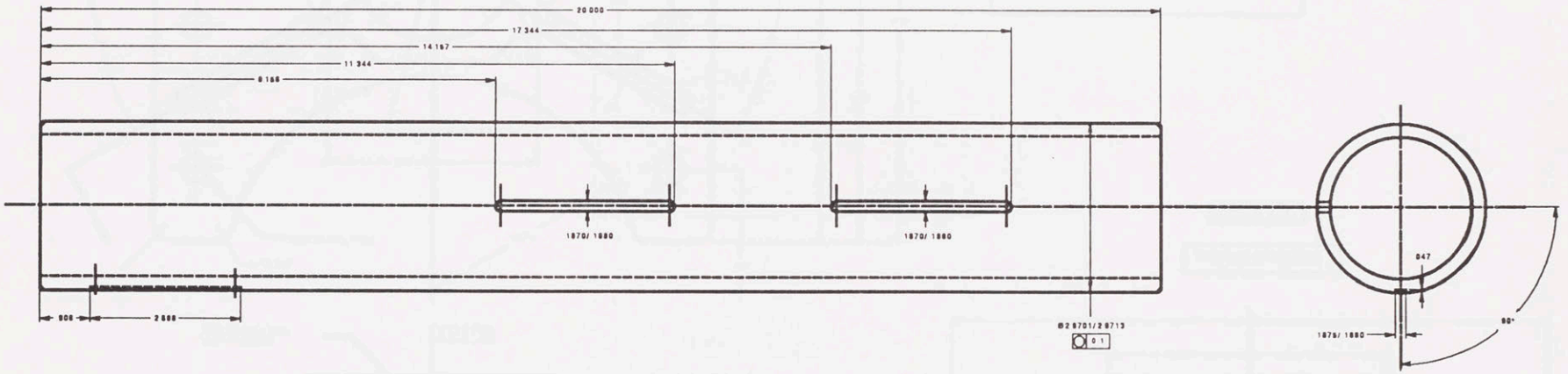

NOTE

1. CUT FROM STANDARD 6061-T6 ALUMINUM ALLOY TUBE STRUCTURE WITH Ø3.00 O.D. AND 0.25 WALL THICKNESS
2. .063 FOR ALL FILLETS AND CHAMFERS UNLESS SPECIFIED

ACCESSORIES LIST
1. BERGS SC-10-21 BRASS TIP SCREW 2 REQ.

Material: 6061-T6 Aluminum Alloy Ø3.00 OD .25 wall thickness	Tolerances: X ±.xx, XX ±.xx, XXX ±.xxx Unless specified	Manual Teaching Aid	
Finish: Black Anodize		Mounting Column	
Quantity Req.: 1	Scale 1 : 1	B03	Drw by: Jaim Charnnarong / App by: Dr. Anita Sharon
		1/24/91	Massachusetts Institute of Technology

DWG# B04A

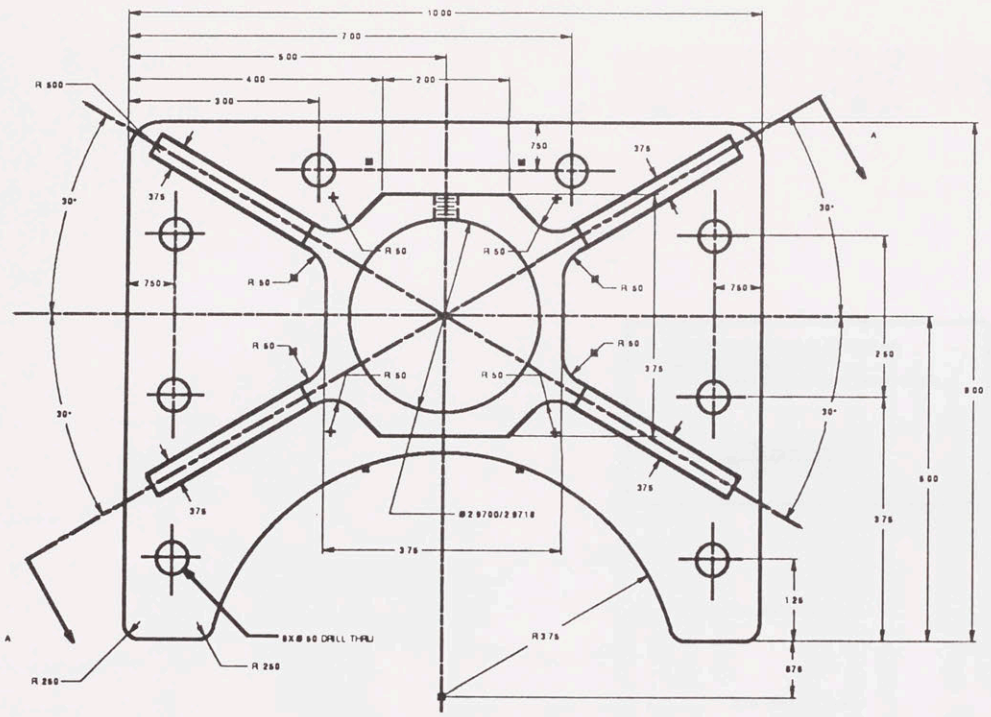

SEE DWG# B04C FOR MILLING CUTTER POSITIONING DATA

SECTION A-A

TRUE SIZE OF THE RIBS

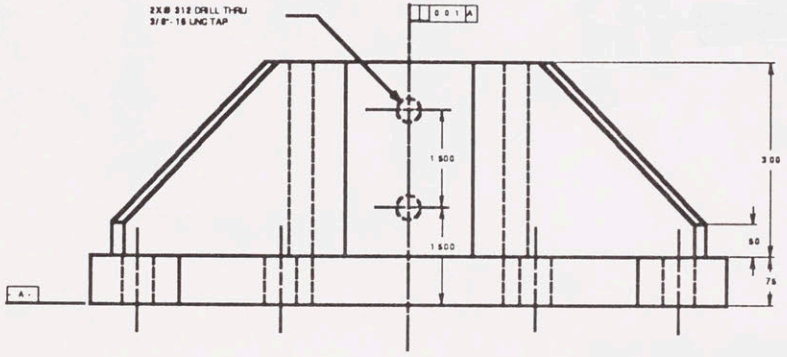

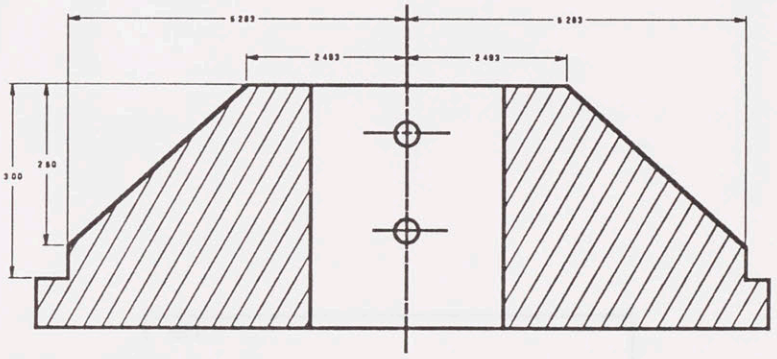

ACCESSORIES LIST
1. SOCKET HEAD CAP SCREW 1/2"-20 UNF 2" UNDER HEAD LENGTH 8 REQ.
2. BERGS SC-10-21 BRASS TIP SCREW 2 REQ.

Material: 6061-T6 Aluminum Alloy	Tolerances: X ±.xx, XX ±.xxx, XXX ±.xxx Unless specified	Manual Teaching Aid	
Finish: Black Anodize		Mounting Base	
Quantity Req. 1	Scale 1 : 1	B04A	Drw. by Jack Chenevert
		1/24/91	Massachusetts Institute of Technology

Appr. by Dr. Agata Sharon

DWG# B05

Standard heat treated alloy steel
Socket head cap screw
1/4"-20 UNC 0.75" under head length

Cut and modiffy to

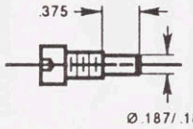

Note

1. .03 for all fillets and chamfers unless specified

Material: Cut from standard heat treated alloy steel socket head cap screw	Tolerances: X ±.015, XX ±.010, XXX ±.005, Unless specified	Manual Teaching Aid	
		Mounting Column Index Pin	
Quantity Req. 4	Scale 1 : 1	B05	Drw. by Jain Charnnarong / App. by Dr. Andre Sharon
		1/24/91	Massachusetts Institute of Technology

Appendix A.3 : End-Effector Subassembly

Drawing No.	Name	Page No.
ASB E01	End-Point Effector Assembly	235
E01	End-Point Pivot Shaft	236
E02	Main Structure	237
E03	Pronation/Supination Motor Base	238
E04	Differential Gear Supporter	239
E05	Pronation/Supination Joint	240
E06	Pronation/Supination Joint Shaft	241
E08	Crank Follower	242
E09A	Pronation/Supination Motor Connecting Rod	243
E09B	Pronation/Supination Connecting Rod	243
E10	Splint Holder Guide Rod	244
E11	Splint Holder Lock	245
E12	Splint Holder	246
E14	Flexion/Abduction S-Rod	247
E15A	Flexion/Abduction Connecting Rod	248
E15B	Flexion/Abduction Palm Connector	248
E16	Flexion/Abduction Connecting Shaft	249

DWG# ASB E01

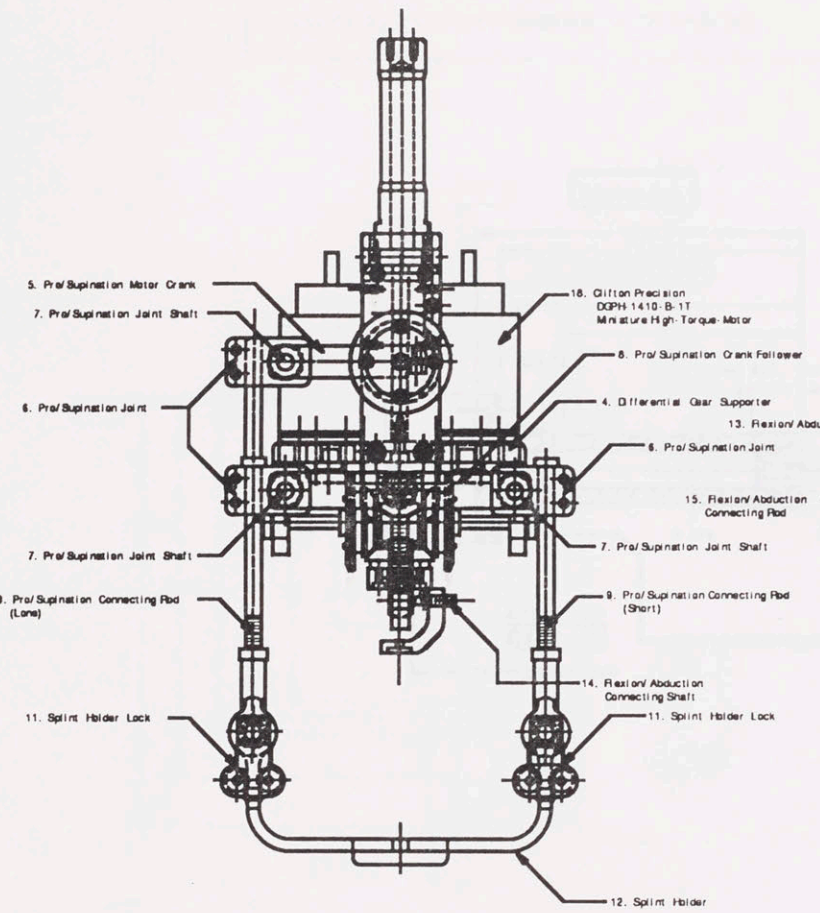

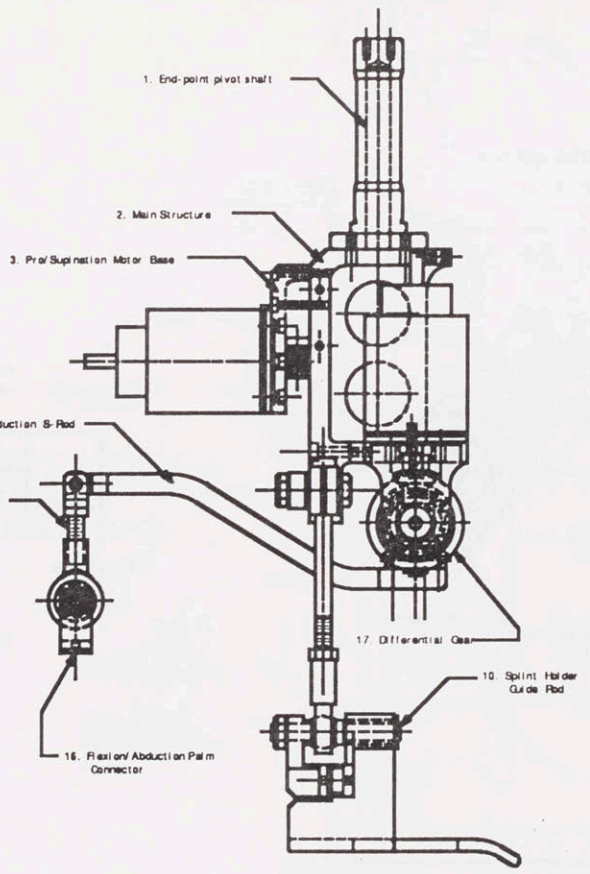

1. End-point pivot shaft	See DWG# E01
2. Main Structure	See DWG# E02
3. Pro/Supination Motor Base	See DWG# E03
4. Differential Gear Supporter	See DWG# E04
5. Pro/Supination Motor Crank	See DWG# E07
6. Pro/Supination Joint	See DWG# E05
7. Pro/Supination Joint Shaft	See DWG# E06
8. Pro/Supination Crank Follower	See DWG# E08
9. Pro/Supination Connecting Rod	See DWG# E09 A, B
10. Splint Holder Guide Rod	See DWG# E10
11. Splint Holder Lock	See DWG# E11
12. Splint Holder	See DWG# E12
13. Flexion/Abduction S-Rod	See DWG# E14
14. Flexion/Abduction Connecting Shaft	See DWG# E16
15. Flexion/Abduction Connecting Rod	See DWG# E15A
16. Flexion/Abduction Palm Connector	See DWG# E15B
17. Differential Gear	
18. Clifton Precision DGPH-1410-B-1T Miniature High-Torque-Motor	

Tolerances .X ±.xx .XX ±.xxx .XXX ±.xxx Unless specified	Manual Teaching Aid		
	End-point Effector Assembly		
Scale 1 : 1	ASB E01	Drw by Jain Charnnarong	App by Dr. Angela Sharon
	1/24/91	Massachusetts Institute of Technology	

DWG# E01

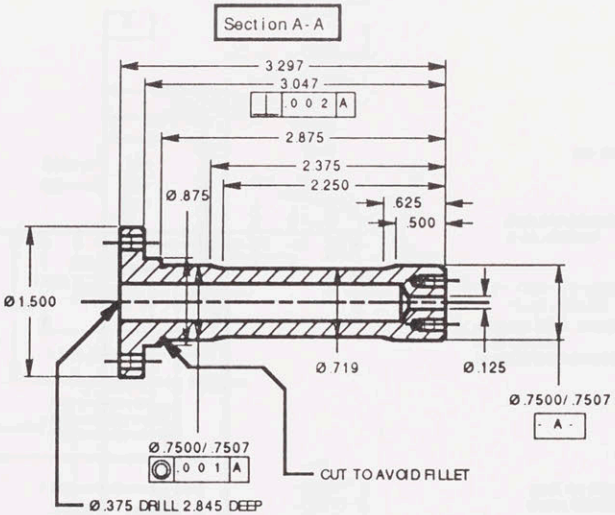

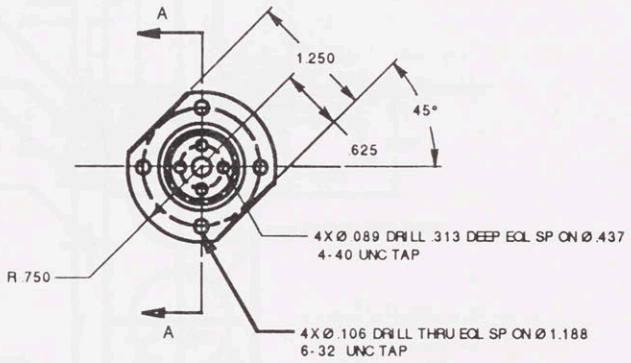

NOTE

1. R.030 FOR ALL FILLETS AND CHAMFERS UNLESS SPECIFIED

ACCESSORIES LIST

1. FLAT HEAD SOCKET HEAD CAP SCREW 4-40 UNC 5/16" OVERALL LENGTH 4 REQ.
2. SOCKET HEAD CAP SCREW 6-32 UND 1/2" UNDER HEAD LENGTH 4 REQ.

Material: 6061-T6 Aluminium Alloy	Tolerances: .X ±.015, .XX ±.010, .XXX ±.005 Unless specified	Manual Teaching Aid	
Finish: Black Anodize		End-Point Pivot Shaft	
Quantity Req.: 1	Scale 1 : 1	E01	Drw. by: Jain Charnnarong / App. by: Dr. Andre Sharon
		1/24/91	Massachusetts Institute of Technology

DWG# E02

NOTE

1. .030 FOR ALL FILLETS AND CHAMFERS UNLESS SPECIFIED

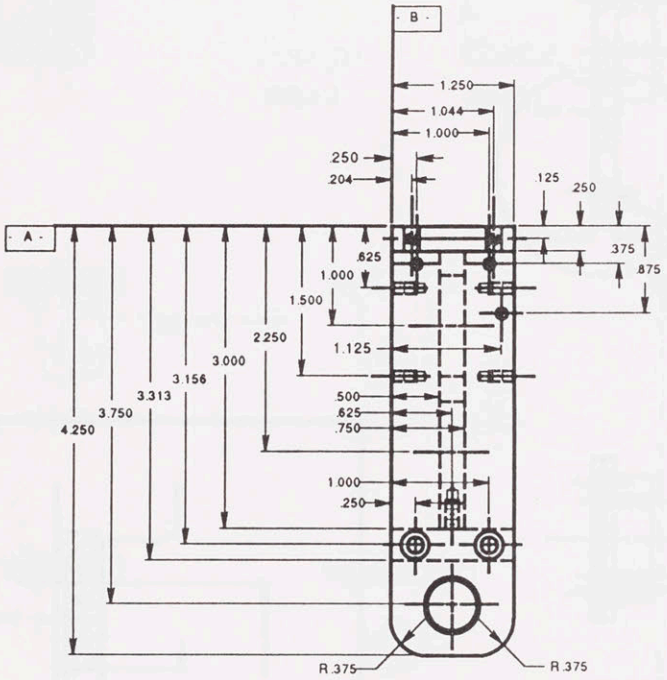

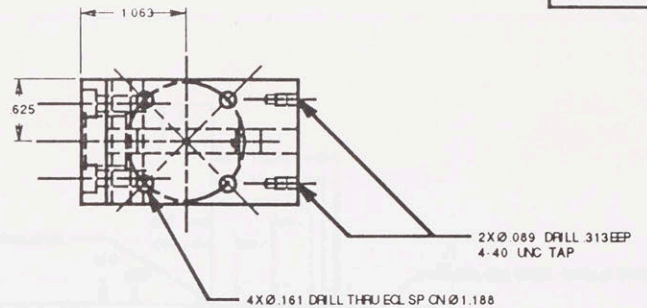

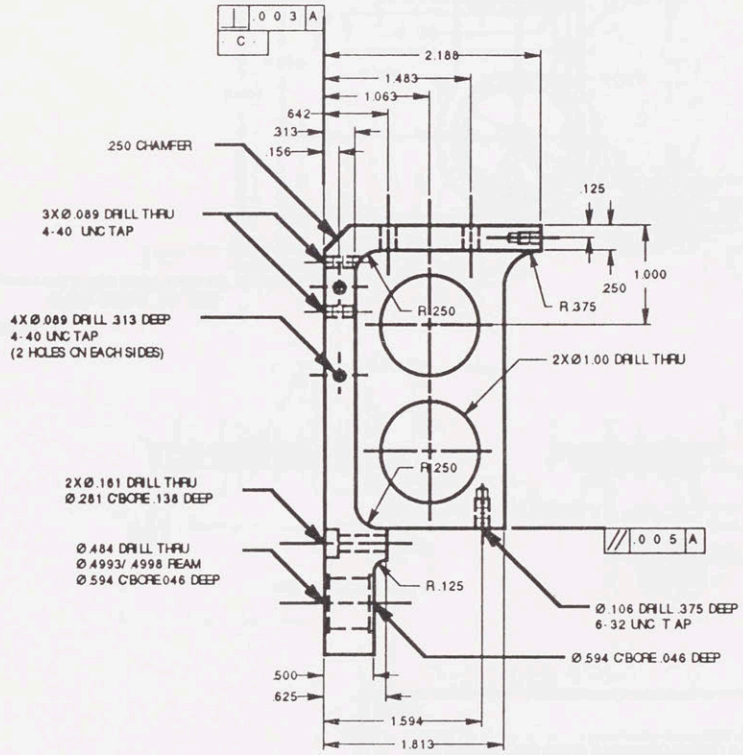

ACCESSORIES LIST

1. BERGS BALL BEARING B2-11S 2 REQ.
2. SOCKET HEAD CAP SCREW 6-32 UNC 3/8" UNDER HEAD LENGTH 1 REQ.
3. SOCKET HEAD CAP SCREW 4-40 UNC 3/4" UNDER HEAD LENGTH 3 REQ.

Material: 6061-T6 Aluminium Alloy	Tolerances: .X ±.015, .XX ±.010, .XXX ±.005, Unless specified	Manual Teaching Aid	
Finish: Black Anodize		Main structure	
Quantity Req.: 1	Scale 1 : 1	E02	Drw. by: Jain Charnnarong; App. by: Dr. Andre Sharon
		1/24/91	Massachusetts Institute of Technology

DWG# E03

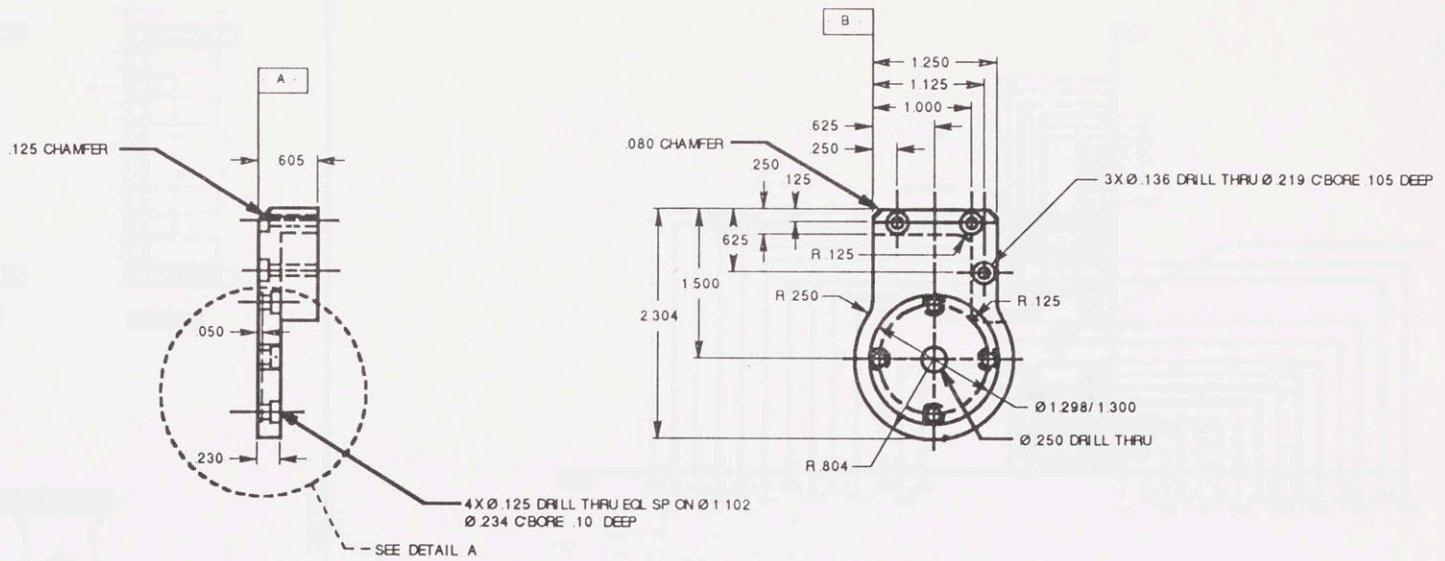

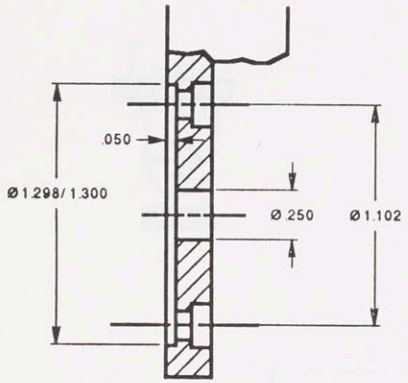

Detail A
scale 2:1

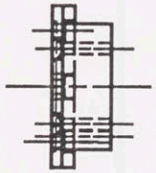

NOTE

1. .030 FOR ALL FILLETS AND CHAMFERS UNLESS SPECIFIED

Material: 6061-T6 Aluminium Alloy	Tolerances: .X ±.015, .XX ±.010, .XXX ±.005, Unless specified	Manual Teaching Aid	
Finish: Black Anodize		Pro/supi motor base	
Quantity Req.: 1	Scale 1 : 1	E03	Drw. by Jain Charnnarong / App. by Dr. Andre Sharon
		1/24/91	Massachusetts Institute of Technology

DWG# E04

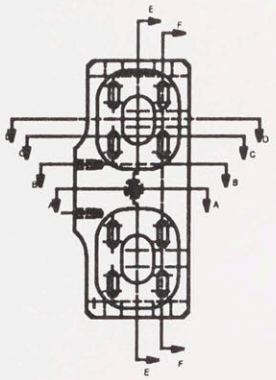

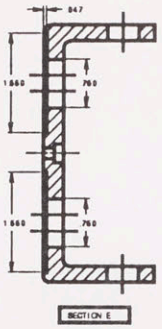

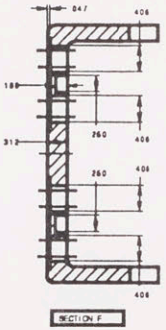

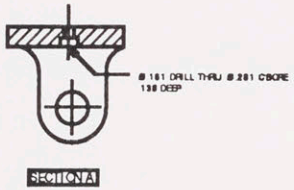

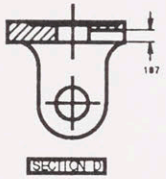

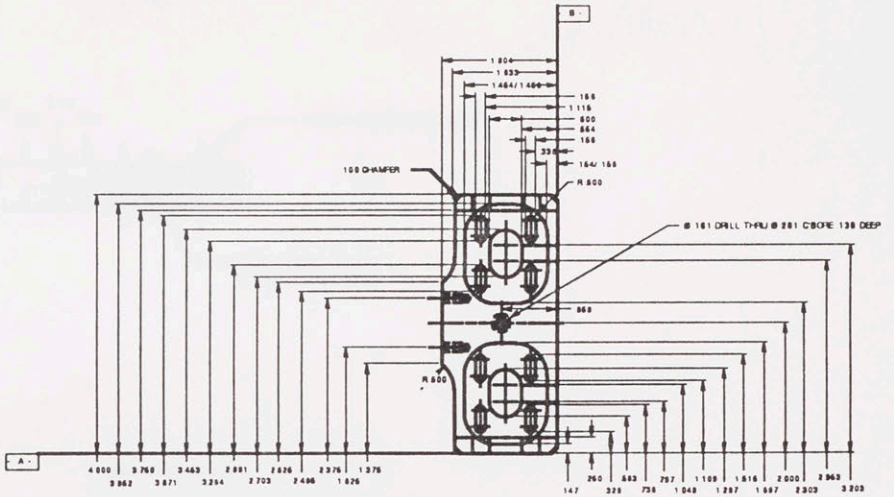

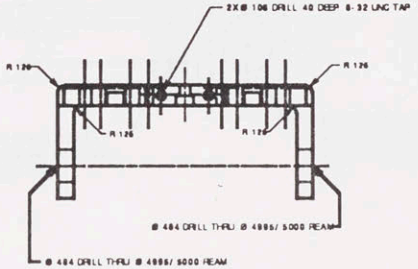

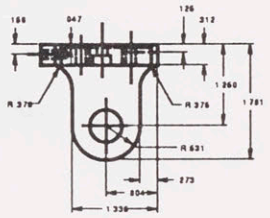

ACCESORIES LIST
1. BERGS B2-6-S BALL BEARING 2 REQ.
2. BERGS E11 BALL BEARING DIFFERENTIAL GEAR SET 1 REQ.
3. BERGS M64N-3 MITTER AND BEVEL GEAR 2SET REQ.
4. BERGS CG1-27 SPLIT HUB CLAMB
5. SOCKET HEAD CAP SCREW 6-32 UNC 3/4" UNDER HEAD LENGTH 2 REQ.
6. METRIC SOCKET HEAD CAP SCREW M3 - 15MM UNDER HEAD LENGTH 8 REQ.

NOTE
1. 0.030 FOR ALL FILLETS AND CHAMFERS UNLESS SPECIFIED

Material 6061-T6 Aluminium Alloy	Tolerances X ±.xxx XX ±.xxx XXX ±.xxx Unless specified	Manual Teaching Aid	
Finish Black Anodize		Differential Gear Supporter	
Quantity Req. 1	Scale 1 : 1	E04	Drw by Jian Chennareng / App by Dr. Andre Sharon
		1/24/91	Massachusetts Institute of Technology

DWG# E05

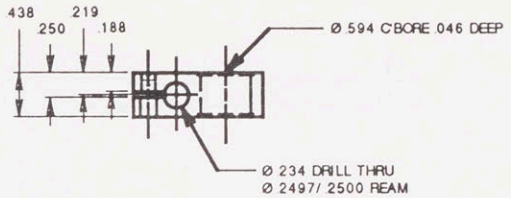

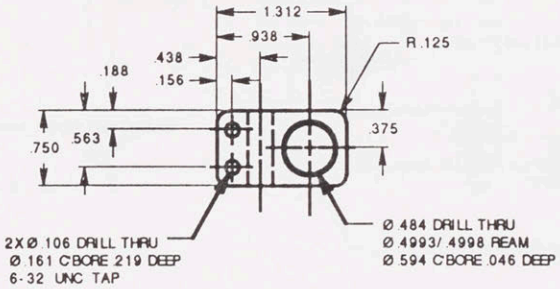

NOTE

1. R.030 FOR ALL FILLETS AND CHAMFERS UNLESS SPECIFIED

ACCESSORIES LIST

1. BERG'S B2-11-S BEARING 6 REQ.
2. SOCKET HEAD CAP SCREW 6-32 UNC 3/8" UNDER HEAD LENGTH 6 REQ.

Material: 6061-T6 Aluminium Alloy	Tolerances: .X ±.015, .XX ±.010, .XXX ±.005, Unless specified	Manual Teaching Aid	
Finish: Black Anodize		Pro/Supination joint	
Quantity Req.: 3	Scale 1 : 1	E05	Drw. by: Jain Charnnarong; App. by: Dr. Andre Sharon
		1/24/91	Massachusetts Institute of Technology

DWG# E06

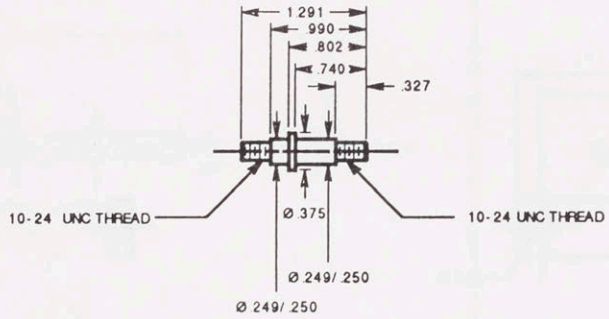

NOTE

1. R.030 FOR ALL FILLETS AND CHAMFERS UNLESS SPECIFIED

ACCESSORIES LIST

1. BERGS 10-24 UNC HEXAGONAL NUT Y5-11 8 REQ.

Material: 303 Stainless Steel	Tolerances: .X ±.015, .XX ±.010, .XXX ±.005 Unless specified	Manual Teaching Aid	
Finish: Black Oxide		Pro/Supination joint shaft	
Quantity Req.: 4	Scale 1 : 1	E06	Drw. by Jain Charnnarong / App. by Dr. Andre Sharon
		1/24/91	Massachusetts Institute of Technology

DWG# E08

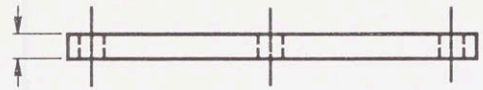

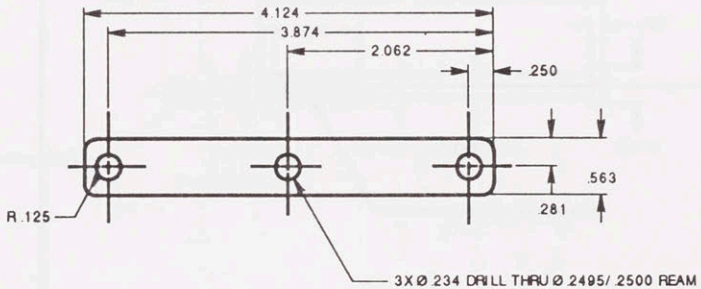

NOTE

1. .03 FOR ALL FILLETS AND CHAMFERS UNLESS SPECIFIED

Material: 6061-T6 Aluminium Alloy	Tolerances: .X ±.015, .XX ±.010, .XXX ±.005 Unless specified	Manual Teaching Aid	
Finish: Black Anodize		Crank Follower	
Quantity Req.: 1	Scale 1 : 1	E08	Drw. by Jain Charnnarong / App. by Dr. Andre Sharon
		1/24/91	Massachusetts Institute of Technology

DWG# E09A

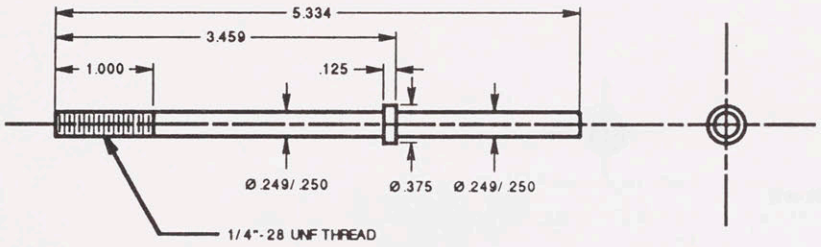

NOTE

1. R.030 FOR ALL FILLETS AND CHAMFERS UNLESS SPECIFIED

Material: 303 Stainless Steel	Tolerances: .X ±.015, .XX ±.010, .XXX ±.005, Unless specified	Manual Teaching Aid		
Finish: Black Oxide		Pro/supi motor connecting rod		
Quantity Req.: 1	Scale 1 : 1	E09A	Drw. by Jain Charnnarong	App. by Dr. Andre Sharon
		1/24/91	Massachusetts Institute of Technology	

DWG# E09B

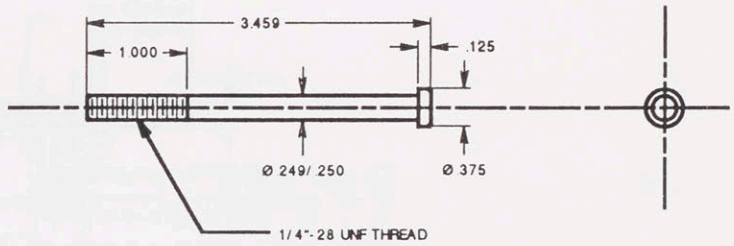

NOTE

1. R.030 FOR ALL FILLETS AND CHAMFERS UNLESS SPECIFIED

Material: 303 Stainless Steel	Tolerances: .X ±.015, .XX ±.010, .XXX ±.005, Unless specified	Manual Teaching Aid		
Finish: Black Oxide		Pro/supi connecting rod		
Quantity Req.: 1	Scale 1 : 1	E09B	Drw. by Jain Charnnarong	App. by Dr. Andre Sharon
		1/24/91	Massachusetts Institute of Technology	

DWG# E10

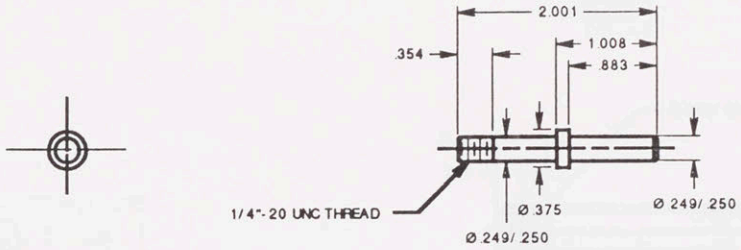

NOTE

1. R.030 FOR ALL FILLETS AND CHAMFERS UNLESS SPECIFIED

ACCESSORIES LIST

1. BERGS 1/4"-20 UNC HEX NUT Y5-12 2 REQ.

Material: 303 Stainless Steel	Tolerances: .X ±.015, .XX ±.010, .XXX ±.005 Unless specified	Manual Teaching Aid	
Finish: Black Oxide		Splint Holder Guide Rod	
Quantity Req.: 2	Scale 1 : 1	E10	Drw. by Jain Charnnarong / App. by Dr. Andre Sharon
		1/24/91	Massachusetts Institute of Technology

DWG# E11

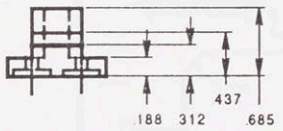

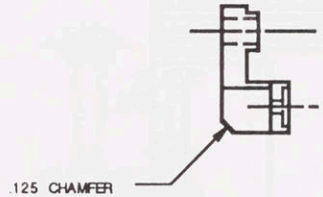

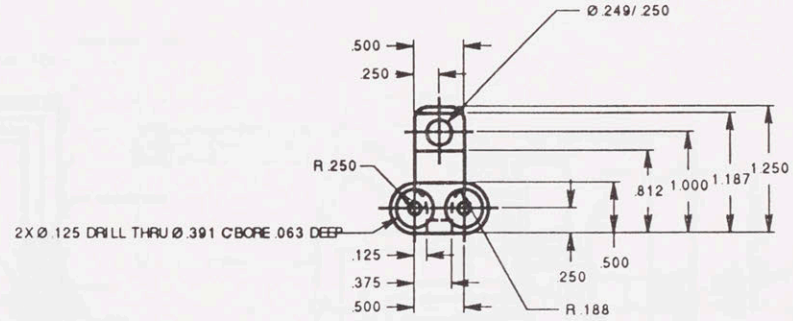

NOTE

1. R.125 FOR ALL FILLETS AND CHAMFERS UNLESS SPECIFIED

ACCESSORIES LIST

1. EDMUND SCIENTIFICS D35,104 NEODYMIUM-IRON-BORON MAGNETS 4 REQ.

Material: 6061-T6 Aluminium Alloy	Tolerances: .X ±.015, .XX ±.010, .XXX ±.005 Unless specified	Manual Teaching Aid	
Finish: Black Anodize		Splint Holder Lock	
Quantity Req.: 2	Scale 1 : 1	E11	Drw. by: Jain Charnnarong; App. by: Dr. Andre Sharon
		1/24/91	Massachusetts Institute of Technology

DWG# E12

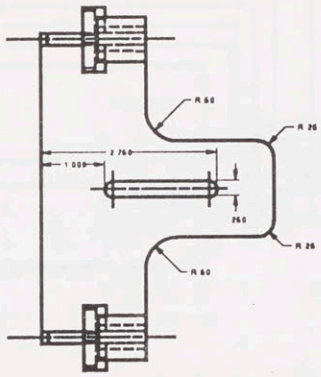

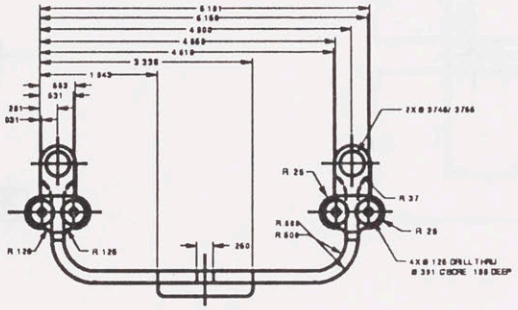

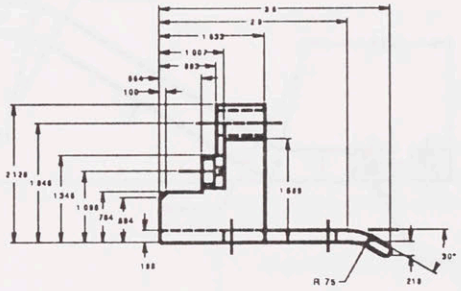

NOTE

1. .030 FOR ALL FILLETS AND CHAMFERS UNLESS SPECIFIED

ACCESSORIES LIST

1. BERGS CYL-LESS BEARING BS-54 2 REQ.
2. SMALL PARTS' THREE-ARM KNOB C-TAK-1 2 REQ.
3. EDMUND SCIENTIFIC'S D35,104 8 REQ.

Material 6061-T6 Aluminium Alloy	Tolerances X ±.xx XX ±.xxx XXX ±.xxx Unless specified	Manual Teaching Aid	
Finish Black Anodize		Splint Holder	
Quantity Req. 1	Scale 1 : 1	E12	Drw by Jan Chamnarong
		1/24/91	Massachusetts Institute of Technology

Apr by Dr. Andris Sharan

DWG# E14

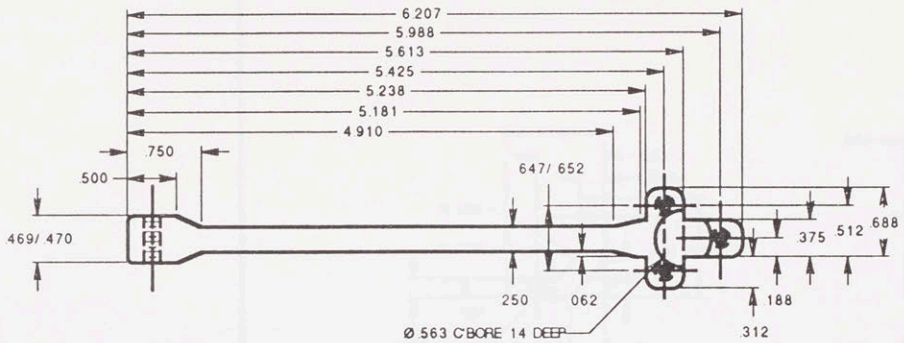

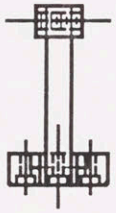

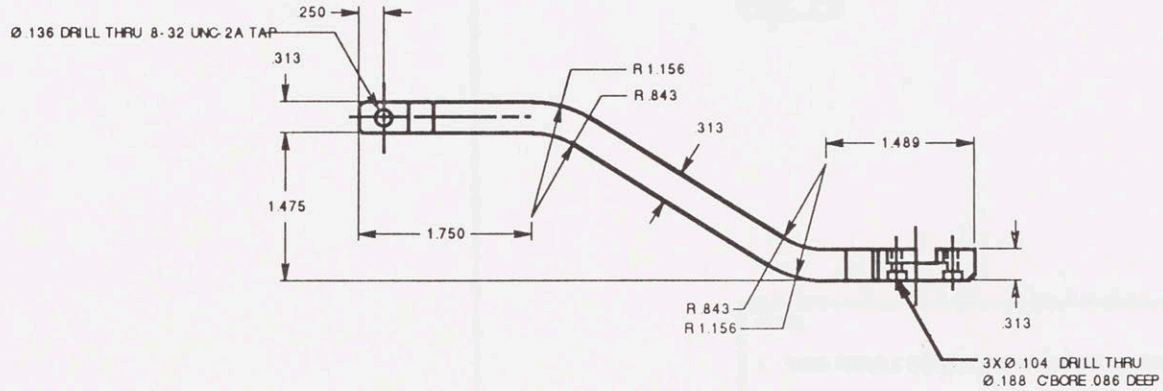

NOTE

1. R.030 FOR ALL FILLETS AND CHAMFERS UNLESS SPECIFIED

ACCESSORIES LIST

1. BERG'S PL-6 SHOULDER SCREW 2 REQ.
2. SOCKET HEAD CAP SCREW 2-56 UNC 5/16" UNDER HEAD LENGTH

Material: 6061-T6 Aluminium Alloy	Tolerances: .X ±.015, .XX ±.010, .XXX ±.005 Unless specified	Manual Teaching Aid	
Finish: Black Anodize		Flexion/abduction S-Rod	
Quantity Req.: 1	Scale 1 : 1	E14	Drw. by Jain Charnnarong / App. by Dr. Andre Sharon
		1/24/91	Massachusetts Institute of Technology

DWG# E15A

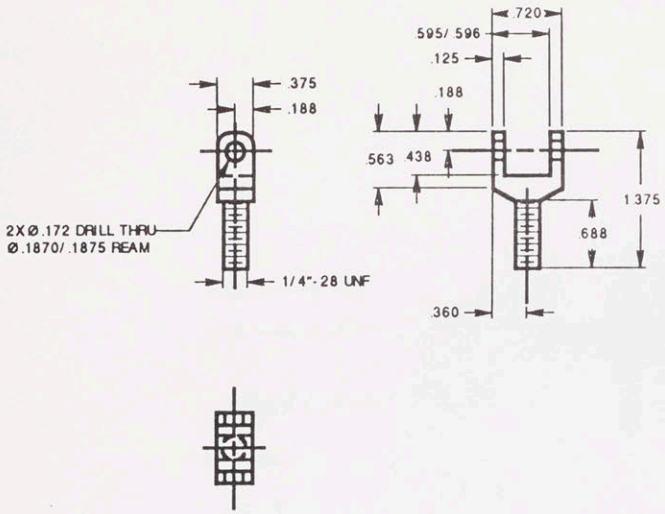

NOTE

1. R.030 FOR ALL FILLETS AND CHAMFERS UNLESS SPECIFIED

Material: 303 Stainless Steel	Tolerances: X ±.015, .XX ±.010, .XXX ±.005, Unless specified	Manual Teaching Aid		
Finish: Black Oxide		Flex/ Abduction connecting rod		
Quantity Req.: 1	Scale 1 : 1	E15A	Drw. by Jain Charnnarong	App. by Dr. Andre Sharon
		1/24/91	Massachusetts Institute of Technology	

DWG# E15B

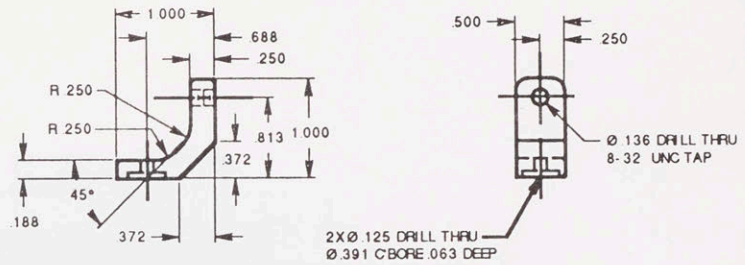

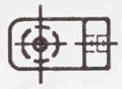

NOTE

1. R.030 FOR ALL FILLETS AND CHAMFERS UNLESS SPECIFIED

ACCESSORIES LIST

1. EDMUND SCIENTIFIC D35,104 NEODYMIUM-IRON-BORON MAGNET 2 REQ.

Material: 6061-T6 Aluminium Alloy	Tolerances: X ±.015, .XX ±.010, .XXX ±.005, Unless specified	Manual Teaching Aid		
Finish: Black Anodize		Flex/ Abduction Palm Connector		
Quantity Req.: 1	Scale 1 : 1	E15B	Drw. by Jain Charnnarong	App. by Dr. Andre Sharon
		1/24/91	Massachusetts Institute of Technology	

DWG# E16

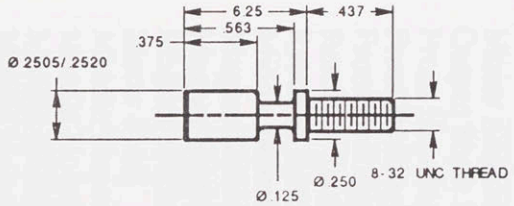

NOTE

1. 0.03 FOR ALL FILLETS AND CHAMFERS UNLESS SPECIFIED

Material: AISI 410 Stainless Steel	Tolerances: X ±.015, .XX ±.010, .XXX ±.005 Unless specified	Manual Teaching Aid	
Finish: Black Oxide		Flex/ abd Palm Connecting Shaft	
Quantity Req.: 1	Scale 2 : 1	E16	Drw. by: Jain Charnnarong / App. by: Dr. Andre Sharon
		1/24/91	Massachusetts Institute of Technology

Appendix A.4 : Actuator Package Subassembly

Drawing No.	Name	Page No.
ASB M01	Motor Assembly	251
M01	Output Shaft Flange Connector	252
M02	Front Housing	253
M03A	Front Bearing Outer Retainer	254
M03B	Front Bearing Inner Retainer	254
M04A	Resolver Stator Retainer	255
M04B	Resolver Rotor Retainer	255
M05A	Middle Bearing Retainer	256
M05B	Magnet Shield Plate	257
M05C	Magnet Shield Retainer	258
M05D	Magnet Shield Separator	258
M06	Motor Shaft	259
M07A	Middle Housing, Overview	260
M07B	Middle Housing, Left-Side View	261
M07C	Middle Housing, Right-Side View	262
M07D	Middle Housing, Wiring Slot	263
M08A	Rear Housing	264
M08B	Rear Housing, Ports	265
M09	Rear Cover Plate	266
M10A	Motor Stator Retainer	267
M10B	Motor Rotor Retainer	267
M11	Tachometer Retainer	268
M12	Resolver Key	269
M13	Motor Keyways	270

DWG# ASB M01

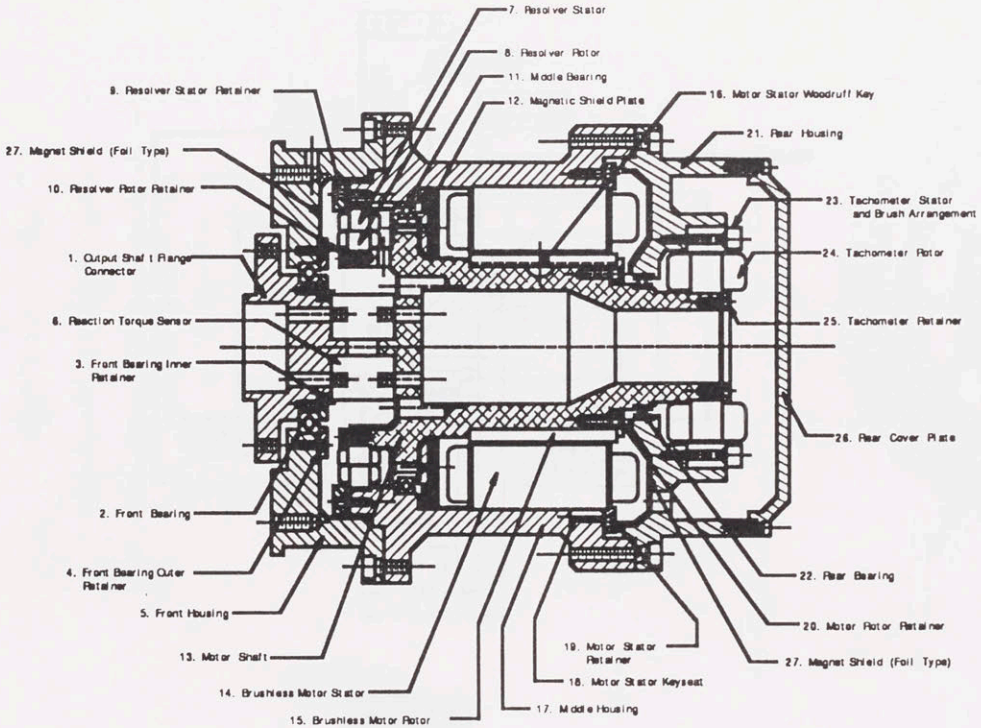

1. Output Shaft Flange Connector	See DWG# M01
2. Front Bearing	Kaydon KB030XP3 Four-point-contact bearing
3. Front Bearing Inner Retainer	See DWG# M03B
4. Front Bearing Outer Retainer	See DWG# M03A
5. Front Housing	See DWG# M02
6. Reaction Torque Sensor	Transducer Techniques TRT-200
7. Resolver Stator	Clifton Precision SSJH-44-B-2
8. Resolver Rotor	Clifton Precision SSJH-44-B-2
9. Resolver Stator Retainer	See DWG# M04A
10. Resolver Rotor Retainer	See DWG# M04B
11. Middle Bearing	Kaydon KA040CP4
12. Magnetic Shield Plate	See DWG# M05A,B,C,D
13. Motor Shaft	See DWG# M06
14. Brushless Motor Stator	Inland Motor RBE 3003-ACK
15. Brushless Motor Rotor	Inland Motor RBE 3003-ACK
16. Motor Stator Woodruff Key	See DWG# M12
17. Middle Housing	See DWG# M07A,B,C
18. Motor Stator Keyseat	See DWG# M07A,B,C
19. Motor Stator Retainer	See DWG# M10A
20. Motor Rotor Retainer	See DWG# M10B
21. Rear Housing	See DWG# M08A, B
22. Rear Bearing	NHBB SSR1-544EE
23. Tachometer Stator and Brush Arrangement	Inland Motor TG-2936-B
24. Tachometer Rotor	Inland Motor TG-2936-B
25. Tachometer Retainer	See DWG# M10A, B
26. Rear Cover Plate	See DWG# M09
27. Magnet Shield (Foil Type)	Note the installed locations

Tolerances .X ±.xx .XX ±.xxx .XXX ±.xxx Unless specified	Manual Teaching Aid	
	Motor Assembly	
Scale 1 : 1	ASB M01	Drw. by Jein Charnnarong / App. by Dr. Andre Sharon
	1/24/91	Massachusetts Institute of Technology

DWG# M01

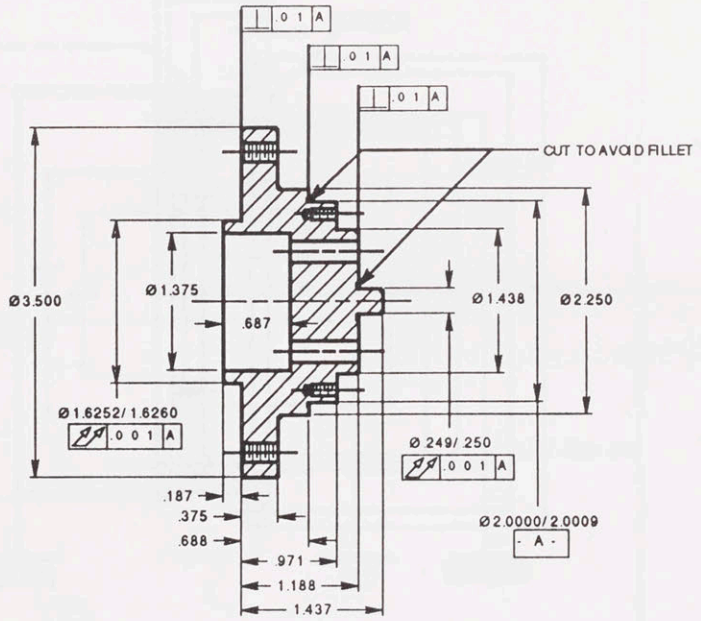

Section A-A

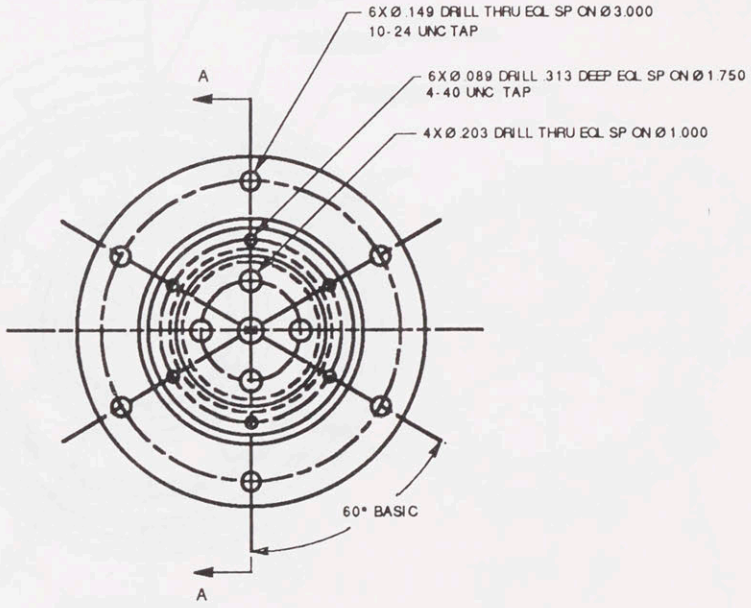

NOTE

1. .025 FOR ALL FILLETS AND CHAMFERS UNLESS SPECIFIED

ACCESSORIES LIST

1. KAYDON'S KB020XP3 4-POINT-CONTACT BEARING 2 REQ.
2. FLAT HEAD SOCKET HEAD CAP SCREW 4-40 UNC 3/8" OVERALL LENGTH 12 REQ.
3. SOCKET HEAD CAP SCREW 10-24 UNC 1/2" UNDER HEAD LENGTH 12 REQ.
4. SOCKET HEAD CAP SCREW 10-24 UNC 1" UNDER HEAD LENGTH 8 REQ.

Material: 6061-T6 Alluminium Alloy	Tolerances: .X ±.015, .XX ±.010, .XXX ±.005 Unless specified	Manual Teaching Aid	
Finish: Black Anodize		Output Shaft Flange Connector	
Quantity Req.: 2	Scale 1 : 1	M01	Drw. by Jain Charnnarong / App. by Dr. Andre Sharon
		1/24/91	Massachusetts Institute of Technology

DWG# M02

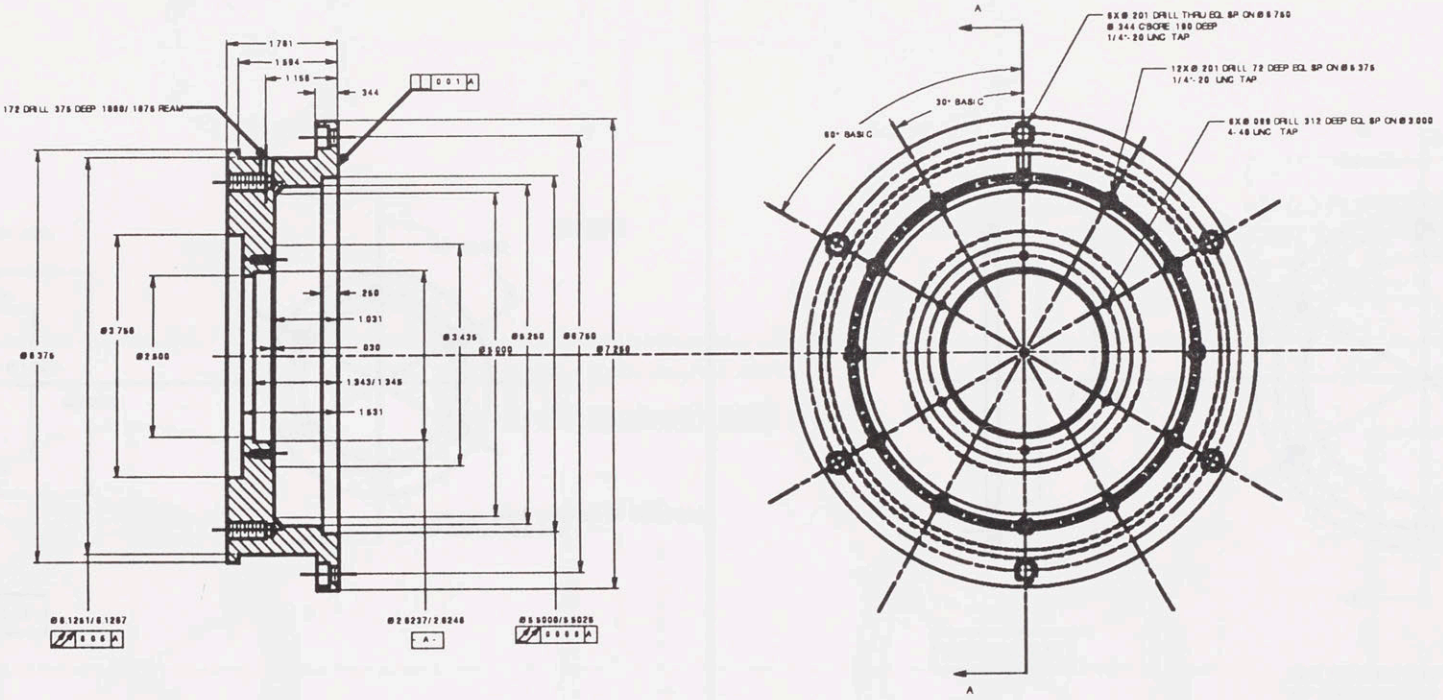

SECTION A-A

NOTE

1. 0.025 FOR ALL FILLETS AND CHAMFERS UNLESS SPECIFIED

ACCESSORY LIST

1. MOTION LIMITTER ; MINOR RUBBER CO. VBM-5014 #228379 5 REQ.
2. BERGS DOWEL PIN D-27-6 2 REQ.
3. FLAT HEAD SOCKET HEAD CAP SCREW 4-40 UNC 3/8" OVERALL LENGTH 12 REQ.

Material: 6061-T6 Aluminium alloy	Tolerances: X .xx, XX .xxx, XXX .xxx unless specified	Manual Teaching Aid	
Finish: Black Anodize		Front Housing	
Quantity Req.: 2	Scale 1 : 1	M02	Drw by: Jan Charmerang; App by: Dr. Agrawal
		1/23/91	Massachusetts Institute of Technology

DWG# M03B

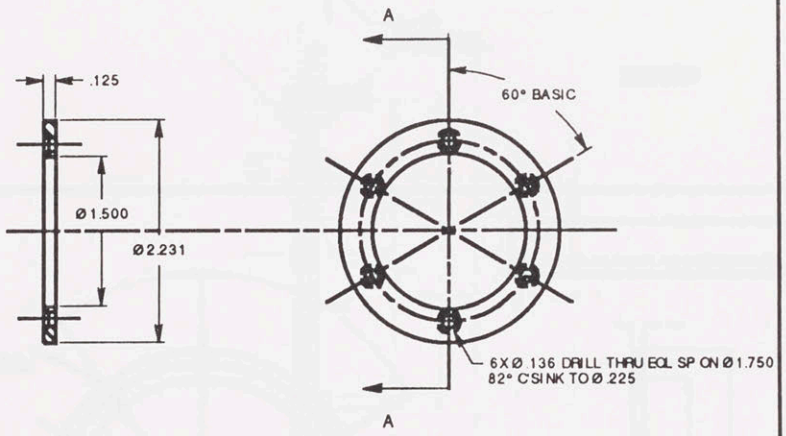

SECTION A-A

NOTE

1. .025 FOR ALL FILLETS AND CHAMFERS UNLESS SPECIFIED

Material: 303 Stainless Steel	Tolerances: .X ±.015, .XX ±.010, .XXX ±.005, Unless specified	Manual Teaching Aid		
Finish: Black Oxide		Front Bearing Inner Retainer		
Quantity Req.: 2	Scale 1 : 1	M03B	Drw. by Jain Charnnarong	App. by Dr. Andre Sharon
		1/24/91	Massachusetts Institute of Technology	

DWG# M03A

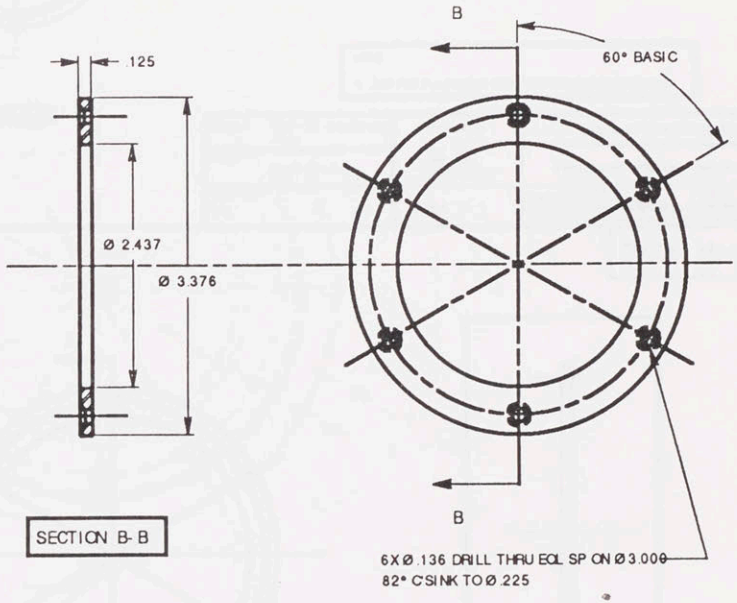

SECTION B-B

NOTE

1. .025 FOR ALL FILLETS AND CHAMFERS UNLESS SPECIFIED

Material: 303 Stainless Steel	Tolerances: .X ±.015, .XX ±.010, .XXX ±.005, Unless specified	Manual Teaching Aid		
Finish: Black Oxide		Front Bearing Outer Retainer		
Quantity Req.: 2	Scale 1 : 1	M03A	Drw. by Jain Charnnarong	App. by Dr. Andre Sharon
		1/24/91	Massachusetts Institute of Technology	

DWG# M04B

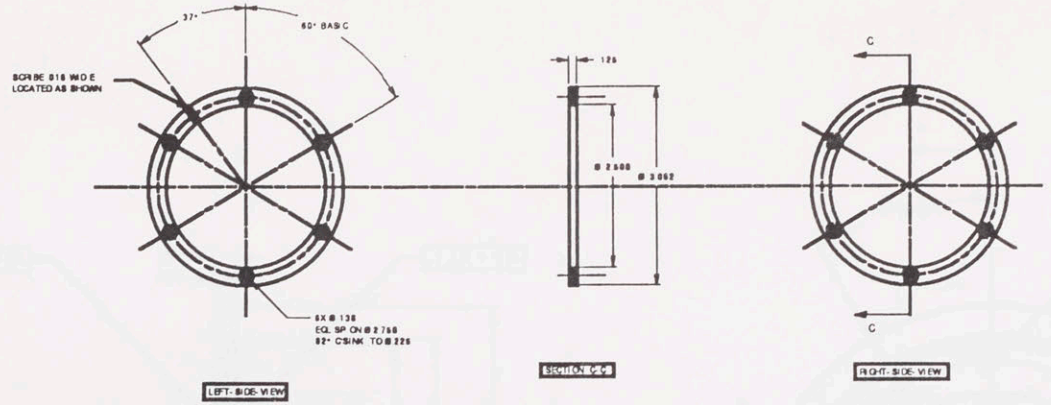

LEFT-SIDE-VIEW

SECTION C-C

RIGHT-SIDE-VIEW

NOTE

1. .025 FOR ALL FILLETS AND CHAMFERS UNLESS SPECIFIED

Material: 6061-T6 Aluminium Alloy	Tolerances: X ±.xxx, XX ±.xxx, XXX ±.xxx Unless specified	Manual Teaching Aid	
Finish: Black Anodize		Resolver Rotor Retainer	
Quantity Req.: 2	Scale 1 : 1	M04B	Drw by Jien Chennareng / App by Dr. Agata Sharan
		5/12/90	Massachusetts Institute of Technology

DWG# M04A

NOTE

1. .025 FOR ALL FILLETS AND CHAMFERS UNLESS SPECIFIED

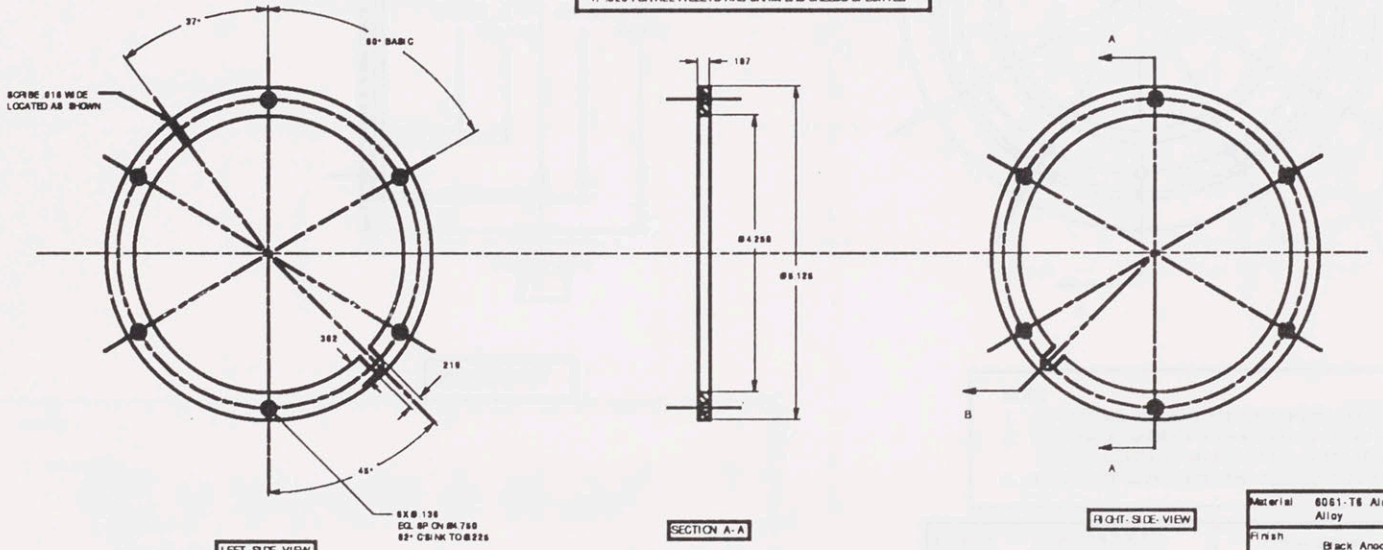

LEFT-SIDE-VIEW

SECTION A-A

RIGHT-SIDE-VIEW

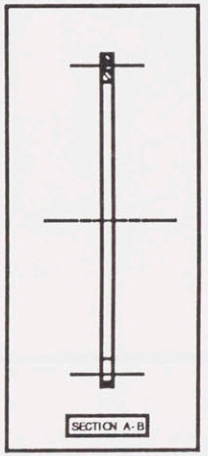

SECTION A-B

Material: 6061-T6 Aluminium Alloy	Tolerances: X ±.xxx, XX ±.xxx, XXX ±.xxx Unless specified	Manual Teaching Aid	
Finish: Black Anodize		Resolver Stator Retainer	
Quantity Req.: 2	Scale 1 : 1	M04A	Drw by Jien Chennareng / App by Dr. Agata Sharan
		5/12/90	Massachusetts Institute of Technology

DWG# M05A

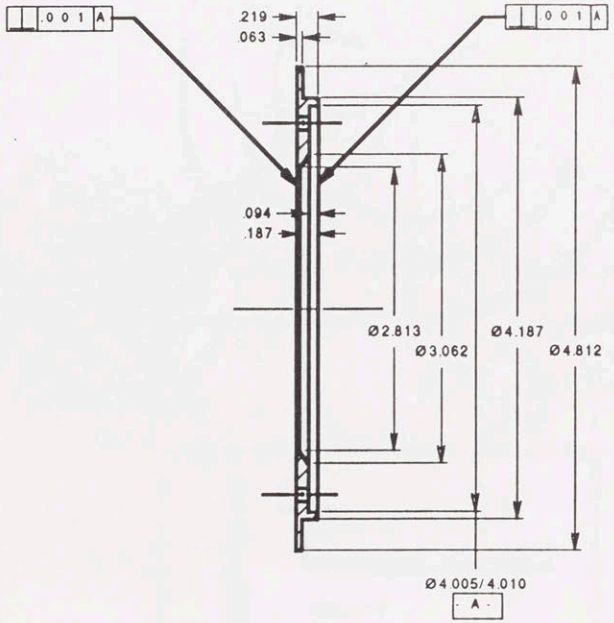

SECTION A-A

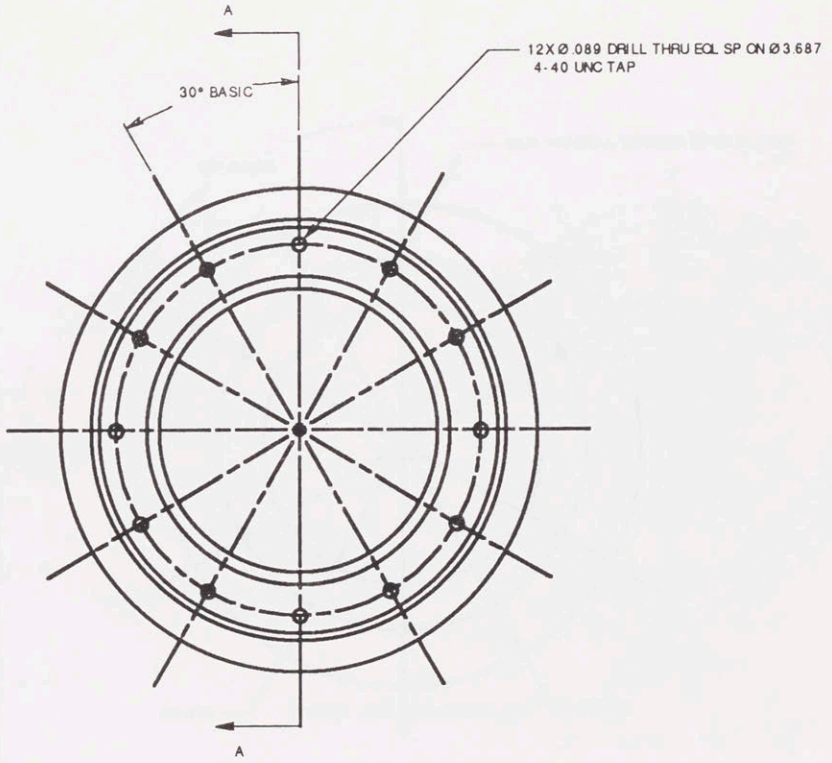

NOTE
1. .03 FOR ALL FILLETS AND CHAMFERS UNLESS SPECIFIED
2. THE TRADE NAME OF 99.8% IRON IS CORO-STEEL
   PLEASE CONTACT MAJOR STEEL SUPPLIER
3. IN CASE OF ANY PROBLEMS PLEASE CONTACT JAIN CHARNNARONG @617-254-6803

Material: Iron (99.8% Fe) Annealed	Tolerances: .X ±.015, .XX ±.010, .XXX ±.005 Unless specified	Manual Teaching Aid		
Finish		Middle Bearing Retainer		
Quantity Req. 2	Scale 1 : 1	M05A	Drw. by Jain Charnnarong	App. by Dr. Andre Sharon
		1/24/91	Massachusetts Institute of Technology	

DWG# M05B

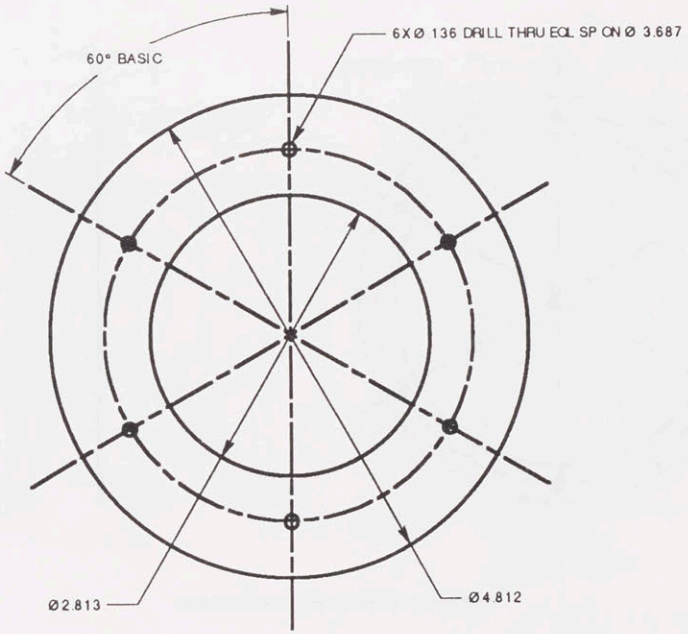

NOTE

1. MATERIAL :
   ADMU-80 FULL ANNEALED 80% NICKEL .032" THICK- 2 PIECES
   ADMU-40 FULL ANNEALED 40% NICKEL .032" THICK- 4 PIECES
   PRODUCT OF
   ADVANCE MAGNETIC
   625 MONROE ST.
   ROCHESTER, INDIANA 49675
   TEL. 219 223-3158

Material SEE ABOVE NOTE	Tolerances .X ±.015 .XX ±.010 .XXX ±.005 Unless specified	Manual Teaching Aid	
Finish		Magnet Shield Plate	
Quantity Req. ADMU-80 2 PIECES ADMU-40 4 PIECES	Scale 1 : 1	M05B	Drw. by Jain Charnnarong / App. by Dr. Andre Sharon
		1/24/91	Massachusetts Institute of Technology

DWG# M05C

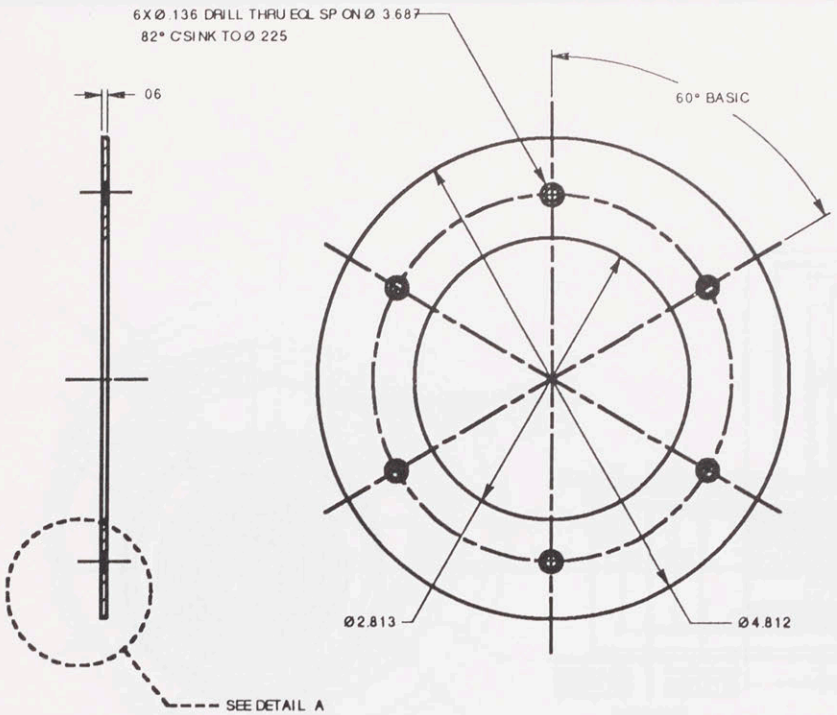

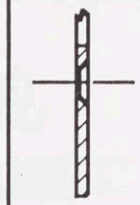

DETAIL A

COUNTERSINK ARRANGEMENT

SCALE 2 : 1

ACCESSORIES LIST

1. FLAT HEAD SOCKET HEAD CAP SCREW 4-40 UNC 1/2" OVERALL LENGTH 12 REQ.

Material: ADMU-80 ANNEALED	Tolerances: .X ±.015, .XX ±.010, .XXX ±.005 Unless specified	Manual Teaching Aid		
Finish		Magnet Shield Retainer		
Quantity Req. 2	Scale 1 : 1	M05C	Drw. by Jain Charnnarong	App. by Dr. Andre Sharon
		1/24/91	Massachusetts Institute of Technology	

DWG# M05D

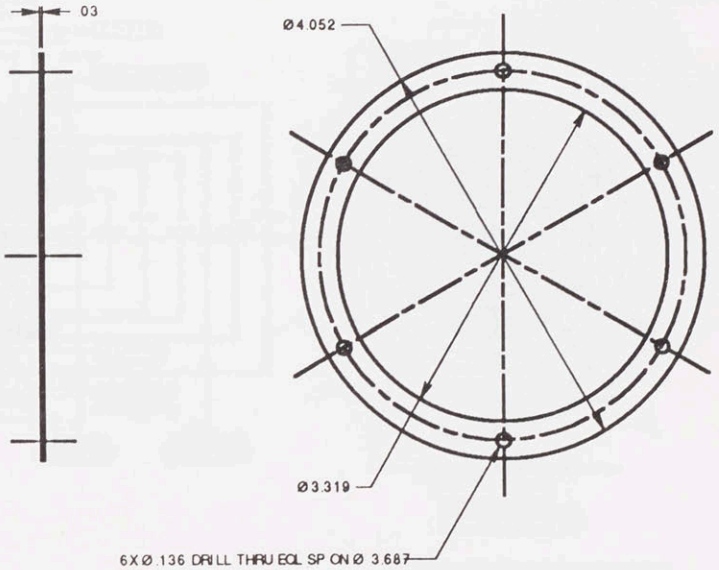

Material: ADMU-80 ANNEALED	Tolerances: .X ±.015, .XX ±.010, .XXX ±.005 Unless specified	Manual Teaching Aid		
Finish		Magnet Shield Separator		
Quantity Req. 2	Scale 1 : 1	M05D	Drw. by Jain Charnnarong	App. by Dr. Andre Sharon
		1/24/91	Massachusetts Institute of Technology	

DWG# M06

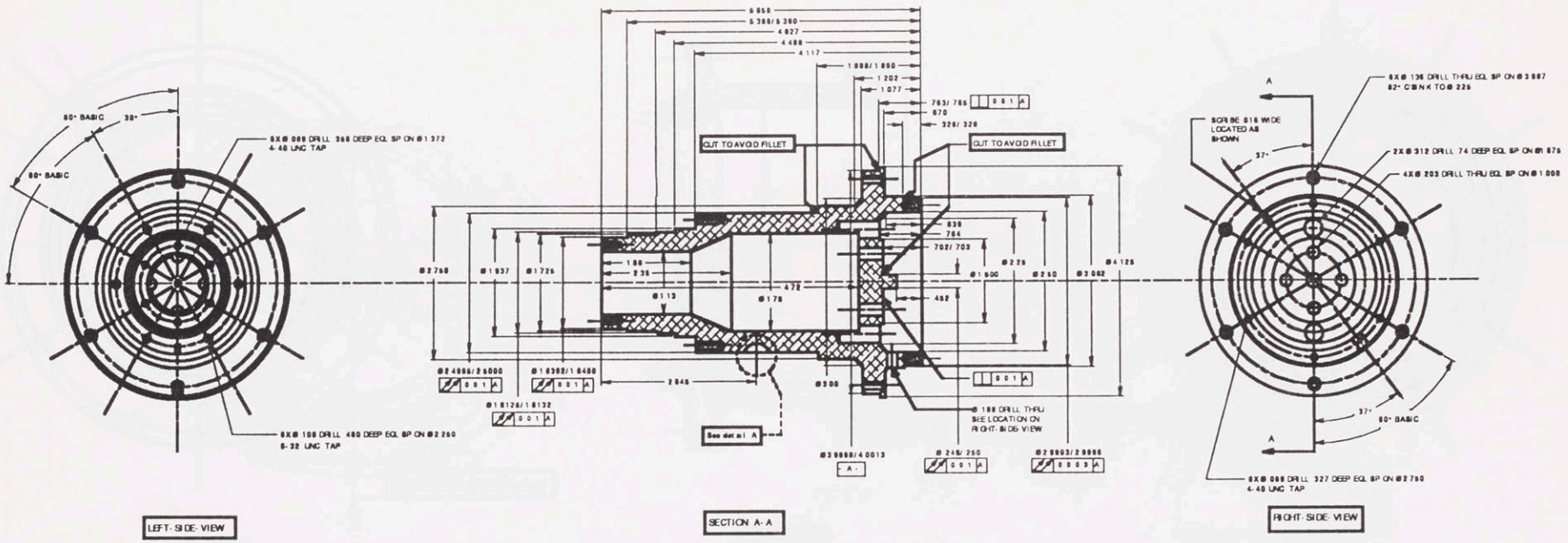

LEFT-SIDE VIEW

SECTION A-A

RIGHT-SIDE VIEW

DETAIL A

SCALE 2:1

ACCESSORIES LIST

1. SOCKET HEAD CAP SCREW 4-40 UNC 3/8" UNDER HEAD LENGTH 12 REQ.
2. FLAT HEAD SOCKET HEAD CAP SCREW 6-32 UNC 1/2" OVERALL LENGTH 12 REQ.
3. FLAT HEAD SOCKET HEAD CAP SCREW 4-40 UNC 3/8" OVERALL LENGTH 12 REQ.
4. SOCKET HEAD CAP SCREW 10-24 UNC 3/4" UNDER HEAD LENGTH 8 REQ.
5. BERG'S K-8 WOODRUFF KEY 2 REQ.
6. KAYDON RADIAL BALL BEARING KA040CP4 2 REQ.
7. NHBB SSR1-544EE BALL BEARING 2 REQ.

NOTE
1. .025 FOR ALL ROUNDS, FILLETS, AND CHAMFERS UNLESS SPECIFIED

Material: 6061-T6 Aluminium Alloy	Tolerances: X ±.03, XX ±.010, XXX ±.005 unless specified	Manual Teaching Aid	
Finish: Black Anodize		Motor Shaft	
Quantity Req.: 2	Scale: 1 : 1	MD6	Drw. by: Jain Chennarsamy; App. by: Dr. Andre Sharon
		1/24/91	Massachusetts Institute of Technology

DWG# M07A

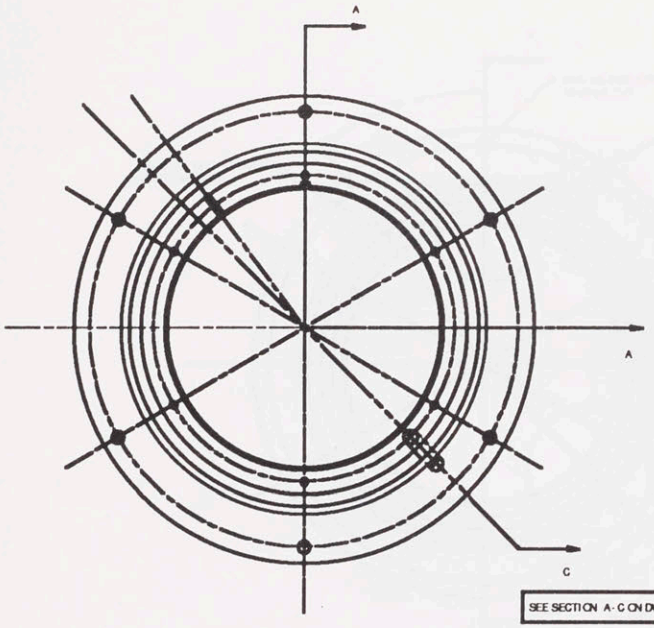

SEE SECTION A-C ON DWG# M07D

LEFT-SIDE-VIEW

SEE DWG# M07B FOR LEFT-SIDE-VIEW DETAIL

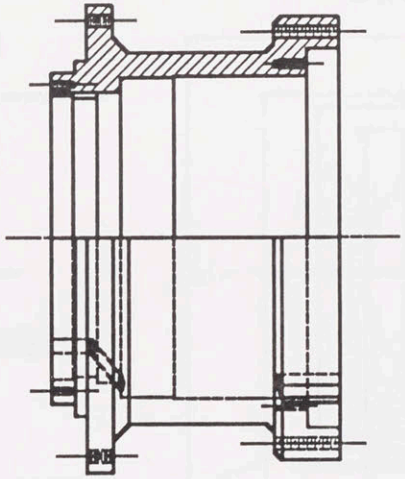

SECTION A-A

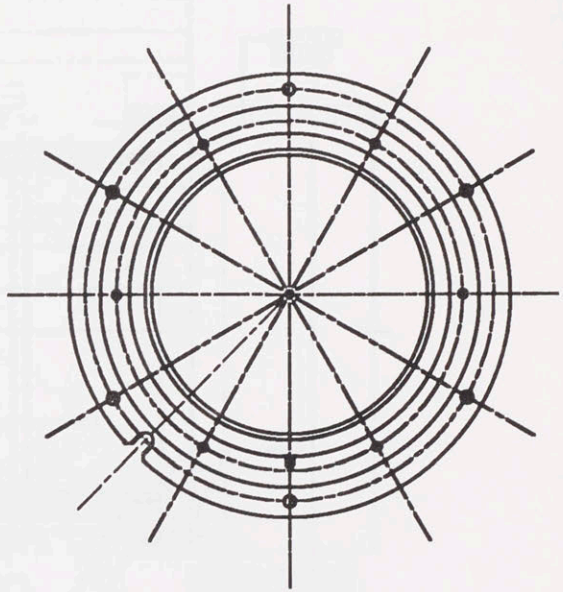

RIGHT-SIDE-VIEW

SEE DWG# M07C FOR RIGHT-SIDE-VIEW DETAIL

Material: 6061-T6 Aluminium Alloy	Tolerances: X ±.xx, XX ±.xxx, XXX ±.xxx Unless specified	Manual Teaching Aid	
Finish: Black Anodize		Middle Housing, Overview	
Quantity Req.: 2	Scale 1 : 1	M07A	Drw by: Jain Chennareng; App by: Dr. Andris Sharon
		1/24/91	Massachusetts Institute of Technology

DWG# M07B

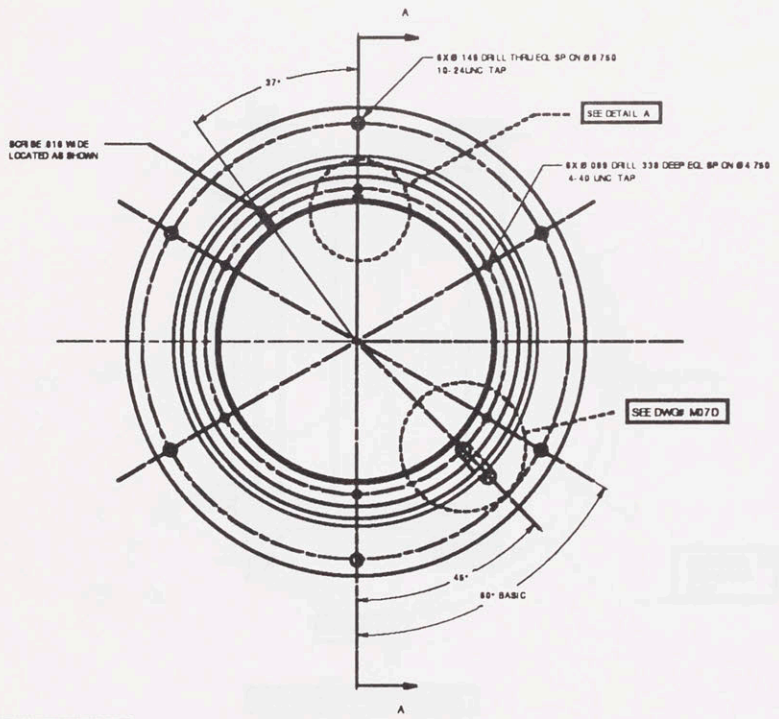

LEFT-SIDE-VIEW

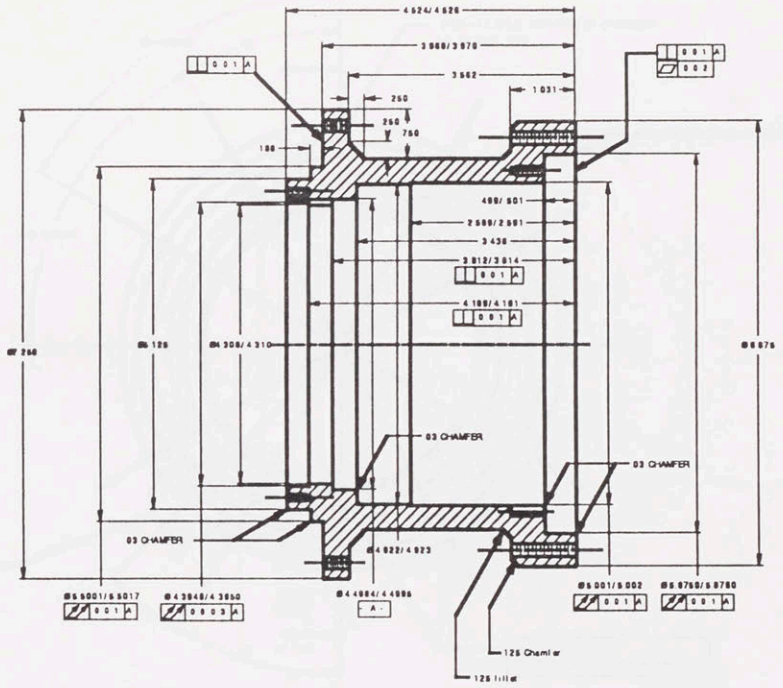

SECTION A-A

DETAIL A

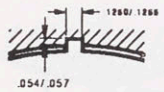

Keyway

Scale 2:1

DETAIL OF KEY ARE IN DWG# M12

NOTE
1. .030 FOR ALL FILLETS AND CHAMFERS UNLESS SPECIFIED

ACCESSORIES LIST
1. SOCKET HEAD CAP SCREW 10-24 UNC 1/2" UNDER HEAD LENGTH 12 REQ.
2. SOCKET HEAD CAP SCREW 10-24 UNC 1" UNDER HEAD LENGTH 12 REQ.
3. FLAT HEAD SOCKET HEAD CAP SCREW 4-40 UNC 1/2" OVERALL LENGTH 12 REQ.
4. FLAT HEAD SOCKET HEAD CAP SCREW 6-32 UNC 1/2" OVERALL LENGTH 12 REQ.
5. .1249/.1251 SQUARE KEY .495/.498 LONG

Material: 6061-T6 Aluminum Alloy	Tolerances: .X ±.010, .XX ±.030, .XXX ±.005 Unless specified	Manual Teaching Aid	
Finish: Black Anodize		Middle Housing, L.S. view	
Quantity Req. 2	Scale 1 : 1	M07B	Drw by Jain Chennareng / App by Dr. Andrew Sharon
		1/24/91	Massachusetts Institute of Technology

DWG# M07C

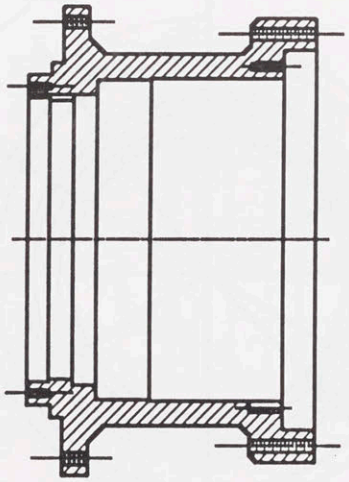

SECTION A-A

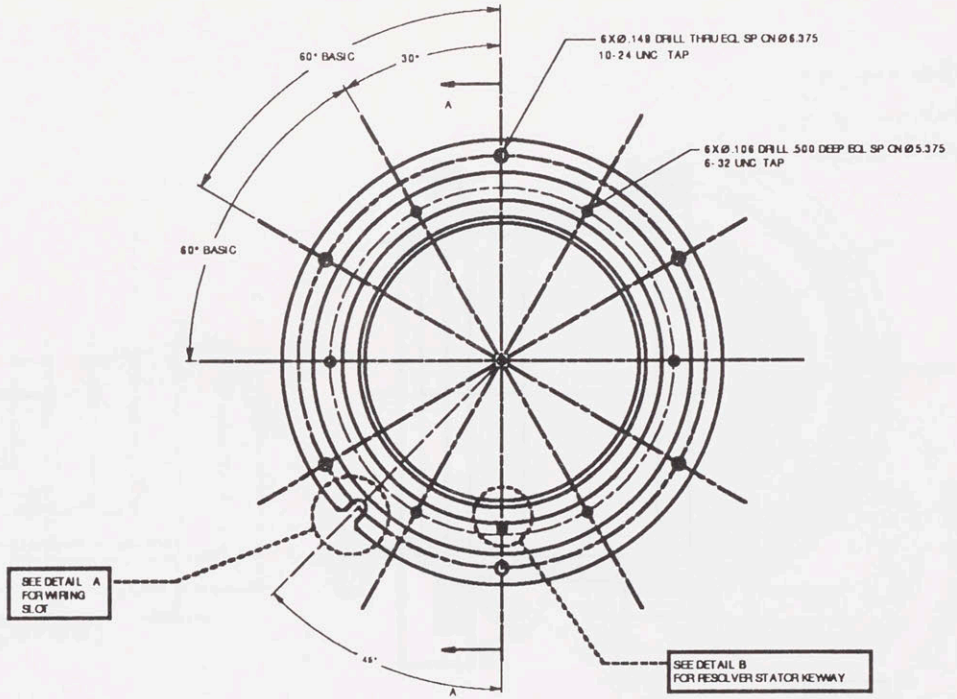

RIGHT-SIDE-VIEW

DETAIL DIMENSIONS ARE IN DWG# M07B

DETAIL A

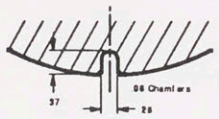

Scal 1:1

DETAIL B

Scale 2:1

Material: 6061-T6 Aluminium Alloy	Tolerances: X ±.xxx, XX ±.xxx, XXX ±.xxx Unless specified	Manual Teaching Aid	
Finish: Black Anodize		Middle Housing, R.S. view	
Quantity Req.: 2	Scale 1 : 1	M07C	Drw by: Jain Charnnarong / App by: Dr. Andrew Shearer
		1/24/91	Massachusetts Institute of Technology

DWG# M07D

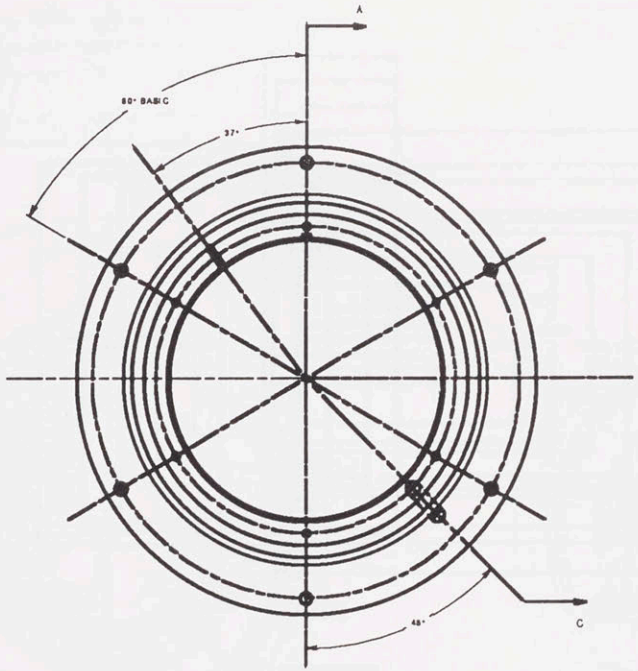

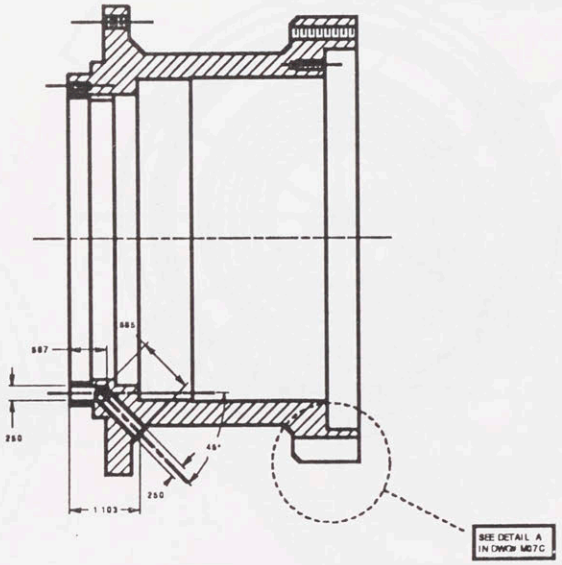

SECTION A-C

Material: 6061-T6 Aluminium Alloy	Tolerances .X ±.xx ±.xxx ±.xxx Unless specified	Manual Teaching Aid	
Finish: Black Anodize		Mid Housing, Wiring Slot	
Quantity Req.: 2	Scale 1 : 1	M07D	Drw. by: Jain Charnnarong / App. by: Dr. Angela Sharon
		1/24/91	Massachusetts Institute of Technology

DWG# M08A

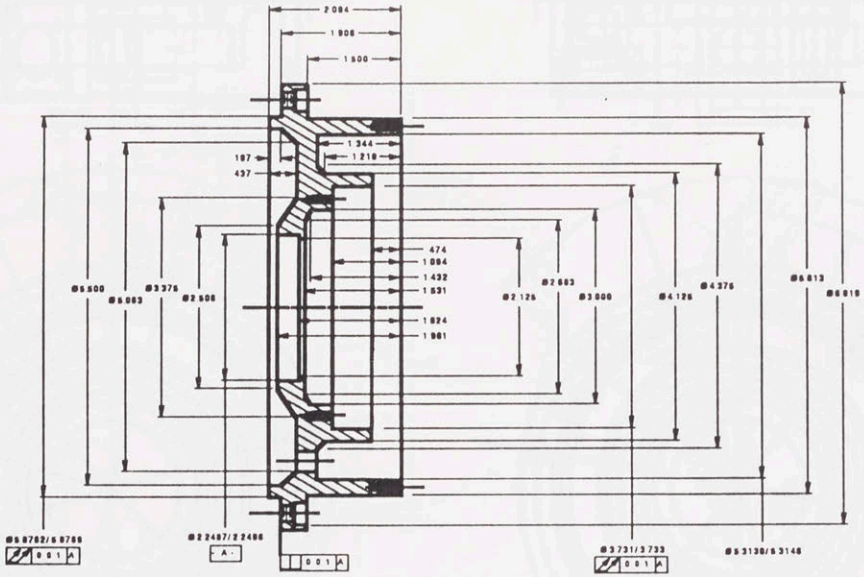

SECTION A-A

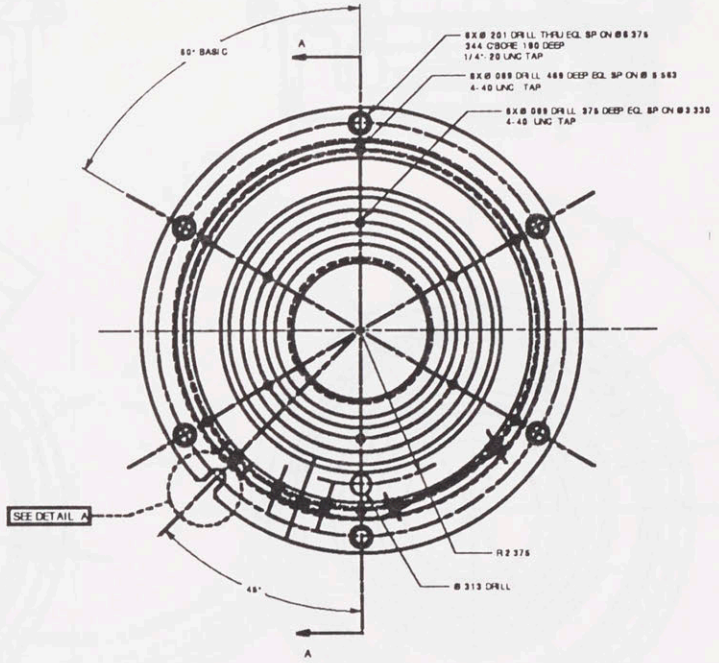

SEE DWG# M08B FOR PORT DETAIL

Detail A

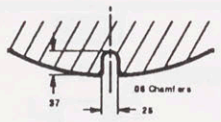

Scal 1:1

ACCESSORIES LIST
1. FLAT HEAD SOCKET HEAD CAP SCREW 4-40 UNC 3/4" OVERALL LENGTH 12 REQ.
2. SOCKET HEAD CAP SCREW 4-40 UNC 3/8" UNDER HEAD LENGTH 12 REQ.
3. AMPLINCL CIRCULAR CONNECTOR 12SL-844P 4-CONTACT 3102A RECEPTACLE 2 REQ.
4. AMPLINCL CIRCULAR CONNECTOR 12SL-844S 4-CONTACT 3106A STRAIGHT PLUG 2 REQ.
5. AMP AMPLIMITE D-SUBMINIATURE CABLE CLAMP 25-PIN TYPE 747913-2 RECEPTACLE 2REQ.
6. AMP AMPLIMITE D-SUBMINIATURE CABLE CLAMP 25-PIN TYPE 747912-2 PLUG 2 REQ.
7. AMP AMPLIMITE D-SUBMINIATURE CABLE CLAMP 9-PIN TYPE 747905-2 RECEPTACLE 4 REQ.
8. AMP AMPLIMITE D-SUBMINIATURE CABLE CLAMP 9-PIN TYPE 747904-2 PLUG 4 REQ.

NOTE
1. .025 FOR ALL FILLETS AND CHAMFERS UNLESS SPECIFIED

Material: 6061-T6 Aluminium Alloy	Tolerances: X ±.xx, XX ±.xx, XXX ±.xxx, Unless specified	Manual Teaching Aid	
Finish: Black Anodize		Rear Housing	
Quantity Req.: 2	Scale 1 : 1	M08A	Drw by: Jain Charmmarong; App by: Dr. Andris Sharan
		1/24/91	Massachusetts Institute of Technology

DWG# M08B

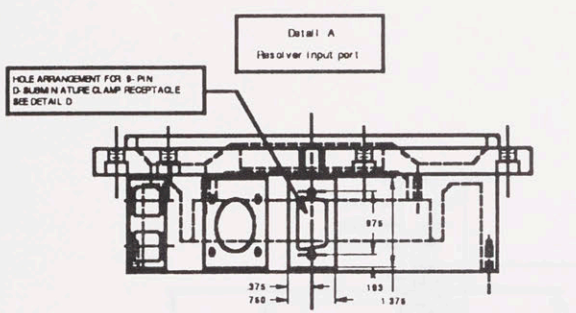

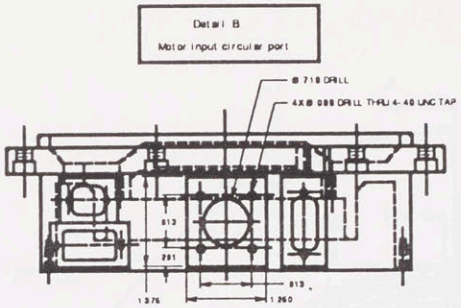

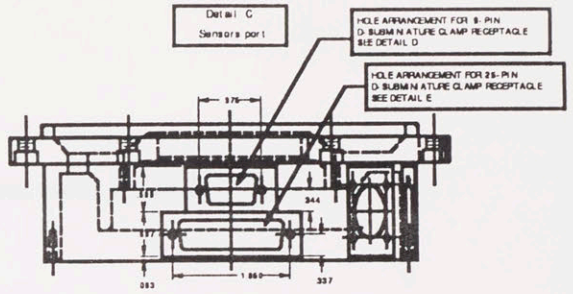

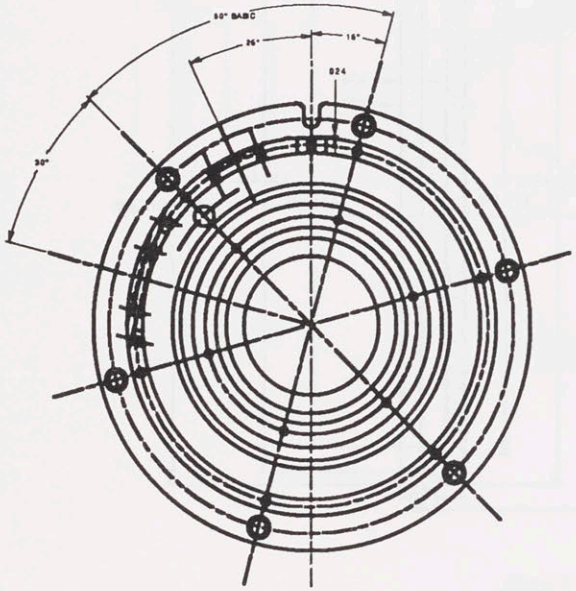

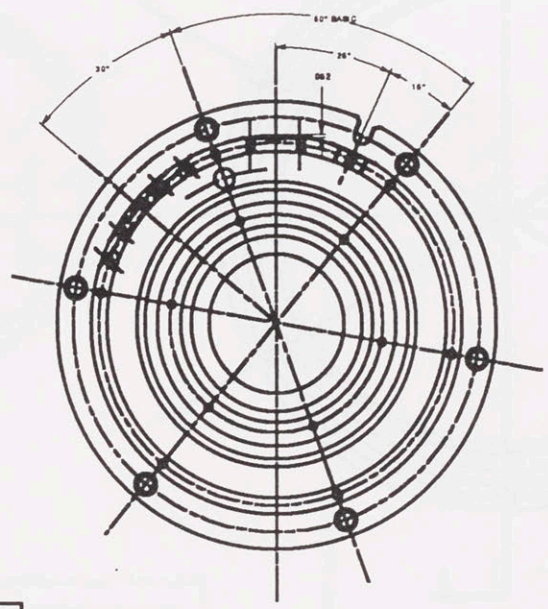

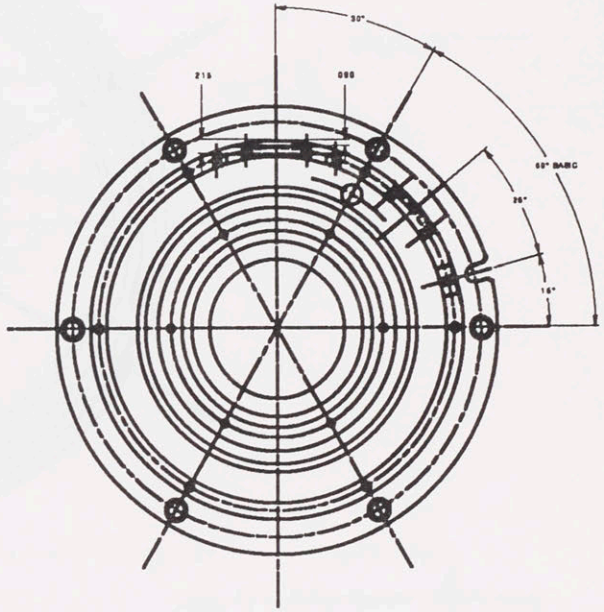

DETAIL D

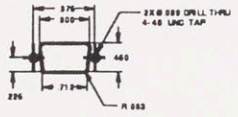

DETAIL E

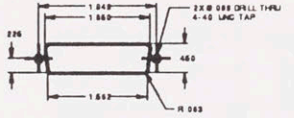

Material: 6061-T6 Aluminium Alloy	Tolerances: X ±.xxx, XX ±.xxx, XXX ±.xxx, Unless specified	Manual Teaching Aid	
Finish: Black Anodize		Rear Housing, Ports	
Quantity Req: 2	Scale 1 : 1	M08B	Drw. by: Jian Chennareng; App. by: Dr. Andre Stanson
		1/24/91	Massachusetts Institute of Technology

DWG# M09

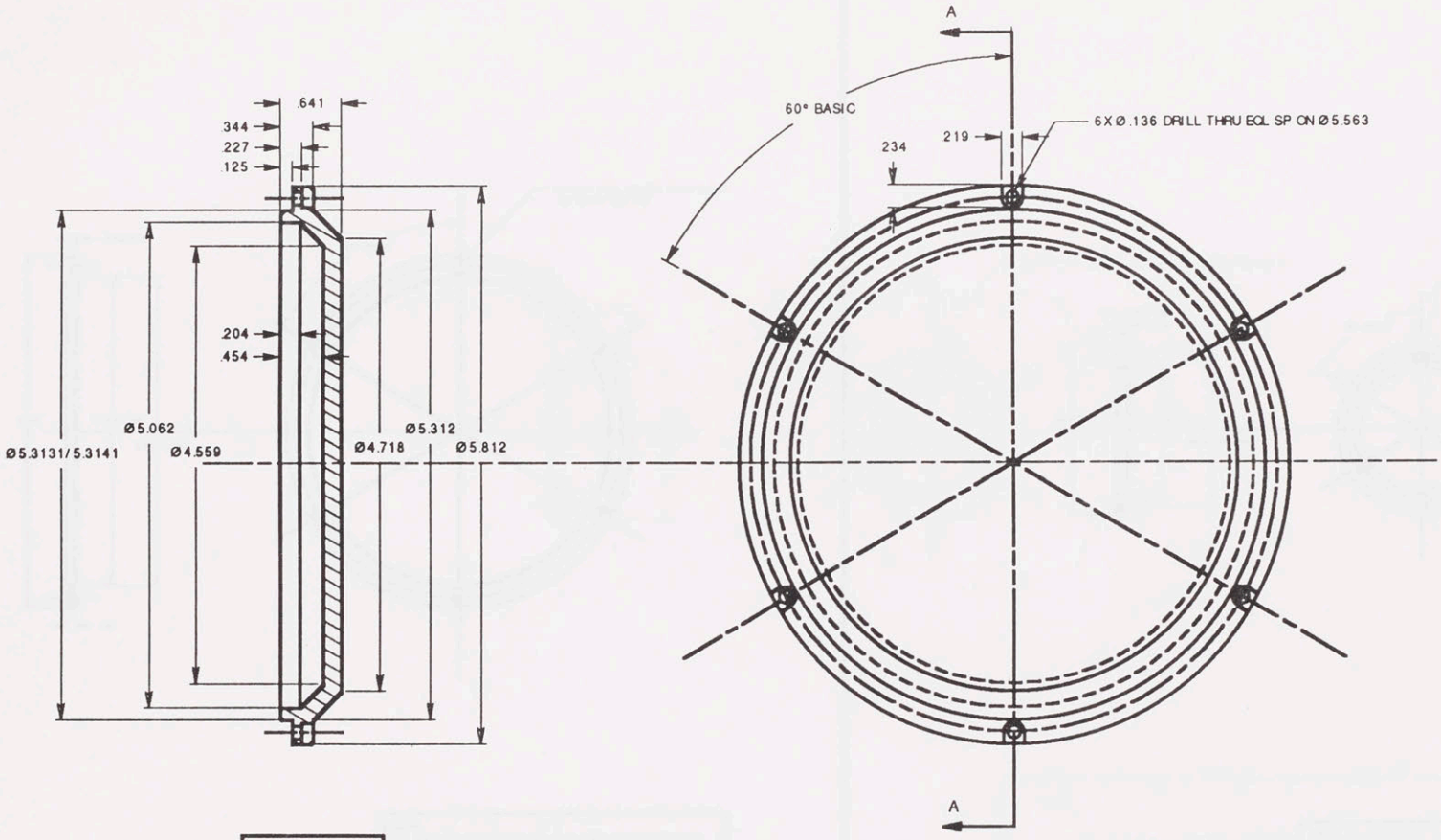

SECTION A-A

NOTE
1. .025 FOR ALL FILLETS AND CHAMFERS UNLESS SPECIFIED

Material: 6061-T6 Aluminium alloy	Tolerances: .X ±.015, .XX ±.010, .XXX ±.005 Unless specified	Manual Teaching Aid	
Finish: Black Anodize		Rear Cover Plate	
Qunatity Req.: 2	Scale 1 : 1	M09	Drw. by Jain Charnnarong / App. by Dr. Andre Sharon
		1/24/91	Massachusetts Institute of Technology

DWG# M10A

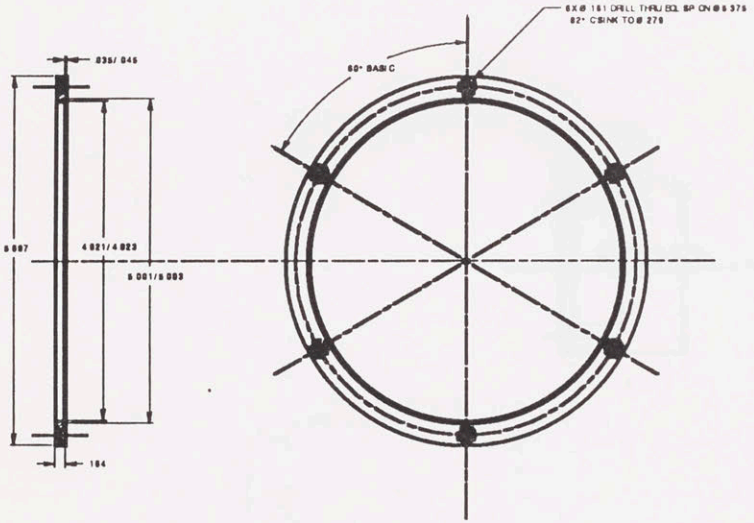

NOTE
1. .025 FOR ALL FILLETS AND CHAMFERS UNLESS SPECIFIED

Material: AISI 303 Stainless Steel	Tolerances: .X ±.xxx, .XX ±.xxx, .XXX ±.xxx, Unless specified	Manual Teaching Aid	
Finish: Black Oxide		Motor Stator Retainer	
Quantity Req.: 2	Scale 1 : 1	M10A	Drw. by: Jain Charnnarong / Date: 1/24/91
			App. by: Dr. Andrew Sharon / Massachusetts Institute of Technology

DWG# M10B

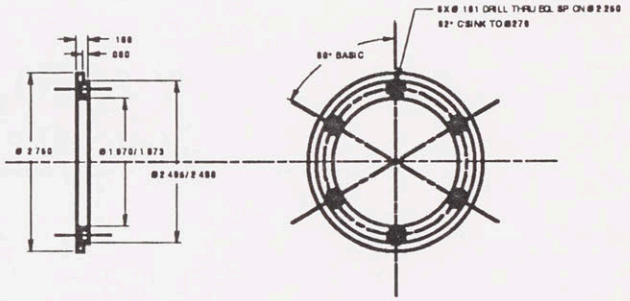

NOTE
1. .025 FOR ALL FILLETS AND CHAMFERS UNLESS SPECIFIED

Material: AISI 303 Stainless Steel	Tolerances: .X ±.xxx, .XX ±.xxx, .XXX ±.xxx, Unless specified	Manual Teaching Aid	
Finish: Black Oxide		Motor Rotor Retainer	
Quantity Req.: 2	Scale 1 : 1	M10B	Drw. by: Jain Charnnarong / Date: 1/24/91
			App. by: Dr. Andrew Sharon / Massachusetts Institute of Technology

DWG# M11

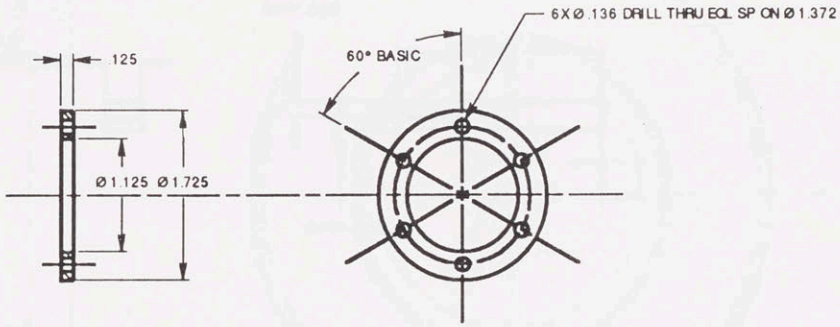

NOTE

1. .025 FOR ALL FILLETS AND CHAMFERS UNLESS SPECIFIED

Material: AISI 303 Stainless Steel	Tolerances: .X ±.015, .XX ±.010, .XXX ±.005, Unless specified	Manual Teaching Aid	
Finish: Black Oxide		Tachometer Retainer	
Quantity Req.: 2	Scale 1 : 1	M11	Drw. by Jain Charnnarong / App. by Dr. Andre Sharon
		1/24/91	Massachusetts Institute of Technology

DWG# M12

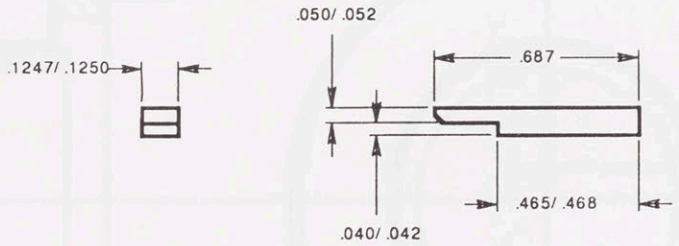

Note
1. R.030 for all fillets and chamfers

Material: AISI 303 Stainless Steel	Tolerances: X ±.015, XX ±.010, XXX ±.005, Unless specified	Manual Teaching Aid	
Finish		Resolver key	
Quantity Req. 2	Scale 3 : 1	M12	Drw. by Jain Charnnarong / App. by Dr. Andre Sharon
		1/24/91	Massachusetts Institute of Technology

DWG# M13

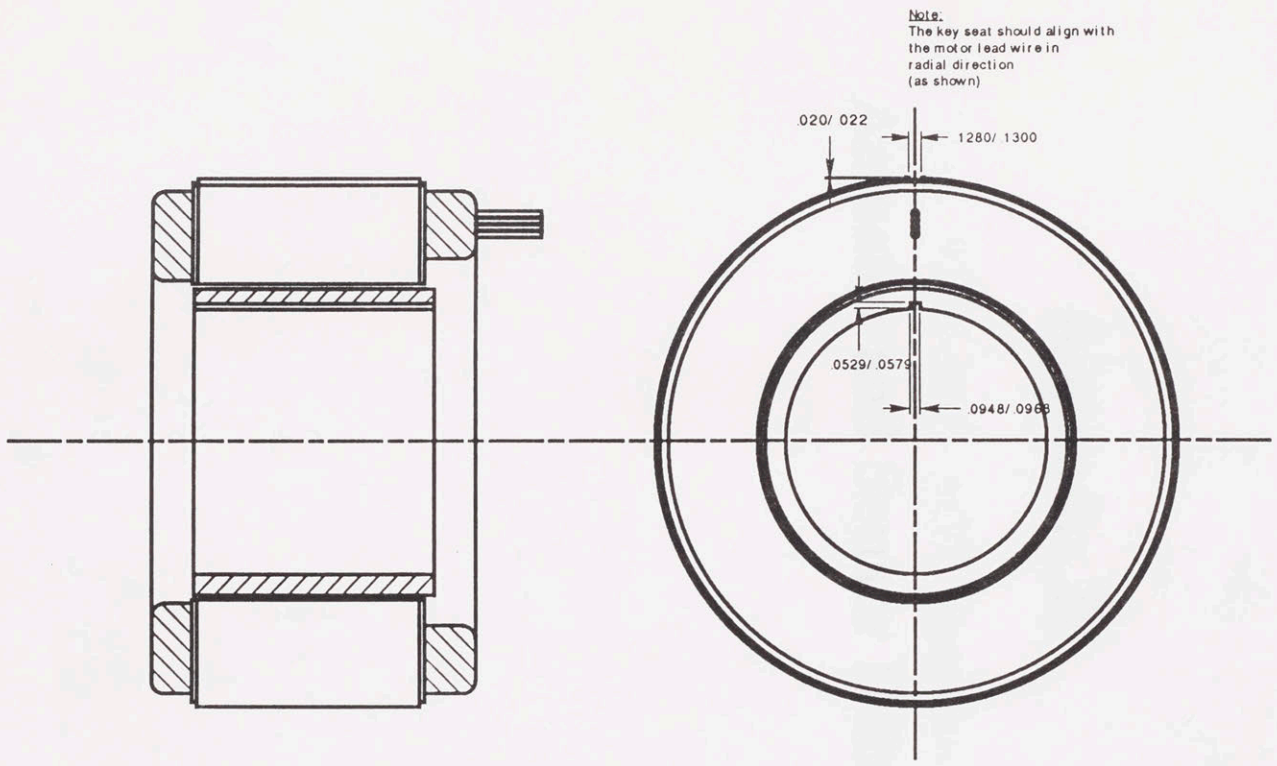

Note

1. INLAND'S RBE 3003 BRUSHLESS DC MOTOR WITH SPECIAL KEY ARRANGEMENT

Tolerances .X ±.015 .XX ±.010 .XXX ±.005 Unless specified	Rehab Robotic Aid Motor Keyways
SCALE 1:1	Drw. by Jain Charnnarong; App. by Dr. Andre Sharon 9/12/90 Massachusetts Institute of Technology

Appendix B

Actuator and Sensor Details

Appendix B.1 : RBE-3003-AOX Brushless Motor

Frameless Motor

MODEL	"A" DIM	"B" DIM	"C" DIM
RBE-03000-_00	.525 (13.3)	.705 (17.9)	1.385 (35.2)
RBE-03001-_00	1.050 (26.7)	1.230 (31.2)	1.910 (48.5)
RBE-03002-_00	1.625 (41.3)	1.805 (45.8)	2.485 (63.1)
RBE-03003-_00	2.150 (54.6)	2.330 (59.2)	3.010 (76.5)
RBE-03004-_00	2.625 (66.7)	2.805 (71.2)	3.485 (88.5)
RBE-03005-_00	3.250 (82.6)	3.430 (87.1)	4.110 (104.4)
RBE-03006-_00	3.750 (95.3)	3.930 (99.8)	4.610 (117.1)

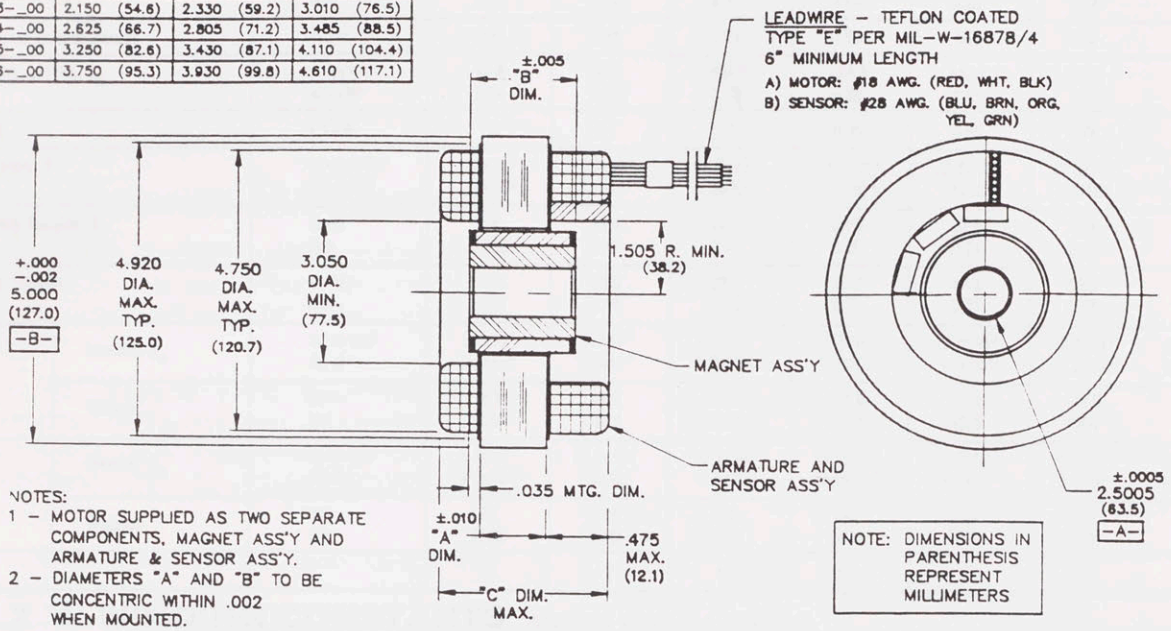

NOTES:
1 – MOTOR SUPPLIED AS TWO SEPARATE COMPONENTS, MAGNET ASS'Y AND ARMATURE & SENSOR ASS'Y.
2 – DIAMETERS "A" AND "B" TO BE CONCENTRIC WITHIN .002 WHEN MOUNTED.
3 – MOUNTING SURFACE BETWEEN 5.000 AND 4.920 DIAMETERS ON BOTH SIDES.

NOTE: DIMENSIONS IN PARENTHESIS REPRESENT MILLIMETERS

Housed Motor

MODEL	LENGTH
RBEH-03000-_00	2.320 (58.9)
RBEH-03001-_00	2.845 (72.3)
RBEH-03002-_00	3.420 (86.9)
RBEH-03003-_00	3.945 (100.2)
RBEH-03004-_00	4.420 (112.3)
RBEH-03005-_00	5.045 (128.1)
RBEH-03006-_00	5.545 (140.8)

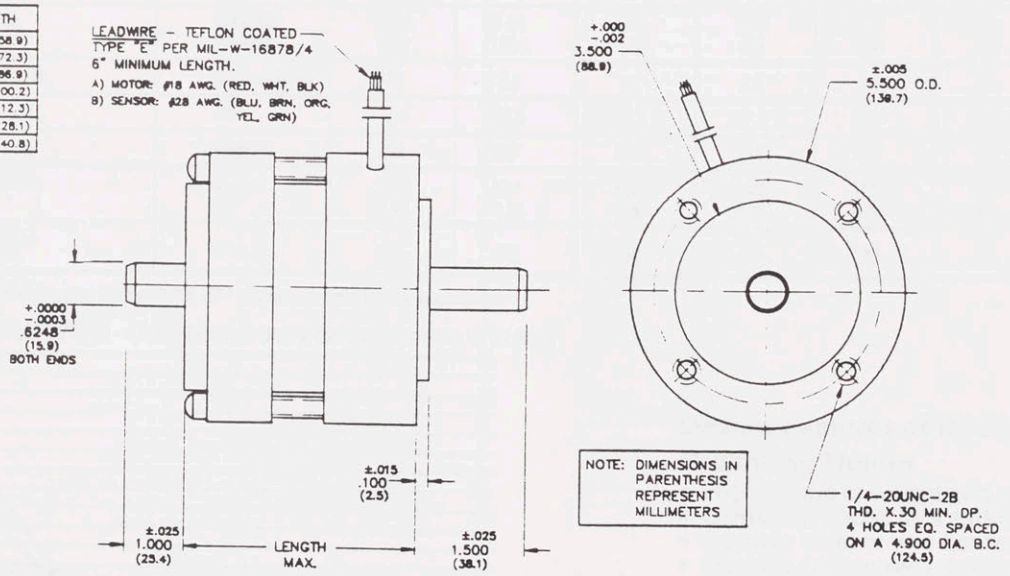

NOTE: DIMENSIONS IN PARENTHESIS REPRESENT MILLIMETERS

RBE(H) 03000 MOTOR SERIES

SIZE CONSTANTS

PARAMETERS / MODEL NO.		UNITS	RBE-03000	RBE-03001	RBE-03002	RBE-03003	RBE-03004	RBE-03005	RBE-03006
Peak Rated Torque, ±25%		oz-in Nm	837 5.9	1607 11.3	2390 16.9	3106 21.9	3752 26.5	4597 32.4	5425 38.3
Power at Peak Rated Torque		Watts	308	402	495	623	687	754	822
Max. Continuous Stall Torque, T_c		oz-in Nm	372 2.63	650 4.59	910 6.42	1114 7.86	1316 9.29	1620 11.4	1890 13.3
Max. Continuous Output Power		Watts	466	596	709	786	865	992	1071
Motor Constant, ± 15%, K_M		oz-in/$\sqrt{W}$ Nm/$\sqrt{W}$	47.8 0.34	80.0 0.56	106.9 0.75	124.8 0.88	142.7 1.01	167.9 1.18	190.1 1.34
TPR, ± 15% †		(°C/W)	1.2	1.1	1.0	0.91	0.85	0.78	0.73
Viscous Damping, F_t		oz-in/RPM Nm/RPM	$5.4x10^{-3}$ $3.8x10^{-5}$	$9.9x10^{-3}$ $7.0x10^{-5}$	$14.4x10^{-3}$ $1.0x10^{-4}$	$18.7x10^{-3}$ $1.3x10^{-4}$	$22.6x10^{-3}$ $1.6x10^{-4}$	$27.6x10^{-3}$ $1.9x10^{-4}$	$33.4x10^{-3}$ $2.4x10^{-4}$
Hysteresis Drag Torque, T_r		oz-in Nm	8.4 0.059	15.4 0.11	22.0 0.16	28.0 0.20	33.6 0.24	40.8 0.29	49.2 0.35
Max. Cogging Torque		oz-in Nm	11.0 0.08	20.0 0.14	28.0 0.20	36.0 0.26	44.0 0.31	53.0 0.38	60.0 0.43
Frameless Motor	Inertia, J_M	oz-in-sec^2 Kg-m^2	$3.2x10^{-2}$ $2.3x10^{-4}$	$5.7x10^{-2}$ $4.0x10^{-4}$	$8.3x10^{-2}$ $5.9x10^{-4}$	$10.7x10^{-2}$ $7.6x10^{-4}$	$12.9x10^{-2}$ $9.1x10^{-4}$	$15.8x10^{-2}$ $11.2x10^{-4}$	$18.1x10^{-2}$ $12.8x10^{-4}$
	Weight	oz gm	38.1 1080	64.0 1814	92.3 2617	118.0 3345	142.0 4026	173.0 4904	199.0 5642
Housed Motor	Inertia, J_M	oz-in-sec^2 Kg-m^2	$6.4x10^{-2}$ $4.5x10^{-4}$	$11.2x10^{-2}$ $7.9x10^{-4}$	$16.5x10^{-2}$ $11.6x10^{-4}$	$21.2x10^{-2}$ $15.0x10^{-4}$	$25.6x10^{-2}$ $18.1x10^{-4}$	$31.3x10^{-2}$ $22.1x10^{-4}$	$35.8x10^{-2}$ $25.3x10^{-4}$
	Weight	oz gm	75 2126	113 3189	155 4376	192 5431	225 6366	272 7698	309 8741
No. of Poles			12	12	12	12	12	12	12

100 VOLT 'A' WINDING CONSTANTS Alternate Windings Available

Peak Torque, ±25%, T_p		oz-in Nm	837 5.9	1607 11.3	2390 16.9	3106 21.9	3752 26.5	4597 32.4	5425 38.3
Peak Current, ± 15%, I_p		Amps	6.5	8.3	10.3	11.9	13.4	15.9	17.4
Torque Sensitivity, ± 10%, K_T		oz-in/Amp Nm/Amp	128 0.904	193 1.37	233 1.64	261 1.84	279 1.97	290 2.05	311 2.20
No Load Speed, ± 10%		RPM	1040	690	575	510	480	460	430
Voltage Constant, ± 10%, K_E		V/Rad/sec V/KRPM	0.904 94.6	1.37 143.4	1.64 172	1.84 193	1.97 206	2.05 214	2.20 230
Terminal Resistance, ± 12%, R_M		ohms @ 25°C	7.2	5.8	4.7	4.4	3.8	3.0	2.7
Terminal Inductance, ±30%, L_M		mH	19.4	22.5	22.3	21.8	20.7	18.2	17.3
Max. Continuous Output Power	Power	Watts	208	247	291	318	354	424	465
	Torque	oz-in Nm	350 2.47	614 4.33	858 6.06	1049 7.40	1238 8.74	1514 10.7	1767 12.5
	Speed	RPM	800	545	460	410	385	380	355

†TPR assumes housed motor mounted to 12.0 x 12.0 x .50" aluminum heat sink or equivalent.

PERFORMANCE CURVES CONTINUOUS DUTY CAPABILITY FOR 75°C RISE

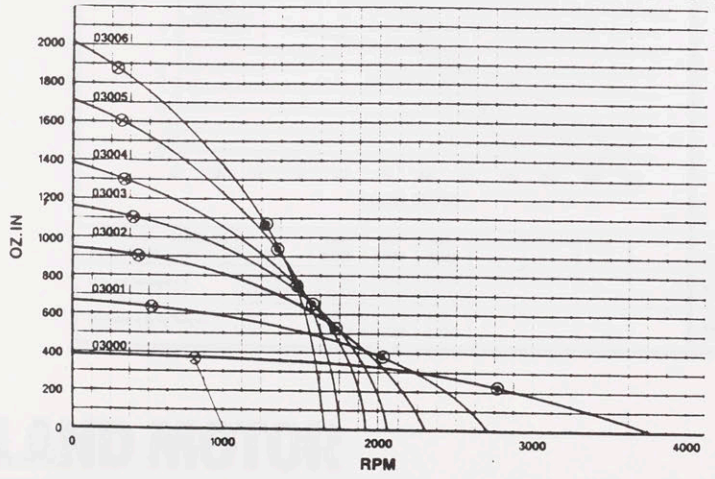

Design Features of RBE(H) Brushless Motors

- High torque to weight and inertia ratios
- Samarium cobalt rare earth magnets
- 3 phase delta or wye connection
- Housed or frameless designs
- Stationary outer stator winding rotating inner permanent magnet rotor
- Stainless steel shafts (housed versions)
- All motors built to MIL-Q-9858A
- Encapsulated windings available for harsh environments
- Built-in Hall effect devices for electronic commutation

HIGH EFFICIENCY LAMINATIONS

The accompanying speed/torque curves represent the performance limits of the RBE(H) brushless motors with high efficiency laminations. The advantage of motors with high efficiency laminations is improved performance at higher operating speeds.

Since these motors are best utilized with custom windings, standard windings are not available. To obtain the optimum winding for your application, please contact our application engineers at the factory.

PERFORMANCE PARAMETERS

The physical dimensions of the motors do not change from standard. Please refer to the outline drawings on the DC brushless motor data sheets.

The Size Constants on the data sheets remain the same with the exception of the Viscous Damping (F_l) and Hysteresis Drag Torque (T_F) coefficients which are detailed with the respective curves.

As stated above, standard windings are not available.

PERFORMANCE CURVES
CONTINUOUS DUTY CAPABILITY FOR 75°C RISE

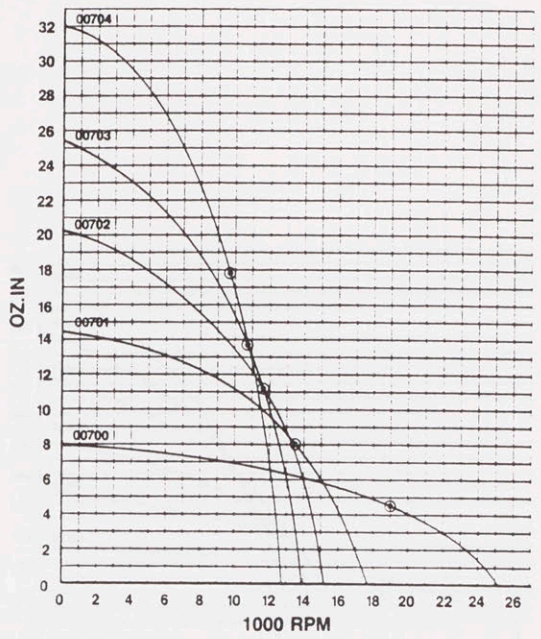

PARAMETERS \ MODEL NO.	UNIT	RBE-00700	RBE-00701	RBE-00702	RBE-00703	RBE-00704
Viscous Damping, F_l	oz-in/RPM	2.2×10^{-5}	4.4×10^{-5}	6.2×10^{-5}	7.9×10^{-5}	9.9×10^{-5}
	Nm/RPM	1.6×10^{-7}	3.1×10^{-7}	4.4×10^{-7}	5.6×10^{-7}	7.0×10^{-7}
Hysteresis Drag Torque, T_F	oz-in	0.15	0.29	0.42	0.53	0.67
	Nm	0.001	0.002	0.003	0.004	0.005

PERFORMANCE CURVES
CONTINUOUS DUTY CAPABILITY FOR 75°C RISE

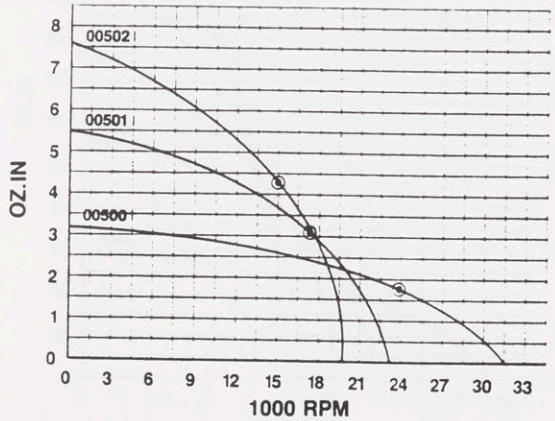

PARAMETERS \ MODEL NO.	UNIT	RBE-00500	RBE-00501	RBE-00502
Viscous Damping, F_l	oz-in/RPM	9.1×10^{-6}	1.8×10^{-5}	2.6×10^{-5}
	Nm/RPM	6.4×10^{-8}	1.2×10^{-7}	1.8×10^{-7}
Hysteresis Drag Torque, T_F	oz-in	0.06	0.12	0.17
	Nm	0.0004	0.0008	0.0012

PERFORMANCE CURVES
CONTINUOUS DUTY CAPABILITY FOR 75°C RISE

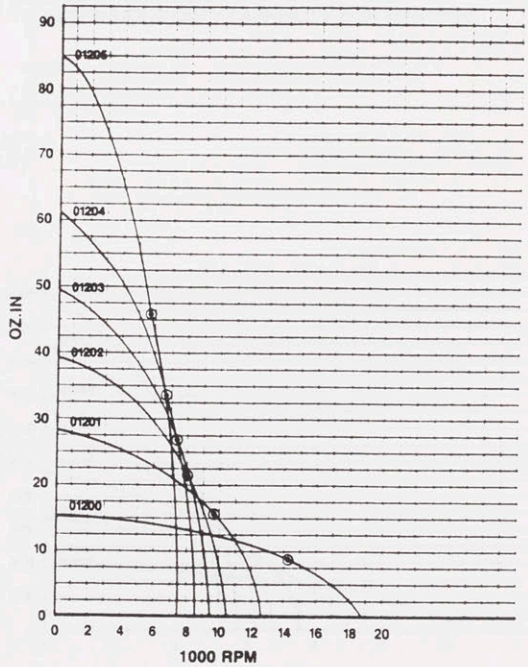

PARAMETERS \ MODEL NO.	UNIT	RBE-01200	RBE-01201	RBE-01202	RBE-01203	RBE-01204	RBE-01205
Viscous Damping, F_l	oz-in/RPM	5.0×10^{-5}	1.1×10^{-4}	1.7×10^{-4}	2.1×10^{-4}	2.8×10^{-4}	4.1×10^{-4}
	Nm/RPM	3.5×10^{-7}	0.8×10^{-6}	1.2×10^{-6}	1.5×10^{-6}	2.0×10^{-6}	2.9×10^{-6}
Hysteresis Drag Torque, T_F	oz-in	0.25	0.56	0.81	1.03	1.35	2.01
	Nm	0.002	0.004	0.006	0.007	0.01	0.014

PERFORMANCE CURVES
CONTINUOUS DUTY CAPABILITY FOR 75°C RISE

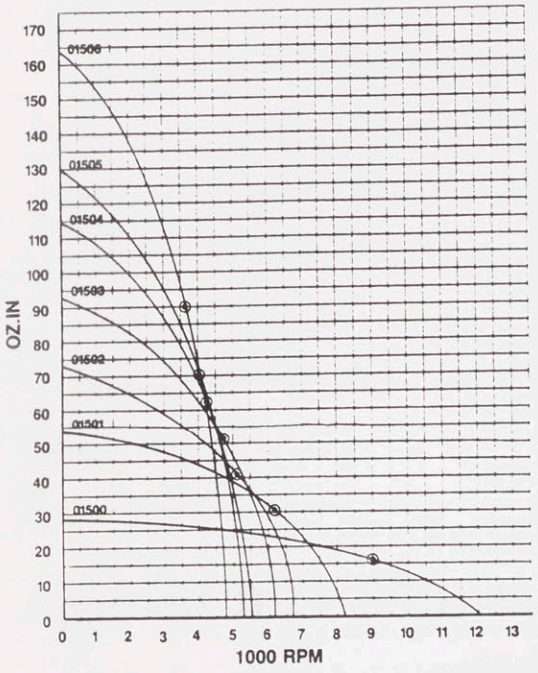

PARAMETERS / MODEL NO.	UNIT	RBE-01500	RBE-01501	RBE-01502	RBE-01503	RBE-01504	RBE-01505	RBE-01506
Viscous Damping, F_1	oz-in/RPM	1.7×10^{-4}	3.6×10^{-4}	5.3×10^{-4}	6.6×10^{-4}	8.5×10^{-4}	9.4×10^{-4}	1.2×10^{-3}
	Nm/RPM	1.2×10^{-6}	2.5×10^{-6}	3.7×10^{-6}	4.7×10^{-6}	6.0×10^{-6}	6.6×10^{-6}	0.9×10^{-3}
Hysteresis Drag Torque, T_1	oz-in	0.54	1.20	1.70	2.15	2.76	3.10	4.08
	Nm	0.004	0.008	0.012	0.015	0.020	0.022	0.029

PERFORMANCE CURVES
CONTINUOUS DUTY CAPABILITY FOR 75°C RISE

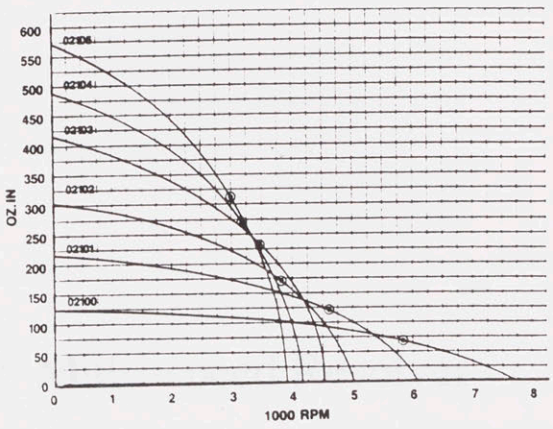

PARAMETERS / MODEL NO.	UNIT	RBE-02100	RBE-02101	RBE-02102	RBE-02103	RBE-02104	RBE-02105
Viscous Damping, F_1	oz-in/RPM	6.9×10^{-4}	1.2×10^{-3}	1.7×10^{-3}	2.2×10^{-3}	2.8×10^{-3}	3.3×10^{-3}
	Nm/RPM	4.9×10^{-6}	0.9×10^{-5}	1.2×10^{-5}	1.6×10^{-5}	2.0×10^{-5}	2.3×10^{-5}
Hysteresis Drag Torque, T_1	oz-in	2.28	3.95	5.71	8.16	9.37	10.94
	Nm	0.016	0.028	0.040	0.058	0.066	0.077

PERFORMANCE CURVES
CONTINUOUS DUTY CAPABILITY FOR 75°C RISE

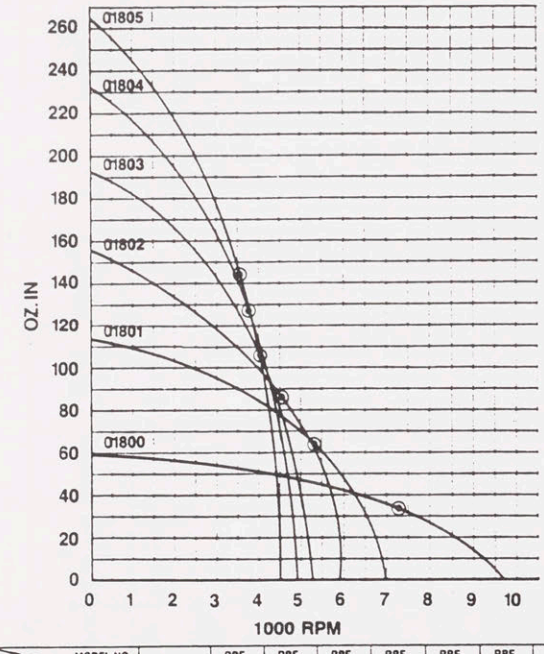

PARAMETERS / MODEL NO.	UNIT	RBE-01800	RBE-01801	RBE-01802	RBE-01803	RBE-01804	RBE-01805
Viscous Damping, F_1	oz-in/RPM	3.4×10^{-4}	6.4×10^{-4}	9.1×10^{-4}	1.2×10^{-3}	1.4×10^{-3}	1.7×10^{-3}
	Nm/RPM	2.4×10^{-6}	4.5×10^{-6}	6.4×10^{-6}	0.9×10^{-5}	1.0×10^{-5}	1.2×10^{-5}
Hysteresis Drag Torque, T_1	oz-in	1.08	2.16	3.03	3.83	4.69	5.57
	Nm	0.008	0.015	0.021	0.027	0.033	0.039

PERFORMANCE CURVES
CONTINUOUS DUTY CAPABILITY FOR 75°C RISE

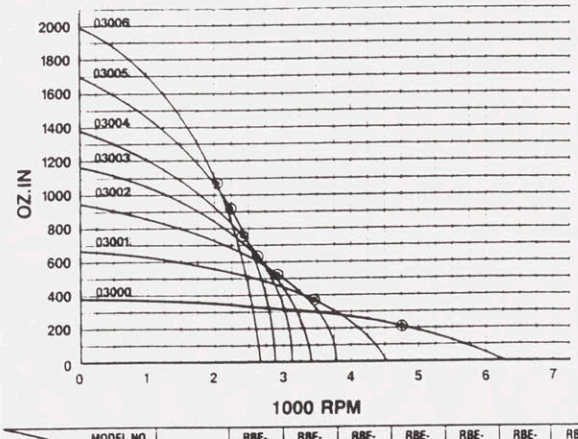

PARAMETERS / MODEL NO.	UNIT	RBE-03000	RBE-03001	RBE-03002	RBE-03003	RBE-03004	RBE-03005	RBE-03006
Viscous Damping, F_1	oz-in/RPM	1.7×10^{-3}	3.1×10^{-3}	4.5×10^{-3}	5.9×10^{-3}	7.1×10^{-3}	8.6×10^{-3}	1.0×10^{-2}
	Nm/RPM	1.2×10^{-5}	2.2×10^{-5}	3.2×10^{-5}	4.2×10^{-5}	5.0×10^{-5}	6.1×10^{-5}	0.7×10^{-4}
Hysteresis Drag Torque, T_1	oz-in	5.54	10.44	15.11	19.57	23.67	28.97	34.87
	Nm	0.039	0.074	0.107	0.138	0.167	0.205	0.246

Appendix B.2 : SSJH-44-B-2 Multi-speed Resolver

Litton
Clifton Precision

P.O. Box 230, Clifton Heights, PA 19018
(215) 622-1000, FAX (215) 623-6344

MULTISPEED PANCAKES (with Integral 1-Speed)

UNIT TYPE	FUNCTION	PRIMARY	SPEED	INPUT (volts-Hz)	OUTPUT (volts)	ACCU-RACY	TR	PHASE SHIFT (deg)	NULL VOLTAGE (mV)	INPUT CURRENT (mA)	INPUT POWER (mW)	IMPEDANCES (ohms)			DIMENSIONS (inches)			WEIGHT (g)	NOTES
												ZPO	ZPS	ZSO	OD	ID	OAW		
SGJH-19-B-1	SYNCHRO CX	ROTOR	1 36	10V-1200	6.38 1.82	± 20′ ± 30″	.638 .182	5.8 43.0	20 10	4.6 34	10 235	457 + j2125 202 + j212	—	207 + j700 138 + j74	1.84	.84	.525	85	—
SSJH-23-A-1	RESOLVER RX	ROTOR	1 36	7V-1000	3.44 1.64	± 6′ ± 20″	.492 .234	13.0 49.0	10 8	114	594	46 + j41	—	277 + j54 335 + j83	2.25	1.00	.437	114	1, 2
SSJH-27-B-1	SYNCHRO CX	ROTOR	1 36	26V-400	11.80 11.80	± 15′ ± 15″	.454 .454	10.0 57.0	25 25	5 80	32 1730	1275 + j5100 270 + j175	—	450 + j900 1375 + j940	2.63	1.22	.620	230	—
SGJH-31-B-1	SYNCHRO CX	ROTOR	2 72	26V-400	2.95 2.95	± 10′ ± 20″	.114 .114	32.0 76.0	20 10	29 116	413 2950	491 + j732 219 + j48	—	—	3.03	.39	.510	215	1, 2
SSJH-31-D-2	RESOLVER RX	ROTOR	1 8	26V-400	11.80 11.80	± 5′ ± 1′	.454 .454	12.5 45.0	25 25	9.7 76	74 1360	785 + j2550 235 + j250	—	—	3.03	1.20	.485	165	1, 2
SSJH-31-S-6	RESOLVED RX	ROTOR	1 36	26V-400	3.51 3.51	± 5′ ± 30″	.135 .135	12.0 54.0	25 25	6.5 75	56 1600	1400 + j3900 290 + j200	—	—	3.03	1.20	.530	160	1, 2
SGJH-40-A-2	SYNCHRO CX	ROTOR	2 36	115V-400	90.00 90.00	± 20′ ± 20″	.783 .783	5.4 25.0	225 225	11.8 51.5	200 2600	1360 + j9530 970 + j2020	2420 + j515 1220 + j1575	1085 + j4780 2340 + j3910	4.00	2.19	1.015	695	—
SSJH-44-B-2	RESOLVER RX	ROTOR	1 36	28V-800	28.00 5.04	± 8′ ± 8″	1.000 .180	5.4 41.5	50 16	11 70	150 1300	1150 + j2190 260 + j295	—	1690 + j2495 105 + j62	4.40	3.00	.636	400	1
SSJH-47-A-1	RESOLVER RX	ROTOR	1 16	26V-400	6.50 5.20	± 10′ ± 30″	.250 .200	24.0 64.5	30 20	158	3570	143 + j82	—	240 + j120 730	4.70	.50	.750	—	1, 2
SGJH-50-A-1	SYNCHRO CX	ROTOR	2 72	26V-400	11.80 11.80	± 10′ ± 30″	.454 .454	7.7 45.3	60 20	5.2 54	43.6 1020	1700 + j5000 350 + j330	—	—	5.00	3.46	1.500	1040	—
SSJH-50-A-1	RESOLVER RX	ROTOR	1 36	28V-800	2.80 5.04	± 12′ ± 8″	1.000 .180	2.5 20.0	85 20	14 84	188 850	950 + j1750 120 + j310	—	1600 + j2300 50 + j48	5.00	3.46	.750	520	—
SJH-60-D-1	RESOLVER RX	ROTOR	1 16	115V-400	90.00 90.00	± 20′ ± 40″	.783 .783	6.2 17.7	200 200	5.7 67	260 2520	7978 + j17680 560 + j1668	—	5100 + j12228 2216 + j2380	6.00	3.46	1.000	1360	—
SSJH-63-A-1	RESOLVER RX	ROTOR	1 16	26V-400	11.80 11.80	± 10′ ± 60″	.454 .454	21.0 36.0	30 30	100	1570	160 + j208	—	570 + j172 430 + j92	6.25	5.01	.610	520	—
SSJH-68-A-1	RESOLVER RX	ROTOR	1 16	26V-400	11.80 11.80	± 10′ ± 60″	.454 .454	15.0 29.0	30 30	6.6 59	93 714	2170 + j3330 205 + j389	1882 + j480 266 + j359	628 + j926 477 + j193	6.73	4.53	1.000	1860	1,
SSJH-90-B-1	RESOLVER RX	STATOR	1 16	26V-400	11.80 11.80	± 10′ ± 60″	.454 .454	7.0 9.2	30 30	7 37	27 361	557 + j754 264 + j266	270 + j118 275 + j135	2318 + j2842 140 + j689	8.99	6.51	1.000	2041	1
SSJH-98-A-1	RESOLVER RX	ROTOR	1 16	26V-400	11.70 11.70	± 10′ ± 60″	.450 .450	7.0 9.3	30 30	7.6 37	120 180	2080 + j2700 130 + j690	1000 + j425 310 + j495	535 + j750 265 + j280	9.75	6.00	1.500	4763	1
SGJH-115-A-2	SYNCHRO CX	ROTOR	1 36	26V-400	10.40 10.40	± 60′ ± 20″	.400 .400	20.0 50.0	120 40	25 125	500 2000	1450 + j1100 215 + j200	—	—	11.50	9.00	.700	2495	
SSJH-200-A-1	RESOLVER RX	ROTOR	1 36	26V-400	12.61 12.22	± 15′ ± 15″	.485 .470	29.5 30.5	45 45	17.2 93	311 1240	1050 + j1090 145 + j240	—	760 + j790 210 + j230	20.00	16.00	1.000	10660	

Notes: 1. Stator ring or housing.
2. Rotor hub or ring.

Although every effort has been made to ensure the accuracy of the information contained within this brochu technical data and dimensions are subject to change without notice. Please contact us to verify all critical para

REVISIONS				
ZONE	LTR.	DESCRIPTION	DATE	APPROVE
—	XA	NEW DRAWING		
D-1	XB	REV. / CN 45369	JM 2-15-79	CE

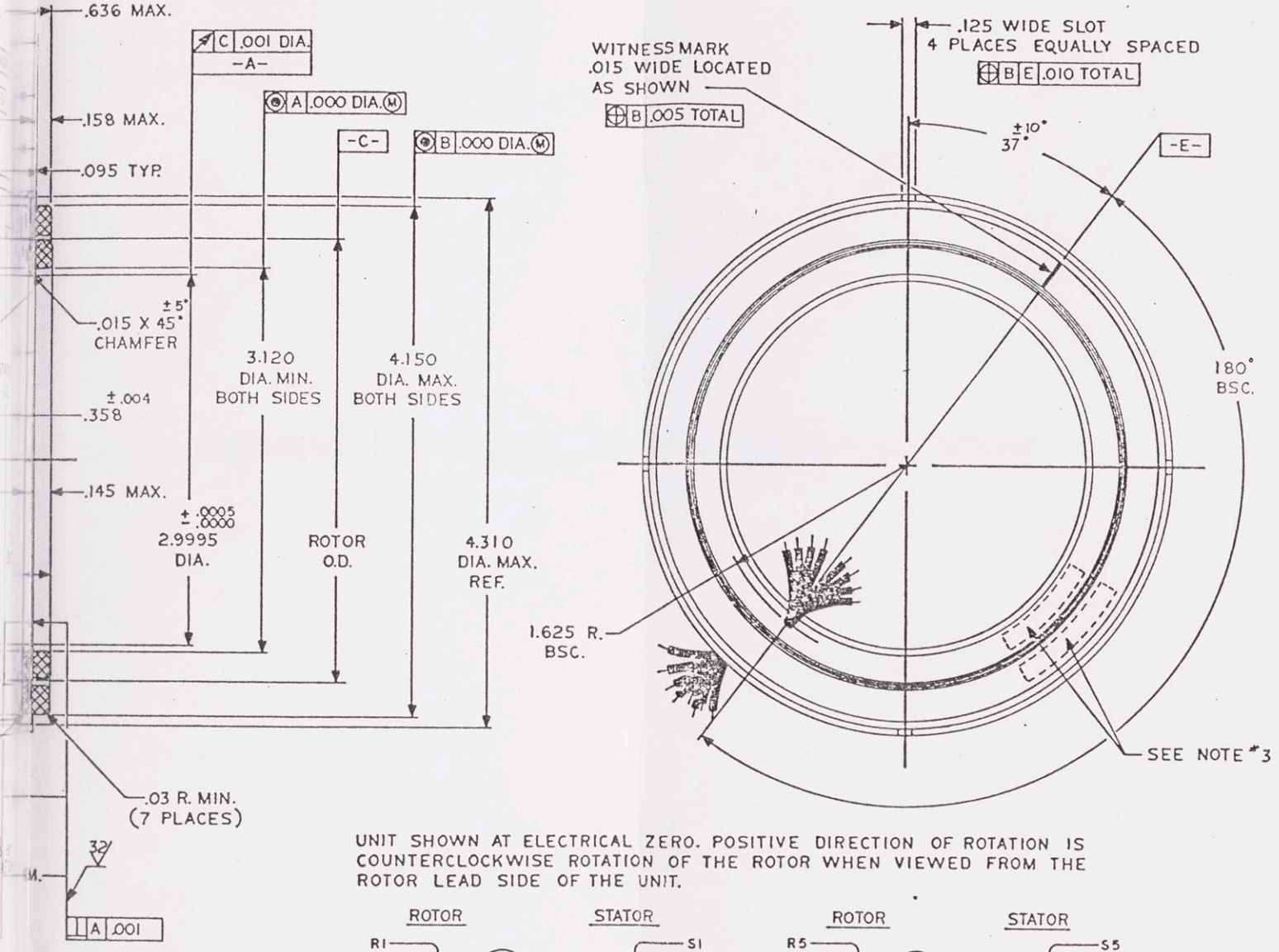

UNIT SHOWN AT ELECTRICAL ZERO. POSITIVE DIRECTION OF ROTATION IS COUNTERCLOCKWISE ROTATION OF THE ROTOR WHEN VIEWED FROM THE ROTOR LEAD SIDE OF THE UNIT.

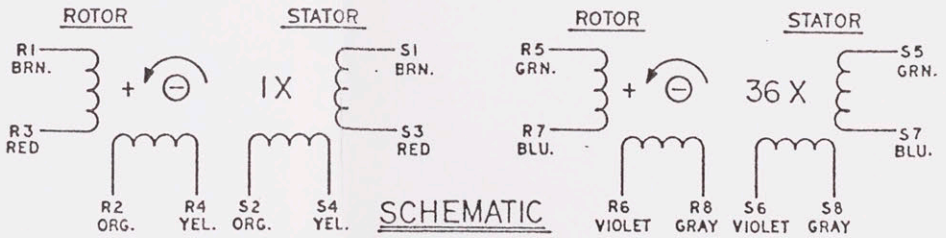

SCHEMATIC

-IL-W-22759/18,
-HCH. MIN.
-RE ALINED, THE
-F ELECTRICAL ZERO.
-NIFICATION.

QTY. REQD.	ITEM NO.	PART OR IDENTIFYING NO.	NOMENCLATURE OR DESCRIPTION	MATERIAL SPECIFICATION	CODE IDENT. NO.	

LIST OF MATERIALS

UNLESS OTHERWISE SPECIFIED
DIMENSIONS ARE IN INCHES
TWO PLACE — .XX ± .010
THREE PLACE — .XXX ± .005
FOUR PLACE — .XXXX ± .0003
HOLES — + .003 - .000
ANGLES — ± 30'
DIMENSIONS TO BE MET AFTER PLATING
REMOVE ALL BURRS & SHARP EDGES
SURFACE ROUGHNESS IN √ AA
MICRO INCHES PER ASA B46

MATERIAL

PROTECTIVE FINISH

NEXT ASSY. | USED ON
APPLICATION

DRAWN	S. Lepatas	5 DATE 78 -26-
DFTG. CHK		
DES. CHK		
ENGR	Carl P. Divirgilio	5/1/78
APPD.		
RELEASED	CES	6.6.78
APPROVED CPPC		
APPROVED CUST		

CLIFTON PRECISION PRODUCTS
DIVISION OF LITTON INDUSTRIES
USA

TITLE
IX & 36X RESOLVER
-OUTLINE-

SIZE	CODE IDENT. NO.	DRAWING
D	86197	SSJH-44-B-2

SCALE — WEIGHT — SHEET 1 OF

Appendix B.3 : TRT-200 Reaction Torque Sensor

LOW CAPACITY (INCH LBS.) GENERAL PURPOSE REACTION TORQUE SENSOR

TRT SERIES

CAPACITY RANGES:
50, 100, 200, 500 INCH LBS.

The TRT & TRS Series' reaction torque sensors offer long-term reliability due to no moving parts and state-of-the-art bonded foil strain gages. The TRS Series is also available as two axis, torque and thrust on special request. Whenever possible, the best approach for precision torque measurements is via reaction torque sensing, eliminating high maintenance of slip rings, bearings and brushes, and high cost.

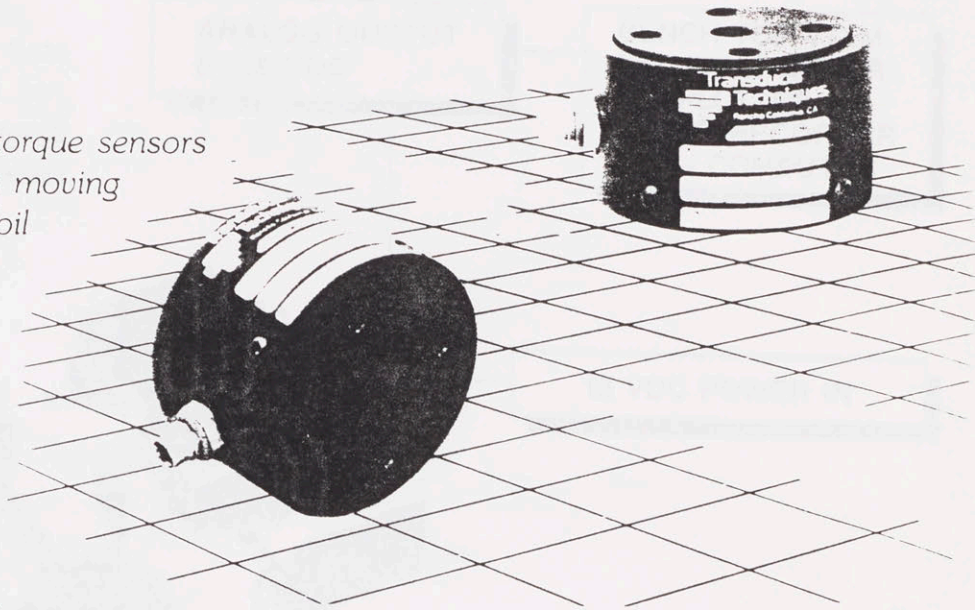

TRT & TRS SPECIFICATIONS

Rated Output (R.O.):	2 mV/V
Nonlinearity:	0.1% of R.O.
Hysteresis:	0.1% of R.O.
Nonrepeatability:	0.05% of R.O.
Zero Balance:	1.0% of R.O.
Compensated Temp. Range:	60 to 160°F
Safe Temp. Range:	–65 to 200°F
Temp. Effect on Output:	0.005% of Load/°F
Temp. Effect on Zero:	0.005% of R.O./°F
Terminal Resistance:	350 OHMs nominal
Excitation Voltage:	10 VDC
Safe Overload:	150% of R.O.

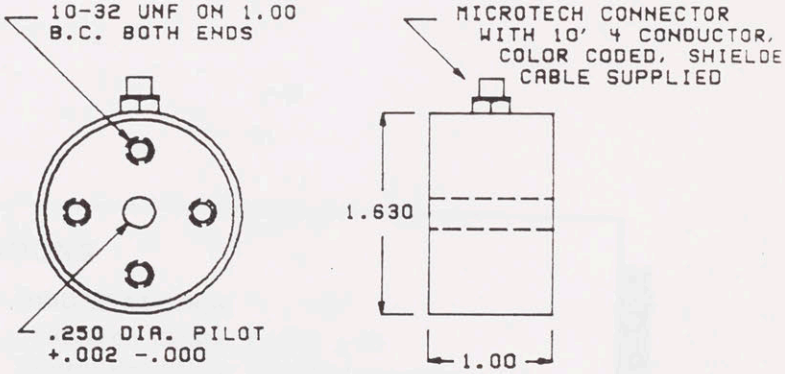

MODEL	CAPACITY INCH LBS.	TORSIONAL STIFFNESS INCH LBS./RAD.	MAX. OVERHUNG MOMENT WXS INCH LBS.	MAX. SHEAR W LBS.	MAX. THRUST P LBS.
TRT-50	50	5,125	50	20	425
TRT-100	100	10,125	100	40	800
TRT-200	200	20,375	200	80	1,400
TRT-500	500	75,875	300	200	2,600

LOW COST 12 VDC POWERED AMPLIFIER / CONDITIONER MODULE

MODEL TM-1

The TM-1 Module provides low cost dedicated conditioning for one bridge type load or pressure sensor. The unit can be placed near the sensor for high level signal transmission. Several units can be powered from a common power supply. Balance and span pots are low Tempco metal film for long-term stability and good resolution.

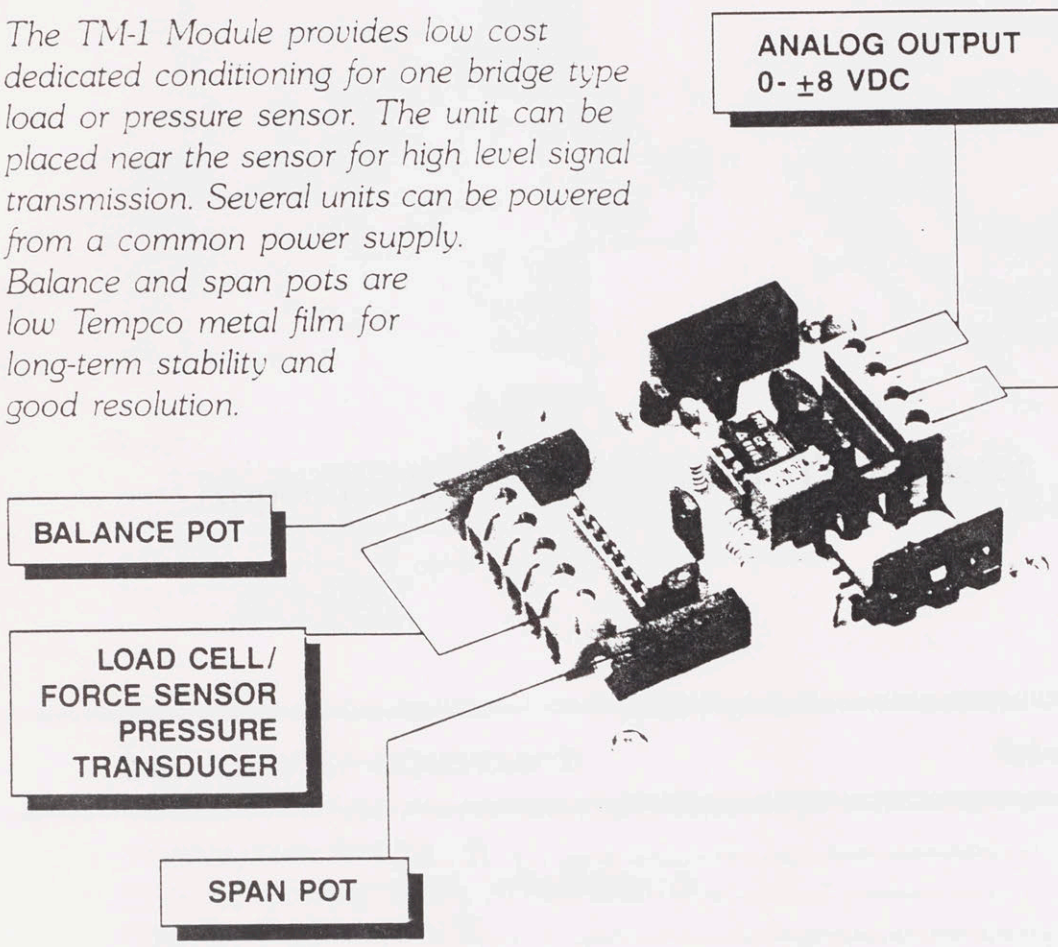

SPECIFICATIONS

AMPLIFIER SECTION

Type:	Bipolar, differential
Gain Range:	75 to 1000
Input Sensitivity:	1 MV/V minimum for 8 V output
Output Voltage:	0 to ±8 VDC (linear to 9.5)
Output Current:	0 to 10 MA
Nonlinearity:	.01% maximum
Compliance:	.1% plus vs. minus full scale
Stability:	±.1% for 24 hours
Tempco:	.01% full scale/°C
Noise and Ripple:	Less than 5 MV P-P at gain = 1000
Filter Type:	2 Pole Butterworth
Frequency Response:	DC to 220 Hz (2.2, 22, 2200 Hz available in lots of 10, no charge)

BRIDGE SECTION

Excitation Voltage:	8 VDC ± 25
Sensor Resistance:	120 OHM minimum, 1000 OHM maximum
Balance Range:	±30% of output (350 OHM bridge)

GENERAL

Weight:	Approx. 2 ozs.
Size:	2.25 x 2.50 x .80 inches tall
Mounting:	Corner standoffs, 4-40 thread
Input/Output:	Via screw terminals
Operating Temp:	0 to 70°C
Power Required:	12 VDC ±.5 at 65 MA

Appendix B.4 : TG-2936-B Tachometer

$ 1655 each

TG-2936

2.20 V per RAD/S (max.)

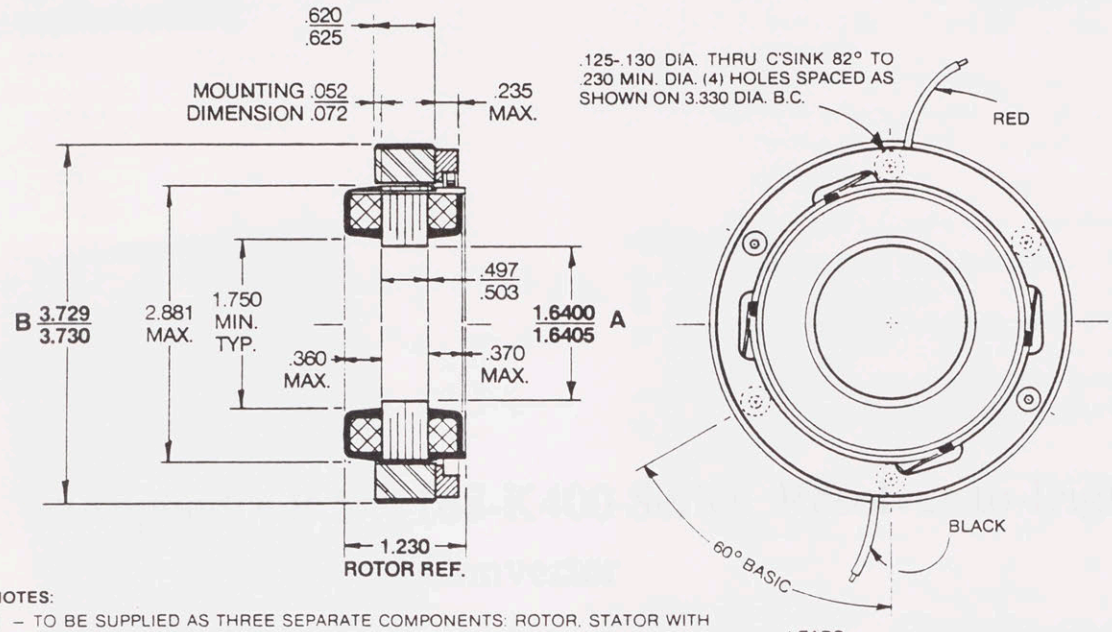

NOTES:

1 – TO BE SUPPLIED AS THREE SEPARATE COMPONENTS: ROTOR, STATOR WITH KEEPER, AND BRUSH ASSEMBLY **CAUTION:** DO NOT REMOVE KEEPER UNTIL ROTOR IS FULLY IN PLACE
2 – MOUNTING REQUIREMENTS: DIAMETERS "A" AND "B" TO BE CONCENTRIC WITHIN .001 (.002 T.I.R.) WHEN MOUNTED.
3 – WITH A C.C.W. ROTATION AS VIEWED FROM BRUSH END, A POSITIVE VOLTAGE SHALL BE GENERATED ON RED LEAD.
4 – GOLD PLATED COMMUTATOR.
5 – METAL GRAPHITE BRUSHES (4).

LEADS:
#24 AWG TYPE "E" TEFLON COATED
PER MIL W-16878 18" MIN. LG.

TACHOMETER CONSTANTS

	Values	Units
Maximum Voltage Sensitivity - K_G	2.20	V per RAD/S
Ripple Voltage (Average to Peak, unfiltered max) - E_R	0.5	PERCENT
Ripple Frequency (Fundamental)	91	CYCLES/REV.
Static Friction (Max.) - T_F	0.014	LB. FT.
Rotor Inertia - J_G	2.1×10^{-4}	LB.FT.S^2
Maximum Terminal Voltage	150	VOLTS
Maximum Speed (Brush Limited)	90	RAD/S
Weight	1.5	LB.

WINDING CONSTANTS

Winding Designations

	UNITS	TOLERANCES	A	B	C	D	E	F	G
Voltage Sensitivity - K_G	V per RAD/S	±10%	1.4	1.75	2.20	1.10	0.343		
Maximum Operating Speed - ω_{MAX}	RAD/S		90	86	68	90	90		
Maximum Output Voltage - V_{MAX}	VOLTS		126	150	150	99	30.9		
DC Resistance (25°C) - R_G	OHMS	±12.5%	475	777	1230	307	29		
Inductance - L_G	HENRIES	±30%	0.44	0.69	1.1	0.27	0.026		
Recommended Load Resistance - R_L	OHMS		47K	78K	120K	30K	2.9K		

we bought this

Appendix B.5 : 168-K400 Series Resolver-to-Digital Converter

synchro resolver-to-digital converter
single module 2-speed 16-bit
series 168K400

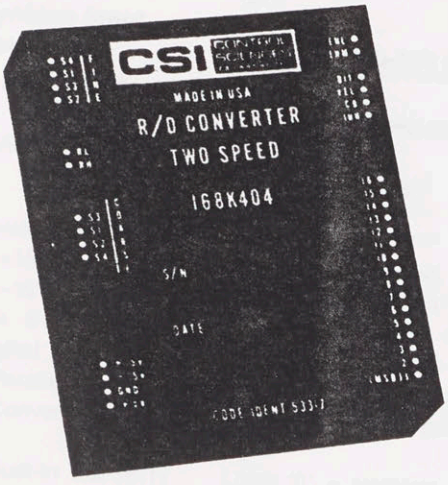

FEATURES

- 1:16, 1:32 or 1:36 speed ratios
- 20-second accuracy
- 16-bit byte/parallel output with 3-state output latches
- 2-speed inputs, multiple pole or geared types
- Insensitive to rotor-to-stator phase shifts up to 70°
- Single module

APPLICATIONS

Radar Tracking — Satellite Tracking — Robotics — Precise Angle Measurements

GENERAL DATA

The Series 168K400 is the first 2-speed, high performance, synchro (or resolver) - to - digital converter specifically designed to operate with multiple pole synchros or resolvers. The converter employs a synthesized reference which corrects for rotor-to-stator phase shifts up to 70° which is common to multipole synchros or resolvers. The module also includes the 2-speed combining, crossover network and stickoff circuits necessary for 2-speed conversion. The binary angle output is 3-state addressable as either two 8-bit bytes or one 16-bit word.

THEORY OF OPERATION

The theory of operation for single-speed tracking synchro-to-digital (S/D) converter is explained first. The same principles apply for a resolver-to-digital converter.

Single-Speed Converter (See Figure 1)

The S/D converter determines the value of the input angle Φ by comparing a digital feedback angle Θ with the synchro input angle. When the difference between the input angle and the feedback angle is zero, the output angle contained in the up-down counter is equal to the synchro input angle.

The Function Generator performs the trigonometric computation:

$$\sin(\Phi-\Theta) = (\sin\Phi\cos\Theta-\cos\Phi\sin\Theta)$$

Note that for small angles, $\sin(\Phi-\Theta)\cong(\Phi-\Theta)$. The equality given by the above equation is true only in the first quadrant, i.e., 0° to 90°. The analog inputs to the Function Generator have different values depending on the quadrant in which the input angle lies.

The $\Phi-\Theta$ is an analog representation of the error between Φ the input angle, and Θ the output angle. This analog error is first demodulated then fed to an analog integrator whose output controls the frequency of a Voltage-Controlled Oscillator (VCO). The VCO clocks the up-down counter. The up-down counter is functionally an integrator, therefore the tracking converter in itself is a closed-loop servomechanism with two lags, making it a "Type II" servo loop. The "Type II" servo loop tracking converter exhibits no velocity errors and only minor acceleration errors.

ELECTRICAL SPECIFICATIONS

Parameter	Value		
Resolution	16-bits (0.0055°)		
Accuracy[1]	20 seconds (1:32 or 1:36)		
	40 seconds (1:16)		
Speed Ratios	1:16, 1:32 or 1:36		
Allowable Synchro Misalignment[2]	±2°		
Allowable Rotor to Stator Phase Shift			
Coarse Input	±20°		
Fine Input	±70°		
Synchro Input Rates[3]	**47-70 Hz**	**350-450 Hz**	**800-1200 Hz**
Maximum Tracking Rate	250°/sec	1000°/sec	1800°/sec
Acceleration Constant (K_a)	4,500 sec^{-2}	75,000 sec^{-2}	230,000 sec^{-2}
Power Supplies[4]			
+15V	30 mA max (25 mA typ)		
−15V	35 mA max (30 mA typ)		
+ 5V	15 mA max (10 mA typ)		
Digital Inputs/Outputs			
Parallel Binary Angle	3-state, 2 TTL loads max.		
Converter Busy (CB)	1 to 2 us positive pulse, 2 TTL loads max.		
Built-In Test (BIT)	Logic '0' = tracking, logic '1' = error 2 TTL loads max.		
Inhibit (INH)[5]	Logic '0' latches angle output		
Enable M (ENM)[6]	Logic '0' enables bits 1-8		
	Logic '1' disables		
Enable L (ENL)[6]	Logic '0' enables bits 9-16		
	Logic '1' disables		
Velocity Output			
Scale Factor	±1.0V ±0.2V for 180°/sec @ 1000 Hz		
	±1.0V ±0.2V for 100°/sec @ 400 Hz		
	±1.0V ±0.2V for 25°/sec @ 60 Hz		
Range	±10V min.		
Loading	10 kohms max.		
Synchro/Resolver Input[7]			
11.8V L-L	75 kohms min.		
90V L-L	600 kohms min.		
Reference Input[7]			
23 to 29 Vrms	180 kohms min.		
103 to 127 Vrms	800 kohms min.		
Input Type[8]	Solid-state differential		
Temperature Ranges			
Operating	0° to 70°		
	−55°C to 105°C (ET)		
Storage	−55°C to 125°C		
Dimensions	3.125″ × 2.625″ × 0.8″		
Weight	7.5 oz		

NOTES:

1. Accuracy applies for:
   (a) ±10% signal amplitude variation
   (b) 10% harmonic distortion in the reference
   (c) over power supply range
   (d) over operating temperature range
2. With two-speed synchro converters, it is important to understand that the output of the fine synchro dominates in the determination of the coarse (1X) shaft angle. No ambiguities will exist unless the allowable misalignment is exceeded.

NOTES: (Continued)

3. Higher tracking and acceleration rates available, consult factory.
4. All units can operate on voltages between ±11.5V to ±16.5V. The tolerance on the +5V supply is ±0.25V.
5. The Inhibit is a CMOS input with a 50 kohm pull-up to +5V.
6. Enable M and L are CMOS inputs with 50 kohm pull-downs to ground.
7. Other voltages available, consult factory.
8. Any one stator and/or rotor line may be grounded. Common mode voltages up to specified L-L voltage have no effect on operation.

Two-Speed Converter (See Figure 2)

The operation of a 2-speed S/D converter is essentially the same as the single speed except there are two Solid State Control Transformers (SSCT) generating two error voltages. Assuming an off-null condition (the input angle does not equal the output angle), the crossover detector feeds the coarse SSCT error signal to the demodulator which is driven by the rotor excitation. As the output angle Θ approaches the input angle Φ the coarse SSCT output approaches a null. When the coarse SSCT output drops below a preset threshold, approximately equivalent to 2.8°, the crossover detector switches the fine SSCT error signal into the demodulator. Simultaneously the source of the demodulator drive voltage is switched to the synthesized reference which is derived from fine stators therefore negating the fine rotor to stator phase shift. The feedback angle Θ to the fine SSCT is multiplied by the speed ratio therefore increasing the voltage gradient of the fine SSCT by the same factor. The servo loop then is able to seek an even finer null. The converter will continue to use the fine error signal for continuous tracking. In order to eliminate false stable nulls of 180°, an angle offset produced by the Digital Adder and the Scaler, which produces the Stick-Off Voltage (SO), is introduced into the coarse SSCT.

The 16-bit parallel binary angle is outputted through 3-state transparent latches which can be enabled as one 16-bit word or two 8-bit bytes. By use of the Inhibit input, the 16-bit angle data can be latched without affecting the operation of the converter servo loop.

DIGITAL INPUTS/OUTPUTS

Digital outputs consist of 16 parallel data bits, a Converter Busy (CB) and a BIT logic output.

The parallel digital outputs are addressable either as one 16-bit word or two 8-bit bytes. When Enable M and L are at logic '0', the outputs are at normal logic '1' or '0'. When Enable M and L are at logic '1' the outputs are in the high impedance state. Outputs are valid 0.5 microseconds after an Enable is driven to logic '0'.

The CB output is a positive 1 to 2 microsecond pulse, and data changes during the CB pulse. Data is valid at the trailing edge of the CB pulse.

The BIT logic output is a built-in test derived from the crossover detector. Whenever the digital output is not tracking the synchro or resolver input within the fine speed range the BIT output goes to logic '1'.

The Inhibit (INH) input locks the 16-bit transparent latch so that the data bits will remain stable while data is being transferred. The output is stable 0.5 microseconds after INH is driven to logic

'0'. If a CB pulse occurs after an INH has been applied, logic '0', the 16-bit latch will remain locked and its data cannot change until INH is driven back to logic '1' and CB returns to logic '0'. If an INH is applied during a CB pluse, the 16-bit latch will not lock until the CB pulse is over. Inhibit commands do not affect the updating of the converter no matter how long they are applied.

TIMING

Whenever an input angle change occurs, the converter changes the digital angle in steps of 1 LSB and generates a CB pulse. During the 1 to 2 microsecond CB time, the output data is changing and should not be transferred. The converter will ignore an INH command applied during a CB interval until that interval is

SINGLE-SPEED CONVERTER BLOCK DIAGRAM
Figure 1

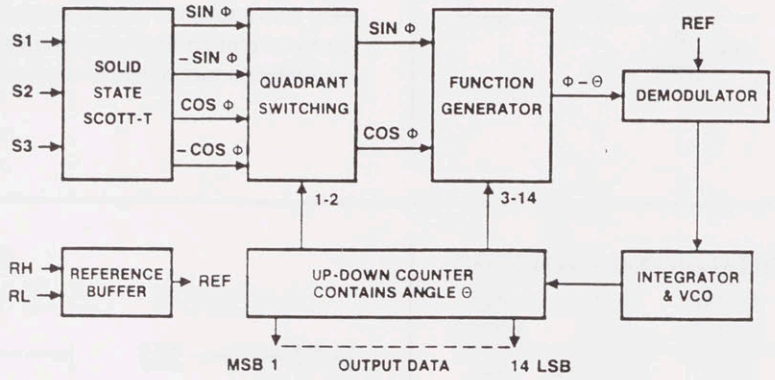

TWO-SPEED CONVERTER BLOCK DIAGRAM
Figure 2

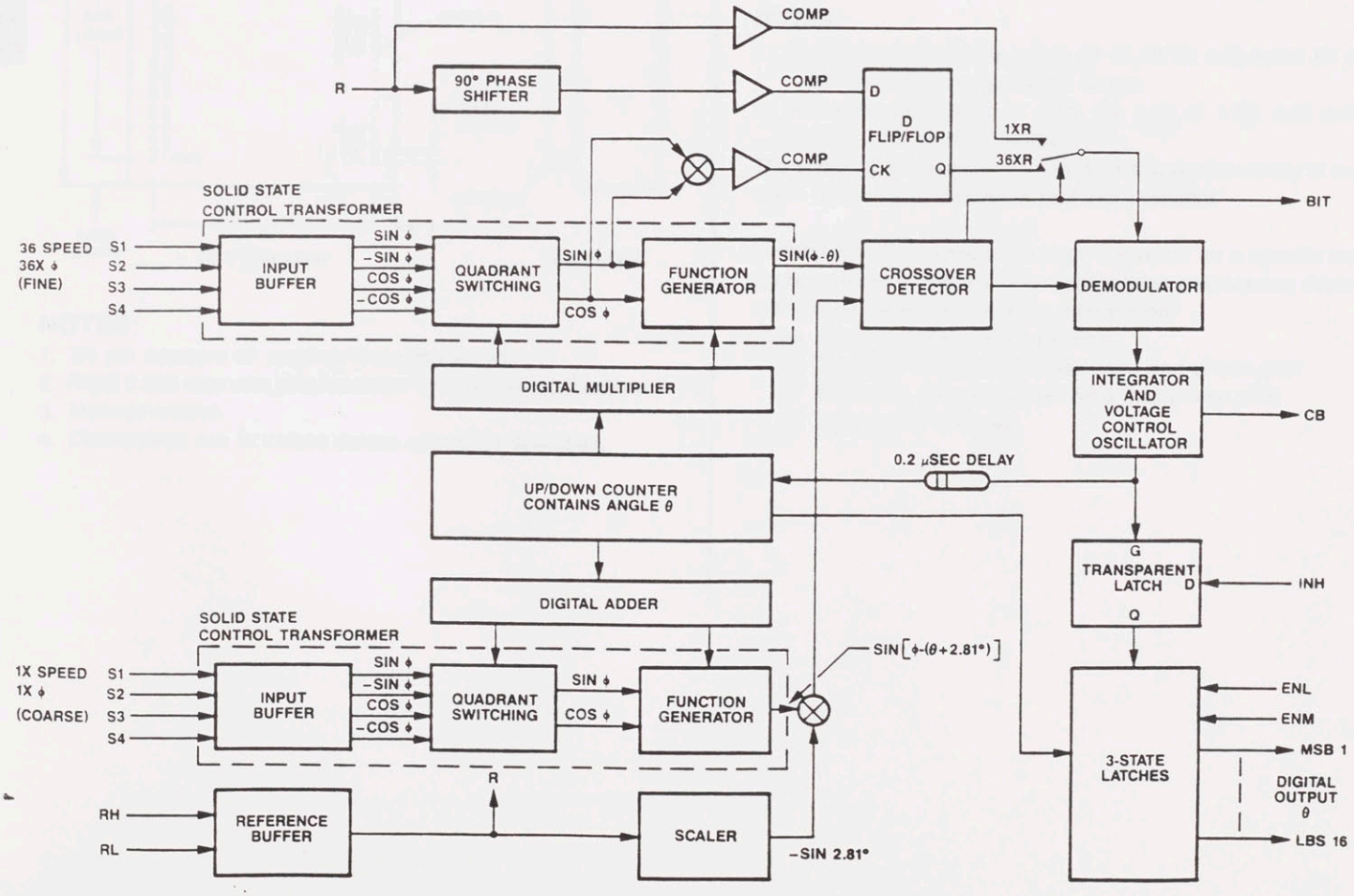

over. There are two methods of interfacing with a computer: (1) synchronous, and (2) asynchronous. A simple method of synchronous loading is to: (a) apply the Inhibit, (b) wait 0.5 microseconds, (c) transfer the data, and (d) release the Inhibit. Asynchronous loading is accomplished by transferring data on the trailing edge of the CB pulse.

ANALOG VELOCITY OUTPUT

Velocity (VEL) is a DC voltage proportional to the angular velocity of the synchro or resolver shaft. Voltage polarity is positive for an increasing digital angle and negative for a decreasing digital angle. Other characteristics are listed in the specifications table.

DYNAMIC PERFORMANCE

The 168K400 series employs a "Type II" servo loop ($K_v = \infty$) and very high acceleration constants (K_a). The loop dynamics are completely independent of power supply variations over their specific ranges. As long as the maximum tracking rate is not exceeded there will be no velocity lag and only minor acceleration lags in the converter output. Acceleration lag can be computed from the following equation:

$$E_a = \frac{\text{acceleration } (°/\text{sec}^2)}{K_a}$$

The open loop transfer functions for all frequency options are given below:

$$G_{60} = \frac{66^2\,(\frac{S}{33}+1)}{S^2\,(\frac{S}{330}+1)} \qquad G_{400} = \frac{266^2\,(\frac{S}{133}+1)}{S^2\,(\frac{S}{1330}+1)}$$

$$G_{1000} = \frac{482^2\,(\frac{S}{277}+1)}{S^2\,(\frac{S}{3333}+1)}$$

MECHANICAL OUTLINE

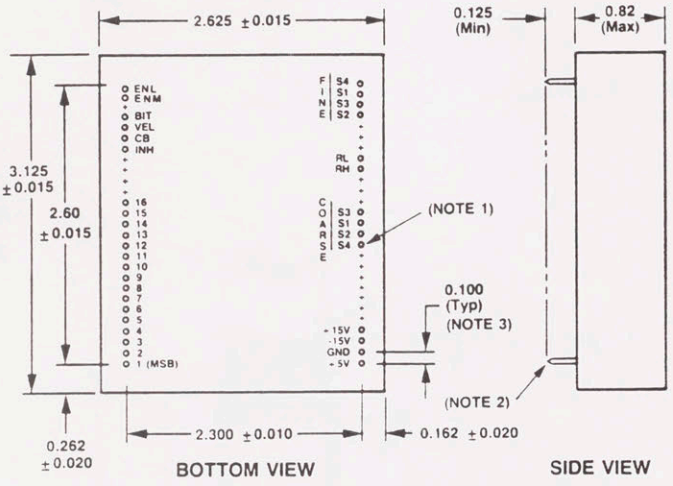

NOTES:

1. S4 pin appears on resolver input model only.
2. Rigid 0.025 diameter pins for solder-in or plug-in applications.
3. Noncumulative.
4. Dimensions are in inches unless otherwise specified.

ORDERING INFORMATION

168K SUFFIX	INPUT TYPE	STATOR VOLTAGE	REFERENCE VOLTAGE	FREQ.	SPEED RATIO
400	SYNCHRO	11.8V	26V	400 Hz	1:36
401	SYNCHRO	90V	115V	400 Hz	1:36
402	SYNCHRO	90V	115V	60 Hz	1:36
403	RESOLVER	11.8V	26V	400 Hz	1:36
404	RESOLVER	11.8V	26V	1000 Hz	1:36

NOTES:

1. Standard temperature range 0° to 70°C; add suffix ET for −55° to 105°C temperature range.
2. Standard speed ratio is 1:36; for 1:16 or 1:32, add suffix −16 or −32 to part number.

The standard part numbers listed do not cover the variety of multipole synchros or resolvers that are available.

In order for CSI to specify the right converter for a specific multipole synchro or resolver our applications engineering department must have the following information:

(a) Rotor voltage and frequency
(b) Coarse (1X) transformation ratio and phase shift
(c) Fine (NX) transformation ratio and phase shift
(d) Z_S (primary shorted)

Appendix B.6 : Bearings

RADIAL BEARINGS WITH PHENOLIC CAGES

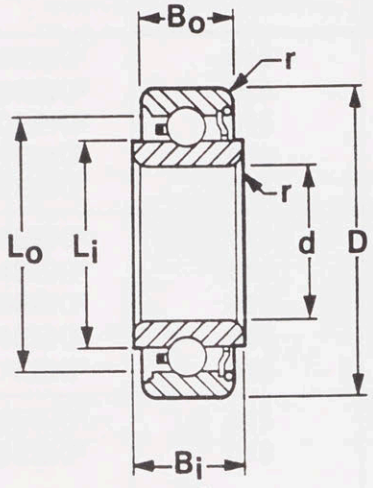

BORE d	O.D. D	WIDTH			
		NARROW	STANDARD		WIDE
		Both (B)	Outer (B_o)	Inner (B_i)	Both (B)
.6250	1.0625	.2500	.2500	.2812	.2812
.7500	1.1875	.2500	.2500	.2812	.2812
.8750	1.3125	.2500	.2500	.2812	.2812
1.0625	1.5000	.2500	.2500	.2812	.2812
1.3125	1.7500	.2500	.2500	.2812	.2812
1.5625	2.0000	.2500	.2500	.2812	.2812
1.8125	2.2500	.2500	.2500	.2812	.2812
2.0625	2.6250	.2500	.2500	.2812	.2812
2.3125	2.8750	.2500	.2500	.2812	.2812
2.5625	3.2500	.3120	.3120	.3750	.3750
2.8125	3.5000	.3120	.3120	.3750	.3750
3.0625	3.8750	.3120	.3120	.3750	.3750

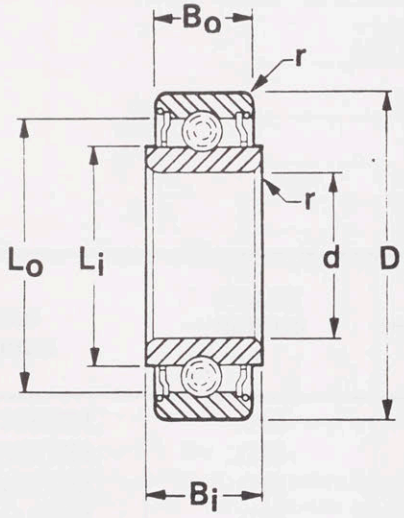

RADIAL BEARINGS WITH TEFLON SLUG SEPARATORS

BORE d	O.D. D	WIDTH			
		NARROW	STANDARD		WIDE
		Both (B)	Outer (B_o)	Inner (B_i)	Both (B)
.6250	1.0625	.2500	.2500	.2812	.2812
.7500	1.1875	.2500	.2500	.2812	.2812
.8750	1.3125	.2500	.2500	.2812	.2812
1.0625	1.5000	.2500	.2500	.2812	.2812
1.3125	1.7500	.2500	.2500	.2812	.2812
1.5625	2.0000	.2500	.2500	.2812	.2812
1.8125	2.2500	.2500	.2500	.2812	.2812
2.0625	2.6250	.2500	.2500	.2812	.2812
2.3125	2.8750	.2500	.2500	.2812	.2812
2.5625	3.2500	.3120	.3120	.3750	.3750
2.8125	3.5000	.3120	.3120	.3750	.3750
3.0625	3.8750	.3120	.3120	.3750	.3750

NOTES:

1. Basic number denotes standard width for open bearing.
2. Basic numbers shown include SS for AISI 440C stainless steel. If SAE 52100 chrome alloy steel is desired, delete SS.
3. ABEC 5T is standard. 7T tolerances also available.
4. r = Maximum shaft or housing fillet radius that bearing corners will clear.
5. Also available with ribbon type cages. Consult NHBB for part number designation.

* Load ratings shown are for chrome alloy steel.

BASIC NUMBER	FILLET RADIUS r	BALL COMPLEMENT		LOAD RATINGS* Lbs		LAND DIAMETER (REFERENCE)	
		NO. Z	SIZE D_b	DYN. C	STATIC C_o	L_I	L_o
SSRI-538EEKF	.015	12	1/8	547	344	.773	.933
SSRI-539EEKF	.015	12	1/8	536	347	.894	1.054
SSRI-540EEKF	.015	14	1/8	581	408	1.019	1.179
SSRI-541EEKF	.015	16	1/8	616	471	1.210	1.370
SSRI-542EEKF	.015	18	1/8	640	534	1.460	1.620
SSRI-543EEKF	.015	25	1/8	761	746	1.706	1.866
SSRI-544EEKF	.015	29	1/8	806	869	1.947	2.116
SSRI-545EEKF	.015	32	1/8	834	963	2.260	2.434
SSRI-546EEKF	.015	34	1/8	879	1024	2.513	2.674
SSRI-547EEKF	.015	26	3/16	1462	1598	2.793	3.019
SSRI-548EEKF	.015	28	3/16	1505	1725	3.043	3.269
SSRI-549EEKF	.015	32	3/16	1606	1977	3.356	3.582

BASIC NUMBER	FILLET RADIUS r	BALL COMPLEMENT		LOAD RATINGS* Lbs		LAND DIAMETER (REFERENCE)	
		NO. Z	SIZE D_b	DYN. C	STATIC C_o	L_I	L_o
SSRI-538EESL	.015	12	1/8	547	344	.773	.933
SSRI-539EESL	.015	13	1/8	567	376	.894	1.054
SSRI-540EESL	.015	15	1/8	608	437	1.019	1.179
SSRI-541EESL	.015	18	1/8	662	530	1.210	1.370
SSRI-542EESL	.015	21	1/8	701	623	1.460	1.620
SSRI-543EESL	.015	25	1/8	761	746	1.706	1.866
SSRI-544EESL	.015	27	1/8	774	809	1.947	2.116
SSRI-545EESL	.015	32	1/8	834	963	2.260	2.434
SSRI-546EESL	.015	36	1/8	916	1084	2.513	2.674
SSRI-547EESL	.015	26	3/16	1462	1598	2.793	3.019
SSRI-548EESL	.015	28	3/16	1505	1725	3.043	3.269
SSRI-549EESL	.015	32	3/16	1606	1977	3.356	3.582

ABEC TOLERANCES

ABEC 1

ABEC standards for dimensional tolerances and terminology have been established by the Anti-Friction Bearing Manufacturers Association. These are shown in the tables below.

INNER RING

Tolerance values in .0001 inch

Bore Diameter (mm)		Mean Bore Diameter Deviation		Single Bore Diameter Variation			Mean Bore Diameter Variation	Radial Runout	Single Width Deviation			Width Variation
				Diameter Series					All	Normal	Modified	
d		Δdmp		Vdp			Vdmp	Kia	ΔBs	ΔBs	ΔBs[4]	VBs
Over	Incl.	High	Low	7,8,9	0,1	2,3,4	Max.	Max.	High	Low	Low	Max.
[1] 0.6	2.5	0	-3	4	3	2.5	2.5	4	0	-16	—	4.5
2.5	10	0	-3	4	3	2.5	2.5	4	0	-47	-98	6
10	18	0	-3	4	3	2.5	2.5	4	0	-47	-98	8
18	30	0	-4	5	4	3	3	5	0	-47	-98	8
30	50	0	-4.5	6	4.5	3.5	3.5	6	0	-47	-98	8
50	80	0	-6	7.5	7.5	4.5	4.5	8	0	-59	-150	10

OUTER RING

Tolerance values in .0001 inch

Outside Diameter (mm)		Mean Outside Diameter Deviation		OPEN BEARINGS			SHIELDED BEARINGS	Mean Outside Diameter Variation	Radial Runout	Single Width Deviation		Width Variation
				Single Outside Diameter Variation[3]								
				Diameter Series								
D		ΔDmp		7,8,9	0,1	2,3,4	0,1,2,3,4	VDmp[3]	Kea	ΔCs		VCs
Over	Incl.	High	Low	VDp			VDp[2]	Max.	Max.	High	Low	Max.
[1] 2.5	6	0	-3	4	3	2.5	4	2.5	6	Identical to ΔBs and VBs of inner ring of same bearing		
6	18	0	-3	4	3	2.5	4	2.5	6			
18	30	0	-3.5	4.5	3.5	3	4.5	3	6			
30	50	0	-4.5	5.5	4.5	3	6.5	3	8			
50	80	0	-5	6.5	5	4	8	4	10			
80	120	0	-6	7.5	7.5	4.5	10	4.5	14			

[1] *This diameter is included in the group.*
[2] *No values have been established for diameter series 7,8,9,0, and 1.*
[3] *Applies before mounting and after removal of internal or external snap ring.*
[4] *This refers to the rings of single bearings made for paired or stack mounting.*

KA SERIES

Bearing Number		Dimensions in Inches				Capacities ①						Weight in Pounds
			Outside	Land	Land	Radial in Lbs.		Thrust in Lbs.		Moment (Lbs-In)		
Current	Former	Bore	Dia.	Dia. L_1	Dia. L_2	Static	Dyn.	Static	Dyn.	Static	Dyn.	
•KA020XPO	KA20XP	2.000	2.500	2.186	2.314		310		780		350	.10
•KA025XPO	KA25XP	2.500	3.000	2.686	2.814		360		890		490	.13
•KA030XPO	KA30XP	3.000	3.500	3.186	3.314		400		1,000		650	.15
•KA035XPO	KA35XP	3.500	4.000	3.686	3.814		430		1,100		810	.18
•KA040XPO	KA40XP	4.000	4.500	4.186	4.314		480		1,170		1,020	.19
×KA042XPO	KA42XP	4.250	4.750	4.436	4.564		500		1,220		1,120	.20
•KA045XPO	KA45XP	4.500	5.000	4.686	4.814		510		1,280		1,210	.22
•KA047XPO	KA47XP	4.750	5.250	4.936	5.064		530		1,300		1,330	.23
•KA050XPO	KA50XP	5.000	5.500	5.186	5.314		540		1,330		1,430	.24
•KA055XPO	KA55XP	5.500	6.000	5.686	5.814	③	580	③	1,440	③	1,660	.25
•KA060XPO	KA60XP	6.000	6.500	6.186	6.314		610		1,500		1,910	.28
•KA065XPO	KA65XP	6.500	7.000	6.686	6.814		640		1,610		2,180	.30
•KA070XPO	KA70XP	7.000	7.500	7.186	7.314		680		1,670		2,460	.31
KA075XPO	KA75XP	7.500	8.000	7.686	7.814		710		1,780		2,760	.34
KA080XPO	KA80XP	8.000	8.500	8.186	8.314		740		1,830		3,070	.38
KA090XPO	KA90XP	9.000	9.500	9.186	9.314		800		2,000		3,700	.44
KA100XPO	KA100XP	10.000	10.500	10.186	10.314		860		2,110		4,390	.50
KA110XPO	KA110XP	11.000	11.500	11.186	11.314		910		2,780		5,120	.52
×KA120XPO	KA120XP	12.000	12.500	12.186	12.314		970		2,390		5,920	.56

SNAPOVER SEPARATOR 1/8" BALLS

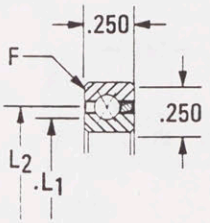

② F = .025

Bearing corners are normally chamfered

KB SERIES

Bearing Number		Dimensions in Inches				Capacities ①						Weight in Pounds
			Outside	Land	Land	Radial in Lbs.		Thrust in Lbs.		Moment (Lbs-In)		
Current	Former	Bore	Dia.	Dia. L_1	Dia. L_2	Static	Dyn.	Static	Dyn.	Static	Dyn.	
•KB020XPO	KB20XP	2.000	2.625	2.231	2.393		440		1,100		510	.16
•KB025XPO	KB25XP	2.500	3.125	2.731	2.893		510		1,260		710	.19
•KB030XPO	KB30XP	3.000	3.625	3.231	3.393		560		1,410		930	.24
•KB035XPO	KB35XP	3.500	4.125	3.731	3.893		610		1,520		1,160	.27
•KB040XPO	KB40XP	4.000	4.625	4.231	4.393		680		1,630		1,450	.30
•KB042XPO	KB42XP	4.250	4.875	4.481	4.643		690		1,690		1,570	.31
•KB045XPO	KB45XP	4.500	5.125	4.731	4.893		720		1,800		1,730	.33
KB047XPO	KB47XP	4.750	5.375	4.981	5.143		740		1,860		1,880	.34
KB050XPO	KB50XP	5.000	5.625	5.231	5.393		770		1,910		2,040	.38
•KB055XPO	KB55XP	5.500	6.125	5.731	5.893		820		2,030		2,390	.41
•KB060XPO	KB60XP	6.000	6.625	6.231	6.393		870		2,140		2,740	.44
•KB065XPO	KB65XP	6.500	7.125	6.731	6.893	③	910	③	2,250	③	3,110	.47
KB070XPO	KB70XP	7.000	7.625	7.231	7.393		960		2,370		3,500	.50
KB075XPO	KB75XP	7.500	8.125	7.731	7.893		1,000		2,480		3,920	.53
•KB080XPO	KB80XP	8.000	8.625	8.231	8.393		1,040		2,590		4,300	.57
•KB090XPO	KB90XP	9.000	9.625	9.231	9.393		1,130		2,820		5,250	.66
KB100XPO	KB100XP	10.000	10.625	10.231	10.393		1,180		2,990		6,090	.73
KB110XPO	KB110XP	11.000	11.625	11.231	11.393		1,240		3,210		7,010	.75
KB120XPO	KB120XP	12.000	12.625	12.231	12.393		1,350		3,380		8,320	.83
KB140XPO	KB140XP	14.000	14.625	14.231	14.393		1,460		3,720		10,480	1.05
×KB160XPO	KB160XP	16.000	16.625	16.231	16.393		1,630		4,060		13,290	1.20
KB180XPO	KB180XP	18.000	18.625	18.231	18.393		1,750		4,390		16,000	1.35
KB200XPO	KB200XP	20.000	20.625	20.231	20.393		1,860		4,730		18,920	1.50

SNAPOVER SEPARATOR 5/32" BALLS

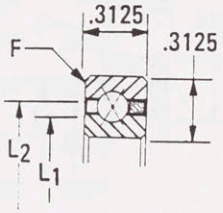

② F = .040

Bearing corners are normally chamfered

• Available from stock — check for availability of other sizes. X — limited availability.

NOTE: ① Capacities listed are not simultaneous. For combined loading see discussion of Bearing Selection and Load Analysis. Dynamic capacities are based upon 500 hours L_{10} life @ 33⅓ RPM (1.0 million revolutions). Moment capacities are in pound-inches.

② "F" is the maximum shaft or housing fillet radius the bearing corners will clear.

③ Consult Kaydon for static capacity ratings.

KA SERIES

SNAPOVER SEPARATOR 1/8" BALLS

Bearing Number		Dimensions in Inches				Radial Capacity (Lbs.) ①		Weight in Pounds
Current	Former	Bore	Outside Diameter	Land Dia. L_1	Land Dia. L_2	Static	Dynamic	
•KA020CPO	KA20CP	2.000	2.500	2.186	2.314		310	.10
•KA025CPO	KA25CP	2.500	3.000	2.686	2.814		360	.13
•KA030CPO	KA30CP	3.000	3.500	3.186	3.314		400	.15
•KA035CPO	KA35CP	3.500	4.000	3.686	3.814		430	.18
•KA040CPO	KA40CP	4.000	4.500	4.186	4.314		480	.19
•KA042CPO	KA42CP	4.250	4.750	4.436	4.564		500	.20
•KA045CPO	KA45CP	4.500	5.000	4.686	4.814		510	.22
•KA047CPO	KA47CP	4.750	5.250	4.936	5.064		530	.23
•KA050CPO	KA50CP	5.000	5.500	5.186	5.314		540	.24
•KA055CPO	KA55CP	5.500	6.000	5.686	5.814	③	580	.25
•KA060CPO	KA60CP	6.000	6.500	6.186	6.314		610	.28
•KA065CPO	KA65CP	6.500	7.000	6.686	6.814		640	.30
•KA070CPO	KA70CP	7.000	7.500	7.186	7.314		680	.31
•KA075CPO	KA75CP	7.500	8.000	7.686	7.814		710	.34
•KA080CPO	KA80CP	8.000	8.500	8.186	8.314		740	.38
•KA090CPO	KA90CP	9.000	9.500	9.186	9.314		800	.44
•KA100CPO	KA100CP	10.000	10.500	10.186	10.314		860	.50
•KA110CPO	KA110CP	11.000	11.500	11.186	11.314		910	.52
•KA120CPO	KA120CP	12.000	12.500	12.186	12.314		970	.56

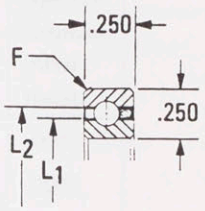

② F = .025

Bearing corners are normally chamfered

KB SERIES

SNAPOVER SEPARATOR 5/32" BALLS

Bearing Number		Dimensions in Inches				Radial Capacity (Lbs.) ①		Weight in Pounds
Current	Former	Bore	Outside Diameter	Land Dia. L_1	Land Dia. L_2	Static	Dynamic	
•KB020CPO	KB20CP	2.000	2.625	2.231	2.393		440	.16
•KB025CPO	KB25CP	2.500	3.125	2.731	2.893		510	.20
•KB030CPO	KB30CP	3.000	3.625	3.231	3.393		560	.24
•KB035CPO	KB35CP	3.500	4.125	3.731	3.893		610	.27
•KB040CPO	KB40CP	4.000	4.625	4.231	4.393		680	.30
•KB042CPO	KB42CP	4.250	4.875	4.481	4.643		690	.31
•KB045CPO	KB45CP	4.500	5.125	4.731	4.893		720	.33
KB047CPO	KB47CP	4.750	5.375	4.981	5.143		740	.34
•KB050CPO	KB50CP	5.000	5.625	5.231	5.393		770	.38
•KB055CPO	KB55CP	5.500	6.125	5.731	5.893		820	.41
•KB060CPO	KB60CP	6.000	6.625	6.231	6.393		870	.44
•KB065CPO	KB65CP	6.500	7.125	6.731	6.893	③	910	.47
KB070CPO	KB70CP	7.000	7.625	7.231	7.393		960	.50
KB075CPO	KB75CP	7.500	8.125	7.731	7.893		1,000	.53
•KB080CPO	KB80CP	8.000	8.625	8.231	8.393		1,040	.57
KB090CPO	KB90CP	9.000	9.625	9.231	9.393		1,130	.66
KB100CPO	KB100CP	10.000	10.625	10.231	10.393		1,180	.73
KB110CPO	KB110CP	11.000	11.625	11.231	11.393		1,240	.75
KB120CPO	KB120CP	12.000	12.625	12.231	12.393		1,350	.83
KB140CPO	KB140CP	14.000	14.625	14.231	14.393		1,460	1.05
KB160CPO	KB160CP	16.000	16.625	16.231	16.393		1,630	1.20
KB180CPO	KB180CP	18.000	18.625	18.231	18.393		1,750	1.35
KB200CPO	KB200CP	20.000	20.625	20.231	20.393		1,860	1.50

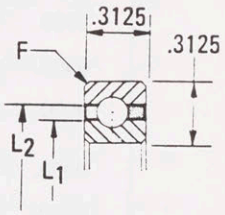

② F = .040

Bearing corners are normally chamfered

- Available from stock — check for availability of other sizes. X — limited availability.

NOTE:
① Capacities listed are not simultaneous. For combined loading see discussion of Bearing Selection and Load Analysis. Dynamic capacities ar based upon 500 hours L_{10} life @ 33⅓ RPM (1.0 million revolutions).
② "F" is the maximum shaft or housing fillet radius the bearing corners will clear.
③ Consult Kaydon for static capacity ratings.

KAYDON CORPORATIO

Kaydon REALI-SLIM Ball Bearings

TYPE C

KAYDON Precision Tolerances and Recommended Fits For REALI-SLIM Ball Bearings in Normal Applications

PRECISION CLASS 1

Bearing Series (All Series)	Bearing Diameters		Radial & Axial Runout		Rotating Shaft		Stationary Shaft				Bearing Diametral Clearance*		
	Bearing Bore	Bearing O.D.			Shaft Diameter	Housing Bore	Shaft Diameter		Housing Bore		Before Installation		Expected Minimum After Instal.
	Nominal +.0000	Nominal +.0000	Inner Race	Outer Race	Nominal +.0000	Nominal +.0000	Nominal		Nominal				
10	−.0004	−.0005	.0005	.0008	+.0004	+.0005	−.0004	−.0008	−.0005	−.0010	.0010	.0016	.0003
15	−.0005	−.0005	.0006	.0008	+.0005	+.0005	−.0005	−.0010	−.0005	−.0010	.0012	.0018	.0003
020	−.0006	−.0005	.0008	.0010	+.0006	+.0006	−.0006	−.0012	−.0006	−.0012	.0012	.0024	.0003
025	−.0006	−.0005	.0008	.0010	+.0006	+.0006	−.0006	−.0012	−.0006	−.0012	.0012	.0024	.0003
030	−.0006	−.0006	.0008	.0010	+.0006	+.0006	−.0006	−.0012	−.0006	−.0012	.0012	.0024	.0003
035	−.0008	−.0006	.0010	.0012	+.0008	+.0006	−.0008	−.0016	−.0006	−.0012	.0016	.0028	.0004
040	−.0008	−.0006	.0010	.0012	+.0008	+.0006	−.0008	−.0016	−.0006	−.0012	.0016	.0028	.0004
042	−.0008	−.0008	.0010	.0014	+.0008	+.0008	−.0008	−.0016	−.0008	−.0016	.0016	.0028	.0004
045	−.0008	−.0008	.0010	.0014	+.0008	+.0008	−.0008	−.0016	−.0008	−.0016	.0016	.0028	.0004
047	−.0010	−.0008	.0012	.0014	+.0010	+.0008	−.0010	−.0020	−.0008	−.0016	.0020	.0034	.0006
050	−.0010	−.0008	.0012	.0014	+.0010	+.0008	−.0010	−.0020	−.0008	−.0016	.0020	.0034	.0006
055	−.0010	−.0010	.0012	.0016	+.0010	+.0010	−.0010	−.0020	−.0010	−.0020	.0020	.0034	.0006
060	−.0010	−.0010	.0012	.0016	+.0010	+.0010	−.0010	−.0020	−.0010	−.0020	.0020	.0034	.0006
065	−.0010	−.0010	.0012	.0016	+.0010	+.0010	−.0010	−.0020	−.0010	−.0020	.0020	.0034	.0006
070	−.0010	−.0012	.0012	.0016	+.0010	+.0012	−.0010	−.0020	−.0012	−.0024	.0020	.0034	.0006
075	−.0012	−.0012	.0016	.0018	+.0012	+.0012	−.0012	−.0024	−.0012	−.0024	.0024	.0042	.0007
080	−.0012	−.0012	.0016	.0018	+.0012	+.0012	−.0012	−.0024	−.0012	−.0024	.0024	.0042	.0007
090	−.0012	−.0012	.0016	.0018	+.0012	+.0012	−.0012	−.0024	−.0012	−.0024	.0024	.0042	.0007
100	−.0014	−.0014	.0018	.0020	+.0014	+.0014	−.0014	−.0028	−.0014	−.0028	.0028	.0048	.0008
110	−.0014	−.0014	.0018	.0020	+.0014	+.0014	−.0014	−.0028	−.0014	−.0028	.0028	.0048	.0008
120	−.0014	−.0014	.0018	.0020	+.0014	+.0014	−.0014	−.0028	−.0014	−.0028	.0028	.0048	.0008
140	−.0016	−.0016	.0018	.0020	+.0016	+.0016	−.0016	−.0032	−.0016	−.0032	.0032	.0052	.0010
160	−.0018	−.0018	.0018	.0020	+.0018	+.0018	−.0018	−.0036	−.0018	−.0036	.0036	.0056	.0011
180	−.0018	−.0018	.0020	.0020	+.0018	+.0018	−.0018	−.0036	−.0018	−.0036	.0036	.0056	.0011
200	−.0020	−.0020	.0020	.0020	+.0020	+.0020	−.0020	−.0040	−.0020	−.0040	.0040	.0060	.0012
250	−.0030	−.0030	.0020	.0020	+.0030	+.0030	−.0030	−.0060	−.0030	−.0060	.0060	.0080	.0018
300	−.0030	−.0030	.0020	.0020	+.0030	+.0030	−.0030	−.0060	−.0030	−.0060	.0060	.0080	.0018
350	−.0040	−.0040	.0020	.0020	+.0040	+.0040	−.0040	−.0080	−.0040	−.0080	.0080	.0100	.0024
400	−.0040	−.0040	.0020	.0020	+.0040	+.0040	−.0040	−.0080	−.0040	−.0080	.0080	.0100	.0024

netral clearance after installation theoretically can range rather widely if all ontributing bearing, housing, and shaft tolerances are at either of their extremes. learances shown are the amounts expected according to the laws of probability.

Race Width Tolerance:

Up thru 12" Bearing Bore	+.000 −.005
Over 12" Bearing Bore	+.000 −.010

All dimensions in inches.

KAYDON Precision Tolerances and Recommended Fits For REALI-SLIM Ball Bearings in Normal Applications

PRECISION CLASS 4

Bearing Size (All Series)	Bearing Diameters: Bearing Bore Nominal +.0000	Bearing Diameters: Bearing O.D. Nominal +.0000	Radial & Axial Runout: Inner Race		Radial & Axial Runout: Outer Race		Rotating Shaft: Shaft Diameter Nominal +.0000	Rotating Shaft: Housing Bore Nominal +.0000	Stationary Shaft: Shaft Diameter Nominal		Stationary Shaft: Housing Bore Nominal		Bearing Diametral Clearance*: Before Installation		Bearing Diametral Clearance*: Expect Min Aft Inst
10	−.0002	−.0002	R.0002,	A.0003	R.0002,	A.0003	+.0002	+.0002	−.0002	−.0004	−.0002	−.0004	.0005	.0009	.0001
15	−.0002	−.0002	R.0002,	A.0003	R.0002,	A.0003	+.0002	+.0002	−.0002	−.0004	−.0002	−.0004	.0005	.0009	.0001
020	−.0003	−.0003	R.0002,	A.0003	R.0003,	A.0004	+.0003	+.0003	−.0003	−.0006	−.0003	−.0006	.0006	.0012	.0002
025	−.0003	−.0003	R.0002,	A.0003	R.0003,	A.0004	+.0003	+.0003	−.0003	−.0006	−.0003	−.0006	.0006	.0012	.0002
030	−.0003	−.0003	R.0002,	A.0003	R.0004,	A.0005	+.0003	+.0003	−.0003	−.0006	−.0003	−.0006	.0006	.0012	.0002
035	−.0003	−.0003	R.0003,	A.0004	R.0004,	A.0005	+.0003	+.0003	−.0003	−.0006	−.0003	−.0006	.0006	.0012	.0002
040	−.0003	−.0003	R.0003,	A.0004	R.0004,	A.0005	+.0003	+.0003	−.0003	−.0006	−.0003	−.0006	.0006	.0012	.0002
042	−.0003	−.0004	R.0003,	A.0004	R.0004,	A.0005	+.0003	+.0004	−.0003	−.0006	−.0004	−.0008	.0008	.0014	.0002
045	−.0003	−.0004	R.0003,	A.0004	R.0004,	A.0005	+.0003	+.0004	−.0003	−.0006	−.0004	−.0008	.0008	.0014	.0002
047	−.0004	−.0004	R.0003,	A.0004	R.0004,	A.0005	+.0004	+.0004	−.0004	−.0008	−.0004	−.0008	.0008	.0014	.0002
050	−.0004	−.0004	R.0003,	A.0004	R.0004,	A.0005	+.0004	+.0004	−.0004	−.0008	−.0004	−.0008	.0008	.0014	.0002
055	−.0004	−.0005	R.0003,	A.0004	R.0005,	A.0006	+.0004	+.0005	−.0004	−.0008	−.0005	−.0010	.0010	.0016	.0003
060	−.0004	−.0005	R.0003,	A.0004	R.0005,	A.0006	+.0004	+.0005	−.0004	−.0008	−.0005	−.0010	.0010	.0016	.0003
065	−.0004	−.0005	R.0003,	A.0004	R.0005,	A.0006	+.0004	+.0005	−.0004	−.0008	−.0005	−.0010	.0010	.0016	.0003
070	−.0004	−.0005	R.0003,	A.0004	R.0005,	A.0006	+.0004	+.0005	−.0004	−.0008	−.0005	−.0010	.0010	.0016	.0003
075	−.0005	−.0005	R.0004,	A.0005	R.0005,	A.0006	+.0005	+.0005	−.0005	−.0010	−.0005	−.0010	.0010	.0016	.0003
080	−.0005	−.0005	R.0004,	A.0005	R.0005,	A.0006	+.0005	+.0005	−.0005	−.0010	−.0005	−.0010	.0010	.0016	.0003
090	−.0005	−.0005	R.0004,	A.0005	R.0005,	A.0006	+.0005	+.0005	−.0005	−.0010	−.0005	−.0010	.0010	.0016	.0003
100	−.0005	−.0005	R.0005,	A.0006	R.0006,	A.0007	+.0005	+.0005	−.0005	−.0010	−.0005	−.0010	.0010	.0016	.0003
110	−.0005	−.0005	R.0005,	A.0006	R.0006,	A.0007	+.0005	+.0005	−.0005	−.0010	−.0005	−.0010	.0010	.0016	.0003
120	−.0005	−.0006	R.0005,	A.0006	R.0007,	A.0008	+.0005	+.0006	−.0005	−.0010	−.0006	−.0012	.0012	.0018	.0003
140	−.0006	−.0006	R.0005,	A.0007	R.0007,	A.0008	+.0006	+.0006	−.0006	−.0012	−.0006	−.0012	.0012	.0018	.0003
160	−.0006	−.0007	R.0007,	A.0008	R.0008,	A.0009	+.0006	+.0007	−.0006	−.0012	−.0007	−.0014	.0014	.0020	.0004
180	−.0006	−.0007	R.0007,	A.0008	R.0008,	A.0009	+.0006	+.0007	−.0006	−.0012	−.0007	−.0014	.0014	.0020	.0004
200	−.0007	−.0008	R.0008,	A.0009	R.0009,	A.0010	+.0007	+.0008	−.0006	−.0014	−.0007	−.0016	.0014	.0022	.0004

Total Width Tolerance – Duplexed Type A Bearings:

Up thru 2" Bearing Bore	+.000 −.020
Over 2" thru 5" Bore	+.000 −.030
Over 5" thru 14" Bore	+.000 −.040
Over 14" Bore	+.000 −.050

Race Width Tolerance – Single Type C, X, A Bearings:

Up thru 12" Bearing Bore	+.000 −.005
Over 12" Bearing Bore	+.000 −.010

*Diametral clearance after installation theoretically can range rather widely if a contributing bearing, housing, and shaft tolerances are at either of their extreme Clearances shown are the amounts expected according to the laws of probability Diametral clearance shown do not apply to type A (angular contact) bearings.

All dimensions in inches.

KAYDON CORPORATION

don REALI-SLIM Ball Bearings

YPE C

YPE X

YPE A

KAYDON Precision Tolerances and Recommended Fits For REALI-SLIM Ball Bearings in Normal Applications

PRECISION CLASS 3

earing Size (All eries)	Bearing Diameters		Radial & Axial Runout		Rotating Shaft		Stationary Shaft				Bearing Diametral Clearance*		
	Bearing Bore	Bearing O.D.			Shaft Diameter	Housing Bore	Shaft Diameter		Housing Bore		Before Installation		Expected Minimum After Instal.
	Nominal +.0000	Nominal +.0000	Inner Race	Outer Race	Nominal +.0000	Nominal +.0000	Nominal		Nominal				
10	−.0002	−.0003	.0003	.0004	+.0002	+.0003	−.0002	−.0004	−.0003	−.0006	.0007	.0011	.0003
15	−.0003	−.0003	.0004	.0004	+.0003	+.0003	−.0003	−.0006	−.0003	−.0006	.0008	.0012	.0003
020	−.0004	−.0004	.0004	.0005	+.0004	+.0004	−.0004	−.0008	−.0004	−.0008	.0008	.0018	.0002
025	−.0004	−.0004	.0004	.0005	+.0004	+.0004	−.0004	−.0008	−.0004	−.0008	.0008	.0018	.0002
030	−.0004	−.0004	.0004	.0006	+.0004	+.0004	−.0004	−.0008	−.0004	−.0008	.0008	.0018	.0002
035	−.0005	−.0004	.0005	.0006	+.0005	+.0004	−.0005	−.0010	−.0004	−.0008	.0010	.0020	.0003
040	−.0005	−.0004	.0005	.0006	+.0005	+.0004	−.0005	−.0010	−.0004	−.0008	.0010	.0020	.0003
042	−.0005	−.0005	.0005	.0008	+.0005	+.0005	−.0005	−.0010	−.0005	−.0010	.0010	.0020	.0003
045	−.0005	−.0005	.0005	.0008	+.0005	+.0005	−.0005	−.0010	−.0005	−.0010	.0010	.0020	.0003
047	−.0006	−.0005	.0006	.0008	+.0006	+.0005	−.0006	−.0012	−.0005	−.0010	.0012	.0022	.0003
050	−.0006	−.0005	.0006	.0008	+.0006	+.0005	−.0006	−.0012	−.0005	−.0010	.0012	.0022	.0003
055	−.0006	−.0006	.0006	.0009	+.0006	+.0006	−.0006	−.0012	−.0006	−.0012	.0012	.0022	.0003
060	−.0006	−.0006	.0006	.0009	+.0006	+.0006	−.0006	−.0012	−.0006	−.0012	.0012	.0022	.0003
065	−.0006	−.0006	.0006	.0009	+.0006	+.0006	−.0006	−.0012	−.0006	−.0012	.0012	.0022	.0004
070	−.0006	−.0007	.0006	.0010	+.0006	+.0007	−.0006	−.0012	−.0007	−.0014	.0014	.0024	.0004
075	−.0007	−.0007	.0008	.0010	+.0007	+.0007	−.0007	−.0014	−.0007	−.0014	.0014	.0024	.0004
080	−.0007	−.0007	.0008	.0010	+.0007	+.0007	−.0007	−.0014	−.0007	−.0014	.0014	.0024	.0004
090	−.0007	−.0007	.0008	.0010	+.0007	+.0007	−.0007	−.0014	−.0007	−.0014	.0014	.0024	.0004
100	−.0008	−.0008	.0010	.0012	+.0008	+.0008	−.0008	−.0016	−.0008	−.0016	.0016	.0026	.0004
110	−.0008	−.0008	.0010	.0012	+.0008	+.0008	−.0008	−.0016	−.0008	−.0016	.0016	.0026	.0005
120	−.0008	−.0009	.0010	.0014	+.0008	+.0009	−.0008	−.0016	−.0009	−.0018	.0018	.0028	.0005
140	−.0008	−.0009	.0012	.0014	+.0008	+.0009	−.0008	−.0016	−.0009	−.0018	.0018	.0028	.0005
160	−.0009	−.0010	.0014	.0016	+.0009	+.0010	−.0009	−.0018	−.0010	−.0020	.0020	.0030	.0005
180	−.0009	−.0010	.0014	.0016	+.0009	+.0010	−.0009	−.0018	−.0010	−.0020	.0020	.0030	.0005
200	−.0010	−.0012	.0016	.0018	+.0010	+.0012	−.0010	−.0020	−.0012	−.0024	.0024	.0034	.0006

ıametral clearance after installation theoretically can range rather widely if all ntributing bearing, housing, and shaft tolerances are at either of their extremes. Clearances shown are the amounts expected according to the laws of probability. Diametral clearances shown do not apply to type A (angular contact) bearings.

All dimensions in inches.

Total Width Tolerance — Duplexed Type A Bearings:

Up thru 2" Bearing Bore	+.000 −.020
Over 2" thru 5" Bore	+.000 −.030
Over 5" thru 14" Bore	+.000 −.040
Over 14" Bore	+.000 −.050

Race Width Tolerance — Single Type C, X, A Bearings:

Up thru 12" Bearing Bore	+.000 −.005
Over 12" Bearing Bore	+.000 −.010

Appendix B.7 : DGPH-1610-B-1T high torque miniature motor

Litton
CLIFTON PRECISION®
Clifton Heights PA 19018 • (215) 622-1000

Housed Torque Motor Generator—Potentiometer
DGPH-1610-B-1T

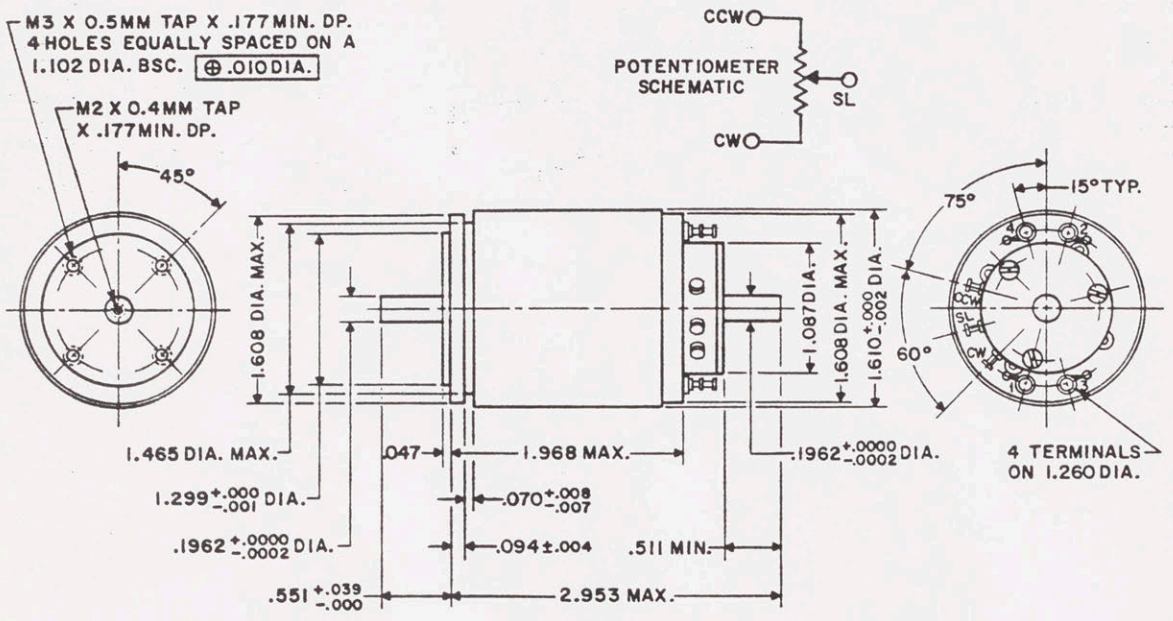

Performance Data:

Electrical Characteristics	Symbol	Values	Units	Tolerance
Peak torque	T_P	15.4	oz-in	nominal
Motor constant	K_M	1.9	oz-in/√watts	nominal
Electrical time constant	T_E	.27	milliseconds	nominal
Mechanical time constant	T_M	54	milliseconds	nominal
Power input, stalled, @ peak torque	P_P	65.2	watts	nominal
Viscous damping coefficient				
Zero impedance source	F_O	.026	oz-in/rad/sec	nominal
Infinite impedance source	F_I	.002	oz-in/rad/sec	nominal
Rotor inertia	J_M	.0014	oz-in-sec²	nominal
Weight		9.2	oz	nominal
Friction torque	T_F	1.1	oz-in	maximum
Ripple torque	T_R	7	percent	maximum
Max winding temperature		150	°C	maximum
Theoretical acceleration	α_M	11000	rad/sec²	maximum
No load speed	ω_{NL}	597	rad/sec	maximum
DC resistance	R_M	24.5	ohms	±12.5%
Volts @ peak torque	V_P	40	volts	nominal
Amps @ peak torque	I_P	1.63	amps	rated

Electrical Characteristics (Cont'd.)	Symbol	Values	Units	Tolerance
Torque sensitivity	K_T	9.5	oz-in/amp	±10%
Back EMF constant	K_E	.067	volts/rad/sec	±10%
Inductance	L_M	6.5	millihenries	±30%

Generator Characteristics	Symbol	Values	Units	Tolerance
DC resistance	R_T	50	ohms	±12.5%
Inductance	L_T	8.2	millihenries	±30%
Voltage sensitivity	K_G	0.07	volts/rad/sec	±10%
Load resistance	R_L	100 K	ohms	minimum
Ripple voltage	T_R	7	percent	maximum

Potentiometer Characteristics	Symbol	Values	Units	Tolerance
Total resistance	R_T	5 K	ohms	±20%
Effective electrical travel	Θ_A	320	degrees	±5°
Linearity		.5	percent	maximum
Power rating		.5	watts	maximum

Although every effort has been made to ensure the accuracy of the information contained within this brochure, the technical data and dimensions are subject to change without notice. Please contact us to verify all critical parameters.